UMONS

Université de Mons

Faculté Polytechnique

Centralized Control of Voltage in the MV Distribution Systems under Deterministic to Uncertain Model

PhD Thesis submitted by

Bashir BAKHSHIDEH ZAD

in partial fulfilment of the requirements for the degree of Doctor of Philosophy (PhD) in Engineering Sciences

Examining Committee:

Prof. Benoît Robyns (HEI-Lille)

Prof. Lieven Vandevelde (UGent)

Prof. Thierry Van Cutsem (ULg)

Prof. Emmanuel De Jaeger (UCL)

Prof. Olivier Debelecker (UMONS)

Prof. Jacques Lobry (UMONS), Supervisor

Prof. François Vallée (UMONS), Co-supervisor

Prof. Véronique Moeyaert (UMONS), President

Contents

Summary

The massive integration of Distributed Generation (DG) units in the electric distribution systems has created serious technical challenges for the Distribution System Operators (DSOs) including the voltage rise and local congestion problems. In order to deal with such arising issues, the conventional passive manner of the distribution network management based on the fit-and-forget policy is being replaced by the Active Network Management (ANM) schemes aiming at operating network in a safe and cost-effective way by taking advantage of the real-time communication and optimal control of the available devices. This thesis addresses the voltage control problem of the Medium-Voltage (MV) distribution systems under deterministic to uncertain model.

Inspired by the ANM framework, in the first part of the thesis, a centralized sensitivity-based voltage control approach is developed which manages the transformer tap position and DG active and reactive powers in order to maintain the node voltages and branch currents within their permitted limits. The sensitivity analysis determines impacts of the control variables on the operational limits of the system. Thanks to the information provided by the proposed sensitivity analysis methods, the voltage control problem is simplified to a linear optimization formulation that can remain tractable in almost real-time. Another important feature of the sensitivity-based voltage control approach is that it does not require the state estimation interface and with limited number of the voltage and power measurements, it can manage the voltage constraints.

In the electric distribution systems, as an accurate and up-to-date model of the system is not available, the calculations and analyses are performed relying on the simplified deterministic model that can lead to erroneous analyses and eventually wrong control decisions. In the second part of the thesis, it is considered that the network model is not deterministic anymore but is rather uncertain varying within the predefined bounds. A probabilistic framework is developed in order to evaluate impacts of the uncertain models of the system components on the voltage control problem of the MV distribution systems. In addition, a robust voltage control algorithm is designed that considers the model uncertainty when taking corrective decisions of the control variables. It determines a solution, which remains immunized against all possible realizations of uncertainties associated with the network component models.

Keywords: MV distribution systems, distributed generation units, voltage constraints management, branch ampacity limits, sensitivity analysis, model uncertainty, Monte Carlo simulation, robust optimization.

Chapter 1: Introduction

1.1. Abstract

In the first chapter of this thesis, generalities about the distribution systems hosting Distributed Generation (DG) units are presented. Then, voltage variation problem in such a network is introduced and voltage control methods for managing the voltage violations are discussed. Afterwards, a complete review is carried out on the existing Voltage Control Algorithms (VCAs) in the literature with a focus on the centralized-based schemes. Finally, the context and motivation of the current thesis is described which is followed by introducing the outline of the thesis.

1.2. The current trends in the medium-voltage distribution systems

In the recent years, the conventional structure of the electric power systems has been changed due to integration of DG units. The electric power that was only generated before in the large stations at small number of locations can be produced currently in the smaller scales but across the distribution systems. Consequently, the electric distribution systems that were designed previously to transfer electric power from the transmission networks to the end users are now changing to active circuits with bi-directional power flows hosting DG units and feeding the loads. Numbers of factors have led to an increasing interest in integration of DG units. The main drivers behind the growth of DGs are

- Diversification of energy resources;
- Energy efficiency issue and rational use of energy;
- Deregulation and competition in energy market;
- National power requirements;
- Reduction of gaseous emissions, etc.

Integration of DG units created new technical challenges for the safe operation and management of the distribution systems. Traditionally, the distribution networks were designed on the basis of the deterministic Load Flow (LF) studies considering the worst case scenarios to meet the forecasted load demands while keeping the branch ampacities and voltage limits. In other words, the system operation was done actually at the planning stage without almost any control on the real-time. This traditional manner of the distribution network management known as the fit-and-forget policy however could not be continued under the context of the active distribution systems integrating DG units given that the latter changes the power flow patterns to bi-directional, increases the fault level, creates local congestions, and induces voltage rise problems. Moreover, volatility of DG powers adds a big source of uncertainty to the network management problem.

The abovementioned shortcoming of the fit-and-forget policy has given rise to the new paradigm called Active Network Management (ANM) according to which, the up-to-date information about the system state and model is in disposal in order to optimally manage the system in real-time by controlling loads, DG active and reactive powers, transformer tap changers, energy storage devices, and circuit breakers [1]. The ANM aims at keeping the network safe by employing an efficient monitoring and control system, maximizing the utilization of the existing network and postponing the network reinforcement. In order to deploy such a control scheme, investments are needed on the automation of the substations and feeders, control centre software like SCADA (Supervisory Control And Data Acquisition), as well as communication and measurement channels. It is expected that the benefits brought by the ANM in long-term will outweigh the costs of these investments [2].

1.3. Voltage variation problem in the current distribution systems

The electric power networks were traditionally operated in a passive mode where the power generated by the large power plants was delivered to the customers through the distribution networks. Thus, the power flow was from the interface of the transmission and distribution networks towards the end users. In such a configuration, voltage decreases towards end of distribution system feeders, as the line impedances cause voltage drops. Thus, the biggest voltage drop happens at the end of the feeder. In presence of DGs, if their generated powers exceed the local demands of loads, the power flow directions will be inversed and we will deal with voltage rise problem at the DG-connected buses. When injected DG powers are maximal and the load demands are low, the voltage rise may exceed the permitted voltage range. Conversely, when the load demands are maximal and DG powers are minimal, it leads to the voltage drop issue that conventionally we dealt with in the distribution systems. Consequently, as both voltage rise and drop issues might happen in the distribution systems with DG units, new voltage control strategies are needed to be designed.

Let consider a simple 2-bus distribution system shown in figure 1-1. When there is only power consumption at node 2, active and reactive powers that flow between nodes 1 and 2 (P_{br1} and Q_{br1}) are equal to the load consumption (P_L+jQ_L) at bus 2 (supposing that power losses in the line are negligible).

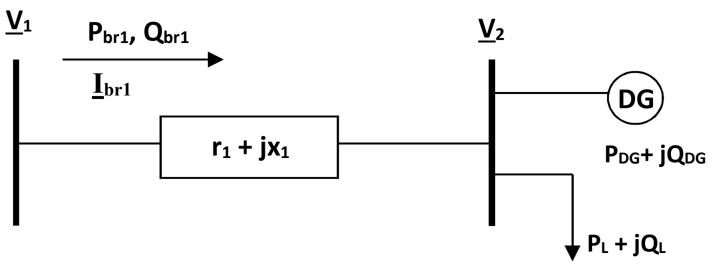

Figure 1-1: A simple 2-bus distribution system

The voltage variation along the line between nodes 1 and 2 is given by

$$\underline{\Delta V}_{12} = \underline{V}_1 - \underline{V}_2 = \underline{I}_{br1}(r_1 + jx_1) \tag{1-1}$$

where $\underline{V}_1$ [1] and $\underline{V}_2$ are complex values of voltages at buses 1 and 2, respectively. Also, r_1 and x_1 are resistance and reactance of the line between nodes 1 and 2, and $\underline{I}$ denotes to the complex current that passes in that line which is given by

$$\underline{I}_{br1} = \frac{P_{br1} - jQ_{br1}}{\underline{V}_1^*} \tag{1-2}$$

Substituting for the line current from (1-2), the voltage variation equation is rewritten as

$$\Delta \underline{V}_{12} = \frac{r_1 P_{br1} + x_1 Q_{br1}}{\underline{V}_1^*} + j\frac{x_1 P_{br1} - r_1 Q_{br1}}{\underline{V}_1^*} \tag{1-3}$$

Due to considerably high resistance and relatively low reactance of the lines in the distribution systems (with respect to the ones in the transmission systems), the voltage angles are small such that the voltage phasors can be represented with their absolute values. Consequently, the imaginary part of the voltage variation vector (1-3) can be neglected [3]. Figure 1-2 shows the vector diagram of the voltages in the above system when a lagging current is absorbed from node 2. As it can be seen, the imaginary part of the voltage variation vector (i.e. equal to $V_2 \sin \theta V_{12}$) over its real part is negligible. It should be noted that in figure 1-2, vectors of voltage variations on the line resistance and reactance have been enlarged for the illustration. In general, they have smaller amplitudes; consequently, ΘV_{12} is smaller than what has been shown in figure 1-2.

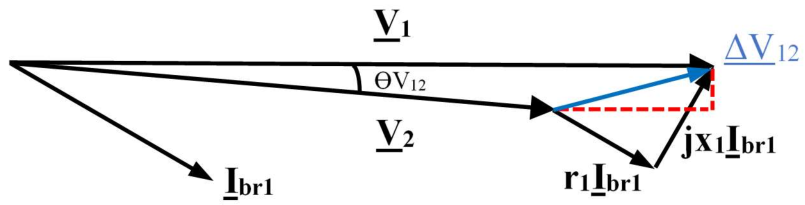

Figure 1-2: Vector diagram of the voltages in the 2-bus system

In addition, considering bus 1 as the slack bus with the voltage magnitude equal to 1 pu and phase angle equal to zero, the voltage variation is simplified to

$$\Delta V_{12} = r_1 P_{br1} + x_1 Q_{br1} \tag{1-4}$$

In presence of both load consumption and DG powers (P_{DG}+jQ_{DG}) at node 2, (1-4) is rewritten as

$$\Delta V_{12} = r_1\left(P_L + P_{DG}\right) + x_1\left(Q_L + Q_{DG}\right) \tag{1-5}$$

Supposing that the injected active power of DG has negative values[2] (i.e. in the opposite direction of the load active power), when its absolute value is sufficiently high, the right side

[1] In the rest of the work, the complex values are presented with a bar in below (e.g.: $\underline{V}_1$) and the complex conjugate values with a bar in below and a star in above (e.g.: $\underline{V}_1^*$). Also, j stands for the imaginary unit (i.e., $j = \sqrt{-1}$).
[2] Appendix 1 presents the adopted convention for directions of load and DG powers.

of (1-5) can become negative leading to V_2 greater than V_1. Thus, injection of DG active power can cause a voltage rise problem at node 2, particularly, when the Resistance to Reactance (R/X) ratio of the line is high that it is normally the case of the distribution grids. Conversely, when DG power is lower than the load demand at bus 2, the power is transferred from bus 1 to 2 and leads to a voltage drop at bus 2 with respect to bus 1. As it can be noticed from (1-5), the voltage variation at bus 2 depends on DG active and reactive powers, load powers and impedance of the line. Due to the fact that load demands and DG active powers are changing continuously, we will deal with both voltage rise and voltage drop problems. The voltage control problem is known as one of the biggest obstacles for increasing the integration of DG units in the distribution grids. If this problem is solved efficiently, then higher DG levels can be allowed to be installed in the system.

1.4. Conventional voltage control techniques

Different methods can be applied to manage the voltage control problem of the distribution systems. In the following sections, the most common voltage control techniques are introduced and their advantages and drawbacks are discussed.

1.4.1. On-load tap changer action

The transformer tap changer modifies the turn ratio of the transformer winding when the voltage value exceeds the predefined voltage range in order to provide the voltage control possibility at the secondary side of the transformer. The tap changer action is normally adjusted by an Automatic Voltage Control (AVC) relay, which continuously monitors the voltage and controls the action of the tap changer. The AVC relay works based on two controlling parameters, which are the reference voltage of the regulated point and a defined voltage deadband. The latter is considered in order to limit the unnecessary action of the tap changer. Voltage regulation using the On-load Tap Changer (OLTC) is a straightforward technique that can be easily implemented, if the transformer is equipped with the OLTC functionality. Given that the OLTC directly changes the node voltages, it will not cause congestion problem in the system branches and will not affect considerably the power losses.

The drawback of the OLTC is that it cannot be used in the voltage regulation of the long radial feeders since it changes the sending-point voltage of the feeder and the biggest voltage violation normally occurs at the end of the line (ending-point of the feeder). In this situation, in order to return the ending-point voltage inside the permitted voltage range, OLTC must change noticeably the sending-point voltage that can cause a voltage violation at that point. In addition, the tap changing operation is done with a time delay due to the slow dynamic response of the OLTC mechanism. As the maintenance costs of the OLTC depend on the number of tap changing operations, there is a tendency to set a long delay for its activation, which results in dealing with some unexpected voltage violations during the time that the OLTC is starting to act. Moreover, the OLTC cannot work efficiently in the voltage regulation of the distribution systems with multiple feeders integrating DG units because depending on DG and load powers, it is possible to deal with voltage rise problem in some feeders while other feeders have the voltage drop issue. It is known that with a unique set-point of the OLTC, it is not possible to manage both voltage rise and drop problems.

In Belgium, the transformer related to the interface of the transmission and Medium-Voltage (MV) distribution systems is not under control of the distribution system operator (e.g. ORES) and it is recognized as the property of the transmission system operator (i.e. ELIA). Therefore, in order to employ the OLTC for the voltage management of the Belgian MV distribution systems, collaboration between the transmission and distribution system operators is required.

1.4.2. Reactive power control of DGs

Reactive power compensation is an old technique for the voltage regulation of the distribution systems. Traditionally, capacitor banks were used in the distribution systems to keep the load power factors close to one and to compensate the voltage drops due to the high load demands. In the DG-connected distribution systems, as we deal with both voltage drop and rise issues, we need a source of reactive power with the ability to work in both capacitive and inductive modes. The reactive power control of DG units can be utilized in this regard as explained in below.

The synchronous machine-based DG unit offers reactive power control capability through modifying the excitation (rotor) current of the machine. Automatic Power Factor Control (APFC) and Automatic Voltage Regulation (AVR) schemes have been designed in [4] in order to achieve the voltage regulation objective by managing reactive power of synchronous machine-based DG unit. In the APFC mode, the reactive power of DG (Q_{DG}) follows any variation of the active power of DG (P_{DG}). Therefore, the $\frac{P_{DG}}{Q_{DG}}$ ratio is maintained constant in order to keep the voltage of the regulated point within the limits. This method is not applicable in the voltage regulation of the distribution systems with a high ratio of R/X. In addition, it is not an accurate approach, as it neglects the load variation of the regulated point. In the AVR mode, the difference between voltage of the regulated point and a predefined reference voltage defines the needed reactive power for the voltage regulation end. This action can be characterized by a droop control. Operation of DG in the AVR mode however can cause problems such as high field currents, overheating and triggering of over current protection systems. In reference [5], a deadband has been defined in order to limit the exchanged reactive power of DG in the unnecessary range. In reference [6], a new voltage control scheme has been proposed which combines the advantages of the AVR and APFC methods.

Regarding the asynchronous machine-based DG units, it is known that reactive power control is not possible in self-excited and squirrel-cage induction generators. In case of Doubly-Fed Induction Generators (DFIG), reactive power control is possible through adjustment of the rotor current but the physical, thermal and converter power limitations must be considered [7]. In the photovoltaic cells-based DGs, reactive power control can be done through the inverter interface considering its capability curve as studied in [8]. Due to the abovementioned limitations of DGs in reactive power control, an alternative source of reactive power can be adopted for the voltage management purpose. Power electronics-based compensators like D-STATCOM (Distribution

Static Synchronous Compensator) can be used in this regard to tackle the limitations of DGs in the reactive power control.

1.4.2.1. Reactive power control by D-STATCOM

D-STATCOM is a member of FACTS (Flexible AC Transmission Systems) devices at the distribution level. It is a voltage source converter-based device, which converts a DC input into a set of three-phase sinusoidal voltage with a fast controllable amplitude and phase angle. D-STATCOM can provide superior solutions for the voltage regulation, flicker elimination, and improvement of power quality. In the voltage regulation mode, thanks to its fast response, the voltage violations can instantly be removed and the voltage can quickly bring back to its targeted voltage value. D-STATCOM as a source of reactive power controls the voltage of the regulated point by providing the required value of injected or absorbed reactive power. When the voltage of the regulated point is lower than the reference voltage, D-STATCOM works in capacitive mode and if it is higher than the reference voltage, it works in inductive mode. As long as the exchanged reactive power stays within its maximal and minimal limits, the voltage of the regulated point is kept at the targeted value. Application of D-STATCOM in the distribution system management and control is currently limited due to its high cost.

In reference [9], coordinated control of OLTC and STATCOM based on the artificial neural network has been investigated in order to maintain the voltage within the limits while minimizing tap changing operations and increasing reactive power capability margin of the STATCOM. Coordination of the OLTC and STATCOM for improvement of the transient and steady-state voltage responses of a wind park connected to the high-voltage grid has been studied in [10]. A coordinated voltage control method based on the OLTC and D-STATCOM has been presented in [11] and [12] in order to keep the voltages within the permitted limits and to reduce the power losses.

1.4.3. Curtailment of DG active powers

As it can be noticed from (1-5), the voltage rise problem is caused by the injected power of DG. Therefore, by curtailing the DG active power, we can mitigate the voltage rise issue. The drawback of this method is that the benefits of integrating DG units cannot be maximized since we need to cut the DG active powers. In the wind turbines, curtailment of the active power is done through pitch control of the turbine blades.

1.4.4. Other voltage control techniques

Beside the abovementioned voltage control methods, which are the most common ones in the MV distribution systems, network reconfiguration can be implemented for the voltage regulation end. In this method, circuit breakers of the system with voltage violations are managed (by opening or closing them) in order to form a new network topology in which the voltage regulation problem is solved. In addition, load side management and energy storage can be used in the voltage management of the distribution systems. Finally, given that the voltage violations strictly depend on the line impedances, network reinforcement (resizing the cables) is another approach for the voltage regulation. However, it is an expensive method, which cannot be implemented in a short time, and it is considered normally as the last possible option.

1.5. A review on the existing voltage control algorithms

The voltage control schemes in the literature can be classified into two main categories namely centralized and distributed (or decentralized) approaches. The distributed approaches (e.g.: [13], [14], and [15]) are mostly based on the local control of the OLTC of the transformer or local power factor control of DG units. In the centralized algorithms (e.g.: [16], [17], [18], [19], [20], [21], [22], [23], [24], and [25]) a global solution for the entire network is defined. Then, the corrective control commands are sent to the controllers through the communication links.

In [13], a decentralized voltage control approach based on the multi-agent concept is designed to manage the energy storage systems located in the clustered control zones. The partitioning of the control zones and linearization of the equations are implemented through the voltage sensitivity analysis. In [14], a partitioning model based on the sensitivity analysis is proposed where the particle swarm optimization algorithm is used to manage the reactive powers of DGs in order to keep the system voltages within the predefined limits. A coordinated distributed scheme for the voltage regulation of the distribution systems with multiple feeders is suggested in [15], which uses the Remote Terminal Units (RTUs) to construct a multi-agent system.

A centralized VCA employing the discrete and continuous control variables has been introduced in [16]. The model predictive control using the voltage sensitivity data establishes a multi-step centralized voltage control scheme in [17] and [18]. A coordinated scheme for minimizing the cost of the system operation (which includes cost of the energy losses, cost of the curtailed energy and cost of the reactive power support) while maintaining the system voltages within the limits has been formulated as a linear optimization problem in [19]. Also, an algorithm for short-term scheduling of distribution systems has been developed in [20] which has a non-linear formulation and is linearized by the use of the voltage sensitivity coefficients. In addition, an ANM scheme that employs control of DG active and reactive powers to maintain the voltage and thermal limits has been developed in [21].The optimal reactive power control of DGs for voltage management of the radial distribution systems using the sensitivity analysis has been addressed in [22]. Volt-var control problem in the 3-phase balanced and unbalanced distribution systems is formulated as a mixed-integer linear programming in [23] and [24]. Soft open point, which is a power electronics-based device that can provide continuous reactive power, is integrated in the volt-var problem in [25] in order to realize a fast voltage regulation possibility.

Comparative study of the distributed and centralized voltage control approaches for determining the hosting capacity of DG in an existing system has been done in [4]. In general, the centralized VCA has an overall view of the system states; eventually, it can manage the network in a more optimal way than the decentralized one. On the other hand, it needs extra measurements and data. Hybrid voltage control methods combining the centralized and localized schemes in the MV and Low-Voltage (LV) distribution levels have been developed in [26] and [27], respectively.

The existing voltage control algorithms can be categorized also based on their employed control strategies. The OLTC action in [11], [12], [15], [17], [20], [26], [27], [28], active power generation curtailment of DGs in [16], [17], [18], [19], [20], [26], [27], [29] and reactive power control of DGs in [16], [17], [18], [19], [20], [22], [23], [24], [26], [27] are used to provide the voltage control possibility. Other voltage control methods such as system reconfiguration in [16], [19], [30], load side management in [3], and integration of energy storage devices in [13] have been also utilized in the literature.

The MV distribution systems are mostly assumed to have balanced characteristics within the phases, while in some limited works like [14], [24] and [31], the unbalanced model of the network is taken into account. Moreover, in most of the works, it is assumed that the load powers are independent of the voltage (i.e. the power constant load model). In [23], the load models are also incorporated in the volt-var problem. Impacts of the load models on the voltage regulation problem using reactive power compensation are studied in [32]. The latter topic is further studied in chapter 6 of the thesis.

1.6. Centralized voltage control approach

As it can be concluded from section 1-4, each of the introduced voltage control techniques has its own advantages and drawbacks and there is no perfect single voltage regulation method. Therefore, in order to have an efficient voltage control system, it is needed to employ different voltage control techniques in a coordinated manner. The centralized voltage control approach on the basis of an optimization process can take advantage of different control methods to efficiently manage the system voltages. In other words, while there are different possibilities for actions of the existing controllers, the centralized voltage control algorithm determines the most optimal solution according to its defined objective function.

In order to deploy such a voltage regulation scheme, the first step is to evaluate the current state of the system. The real-time measurement and communication infrastructure play a major role here. Since in the distribution systems, limited real-time measurement data are available, the state estimation techniques can be used to define the current state of the system [33]. Then, if a voltage violation is found, the next step is to determine the optimal corrective decisions of the controllers in order to manage the voltage violation problem. The Optimal Power Flow (OPF) as described in below can be used in this regard.

1.6.1. Centralized voltage control approach based on the optimal power flow

OPF can be used as the central decision maker to define the most optimal control strategy while operating the system within its predefined limits. OPF can be introduced as an optimization algorithm, which is embedded in the conventional LF study. The LF programme with no optimization part determines the system voltages and currents according to a fixed set of values relating to the power injections and consumptions. Therefore, there is no degree of freedom in the LF calculations. However, active and reactive powers of generators (for instance) can be considered as the adjustable variables. Moreover, node voltages and branch currents can be treated as the flexible variables changing within the predefined ranges in order to provide additional degree of freedom. OPF by adding an optimization layer to the conventional LF programme takes advantage of the provided flexibility to adjust the control variables such that, it optimizes the defined objective function while the system variables are kept within their predefined bounds. In other words, OPF seeks to optimize a given objective function by controlling the power flows within an electrical network without violating the network LF constraints and operating limits. Like conventional LF, OPF determines voltage, current, and power throughout the system. However, unlike the conventional LF, OPF works with an under-constrained system, which means that multiple solutions are possible. Therefore, it performs multiple LF iterations, modifying the under-constrained variables in order to advance the objective [34].

Since the early 60s when OPF has been firstly introduced, it has been applied to manage the power system operation and control problems. Different forms of formulations in a single or multi-objective sense have been utilized to minimize power losses, optimize operation costs of the system, maximize the social welfare, minimize the system emission etc. [34], [35]. OPF in a general form is formulated as a constrained optimization problem given in below.

$$\begin{aligned} \textbf{Min:} \quad & f(u,x) \\ \textbf{Subject to:} \quad & g(u,x) = 0 \\ & h(u,x) \leq 0 \end{aligned} \tag{1-6}$$

where *f(u,x)* is the objective function, *g(u,x)* and *h(u,x)* are the equality and inequality constraints, respectively. Also, u and x denote the controllable and state variables. The equality constraints take into account the nodal power balance equations, similarly to the LF programme. The nodal power balance equations are represented in the rectangular or polar coordinate. Consequently, they are inherently non-linear as they include quadratic or trigonometric terms. The inequality constraints are linked to the operational limits of the system (e.g. node voltages and branch currents). The OPF formulated for managing the operational limits aims at minimizing the total costs of the controllable variables while maintaining the voltage and current values within their predefined limits.

In reference [36], application of the OPF in the voltage regulation of transmission systems by linearizing the objective function has been investigated. In the distribution systems management, OPF is utilized in order to calculate the DG hosting capacity in [37]. A research has been carried out on using OPF for curtailment of DG active powers in order to maintain the system voltages within the safe range in [38]. A comprehensive centralized approach for voltage constraints management based on the OPF formulation has been introduced in [16], which takes advantage of the continuous and discrete control variables. In addition, OPF in a 5-min time horizon employs the ANM of DG active and reactive powers to maintain the voltage and thermal limits in [21].

1.7. Context and motivation of the thesis

OPF problem is a non-linear non-convex optimization problem that in practice, is difficult to solve. In addition, OPF can fail to converge in particular cases as studied in [39]. In the literature, different approaches have been proposed to solve the OPF problem, which can be classified into three main groups. In the first group, it is attempted to simplify the LF-related constraints of the OPF formulation. The most known example of this category is the DC-OPF formulation according to which, line resistances, voltage magnitudes, reactive power flows and power losses are neglected to derive the linear counterparts of the LF-related constraints (i.e. inherently non-linear) of the generic OPF formulation. This is not definitely a proper approach to be used in the distribution systems, which have lines with a high ratio of R/X, and important reactive power flows. The second group aims at solving the non-linear problem with the analytical-based or heuristic-based optimization methods. The drawback of this methodology is that the determination of the global optimal point cannot be guaranteed, given that the non-convexity of the OPF formulation is not taken into account. Moreover, the heuristic-based optimization methods lead generally to long calculation time, which is not compatible with the context of the real-time voltage management. In the last group, it is tried to convexify the LF-related constraints of the OPF problem. Then, the derived convex counterpart of the generic OPF formulation is solved. It should be noted that the objective function of the OPF applied for the operational limits management is usually convex and even linear (e.g., [16]), therefore, the non-convexity lies in the equality constraints related to the LF equations. The convexification procedure however requires extensive and complicated mathematical formulations. References [40] and [41] have presented approaches for the convex relaxation of the OPF in the meshed and radial distribution networks, respectively. In addition, convexification of the OPF problem according to the semidefinite programming and conic programing formulations has been investigated in [42] and [43], respectively. The convex relaxation of the LF-related constraints in the bus injection model and branch flow model has been studied in [44].

Moreover, OPF needs comprehensive data regarding the network model and variable states. Given that in the distribution systems, the network variables are partially known due to the lack of sufficient measurements, a state estimation interface is required to provide the network state to the OPF. Therefore, the OPF works with an assumption that the network state is available through the pre-processing stage of the state estimation.

In the first part of this thesis, motivated by the complexity of the generic OPF problem and unobservability of the network state, a centralized sensitivity-based voltage control approach is designed that includes a linear objective function and linear constraints. The sensitivity analysis determines impacts of the control variables on the operational limits of the system. Thanks to the information provided by the sensitivity analysis, the OPF problem presented in (1-6) is linearized around the system working point. Therefore, there is no need to consider the LF-related constraints of the generic OPF problem, which indicates that the equality constraints corresponding to nodal power balance equations can be deleted from (1-6). As a result, the generic OPF formulation is simplified to a linear optimization formulation that has less computational complexity and eventually, it can be solved in a faster and more straightforward manner. If the accuracy of the results obtained by the sensitivity-based voltage control approach is confirmed, then, it can be concluded that the proposed method is more suitable than the VCA based on the conventional OPF formulation for the voltage constraints management of the MV distribution systems, particularly for the threefold reasons. Firstly, the sensitivity-based voltage control approach has a much simpler formulation compared to the OPF-based one and can give us a better understanding about the voltage control procedure. Secondly, due to its simplified formulation, the solution of the optimization problem of the sensitivity-based voltage control approach can be obtained in a faster way, which makes it more suitable for the on-line management of the operational limits. Finally, the sensitivity-based voltage control approach does not require the state estimation interface and with limited number of voltage and power measurements, it can manage the operational limits of the system. The **main features** of the proposed linear voltage control scheme are as follows.

- **Centralized**

The proposed voltage control scheme as a central decision maker receives the network state through the limited number of the voltage and power measurements (or from an initial LF study). Once its corrective decisions are executed based on the defined optimization procedure, they will be sent to the network from a unique point.

- **Sensitivity-based**

The proposed voltage control approach uses the sensitivity analysis to linearize the system around its operating point and to eliminate the LF-related equations in its optimization formulation.

- **On-line**

The corrective decision of the proposed voltage control scheme should be executed in a very short time (close to real-time) so that the developed control tool can be used for the on-line management of the operational limits.

- **Coordinated**

Different voltage control methods will be employed in the VCA including the OLTC action of the substation transformer, reactive power control of DGs and generation curtailment of DGs. The above controllers are utilized in the voltage control procedure based on the impacts that they have on the operational limits (i.e. known from the sensitivity analysis).

- **Selective**

The proposed voltage control scheme distinguishes between the available control options based on their operating costs. Therefore, the priority is given to the voltage control option that has a high impact on the operational limits and a low operating cost.

- **Closed-loop or open-loop**

The sensitivity data are used to develop two voltage control algorithms in the open-loop and closed-loop forms. In the former type, the voltage violations are managed at once while in the latter one, the working point with violations is moved to the safe state within some steps. The corrective commands of the closed-loop VCA are applied to the controllers in each step. The voltage control procedure continues as long as a voltage violation exists in the system.

- **Static**

The proposed voltage control approach does not incorporate the dynamic response of the controllers. It means that the evolution of the system from the initial point (with the violation of the operational limits) towards the safe state is neglected. The choice is motivated by the fact that the reactive power control of DG (i.e., here the DFIG-based type) has very fast dynamic response thanks to its power electronics-based control structure. The active power curtailment of DG and OLTC action are implemented with longer delays in order of a few seconds to 10 seconds.

- **Snapshot-based**

Assuming that the network model is in our disposal, the proposed VCA receives the state variables (i.e. nodal voltages and powers) as an input. When a violation of the predefined limits is found, the VCA determines a corrective solution, which is optimal with respect to the considered working point. The set-point of the control variables is remained unchanged until a new violation is observed. Alternatively, an outer optimization layer with a longer activation delay can be implemented in order to minimize the network losses, similarly to the 3-level hierarchical voltage control method of the transmission systems [45]. In the latter context, our proposed VCA belongs to the innermost loop known as the primary voltage control, which compensates against rapid voltage variations. Note that in this thesis, we will not focus on the loss minimization loop.

The voltage control approach developed in the first part of this thesis relies on a simplified deterministic network model by adopting certain **assumptions** given in below.

- **3-phase balanced model**

Given that the voltage control problem of the MV distribution systems is addressed, it is supposed that the nodal powers are balanced within the three phases.

- **Power constant model**

In addition, it is assumed that DG and load powers are of the voltage independent type (i.e., power constant model).

- **Short-length line model**

Finally, system lines are modelled with the series impedances similar to the most of the practical cases in the distribution systems. This means that the shunt admittances of the lines are neglected.

In the second part of this thesis, which includes chapters 6 and 7, we consider that the network model is not anymore deterministic (as before) but it is rather uncertain varying within the predefined bounds. Firstly, a probabilistic framework is proposed in order to determine the upper and lower bounds of voltage variations arisen from the uncertainties of the network component models. The obtained bounds can be utilized in order to reset the targeted points of the VCA such that the VCA solutions remain robust against uncertainties of the system component models. Then, in the end of this part, uncertainties associated with the network models are considered in the VCA when taking corrective decisions of the control variables. The proposed VCA of the last chapter determines a solution, which remains robust against all possible realizations of uncertainties associated with the network component models. Based on our best knowledge, the only work that considers the uncertainty of the network model in the voltage constraints management problem has been published in 2017 [46]. In the latter paper, the uncertainty is arisen from the thermal dependency effects of the lines. In the last chapter of this thesis, we further extend this subject by developing a robust VCA that accounts for uncertainties associated with the voltage dependency of loads, power factor of loads, thermal dependency of lines, shunt admittances of lines and internal resistance of substation transformer.

In view of the above discussion, the main objectives of the current thesis are as follows.

- To extract the dependencies between the control variables (i.e. OLTC as well as DG active and reactive powers) and the node voltages.
- To formulate the centralized sensitivity-based voltage control approach as a linear optimization problem.
- To validate the accuracy of the proposed sensitivity-based voltage control approach and evaluate its computation time.
- To determine the model uncertainty impacts on the VCA results relying on the simplified deterministic models of the network components.
- To derive the robust counterpart of the sensitivity-based VCA and validate it under uncertainty of the network model.

The outline of the thesis is presented in the next section.

1.8. Thesis outline

The rest of this thesis is organized as follows:

In the next chapter, a centralized sensitivity-based voltage control scheme is designed in order to bring back the violated voltages within the predefined voltage limits through optimal management of DG reactive powers while keeping the ampacity limits of the system branches. A novel voltage sensitivity analysis method is developed which extracts the relations between the node voltages and reactive powers directly on the basis of the topological structure of the network. Moreover, a new formulation is proposed in order to consider the branch ampacity limits as a function of DG reactive power changes. The voltage control problem is formulated as an optimization problem, which uses the sensitivity analysis for linearizing the relations between the operational limits and the DG reactive powers.

In chapter 3, the direct voltage sensitivity analysis method developed in chapter 2 is used to linearize the relationships between the system voltages and the nodal active and reactive powers. The VCAs presented in chapter 2 in the single-step and multi-step forms are equipped with a complementary functionality to control (curtail) active powers of DG units. Therefore, in this chapter, the proposed VCAs modify both active and reactive powers of DG units in order to return the system voltages within the permitted voltage range while maintaining the branch ampacity limits. The proposed VCAs distinguish between the cheap and expensive control options using the defined weighting coefficients in their objective functions.

In chapter 4, the improved direct sensitivity analysis method is developed. It is a complementary representation of the direct voltage sensitivity analysis method, which considers impacts of power loss variations due to nodal power changes on the system voltages. Effectiveness of the improved direct sensitivity analysis method is investigated and compared with the voltage results obtained through other studied methods. To this end, firstly, the considered voltage sensitivity methods are tested when active or reactive power is changed at the selected nodes of the studied test system. Then, performance of the considered voltage sensitivity methods is examined when they are separately embedded in the single-step and multi-step VCAs.

In chapter 5, functionality of the sensitivity-based VCAs presented in chapter 3 is evolved by adding the possibility of controlling the voltage level at the secondary side of the substation transformer through the transformer OLTC. Due to introduction of the latter with a discrete model, the voltage control problem is converted into the mixed-integer linear programing having the DG active and reactive powers as the continuous variables and the OLTC set-point as the discrete one. In the end of this chapter, it is explained how the proposed sensitivity-based voltage control approach should be modified in order to be compatible with the practical context of the MV distribution systems.

In chapter 6, a framework is proposed in order to evaluate impacts of the uncertain models of the system components on the voltage control problem of the MV distribution systems. To this end, firstly, the voltage constraints are managed using the sensitivity-based VCA relying on the simplified deterministic models of the system components. The system loads and lines as well as the substation transformer are then modelled with the uncertain variables, which are bounded in the predefined ranges. Monte Carlo simulations are utilized to create series of scenarios that cover the possible values that the parameters of the system components can take. The model uncertainty impacts on the voltage control problem are finally evaluated by the LF calculations considering the scenarios created by the Monte Carlo simulations and the set-point obtained by the VCA.

In chapter 7, uncertainties related to the network component models are considered in the VCA when taking corrective decisions of the control variables. The proposed VCA of this chapter determines a solution, which remains robust against all possible realizations of uncertainties associated with the network component models. To this end, prior to formulating the voltage control problem, Monte Carlo simulations are used to characterize the uncertain models of the network components and LF calculations are carried out to evaluate their impacts. The robust optimization counterpart of the proposed VCA is derived based on the results obtained through the Monte Carlo simulations and LF calculations. Once the robust optimization problem is solved, in order to check the robustness of the solution, system voltages are evaluated using the LF calculations considering the new set-points of control variables and uncertainties of the network component models.

Finally, in chapter 8, main contributions of the thesis are summarized, the overall conclusions are presented, applications of the conducted research are discussed, and its future perspectives are highlighted.

Chapter 2: Optimal reactive power control of DGs for managing the voltage constraints

2.1. Abstract

In this chapter, a centralized sensitivity-based voltage control scheme is designed in order to bring back the violated voltages within the predefined voltage limits through optimal management of DG reactive powers while maintaining the ampacity limits of the branches. The proposed voltage control technique consists of three parts, which are the LF calculation, sensitivity analysis and optimization formulation. The LF study is used to evaluate the node voltages and branch currents and to check if there is any violation of the limits. An efficient LF approach tailored for the MV distribution systems is introduced in this chapter, which works on the basis of the network topology. The sensitivity analysis determines impacts of DG reactive powers on the operational limits of the system. A novel Voltage Sensitivity Analysis (VSA) method is derived from the introduced LF approach. As a result, the proposed VSA is also based on the topological structure of the network and remains independent of the network operating point. Therefore, once it is calculated with the LF program, it can be used in all the system working conditions. Moreover, a new formulation is proposed in order to take the ampacity limits of the system branches into account when reactive powers of DGs are changed for the voltage regulation purpose. The voltage control problem is finally formulated as an optimization problem, which aims at minimizing the total changes of DG reactive powers while returning the violated voltages within the predefined voltage limits and keeping currents of the system branches within their permitted ampacity limits.

2.2. Direct load flow approach for the distribution systems

The idea of the Direct Load Flow (DLF) approach in the distribution systems has been presented in [47]. In the DLF approach, two matrices named BIBC (bus injection to branch current) and BCBV (branch current to bus voltage) are constructed. These matrices present the topological structure of the network. The BIBC matrix is responsible for the relations between the node current injections and branch currents. Thus, branch current variations, which are created by the node current changes, can be found through the BIBC matrix. The BCBV matrix presents the relations between the branch currents and node voltages. The variations of system voltages caused by the branch current changes are found through the BCBV matrix. In order to introduce the DLF method, let consider the 5-bus distribution system shown in figure 2-1 where bus number 1 is supposed to be the slack bus with a constant voltage magnitude equal to 1 pu and a phase angle equal to zero.

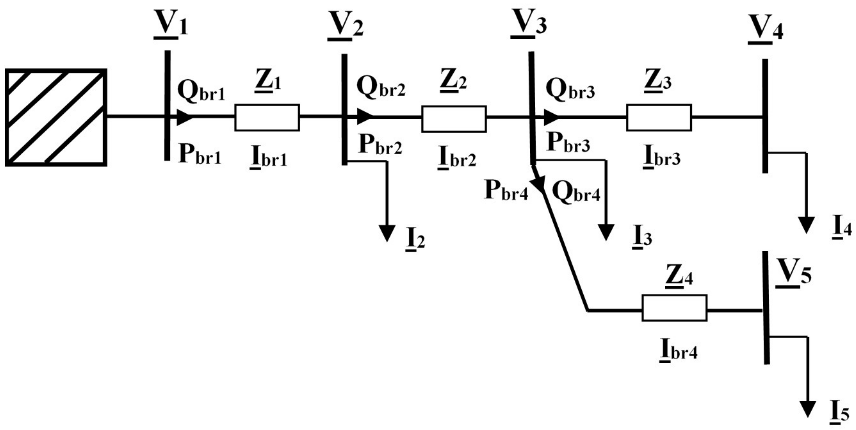

Figure 2-1: Simple 5-bus radial distribution system

In the above 5-bus system, the currents of branches 1 to 4 denoted respectively by $\underline{I}_{br1}$, $\underline{I}_{br2}$, $\underline{I}_{br3}$, and $\underline{I}_{br4}$ can be obtained by applying the Kirchhoff's current law to the nodal currents $\underline{I}_2$, $\underline{I}_3$, $\underline{I}_4$ and $\underline{I}_5$ (related to nodes 2 to 5, respectively) as follows.

$$\underline{I}_{br1} = \underline{I}_2 + \underline{I}_3 + \underline{I}_4 + \underline{I}_5 \qquad (2\text{-}1)$$

$$\underline{I}_{br2} = \underline{I}_3 + \underline{I}_4 + \underline{I}_5 \qquad (2\text{-}2)$$

$$\underline{I}_{br3} = \underline{I}_4 \qquad (2\text{-}3)$$

$$\underline{I}_{br4} = \underline{I}_5 \qquad (2\text{-}4)$$

In the matrix form, the above equations can be written as

$$\begin{bmatrix} \underline{I}_{br1} \\ \underline{I}_{br2} \\ \underline{I}_{br3} \\ \underline{I}_{br4} \end{bmatrix} = \begin{bmatrix} 1 & 1 & 1 & 1 \\ 0 & 1 & 1 & 1 \\ 0 & 0 & 1 & 0 \\ 0 & 0 & 0 & 1 \end{bmatrix} \begin{bmatrix} \underline{I}_2 \\ \underline{I}_3 \\ \underline{I}_4 \\ \underline{I}_5 \end{bmatrix} \qquad (2\text{-}5)$$

The **BIBC** matrix, which gives the relationships between branch currents and nodal currents is obtained from (2-5) as

$$[\mathbf{I_{br}}] = [\mathbf{BIBC}][\mathbf{I}] \qquad (2\text{-}6)$$

Similarly, the relations between node voltage variations (with respect to the slack bus voltage) and branch currents can be written in the matrix form as below.

$$\begin{bmatrix} \underline{V}_1 \\ \underline{V}_1 \\ \underline{V}_1 \\ \underline{V}_1 \end{bmatrix} - \begin{bmatrix} \underline{V}_2 \\ \underline{V}_3 \\ \underline{V}_4 \\ \underline{V}_5 \end{bmatrix} = \begin{bmatrix} \underline{Z}_1 & 0 & 0 & 0 \\ \underline{Z}_1 & \underline{Z}_2 & 0 & 0 \\ \underline{Z}_1 & \underline{Z}_2 & \underline{Z}_3 & 0 \\ \underline{Z}_1 & \underline{Z}_2 & 0 & \underline{Z}_4 \end{bmatrix} \begin{bmatrix} \underline{I}_{br1} \\ \underline{I}_{br2} \\ \underline{I}_{br3} \\ \underline{I}_{br4} \end{bmatrix} \qquad (2\text{-}7)$$

where $\underline{V}_1$ to $\underline{V}_5$ correspond to voltages at buses 1 to 5, respectively. Also, $\underline{Z}_1$, $\underline{Z}_2$, $\underline{Z}_3$ and $\underline{Z}_4$ respectively denote series impedances of the branches 1 to 4. The BCBV matrix can be obtained from the over-mentioned equation.

$$[\mathbf{\Delta V}] = [\mathbf{BCBV}][\mathbf{I_{br}}] \tag{2-8}$$

Substituting for $\mathbf{I_{br}}$ from (2-6), a direct relation between $\mathbf{\Delta V}$ (i.e. vector of nodal voltage variations with respect to the slack voltage) and $\mathbf{I}$ (i.e. vector of nodal current injections) is obtained through the so-called **DLF** matrix through multiplication of **BCBV** and **BIBC** matrices, as follows.

$$\begin{aligned} [\mathbf{\Delta V}] &= [\mathbf{BCBV}][\mathbf{BIBC}][\mathbf{I}] \\ &= [\mathbf{DLF}][\mathbf{I}] \end{aligned} \tag{2-9}$$

The **DLF** matrix is built once for a given network and it remains constant as it contains the topological structure of the network. In order to solve the LF problem, (2-9) is used in an iterative-based procedure. In the first iteration (*it*=1), assuming that all node voltages are equal to 1 pu with phase angles equal to zero, the node current injections are calculated using the following equation

$$\underline{I}_k^{it} = \left(\frac{P_k + jQ_k}{\underline{V}_k^{it}} \right)^* \tag{2-10}$$

where $\underline{I}_k^{it}$ and $\underline{V}_k^{it}$ are the node current and voltage at bus k ($k \in NL$, NL is set of the load buses) at the iteration number it, respectively. Also, P_k and Q_k are the net active and reactive powers of bus k, respectively. Then, the obtained node currents in *it*=1 are used to calculate the vector of node voltage variations for the second iteration using (2-11). Afterwards, node voltages are updated by (2-12).

$$\left[\mathbf{\Delta V^{it+1}}\right] = [\mathbf{DLF}]\left[\mathbf{I^{it}}\right] \tag{2-11}$$

$$\left[\mathbf{V^{it+1}}\right] = [\mathbf{V_1}] - \left[\mathbf{\Delta V^{it+1}}\right] \tag{2-12}$$

where $\mathbf{V_1}$ is vector of reference voltages equal to 1 pu (considered for all load buses). The node voltages obtained by (2-12) are used to update the node currents using (2-10) in the second iteration. Similarly, the voltage variation vector and node voltages are again updated by the last node currents. The new available node voltages create the new node currents and this procedure continues. The solution of the LF problem is obtained when the difference between the absolute value of voltage at bus k in two consecutive iterations is less than a predefined error ($\forall k, k \in NL$).

In the DLF approach, time-consuming LU decomposition and forward/backward substitution of the Jacobian matrix or admittance matrix required in the traditional LF methods are no longer necessary and only, the **DLF** matrix is used to solve the LF problem [47]. Therefore, a considerable computation time can be saved in this method that makes it suitable for the on-line operation and management of the distribution systems.

2.3. Voltage sensitivity analysis

As known, changing any parameter of an electric power system has an effect on the system performance (state). While some parameters have significant impacts on the system state, others can have less important impacts. The VSA, in particular, gives us the impacts of changing nodal active and reactive powers on the system voltages. It determines relations between the nodal voltages and the powers through the linear approximations. The VSA is a known topic in control and operation of the electric power systems. A review on the existing VSA methods is carried out in the following section.

2.3.1. Review on the existing voltage sensitivity analysis methods

Sensitivity of system voltages with respect to the active and reactive powers is conventionally obtained from the inverse of the Jacobian matrix in the Newton-Raphson Load Flow (NRLF) study. The NRLF method has been basically developed for the LF study in the transmission systems which have different characteristics compared to the distribution systems, particularly, regarding the Resistance to Reactance ratio of their lines. Distribution networks by having the lines with wide range of lengths, high R/X ratio, and the radial structure fall into the category of ill-conditioned systems for the NRLF algorithm [48] and [49]. As a result, application of the Jacobian-Based Sensitivity Analysis (JBSA) approach in the distribution systems may encounter problems including inaccuracy or convergence failure [31], [50] and [51]. Moreover, when the NRLF method is not used for the LF calculation, the Jacobian matrix would not be available in order to derive the voltage sensitivity coefficients. In addition, the JBSA approach cannot give us sensitivity of power losses and branch currents with respect to the nodal power changes. In order to tackle these shortcomings of the JBSA method, some research has been carried out in the literature aiming at proposing new VSA approaches that are tailored for the distribution systems.

An analytical sensitivity analysis method has been proposed in [46] in order to calculate the sensitivity of nodal voltages and currents with respect to the active and reactive power variations in the 3-phase unbalanced distribution system. In this method, it is assumed that the phasors of all system voltages are known through a state estimation tool. Also, a new VSA approach based on the Gauss-Seidel LF method and Z-bus matrix has been introduced in [50] in order to derive the voltage and loss sensitivity factors. It is shown that with this proposed VSA method, some results similar to the ones using JBSA approach can be obtained. In [51], voltage and loss sensitivity coefficients with respect to the node powers are obtained by running an initial LF calculation and forming a matrix based on the topological structure of the system. The drawback of this method is that all DG-connected buses should be modelled as the voltage-controlled (PV) nodes with fixed voltage magnitudes. A VSA method for the radial MV distribution system considering the constant current models for loads and generators is developed in [52]. However, it is known that all types of DG units cannot be modelled with the constant current model as studied in [53]. A software toolkit is implemented in [54] based on the perturb-and-observe sensitivity analysis approach in order to determine the relations between system voltages and nodal powers in MV distribution systems. Application of the Tellegen's theorem for calculating sensitivity indices based on the adjoint network is studied in [55], [56] and [57] for the transmission and distribution levels.

2.3.2. The proposed direct sensitivity analysis method

In this chapter, a new VSA method is proposed which defines the dependencies between the nodal voltages and powers directly on the basis of the network topology. The proposed method named Direct Sensitivity Analysis (DSA) is independent of the network operating point given that it is derived from the network structure. Therefore, once the sensitivity coefficients are obtained for a given network, they remain constant for all working points of that system. This is the main advantage of the proposed DSA method over the classical JBSA or other approaches introduced in the previous section since in a real-time voltage control application, updating the VSA data is time-consuming procedure, which results in increasing the execution time of the developed voltage control algorithm. The DSA method is introduced as follows.

Let consider again the simple 2-bus system shown in figure 1-1. In equation (1-5) which gives the voltage variation at bus 2 with respect to the voltage at bus 1 (i.e. the slack bus). It is observed that the active power that flows in the line (P_{br1}) is coupled with the resistance of the line (r_1) and the reactive power that flows in the line (Q_{br1}) is coupled with the reactance of the line (x_1). The voltage variation at bus 2 is a function of the active and reactive power flows of the line located between nodes 1 and 2, but the influence degrees of P_{br1} and Q_{br1} on voltage at bus 2 depend on r_1 and x_1, respectively. Now, let refer to the 5-bus radial distribution system shown in figure 2-1. Supposing that node voltages are nearly close to 1 pu and the imaginary parts of the voltage variation vectors are negligible, (1-5) can be recursively applied to the 5-bus system as below.

$$\begin{bmatrix} V_1 \\ V_1 \\ V_1 \\ V_1 \end{bmatrix} - \begin{bmatrix} V_2 \\ V_3 \\ V_4 \\ V_5 \end{bmatrix} = \begin{bmatrix} r_1 & 0 & 0 & 0 \\ r_1 & r_2 & 0 & 0 \\ r_1 & r_2 & r_3 & 0 \\ r_1 & r_2 & 0 & r_4 \end{bmatrix} \begin{bmatrix} P_{br1} \\ P_{br2} \\ P_{br3} \\ P_{br4} \end{bmatrix} + \begin{bmatrix} x_1 & 0 & 0 & 0 \\ x_1 & x_2 & 0 & 0 \\ x_1 & x_2 & x_3 & 0 \\ x_1 & x_2 & 0 & x_4 \end{bmatrix} \begin{bmatrix} Q_{br1} \\ Q_{br2} \\ Q_{br3} \\ Q_{br4} \end{bmatrix} \tag{2-13}$$

where P_{br1}, P_{br2}, P_{br3} and P_{br4} stand for the active powers entering to branches 1 to 4, respectively, as shown in figure 2-1. Similarly, reactive power flows in these branches are given by Q_{br1}, Q_{br2}, Q_{br3} and Q_{br4}. Also, r_1 and x_1 are the resistance and reactance of the branch 1. The same notation is adopted for resistances and reactances of other branches. Due to the fact that the sensitivity of bus voltages with respect to nodal powers is needed, the branch power flows in above equation must be replaced by the nodal powers. The relations between branch power flows and the nodal powers can be obtained through the **BIBC** matrix in the DLF approach, similarly to (2-5) which gives relations between branch current flows and nodal currents. For the active powers, we have

$$\begin{bmatrix} P_{br1} \\ P_{br2} \\ P_{br3} \\ P_{br4} \end{bmatrix} = \begin{bmatrix} 1 & 1 & 1 & 1 \\ 0 & 1 & 1 & 1 \\ 0 & 0 & 1 & 0 \\ 0 & 0 & 0 & 1 \end{bmatrix} \begin{bmatrix} P_2 \\ P_3 \\ P_4 \\ P_5 \end{bmatrix} \tag{2-14}$$

where P_2, P_3, P_4 and P_5 denote the net active powers of the buses 2, 3, 4 and 5, respectively. It is worth noting that in the above equation, active power losses of the lines are assumed to be negligible. Similarly, relations between the branch reactive power flows and the nodal reactive powers can be also obtained by the BIBC matrix.

$$\begin{bmatrix} Q_{br1} \\ Q_{br2} \\ Q_{br3} \\ Q_{br4} \end{bmatrix} = \begin{bmatrix} 1 & 1 & 1 & 1 \\ 0 & 1 & 1 & 1 \\ 0 & 0 & 1 & 0 \\ 0 & 0 & 0 & 1 \end{bmatrix} \begin{bmatrix} Q_2 \\ Q_3 \\ Q_4 \\ Q_5 \end{bmatrix} \tag{2-15}$$

where Q_2, Q_3, Q_4 and Q_5 denote the net reactive powers of the buses 2, 3, 4 and 5, respectively. Substituting for the branch power flows from (2-14) and (2-15), (2-13) is rewritten as follows.

$$\begin{gathered} \begin{bmatrix} V_1 \\ V_1 \\ V_1 \\ V_1 \end{bmatrix} - \begin{bmatrix} V_2 \\ V_3 \\ V_4 \\ V_5 \end{bmatrix} = \begin{bmatrix} r_1 & r_1 & r_1 & r_1 \\ r_1 & r_1+r_2 & r_1+r_2 & r_1+r_2 \\ r_1 & r_1+r_2 & r_1+r_2+r_3 & r_1+r_2 \\ r_1 & r_1+r_2 & r_1+r_2 & r_1+r_2+r_4 \end{bmatrix} \begin{bmatrix} P_2 \\ P_3 \\ P_4 \\ P_5 \end{bmatrix} + \\ \begin{bmatrix} x_1 & x_1 & x_1 & x_1 \\ x_1 & x_1+x_2 & x_1+x_2 & x_1+x_2 \\ x_1 & x_1+x_2 & x_1+x_2+x_3 & x_1+x_2 \\ x_1 & x_1+x_2 & x_1+x_2 & x_1+x_2+x_4 \end{bmatrix} \begin{bmatrix} Q_2 \\ Q_3 \\ Q_4 \\ Q_5 \end{bmatrix} \end{gathered} \tag{2-16}$$

The above equation gives the relations between bus voltages and nodal active and reactive powers. In a matrix form, it can be shown as

$$[\mathbf{V_1}]-[\mathbf{V_k}]=[\mathbf{R}][\mathbf{P}]+[\mathbf{X}][\mathbf{Q}] \tag{2-17}$$

where $\mathbf{V_k}$ is vector of voltages at the load buses. Also, **P** and **Q** stand for vectors of the nodal active and reactive powers, respectively. **R** and **X** contain data regarding the sensitivity of system voltages with respect to nodal active and reactive powers, respectively. Given that bus number 1 is the slack bus, its voltage is always constant, which indicates that $\frac{\partial V_1}{\partial P_n} = \frac{\partial V_1}{\partial Q_n} = 0$ ($n \in NL, NL = \{2, 3, 4, \dots, nbus\}$, $nbus$ is the total number of the system buses). Therefore, voltage sensitivity at bus k with respect to active or reactive power at bus n is obtained by the following rules.

$$\frac{\partial V_k}{\partial P_n} = -R_{k\text{-}1,n\text{-}1} \tag{2-18}$$

$$\frac{\partial V_k}{\partial Q_n} = -X_{k-1,n-1} \tag{2-19}$$

The entry $R_{k-1,n-1}$ which is the (k-1)th row and the (n-1)th column of **R** equals to the sum of the resistances of the branches in which both P_k and P_n flow. For instance, in order to obtain $R_{3,2}$ (i.e. entry of **R** in the third row and the second column), the branch resistance between nodes 1 and 2 as well as the one between nodes 2 and 3 in which both P_4 and P_3 flow are considered. According to the abovementioned rule, $R_{3,2}$ gives the sensitivity of voltage at bus 4 with respect to the active power at bus 3 as below.

$$\frac{\partial\left(V_1 - V_4\right)}{\partial P_3} = \frac{-\partial V_4}{\partial P_3} = R_{3,2} = r_1 + r_2 \tag{2-20}$$

The DSA is formulated on the basis of the topological structure of the network. The sensitivity coefficients are built considering the directions in which active and reactive powers flow. The matrices **R** and **X** determine the relationships between bus voltages and nodal active and reactive powers. The same procedure has been followed to develop the **DLF** matrix in the DLF approach. The **DLF** matrix is built in the same way as matrices **R** and **X**. It presents the relationships between **ΔV** and **I**. The **DLF** matrix contains the same data as matrices **R** and **X**. The only difference is that **DLF** matrix includes resistance and reactance together in each of its entries in the complex (impedance) form. Thus, we have

$$[\mathbf{DLF}] = [\mathbf{R}] + j[\mathbf{X}] \tag{2-21}$$

Consequently, in the DSA method, the voltage sensitivity coefficients are obtained from the **DLF** matrix in the DLF approach. The real part of the **DLF** matrix composes the **R** and its imaginary part gives the **X**. It is worth noting that the proposed DSA method needs only branch parameters (i.e. resistances and reactances) and network topology as the input data, while the VSA methods introduced in section 2.3.1 require the state estimation interface or data regarding the state variables such as voltage phasors, node powers, etc.

2.4. The proposed method to consider the branch ampacity limit as a function of the DG reactive power

In this section, a new formulation is proposed in order to consider the ampacity limits of the system branches in the voltage control problem. The objective is to keep the branch currents within the maximal ampacities of the system conductors when the reactive powers of DGs vary for the voltage regulation purpose. In order to introduce the proposed method, let us consider again the simple 2-bus distribution system shown in figure 1-1. We suppose that the current in the branch 1 between nodes 1 and 2 must be maintained within the predefined ampacity of the branch named I_{br1}^{max} when reactive power of DG at bus 2 changes. We consider also that the initial current of the branch 1 is known as $\underline{I}_{br1}^{init} = I_{br1}^{init} e^{j\theta_{I1}}$. The active and reactive powers flowing in the branch 1 are given by

$$P_{br1} + jQ_{br1} = \underline{V}_1 \left(\underline{I}_{br1}^{init}\right)^* \tag{2-22}$$

Given that bus number one is the slack bus, voltage at bus 1 is equal to 1 pu and its phase angle is zero. Therefore, above equation can be simplified as

$$P_{br1} + jQ_{br1} = \left(\underline{I}_{br1}^{init}\right)^*$$
$$= P_{br1} + jQ_{br1} = I_{br1}^{init}\cos\theta_{I1} - jI_{br1}^{init}\sin\theta_{I1} \tag{2-23}$$

Now, if we change the reactive power of DG (at bus 2) equal to ΔQ_{DG}, it can be noticed from (2-23) that the real part of $\underline{I}_{br1}^{init}$ remains constant and it only affects the imaginary part of the initial current [58]. In other words, we have

$$P_{br1} + j(Q_{br1} + \Delta Q_{DG}) = I_{br1}^{init}\cos\theta_{I1} - jI_{br1}^{init}\sin\theta_{I1} + j\Delta Q_{DG} \tag{2-24}$$

After the reactive power variation at bus 2, the new current of the branch 1 ($\underline{I}_{br1}^{new}$) is equal to

$$\underline{I}_{br1}^{new} = I_{br1}^{init}\cos\theta_{I1} + jI_{br1}^{init}\sin\theta_{I1} - j\Delta Q_{DG} \tag{2-25}$$

The absolute value of the new current of the branch is given by

$$I_{br1}^{new} = \sqrt{(I_{br1}^{init})^2 + \Delta Q_{DG}^2 - 2\Delta Q_{DG} I_{br1}^{init}\sin\theta_{I1}} \tag{2-26}$$

In order to maintain the branch current within its predefined ampacity limit, the absolute value of the new current should be smaller than or equal to the maximal ampacity of the branch ($I_{br1}^{new} \leq I_{br1}^{max}$). The maximum possible reactive power variation in branch 1 denoted by ΔQ_{br1}^{max} (caused by the reactive power change at bus 2) which creates a current equal to the permitted ampacity of the branch 1 is obtained as follows.

$$I_{br1}^{\max} = \sqrt{(I_{br1}^{init})^2 + \left(\Delta Q_{br1}^{\max}\right)^2 - 2\Delta Q_{br1}^{\max} I_{br1}^{init}\sin\theta_{I1}}$$

$$\left(\Delta Q_{br1}^{\max}\right)^2 - 2\Delta Q_{br1}^{\max} I_{br1}^{init}\sin\theta_{I1} + (I_{br1}^{init})^2 - (I_{br1}^{\max})^2 = 0 \tag{2-27}$$

Assuming that the initial current value of the branch and its phase angle are known, ΔQ_{br}^{max} for a given I_{br1}^{max} can be obtained by solving the above quadratic equation. In other words, roots of the above equation give the maximum possible variations of DG while keeping the current in the branch 1 within its predefined ampacity limit. There are two roots for the above equation that correspond to the reactive power variations towards the inductive and capacitive directions. In order to make it more vivid, let consider figure 2-2 that shows the vector diagram of the currents in the simple 2-bus system. In this figure, it is assumed that the vector of the initial branch current is behind the voltage vector (i.e. the reference axe). The maximal ampacity of the branch 1 is found on the plotted circle with the radius equal to I_{br1}^{max}.

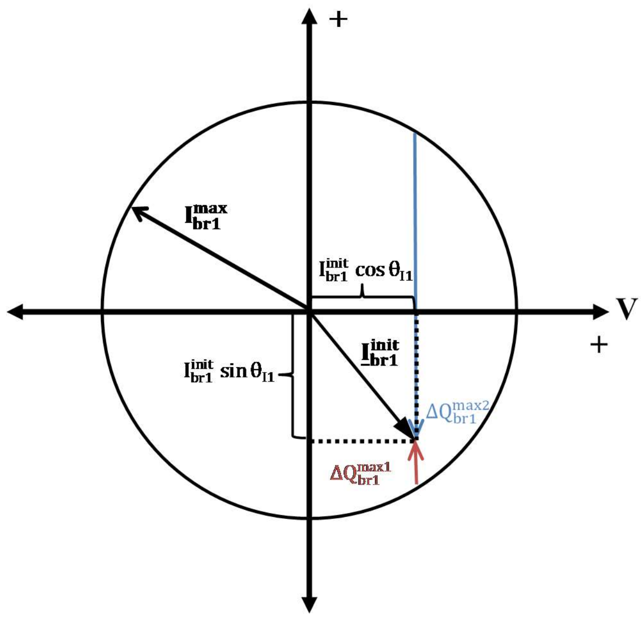

Figure 2-2: Current variations with respect to the reactive power changes

Given that reactive power variation of DG changes the imaginary part of the initial current in the considered branch, roots of (2-27) can be graphically shown with two vertical lines that connect ending point of $\underline{I}_{br1}^{init}$ to the circle of I_{br1}^{max}. In figure 2-2, ΔQ_{br1}^{max1} and ΔQ_{br1}^{max} show the maximum permitted reactive power variations of DG towards the inductive and capacitive directions, respectively. As the initial current has a lagging phase with respect to the voltage, the absolute value (length) of ΔQ_{br1}^{max1} (i.e. the maximum permitted inductive reactive power changes while keeping the ampacity limit of branch 1) is smaller than that of ΔQ_{br1}^{max2} (that corresponds to the maximum permitted capacitive changes).

In figure 2-2, the initial branch current is placed inside the circle of maximum current meaning that $I_{br1}^{init} < I_{br1}^{max}$. When the initial branch current exceeded the maximum branch current, if it has a lagging phase, the roots of (2-27) are both negative since the capacitive reactive power changes will return I_{br1}^{init} to circle of I_{br1}^{max}. In case of leading current with $I_{br1}^{init} > I_{br1}^{max}$, both roots of (2-27) are positive as inductive reactive power changes are needed to bring back the branch current within the limit. The smaller root corresponds to the nearest vertical distance between $\underline{I}_{br1}^{init}$ and circle of the maximum current and the bigger one shows the vertical distance that passes along the circle and reaches the surface of the circle of maximum current.

The proposed approach to consider the branch ampacity limit has been applied to 2-bus distribution system where the voltage at bus one is equal to 1 pu and its phase is zero. In the realistic distribution systems, this assumption does not hold, as a consequence, an error is found in the presented methodology. The accuracy of the proposed formulation will be tested later in this chapter through the numerical simulations.

2.5. Sensitivity-based voltage control scheme managing reactive powers of DGs

A centralized sensitivity-based voltage control approach is proposed here in order to maintain the node voltages and branch currents within their predefined limits through the reactive power control of DGs. It consists of three parts, which are the LF calculation, sensitivity analysis and the optimization formulation. In contrast with the classical OPF-based VCA which includes the LF-related (i.e. nodal power balances) constraints inside the optimization problem, in the proposed method, LF program and optimization part can be decoupled thanks to information provided by the sensitivity analysis. In the proposed voltage control approach, the DLF method is used to define the initial voltages and currents of the system and to check if there is any voltage and current violations. Sensitivity analysis gives us information regarding the influence of changing reactive powers of DGs on the node voltages and branch currents. Therefore, there is no need to consider the LF-related constraints inside the optimization problem. Using the sensitivity analysis, the voltage control problem is linearized around its operating point. The optimization part aims at determining the required modifications of control variables in order to satisfy the voltage and current constraints. On the basis of the above framework, two voltage control algorithms are developed in this chapter using which the initial system working point (with operational limit violations) is directed towards the targeted (safe) point at once in a single step or progressively within some steps. The former constructs an open-loop VCA and the latter works as a closed-loop VCA. The proposed VCAs will be introduced further in the following sections.

2.5.1. Multi-step voltage control algorithm

In the Multi-Step Voltage Control Algorithm (MSVCA), the priority of voltage regulation is given to the bus with the biggest voltage violation such that in each step (or iteration) of the voltage regulation procedure, voltage violation problem at the worst bus (i.e. the one with the biggest voltage violation) is removed. The MSVCA starts with running an initial LF calculation. If the voltage violations are found in the system, the main iterative-based procedure of the MSVCA starts with I=1. In the first iteration (I=1), the bus with the biggest voltage violation is selected and the value of voltage violation at that bus from the permitted voltage range is determined. It gives us the needed value of voltage modification in order to return voltage of that bus inside the permitted voltage range. In case of the voltage drop problem, the required value of voltage modification to remove the voltage violation problem at the worst bus is calculated with respect to the lower permitted voltage limit (i.e. 0.97 pu [59]) as follows.

$$\Delta V_w^{req} = 0.97 - V_w \tag{2-28}$$

where ΔV_w^{req} gives the required value of voltage modification to solve the voltage violation problem at the worst bus. Also, w is index relating to the bus with the worst voltage violation. The main objective of the MSVCA is to bring back the voltage of the worst bus inside the permitted voltage range through the optimal management of the DG reactive powers. In addition, thermal limits of the branches and physical limits of DGs in reactive power production are taken into consideration. Voltage control problem of the MSVCA at I=1 is formulated as an optimization problem given in below.

$$\textbf{Minimize:}\, OF = \sum_{x=1}^{N_G} \Delta Q_{DGx} \tag{2-29}$$

$$\sum_{x=1}^{N_G} \frac{\partial V_w}{\partial Q_{DGx}} \Delta Q_{DGx} \geq \Delta V_w^{req} \tag{2-30}$$

$$I_{brs} \leq I_{brs}^{\max} \quad \forall s,\ s \in C \tag{2-31}$$

$$\Delta Q_{DGx}^{\min} \leq \Delta Q_{DGx} \leq \Delta Q_{DGx}^{\max} \quad \forall x,\ x \in G \tag{2-32}$$

where N_G is the total number of DG units that contribute in the voltage control problem. ΔQ_{DGx} gives the reactive power change of the DG number x. Also, $\frac{\partial V_w}{\partial Q_{DGx}}$ denotes the voltage sensitivity of the worst bus with respect to the reactive power change of DG number x. The inequality constraint (2-30) represents the fact that the reactive power changes of DGs must return the voltage of the bus with the biggest voltage violation inside the permitted voltage range. The left side of (2-30) gives the voltage modification at the worst bus due to reactive power variations of DGs. The inequality constraint (2-31) takes into consideration the ampacity limits of the branches according to the method presented in section 2-4. Thus, the reactive powers of DGs are changed taking into account the maximum current limits of the system branches. For the sake of simplicity, the thermal limits are considered in some selected branches given by the set *C*. The inclusion of ampacity limits in the voltage control problem is discussed more in section 2.6.1. Furthermore, the reactive power contribution of DGs is limited by several factors as studied in [7] and [60]. The reactive power limitations of DGs are considered in the MSVCA as inequality constraint (2-32) representing the capability curves of DGs.

In the presented optimization problem, the reactive power changes of DGs are restricted in the range from negative to positive values corresponding to capacitive and inductive reactive powers. The solution of the linear optimization problem when control variables are unrestricted in sign would be the lower or upper bound of the variables. This is not definitely a proper solution for the voltage control problem. Therefore, the presented optimization problem must be rewritten in the standard form of the linear optimization problem according to [61] such that it only includes the control variables with non-negative bounds. To this end, the reactive power changes of DGs will be replaced by two new auxiliary variables as

$$\Delta Q_{DGx} = \Delta Q_{DGx}^{ind} - \Delta Q_{DGx}^{cap} \tag{2-33}$$

where ΔQ_{DGx}^{ind} represents the reactive power changes of DGs towards the inductive direction and ΔQ_{DGx}^{cap} takes into account the capacitive reactive power changes of DGs. Both new auxiliary variables are restricted in the non-negative ranges. Substituting for ΔQ_{DGx} from (2-33), the aforementioned optimization problem is rewritten as

$$\textbf{Minimize: } OF = \sum_{x=1}^{N_G} \left| \Delta Q_{DGx}^{ind} - \Delta Q_{DGx}^{cap} \right| \tag{2-34}$$

$$\sum_{x=1}^{N_G} \left(\frac{\partial V_w}{\partial Q_{DGx}} (\Delta Q_{DGx}^{ind} - \Delta Q_{DGx}^{cap}) \right) \geq \Delta V_w^{req} \tag{2-35}$$

$$I_{brs} \leq I_{brs}^{\max} \quad \forall s,\ s \in C \tag{2-36}$$

$$\Delta Q_{DGx}^{\min} \leq \Delta Q_{DGx}^{ind} - \Delta Q_{DGx}^{cap} \leq \Delta Q_{DGx}^{\max} \quad \forall x,\ x \in G \tag{2-37}$$

$$\Delta Q_{DGx}^{ind}, \Delta Q_{DGx}^{cap} \geq 0 \quad \forall x,\ x \in G \tag{2-38}$$

In order to have always a positive objective function, ΔQ_{DGx} in (2-29) is replaced by the absolute value of its equivalence given in (2-33) as it can be seen in (2-34). In the above optimization problem, the voltage sensitivity coefficients are known parameters, which are obtained from the matrix **X**. The required value of voltage change (ΔV_w^{req}) for solving the voltage problem of the worst bus is also a defined parameter but ΔQ_{DGx}^{ind} and ΔQ_{DGx}^{cap} ($x \in G$, $G=\{1, 2, 3, \ldots, N_G\}$) are decision variables that must be optimally selected. The linear programming solver of MATLAB optimization toolbox is used to solve the optimization problem of the MSVCA. Due to the fact that ΔV_w^{req} is positive in the voltage drop situation (see (2-28)), and the voltage sensitivity coefficients extracted from the matrix **X** are negative (see (2-19)), reactive power changes towards the capacitive direction (through ΔQ_{DGx}^{cap}) will satisfy the voltage constraint of bus w. The positive objective function guarantees that as soon as the Left-Hand Side (LHS) of (2-35) reaches its Right-Hand Side (RHS) (and when other constraints are satisfied too), the optimal solution is obtained. It should be noted that since $-\Delta Q_{DGx}^{cap}$ is always non-positive, by removing the absolute operator in the objective function, the optimal solution tends towards the lower bound of (2-37) because increasing ΔQ_{DGx}^{cap} will minimize the objective function. The latter solution however will lead to unnecessary reactive power changes. To avoid such an issue, the absolute operator is used in the objective function.

Once the optimization problem regarding I=1 is solved, the needed reactive power changes of DGs in order to manage the biggest voltage violation in I=1 are determined. Then, a new LF calculation is done at the end of the iteration one (including the new set-points of control variables) in order to define whether the MSVCA must go to the next iteration or it can stop. If a new voltage violation is found, the iteration 2 (I=2) starts, and a new optimization problem is composed (similar to that of the first iteration but with the updated values) in order to bring back the biggest voltage violation of the second iteration within the permitted voltage limits. By solving this new optimization problem, the control commands to return the biggest voltage violation of the second iteration within the permitted voltage range are defined. Again at the end of I=2, a new LF calculation is performed to decide if the next iteration of the MSVCA is needed or not. The iterative procedure of the MSVCA continues as long as there is a voltage violation. The flowchart of the proposed MSVCA is shown in figure 2-3.

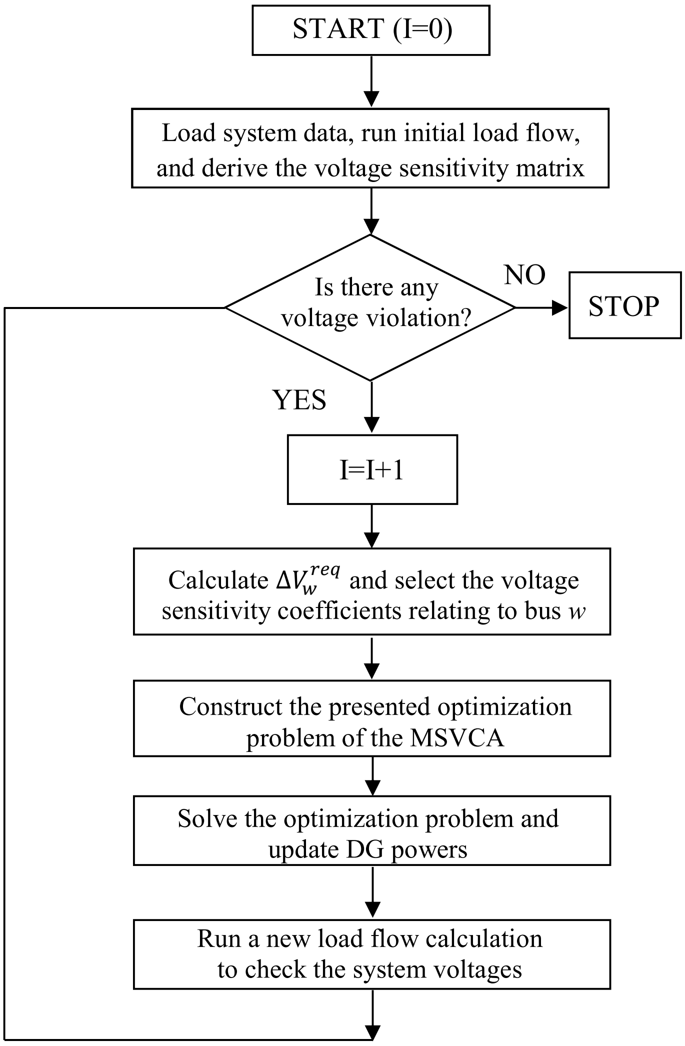

Figure 2-3: Flowchart of the MSVCA

In the voltage rise case, the needed value of voltage change at the bus with the biggest voltage rise is calculated with regard to the permitted upper voltage limit (i.e. 1.03 pu) using the following equation.

$$\Delta V_w^{req} = 1.03 - V_w \tag{2-39}$$

where ΔV_w^{req} gives the required value of the voltage change to remove the voltage violation at the bus with the biggest voltage rise. The optimization problem of the MSVCA mentioned in (2-34) to (2-38) is generally valid for the voltage regulation in the voltage rise state with one exception (difference) that the inequality constraint relating to the required value of voltage change given in (2-35) must be replaced by the following one.

$$\sum_{x=1}^{N_G} \left(\frac{\partial V_w}{\partial Q_{DGx}} (\Delta Q_{DGx}^{ind} - \Delta Q_{DGx}^{cap}) \right) \leq \Delta V_w^{req} \tag{2-40}$$

Given that ΔV_w^{req} is negative in the voltage rise case, and voltage sensitivity coefficients extracted from matrix **X** are also always negative (see (2-19)), in order to satisfy the above constraint, the inductive reactive power changes of DGs will be needed.

2.5.2. Single-step voltage control algorithm

The Single-Step Voltage Control Algorithm (SSVCA) is designed to bring back simultaneously all the violated voltages inside the permitted voltage range through the optimal management of DG reactive powers. It starts with running an initial LF calculation. If voltage violations are found in the system, all buses with the voltage violations are selected. The voltage control problem in the SSVCA is formulated as an optimization problem, which aims at minimizing the total reactive power changes of DGs subject to the voltage constraints relating to all the violated voltages as well as the limits on the branch currents and the bounds on the reactive powers of DGs. Once the optimization problem is solved, the needed reactive power changes of DGs to solve the voltage control problem are determined. Then, a new LF calculation is carried out including the new set-points of DG reactive powers. At this stage, the corrected system voltages obtained by the LF study are plotted and the SSVCA stops. It can be noticed that, unlike the MSVCA, the SSVCA is an open-loop control system as there is no feedback on the corrected voltages. Consequently, in case of error in the VSA, it would not be possible anymore to bring back the system voltages within the permitted voltage range.

We suppose that l denotes index of the buses with the voltage drop issue and L gives the set of the buses with the voltage drop. In the voltage drop case, the needed voltage changes to bring back the violated voltages within the permitted lower limit are given by

$$\Delta V_l^{req} = 0.97 - V_l \quad l \in L \tag{2-41}$$

The voltage control problem of the SSVCA in the voltage drop state is formulated as the following optimization problem.

$$\textbf{Minimize: } OF = \sum_{x=1}^{N_G} \left| \Delta Q_{DGx}^{ind} - \Delta Q_{DGx}^{cap} \right| \tag{2-42}$$

$$\sum_{x=1}^{N_G} \left(\frac{\partial V_l}{\partial Q_{DGx}} (\Delta Q_{DGx}^{ind} - \Delta Q_{DGx}^{cap}) \right) \geq \Delta V_l^{req} \quad \forall l,\ l \in L \tag{2-43}$$

$$I_{brs} \leq I_{brs}^{\max} \quad \forall s,\ s \in C \tag{2-44}$$

$$\Delta Q_{DGx}^{\min} \leq \Delta Q_{DGx}^{ind} - \Delta Q_{DGx}^{cap} \leq \Delta Q_{DGx}^{\max} \quad \forall x,\ x \in G \tag{2-45}$$

$$\Delta Q_{DGx}^{ind}, \Delta Q_{DGx}^{cap} \geq 0 \quad \forall x,\ x \in G \tag{2-46}$$

where $\frac{\partial V_l}{\partial Q_{DGx}}$ is the voltage sensitivity at bus l with respect to the reactive power changes of DGx. It is worth noting that (2-43) is applied to all the buses with the voltage drop given in the set L. Inequality constraints (2-44) to (2-47) are similar to the ones introduced in the MSVCA. The abovementioned optimization problem is generally valid for the voltage control problem in the voltage rise condition with one exception that the constraint (2-43) should be updated in the latter case. In the voltage rise situation, the permitted upper voltage limit is chosen as the targeted point for the violated voltages. Therefore, equation (2-41) is rewritten considering the 1.03 pu voltage limit as

$$\Delta V_u^{req} = 1.03 - V_u \quad \forall u,\ u \in U \tag{2-47}$$

where u stands for the index of the buses with the voltage rise and set U includes all the buses with the voltage rise issue. Consequently, the voltage constraint of the above optimization problem in the voltage rise case is replaced by

$$\sum_{x=1}^{N_G} \frac{\partial V_u}{\partial Q_{DGx}} \left(\Delta Q_{DGx}^{ind} - \Delta Q_{DGx}^{cap} \right) \leq \Delta V_u^{req} \quad \forall u,\ u \in U \tag{2-48}$$

Therefore, the optimization problem of the SSVCA in the voltage rise case is composed of (2-42) as the objective function subject to the inequality constraints given in (2-48), (2-44), (2-45) and (2-46).

2.6. 33-bus test system

In order to test the effectiveness of the proposed voltage control algorithms, a 33-bus, 12.6 kV radial distribution system shown in figure 2-4 is considered. Network parameters regarding the load and line data are given in appendix 2 [62]. Total active and reactive powers of the system loads are 3.72 MW and 2.3 Mvar, respectively. The system under study also consists of 4 DG units, which are located at the buses 6, 12, 18 and 33. The DG units are DFIG-based type and identical with a maximum rated power equal to 1 MW. The capability curve of under study DG units is obtained from [7] and is linearized by the points given in table 2-1. It is approximated as a symmetrical curve. As it can be noticed from table 2-1, the maximum reactive power contribution of DGs is a function of its active power.

In the LF study, bus number 1 is considered as the slack bus and all other buses are load (PQ) buses. The load powers are considered to be voltage independent (i.e. power constant load model). DG active power is modelled as a negative load. The base voltage and power are equal to 12.66 kV and 1 MW. The upper and lower permitted voltage limits are 1.03 and 0.97 pu, respectively, for all the buses [59].

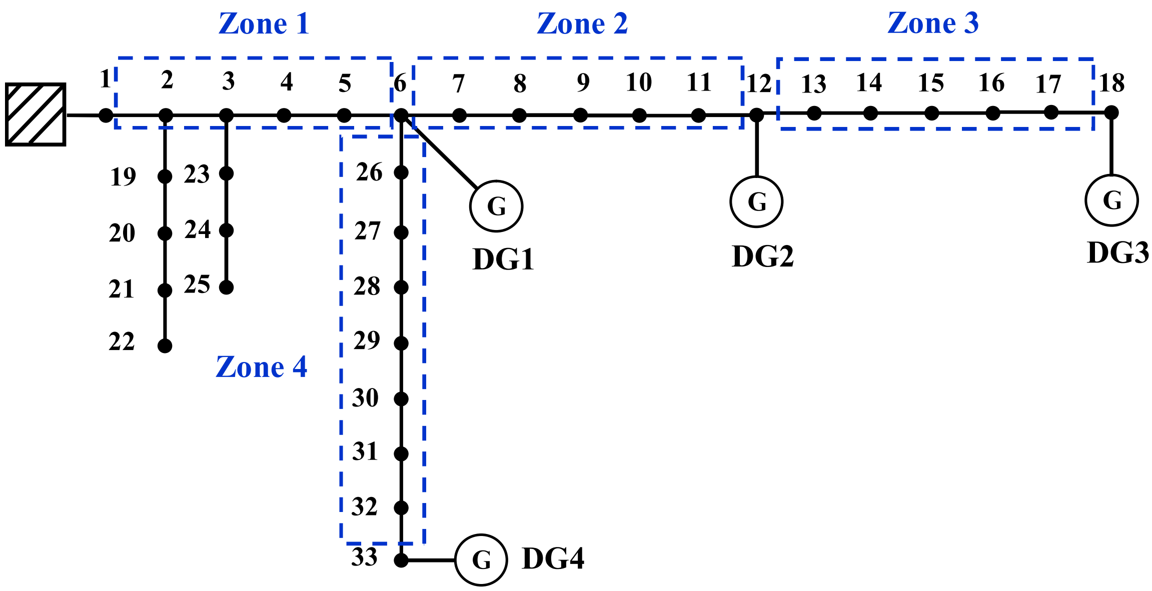

Figure 2-4: 33-bus radial distribution system

TABLE 2-1: POWER CAPABILITY CURVE OF DGS
(% IN DG RATED POWER)

Point	P_{DG}	$Q_{DG}^{max}/Q_{DG}^{min}$
1	0	± 95%
2	25%	± 95%
3	50%	± 90%
4	100%	± 60%

2.6.1. On the consideration of ampacity limits of the branches in the studied test system

As mentioned before, in the proposed VCAs, the branch current limits are not considered in all the system branches. The branches with the ampacity limits are chosen in an optimal manner such that with consideration of the minimum number of branches, we can monitor and control the currents in all the system branches. To do so, firstly, we divide the studied network into 4 zones as shown in figure 2-4. We suppose that the nominal ampacities of the branches located in each zone are identical. Also, the zonal branch limits decrease when moving from slack bus towards the end of feeders. Within such a network topology, in order to keep currents of all the branches in each zone with the predefined limit, it is enough to maintain the currents that enter to and exit from each zone within the predefined current limit of that zone. The idea is motivated by the fact that in the full-load-and-min-generation condition, the first branch of each zone has the smallest available ampacity among all branches of the zone since all the power of the zone enters to the first branch and then it reduces gradually towards the end of the zone. In the full-generation-and-min-load state, the branch that is located in the end of each zone has the lowest free ampacity as the power is flowing from DGs towards the slack bus. Note that there is no DG in the middle of the considered zones. Consequently, if the currents in the branches located in the beginning and ending points of each zone do not exceed the zone limit, currents of other branches placed at that zone will be within the predefined zone current limit. Considering the fact that there are 4 zones in the studied system, we need to take ampacity limits of 8 branches into account as listed in table 2-2.

TABLE 2-2: BRANCH CURRENT LIMITS

Branch	Between nodes	Zone	Rated ampacity (pu)
1	1-2	1	3.6
5	5-6	1	3.6
6	6-7	2	1.6
11	11-12	2	1.6
12	12-13	3	0.8
17	17-18	3	0.8
25	6-26	4	0.8
32	32-33	4	0.8

It is worth noting that the branches located between buses 3 to 25 and the ones between nodes 2 to 22 are not considered in the voltage control problem because the reactive power variations of DGs do not pass from these branches.

The reactive power variations in the selected branches due to reactive power changes of DGs are given by the following equation considering the directions in which DG powers flow.

$$\begin{bmatrix} \Delta Q_{br1} \\ \Delta Q_{br5} \\ \Delta Q_{br6} \\ \Delta Q_{br11} \\ \Delta Q_{br12} \\ \Delta Q_{br17} \\ \Delta Q_{br25} \\ \Delta Q_{br32} \end{bmatrix} = \begin{bmatrix} 1 & 1 & 1 & 1 \\ 1 & 1 & 1 & 1 \\ 0 & 1 & 1 & 0 \\ 0 & 1 & 1 & 0 \\ 0 & 0 & 1 & 0 \\ 0 & 0 & 1 & 0 \\ 0 & 0 & 0 & 1 \\ 0 & 0 & 0 & 1 \end{bmatrix} \begin{bmatrix} \Delta Q_{DG1} \\ \Delta Q_{DG2} \\ \Delta Q_{DG3} \\ \Delta Q_{DG4} \end{bmatrix} \tag{2-49}$$

In a matrix form, above equation is written as

$$\left[\mathbf{\Delta Q_{br}}\right] = \left[\mathbf{DGIB}\right]\left[\mathbf{\Delta Q_{DG}}\right] \tag{2-50}$$

The relations between DG injections and power flows in the selected branches are known through **DGIB** matrix. The latter can be constructed from the **BIBC** matrix in the DLF approach while the rows related to the selected branches and columns associated with the DG-connected buses are only kept and all other rows and columns of the **BIBC** matrix are deleted. Therefore, **DGIB** matrix has 8 rows and 4 columns as can be seen in (2-49). The maximum reactive power variations (towards inductive and capacitive directions) while keeping the branch limit in each of the selected branches are calculated using (2-27). Therefore, the following inequality constraint is introduced in the proposed VCAs in order to maintain the currents of the selected branches within the predefined limits when reactive powers of DGs change for the voltage regulation end.

$$\Delta Q_{brs}^{\max 1} \le \sum_{x=1}^{N_G} DGIB_{b,x} \Delta Q_{DGx} \le \Delta Q_{brs}^{\max 2} \quad \forall s, s \in C \tag{2-51}$$

where s is index for branches with the current limits ($s \in C$, $C = \{1, 5, 6, 11, 12, 17, 25, 32\}$) and b is an index equal to order of element s in set C. For instance, for s=5, b is equal to 2, as 5 is the second element of C. Considering (2-51), reactive powers of DGs are changed such that they create variations within the roots of (2-27) namely ΔQ_{brs}^{max1} and ΔQ_{brs}^{max2} in branch s. As a consequence, the current in the branch s is kept within its predefined ampacity. Replacing ΔQ_{DGx} with the two defined auxiliary variables, the above constraint is rewritten as

$$\Delta Q_{brs}^{\max 1} \le \sum_{x=1}^{N_G} DGIB_{b,x} (\Delta Q_{DGx}^{ind} - \Delta Q_{DGx}^{cap}) \le \Delta Q_{brs}^{\max 2} \quad \forall s, s \in C \tag{2-52}$$

Finally, in the MSVCA and SSVCA, the above constraint is introduced in order to take the current limits in all the selected branches into account when the reactive powers of DGs are changed.

2.7. Simulation results

The proposed VCAs in the single-step and multi-step forms are coded in the MATLAB environment. Effectiveness of the MSVCA and SSVCA is evaluated through the simulations carried out on the 33-bus test system shown in figure 2-4. Two working points corresponding to the full-load-and-min-generation and full-generation-and-min-load states are considered in order to test performance of the proposed VCAs in the voltage drop and rise conditions. The influence of considering ampacity limits of the system branches on the VCA results will be also investigated.

2.7.1. Case A: Working point corresponding to the full-load-and-min-generation situation

In the first studied working point, all the system loads are considered to be at 90% of their nominal values while DG active powers are at 15% of their rated values. The initial reactive powers of DGs are equal to zero. The main objective of this section is to test performance of the proposed VCAs in the voltage drop situation. According to the capability curve of DGs given in table 2-1, the maximum reactive power contribution of each DG in this working point is equal to ±95% of its rated power (= ±0.95 Mvar).

2.7.1.1. *Case A.1: Using multi-step voltage control algorithm when ampacity limits of the system branches are disregarded*

In the first studied case, the MSVCA is used to manage the voltage constraints when ampacity limits of the branches are not considered. As a result, the MSVCA can employ the most efficient DGs to return the system voltages inside the permitted voltage limits. In the studied working point, the worst voltage drop is found at bus 17 with voltage violation equal to -0.0315 pu from the 0.97 pu permitted voltage limit. Table 2-3 presents the demanded reactive power changes of DGs in order to remove the voltage violations. Figure 2-5 shows the initial system voltages as well as the ones obtained after voltage regulation by the MSVCA.

TABLE 2-3: REACTIVE POWER CHANGES OF DGS IN CASE A.1

	I=1	I=2	I=3
ΔV_w^{req} (pu) w	0.0315 17	0.0258 32	0.0028 30
ΔQ_{DG1} (Mvar)	0	0	-0.0278
ΔQ_{DG2} (Mvar)	0	0	-0.0278
ΔQ_{DG3} (Mvar)	-0.5282	0	-0.0167
ΔQ_{DG4} (Mvar)	0	-0.852	-0.098
OF Tot (Mvar)	1.5504		

In table 2-3, the negative values of ΔQ_{DG} mean reactive powers of DGs are changed towards the capacitive direction of the capability curve. Also, *OF Tot* gives the cumulative objective function of the MSVCA in all iterations. At I=1, the voltage control algorithm employs only DG3 (at bus 18) to manage the voltage drop at bus 17 because the sensitivity of voltage at bus 17 with respect to the reactive power change at bus 18 is the highest among all DGs. Also, as the available capacity of DG3 is enough to solve the voltage problem at bus 17 and the thermal limits of the branches are disregarded, DG3 is used alone.

At the second iteration (I=2), the MSVCA must solve the voltage drop at bus 32. DG4 which has the biggest effect on the voltage at bus 32 is used to this end. Finally, at I=3, the voltage drop at bus 30 is removed using the available reactive power changes of DG4 towards the capacitive direction (i.e. -0.95--0.852=-0.098 Mvar). Given that DG4 cannot solve this voltage violation alone, DG1, DG2 and DG3 are used as well. It is worth noting that according to the DSA, reactive power changes of DG1, DG2 and DG3 have the same impacts on the voltage at bus 30 ($\left|\frac{\partial V_{30}}{\partial Q_6}\right| = \left|\frac{\partial V_{30}}{\partial Q_{12}}\right| = \left|\frac{\partial V_{30}}{\partial Q_{18}}\right|$). Therefore, there is no change on the optimal objective function when using each of them. In figure 2-5, the blue dotted line shows the system voltages at the end of the iteration number 3 (I=3) when the MSVCA stops as all system voltages are returned to the predefined voltage limits. Also, hereafter, the red solid line on the 0.97 pu (or 1.03 pu) represents the permitted lower (or upper) voltage limit.

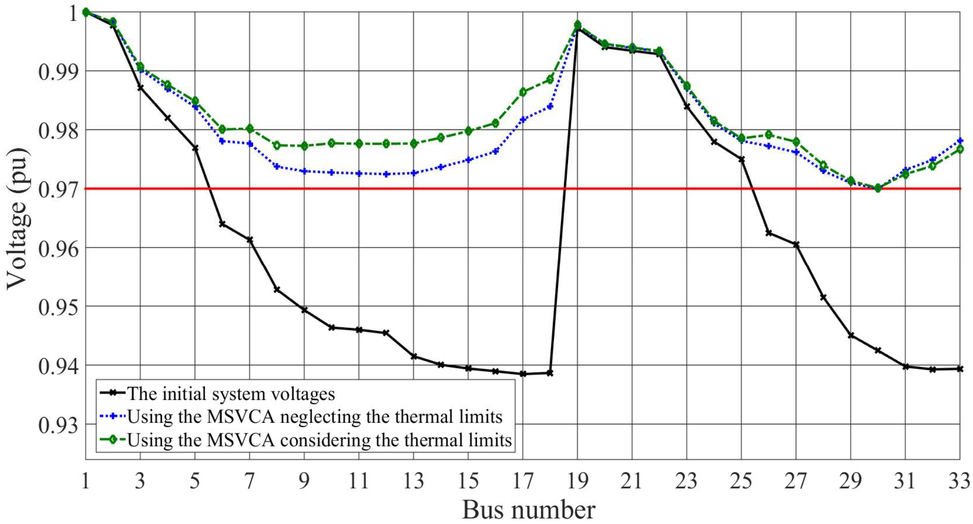

Figure 2-5: System voltages in cases A.1 and A.2 using the MSVCA

2.7.1.2. *Case A.2: Using the multi-step voltage control algorithm when ampacity limits of the system branches are considered*

Considering the same working point as the one of the case A.1, in the current test case, ampacity limits of the selected branches are added to the MSVCA. The objective is to evaluate impact of considering the ampacity limits of the system branches on the MSVCA performance. The corrected voltages obtained using the MSVCA while considering ampacity limits of the system branches are depicted in figure 2-5. Also, table 2-4 presents the reactive power changes of DGs demanded by the MSVCA.

TABLE 2-4: REACTIVE POWER CHANGES OF DGS IN CASE A.2

	I=1	I=2
ΔV_w^{req} (pu) w	0.0315 17	0.0098 30
ΔQ_{DG1} (Mvar)	0	-0.2492
ΔQ_{DG2} (Mvar)	0	-0.1854
ΔQ_{DG3} (Mvar)	-0.4456	-0.0836
ΔQ_{DG4} (Mvar)	-0.5698	-0.2396
OF Tot (Mvar)	1.7732	

In the considered working point for the full-load-and-min-generation condition, the current of the branch 25 has exceeded the permitted 0.8 pu limit of the zone 4. Therefore, in the first iteration, in addition to managing the voltage drop at bus 17 (i.e. the one with the worst voltage drop), the current violation in the branch 25 should be removed as well. Given that the initial current of the branch 25 is bigger than the maximal branch current, $\underline{I}_{br25}^{init}$ is placed outside of the circle of the maximal current shown in figure 2-2. As a consequence, the roots of (2-27) are both negative values meaning that the capacitive reactive power changes are needed to return the current of the branch 25 within its ampacity limit. In I=1, in branch 25, the reactive power changes between -0.5698 and -1.2239 Mvar can return the current of that branch within the 0.8

pu predefined zone limit. These values are found through solving (2-27). Since the reactive power of branch 25 varies by ΔQ_{DG4}, in order to satisfy the constraint regarding the branch 25, DG4 is used only. On the other hand, DG4 does not have a high impact on the voltage at bus 17, and to manage the voltage drop at bus 17, reactive power changes of DG3 are preferred (rather than ΔQ_{DG4}). Consequently, in I=1, to satisfy the constraint regarding the branch 25, ΔQ_{DG4} is changed by -0.5698 Mvar (the root with smaller absolute value) and to remove the voltage constraint at bus 17, ΔQ_{DG3} is modified by -0.4456 Mvar.

In I=2, bus number 30 has the worst voltage violation. DG4 which has the biggest impact on the voltage at bus 30 is employed by the MSVCA up to the limit defined by the ampacity limit of the branch 32. The latter is capable of transferring reactive powers between -0.2396 to 1.35 Mvar from DG4 while keeping the 0.8 pu predefined limit of the zone 4. Given that the capacitive reactive power changes are needed to solve the voltage drop at bus 30, ΔQ_{DG4} is set to -0.2396 Mvar. The rest of needed reactive power changes to remove the voltage violation at bus 30 is provided by the contribution of other DGs. Figure 2-6 shows the initial branch currents as well as the ones obtained after each iteration of the MSVCA using the LF calculations.

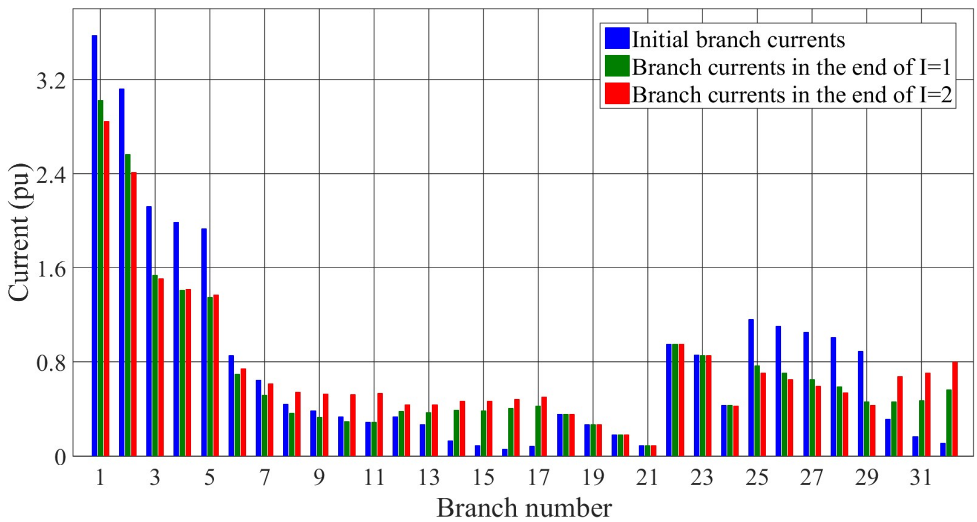

Figure 2-6: The branch currents along the voltage regulation procedure by the MSVCA

As it can be seen in figure 2-6, the initial current violation in the branch 25 has been removed when reactive power changes of I=1 are applied. In addition, the reactive power changes of I=2 do not cause violation of the ampacity limits in the selected branches. More importantly, it is observed that the currents of all branches located in zones 1 to 4 are within the predefined limits which verifies the efficiency of the proposed idea to consider only the ampacity limits in the first and last branches of each zone. The accuracy of the proposed method to calculate the maximal reactive power changes of DGs while keeping the branch ampacity limits can be found in figure 2-6. As it can be seen, in the end of I=1, the current of the branch 25 is smaller than 0.8 pu. Its exact value equals to 0.767 pu which means that the proposed formulation leads to an error equal to 0.8-0.767=0.033 pu. Also, in the end of I=2, the current in the branch 32 reaches 0.798 pu (instead of 0.8 pu) which means that an error of 0.002 pu is arisen from the proposed formulation.

Taking into account figures 2-5 and 2-6, it is verified that the proposed MSVCA not only manages the voltage constraints while keeping the branch ampacity limits, but it also removes the initial branch overloads. Furthermore, considering the results given in tables 2-3 and 2-4, it is noticed that when ampacity limits of the branches are considered, a higher global reactive power changes are needed to solve the same voltage control problem (i.e. 1.7732 Mvar compared to 1.5504 Mvar in case A.1). It is explained by the fact that when ampacity limits are considered, it is not possible to use the most efficient DGs with their maximum available reactive powers (defined by the capability curve) because extra limits on DG reactive powers relating to the branch limits must be taken into account as well. Consequently, beside the efficient DGs (which have high impacts on the violated voltages), it is needed to utilize also DGs at buses which have smaller voltage sensitivity with respect to reactive power changes. Finally, it leads to an increase of the total needed reactive power changes for the voltage regulation purpose.

2.7.1.3. *Case A.3: Using the single-step voltage control algorithm when ampacity limits of the system branches are disregarded*

The SSVCA performance is tested here to manage the voltage constraints of the same working point while ampacity limits of the branches are neglected. As introduced before, the SSVCA finds the optimal combination of DG reactive power changes in order to return simultaneously all the violated voltages inside the permitted voltage range. Table 2-5 presents the reactive power changes of DGs demanded by the SSVCA to manage the voltage constraints.

TABLE 2-5: REACTIVE POWER CHANGES OF DGS IN CASE A.3

ΔQ_{DG1} (Mvar)	-0.1322
ΔQ_{DG2} (Mvar)	-0.2388
ΔQ_{DG3} (Mvar)	-0.397
ΔQ_{DG4} (Mvar)	-0.95
OF (Mvar)	1.7181

In the SSVCA, there will be one inequality constraint per each of the buses with the voltage violation. In the voltage drop state, set L includes all the buses with the voltage drop issue. Cardinality of set L gives the number of the voltage constraints that exist in the SSVCA. In order to remove the initial voltage violations, all these voltage constraints must be satisfied simultaneously. However, all the voltage constraints will not be of the binding type. By definition, in an optimization problem, a constraint is binding if there is no difference between its RHS and LHS in the optimal point [61]. Therefore, if we change its RHS, the objective function of the optimal point will be affected. Thus, it can be concluded that in the optimal point, a binding constraint is satisfied while other constraints (non-binding ones) have been satisfied with less control effort. Consequently, non-binding constraints are the ones that do not impose an increase or decrease of the objective function in the optimal point. Considering the above definition, in the SSVCA context, ‘‘all the voltage constraints are not of the binding type’’ means that there will be one constraint (or more) relating to the binding constraint that needs to be certainly satisfied, and if so, other voltage constraints (non-binding ones) are managed too.

In the considered working point, bus 30 constructs the binding voltage constraint. When the LHS of the voltage constraint relating to bus 30 is equal to its RHS, voltage at bus 30 reaches the targeted point (i.e. 0.97 pu) and all other violated voltages are returned inside the permitted voltage range (having voltage values bigger than 0.97 pu). It should be noted that bus 30 constructs the binding constraint although bus 17 has the worst initial voltage violation. Therefore, the binding constraint does not necessarily belong to the bus with the biggest voltage violation, but it corresponds to the one that demands more control effort to have the LHS equal to the RHS. In fact, voltage drop at bus 17 (the worst voltage violation) does not create binding constraint as the voltage violation at bus 17 can be solved easily by action of DG3. It is mentioned before that reactive power change of DG3 has high impact on the voltage at bus 17. On the contrary, in order to manage the voltage drop at bus 30, reactive power change equal to -0.95 Mvar from DG4 is not sufficient, thus, contribution of other DGs is needed as well, as it can be seen in table 2-5.

Figure 2-7 shows the initial and corrected voltages obtained using the SSVCA. It is seen that after voltage regulation, voltage at bus 30 reaches almost 0.97 pu and all other violated voltages are returned inside the permitted voltage range. It is worth mentioning that the distance between the corrected voltage at bus 30 (i.e. 0.9715 pu) and the 0.97 pu voltage limit represents the error arisen from the linearization of the voltage and reactive power relationships using the DSA method.

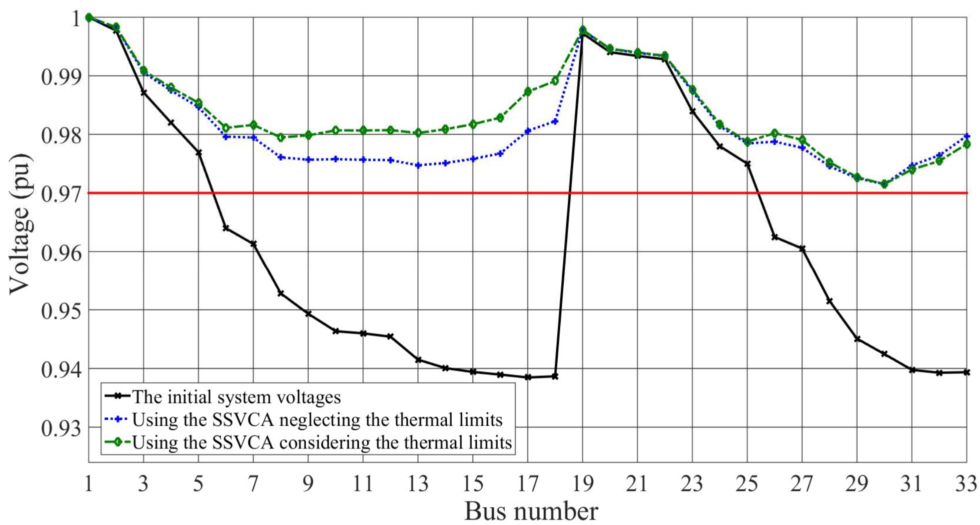

Figure 2-7: System voltages in cases A.3 and A.4 using the SSVCA

2.7.1.4. *Case A.4: Using the single-step voltage control algorithm when ampacity limits of the system branches are considered*

Considering the ampacity limits of the selected branches, the SSVCA is used here in order to manage the voltage control problem of the same working point as before. In case A.2, it was shown that in addition to the existing voltage violations, the initial current in the branch 25 is over its ampacity limit. Therefore, the reactive power modifications of DGs must at once remove the voltage drop of the buses, and return the current in the branch 25 within its ampacity limit while maintaining the currents in all other branches within the predefined limits. Table 2-6 gives the reactive power changes of DGs to this end.

TABLE 2-6: REACTIVE POWER CHANGES OF DGS IN CASE A.4

ΔQ_{DG1} (Mvar)	-0.2618
ΔQ_{DG2} (Mvar)	-0.3509
ΔQ_{DG3} (Mvar)	-0.4520
ΔQ_{DG4} (Mvar)	-0.8334
OF (Mvar)	1.8981

Similarly to case A.2, in order to return the current in branch 25 within its ampacity limit, we need to change reactive power of the branch 25 between -0.5698 to -1.2239 Mvar. In addition, the branch 32 is capable of transferring reactive power changes between the range of -0.8334 to 0.7536 Mvar. The reactive powers of both branches 25 and 32 are only influenced by ΔQ_{DG4}. Given that bus 30 creates the binding voltage constraint and due to the fact that DG4 has the highest impact on the voltage at bus 30, the optimal solution of the SSVCA optimization problem will be to use DG4 with its maximum possible contribution defined by the branch 32 (i.e. -0.8334 Mvar). In this way, the initial violation of the current in branch 25 will be solved too as ΔQ_{DG4}=-0.8334 Mvar is within the range -0.5698 to -1.2239 Mvar. The contribution of other DGs is needed to fully solve the voltage control problem of bus 30. Therefore, in the optimization problem of the SSVCA, the voltage constraint at bus 30 and the current limit in the branch 32 create the binding constraints. As it can be seen in figure 2-7, the corrected voltages do not exceed the permitted voltage range. Also, the voltage at bus 30 is the closest one to the 0.97 pu voltage limit since it was the binding voltage constraint. The difference between the corrected voltage at bus 30 and the 0.97 pu limit shows the error associated with the DSA method. Figure 2-8 depicts the initial branch currents as well as the ones obtained after the SSVCA action.

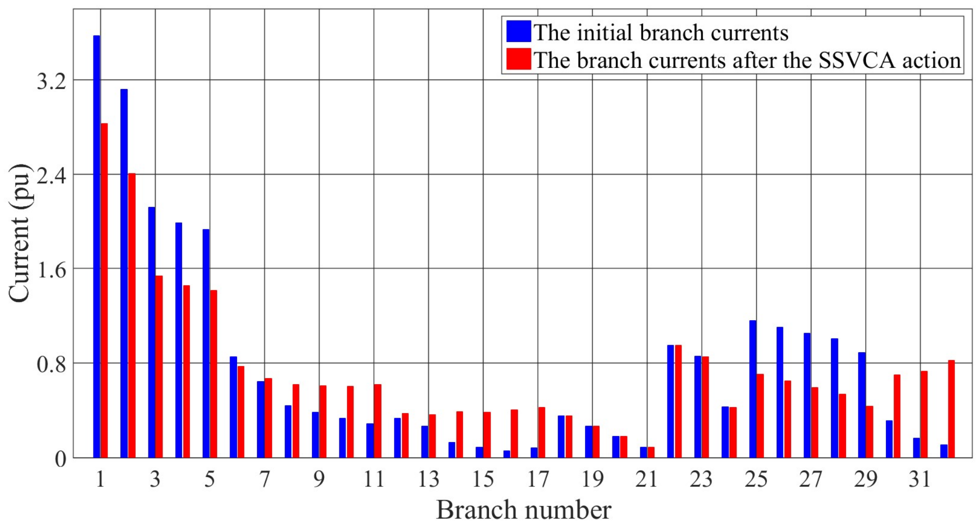

Figure 2-8: The branch currents along the voltage regulation procedure by the SSVCA

As it can be seen in figure 2-8, after the SSVCA action, the initial violation of the current in branch 25 has been removed by reactive power changes of DG4. It can be noticed also that all the branches located in the 4 predefined zones have the currents smaller than their rated ampacity limit except the branch 32. As mentioned before, the latter is one of the binding constraints of the optimization problem. Therefore, the RHS and LHS of that constraint are equal in the optimal solution. This means that the current in the branch 32 must reach 0.8 pu after the SSVCA action. The difference between the real current in the branch 32 (i.e. 0.82 pu) and the 0.8 ampacity limit occurs due to simplification of the relations between branch currents and DG reactive powers in the proposed formulation for considering ampacity limits. As a result, an error equal to 0.02 pu is found in the corrected current of the branch 32.

Comparing results given in tables 2-5 and 2-6, it is observed that in the SSVCA when the branch limits are neglected, total OF equals to 1.7181 Mvar while by considering the ampacity limits, the needed reactive power changes of DGs increase to 1.8981 Mvar.

2.7.2. Case B: Working point corresponding to the full-generation-and-min-load situation

In the second studied working point, load powers and DG active power productions are considered to be at 20% and 70% of their respective rated values while the initial reactive powers of DGs are set to zero. The objective of this section is to examine performance of the MSVCA and SSVCA in the voltage rise condition. According to the capability curve of DGs, the available reactive power changes of DGs are equal to ±0.78 Mvar.

2.7.2.1. Case B.1: Using the multi-step voltage control algorithm when ampacity limits of the system branches are disregarded

In the first test case of the studied working point for the voltage rise state, the MSVCA is used to return the existing voltage violations inside the permitted voltage range. Table 2-7 presents the reactive power changes of DG units to this end. The ampacity limits of the branches are not considered here.

TABLE 2-7: REACTIVE POWER CHANGES OF DGS IN CASE B.1

	I=1	I=2	I=3
ΔV_w^{req} (pu) w	- 0.0460 18	- 0.0033 12	-7.28×10^{-4} 33
ΔQ_{DG1} (Mvar)	0	0	0
ΔQ_{DG2} (Mvar)	0	0.054	0
ΔQ_{DG3} (Mvar)	0.7265	0.0535	0
ΔQ_{DG4} (Mvar)	0	0	0.0217
OF Tot (Mvar)	0.8557		

In the first iteration, the biggest voltage rise is found at bus 18. DG3 which has the biggest effect on the voltage at bus 18 is used to remove that voltage violation. As the ampacity limits of the branches are neglected, DG3 can provide the needed reactive power up to its maximum available reactive power (i.e. 0.78 Mvar). The voltage rise problem at bus 18 is solved by changing reactive power of DG3 by 0.7265 Mvar towards the inductive direction. Then, at I=2, the new bus with the biggest voltage rise (i.e. bus 12) forms a new optimization problem subject to the updated available reactive powers of DGs. Given that DG2 and DG3 have an identical impact on the voltage at bus 12 according to the DSA method, they are both involved in the voltage regulation of bus 12. It should be noted that in I=2, available reactive power change for DG3 is equal to 0.78-0.7265=0.0535 Mvar. Finally, in I=3, the voltage rise problem at bus 33 is solved using DG4 as it has the highest influence on that bus. Figure 2-9 shows the initial voltages as well as the ones obtained after the corrective action of the MSVCA.

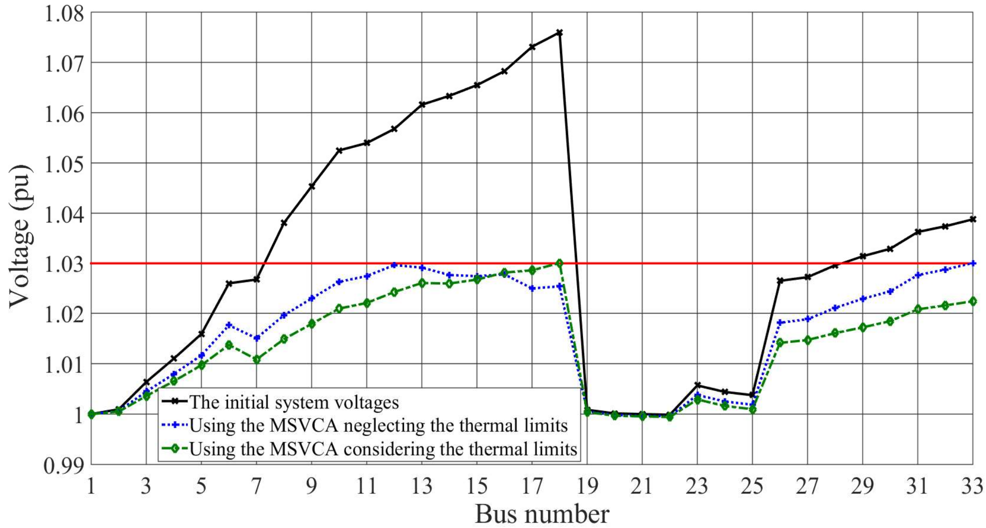

Figure 2-9 System voltages in cases B.1 and B.2 using the MSVCA

In figure 2-9, it is seen that the violated voltages are efficiently brought back to the permitted voltage range using the MSVCA.

2.7.2.2. *Case B.2: Using the multi-step voltage control algorithm when ampacity limits of the system branches are considered*

The MSVCA performance is tested here on the same working point as that of the previous case. However, unlike the case B.1, the ampacity limits of the branches have been also taken into account here. As a result, new constraints are added to the optimization problem of the MSVCA. If there is any binding constraint relating to the ampacity limits of the branches, the optimal point of the MSVCA will be changed with respect to that of the B.1. Table 2-8 presents the reactive power changes of DGs in order to manage the existing voltage violations while keeping the ampacity limits of the branches.

TABLE 2-8: REACTIVE POWER CHANGES OF DGS IN CASE B.2

	I=1
ΔV_w^{req} (pu) w	- 0.0460 18
ΔQ_{DG1} (Mvar)	0.2354
ΔQ_{DG2} (Mvar)	0.4866
ΔQ_{DG3} (Mvar)	0.4388
ΔQ_{DG4} (Mvar)	0.1463
OF (Mvar)	1.307

Although the MSVCA is used, within one iteration, all the voltage violations are removed. Therefore, there is no need to go to the second iteration. In the optimization problem of I=1, there is one constraint regarding the voltage violation at bus 18 and there are 8 constraints relating to ampacity limits of the selected branches. The voltage constraint of bus 18 is certainly a binding one as it is the only voltage constraint of the optimization problem. Reactive power change of DG3 has the highest impact on the voltage of bus 18. Therefore, DG3 is used up to the limit defined by the ampacity of the branch 17 (i.e. 0.8 pu). The latter is capable of transferring reactive powers between the range of -0.5429 to 0.4388 Mvar. The inductive reactive power is needed to remove the voltage rise of bus 18, thus, ΔQ_{DG3} is set to 0.4388 Mvar. However, this is not enough to remove the voltage violation of bus 18. The next DG with the biggest impact on bus 18 is DG2. Utilization of DG2 is restricted by the ampacity limit of the branch 11. Reactive power of branch 11 can change within the range of -1.1631 to 0.9254 Mvar while maintaining its ampacity limit (=1.6 pu). Considering the fact that ΔQ_{DG3}=0.4388 Mvar will be also passed through the branch 11, DG2 changes by 0.9254-0.4388=0.4866 Mvar to not violate the ampacity limit of the branch 11. Finally, DG1 and DG4 are contributed to provide the rest of needed reactive power changes for solving voltage rise of bus 18. As known, DG1 and DG4 have an identical impact on the voltage of bus 18 on the basis of the DSA data. Figure 2-10 depicts the initial branch currents as well as the ones obtained after the MSVCA action using the LF calculation.

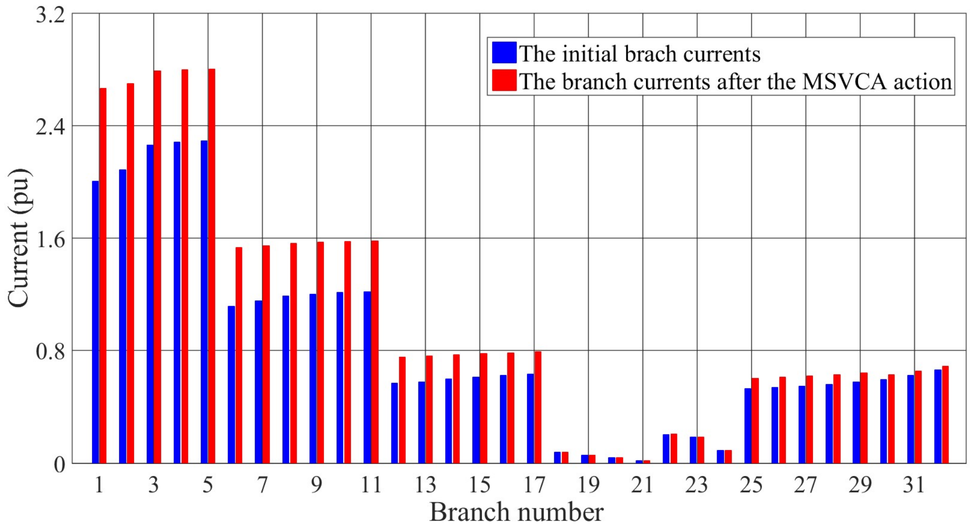

Figure 2-10: The branch currents along the voltage regulation procedure by the MSVCA

As it can be seen in figure 2-10, the reactive power changes of DGs do not violate the ampacity limits of all branches in 4 defined zones. In the optimization problem, constraints relating to the branches 11 and 17 are the binding ones. The error arisen from the proposed formulation for considering the branch limits can be evaluated in these two branches. After the MSVCA action, currents in branches 11 and 17 reach 1.58 pu and 0.792 pu, respectively. Considering the rated ampacities of 1.6 pu and 0.8 pu for these branches, errors equal to 0.02 pu and 0.008 pu are found in branches 11 and 17, respectively.

Comparing the results given in tables 2-7 and 2-8, it can be noticed that when ampacity limits of the branches are considered, the objective function of the MSVCA increases by 0.4513 Mvar compared to case B.1 (which neglects the branch limits). As mentioned before, it is justified by the fact that in presence of the branch limits, we cannot fully employ the DGs with the highest impacts on the violated voltages.

2.7.2.3. Case B.3: Using the single-step voltage control algorithm when ampacity limits of the system branches are disregarded

In this case study, the biggest voltage rise is found at bus 18, but voltage violations at buses 12 and 33 construct the binding constraints of the SSVCA. Given that the biggest voltage violations happened in the buses ending at the bus 18, DG3 is employed to satisfy those voltage constraints. It is worth noting that DG3 and DG2 have the same impacts on the voltage at bus 12, while the former has bigger impacts on buses ending at bus 18. Consequently, DG3 is preferred to DG2. In addition, DG4 is used to remove the voltage violations of nodes 29 to 33. Table 2-9 presents the reactive power changes of DG units in order to manage the system voltages using the SSVCA. Figure 2-11 shows the initial node voltages and the ones obtained after reactive power control of DGs using the SSVCA. As it can be seen, corrected voltages of buses 12 and 33 reach (almost) the 1.03 pu voltage limit and all other violated voltages are returned inside the permitted voltage range. The error arisen from the DSA method in the voltage control procedure can be found in figure 2-11 which is equal to the difference between the 1.03 pu voltage limit and the corrected voltages of buses 12 and 33.

TABLE 2-9: REACTIVE POWER CHANGES OF DGS IN CASE B.3

ΔQ_{DG1} (Mvar)	0
ΔQ_{DG2} (Mvar)	0.1401
ΔQ_{DG3} (Mvar)	0.722
ΔQ_{DG4} (Mvar)	0.0395
OF (Mvar)	0.9016

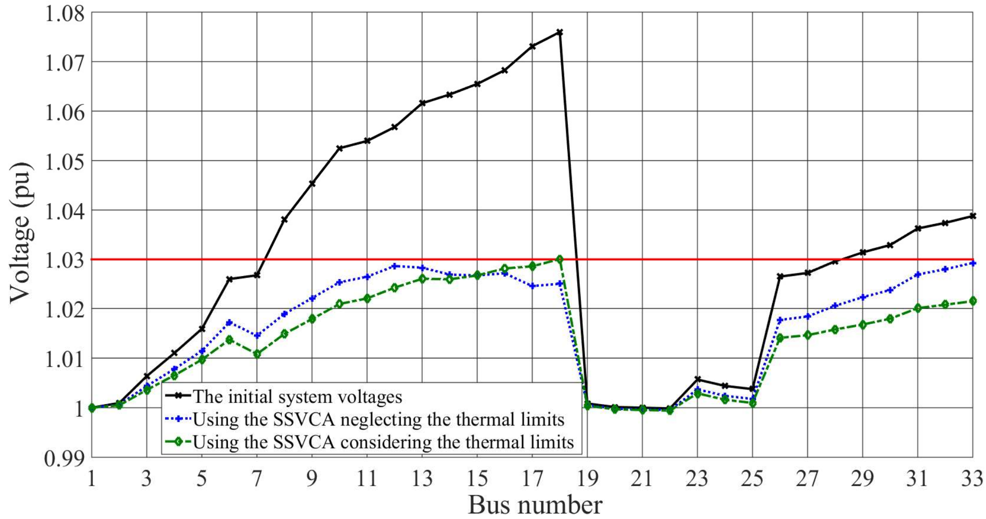

Figure 2-11: System voltages in cases B.3 and B.4 using the SSVCA

2.7.2.4. Case B.4: Using the single-step voltage control algorithm when ampacity limits of the system branches are considered

Finally, in the last case study of this chapter, the SSVCA manages the voltage rise issue of the considered working point while maintaining the ampacity limits of the branches. Similarly to the case B.2, the constraints relating to branches 11 and 17 are binding ones in the optimization problem. As a result, the power changes of DG2 and DG3 are limited to 0.4866 Mvar and 0.4388 Mvar, respectively, like case B.2. Given that branch 17 is capable of transferring maximum 0.4388 Mvar reactive power change from DG3, voltage constraint at bus 18 (having the biggest voltage violation) becomes the binding voltage constraint. In order to satisfy the voltage constraint at bus 18, as the first priority, reactive power of DG3 is changed according to the free capability of branch 17 (=0.4388 Mvar). Then, ΔQ_{DG2}=0.4866 Mvar (which is equal to the maximum reactive power variation of branch 11 while keeping its branch ampacity limit) is applied. Given that contributions of DG2 and DG3 are not sufficient, DG1 and DG4 are also employed in the SSVCA. Table 2-10 presents the reactive power changes of DG units demanded by the SSVCA in order to manage the node voltages considering the ampacity limits of the branches. Figure 2-12 shows the initial branch currents in the considered working point and the branch currents when the SSVCA action is completed.

TABLE 2-10: REACTIVE POWER CHANGES OF DGS IN CASE B.4

ΔQ_{DG1} (Mvar)	0.2169
ΔQ_{DG2} (Mvar)	0.4866
ΔQ_{DG3} (Mvar)	0.4388
ΔQ_{DG4} (Mvar)	0.1648
OF (Mvar)	1.307

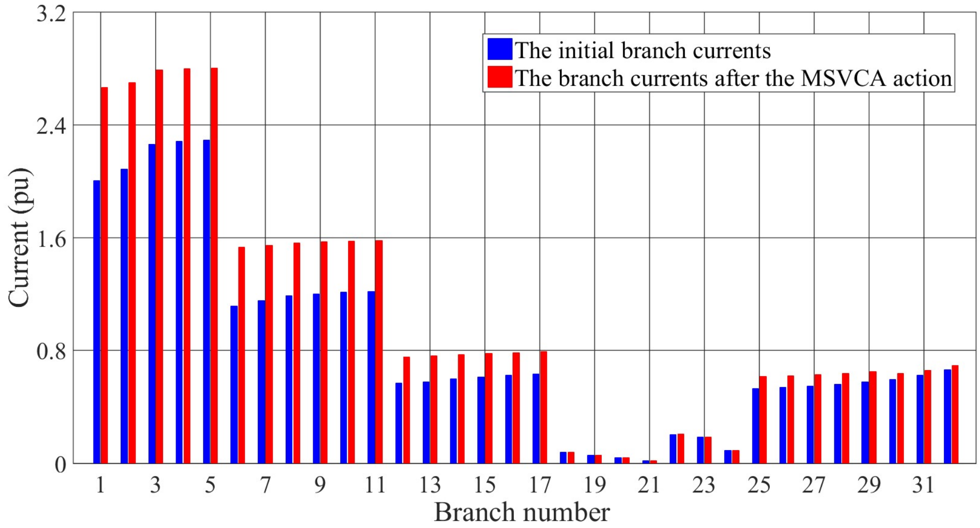

Figure 2-12: The branch currents along the voltage regulation procedure by the SSVCA

In figure 2-12, it is seen that the branch currents do not exceed the permitted defined limit of their own zone when reactive powers of DGs are changed by the SSVCA for the voltage regulation purpose. The constraints belonging to the branches 11 and 17 are the binding ones in the optimization problem. Therefore, after the SSVCA action, currents in branches 11 and 17 reach almost 0.8 and 1.6, respectively, which are the rated ampacity of these branches. The differences between the corrected currents of branches 11 and 17 with their associated ampacity limits give the error arisen from the proposed method for consideration of the branch ampacity limits.

As reported in tables 2-9 and 2-10, objective function of the SSVCA in the case of neglecting the branch ampacity limits is equal to 0.9016 Mvar while by adding the branch constraints, it increases to 1.307 Mvar.

2.8. Discussion on the results

The proposed DSA method has been developed on the basis of an assumption which considers that the voltage variation vector relating to two adjacent buses is equal to the real part of that vector given that the voltage angles are expected to be small in the distribution systems with the high R/X ratio. The error arisen from this assumption in the voltage control procedure can be evaluated in the simulated test cases of this chapter. When there is no error associating with the VSA method, corrected voltage of the binding voltage constraint reaches the 0.97 or 1.03 pu voltage limit (i.e. the targeted point). Consequently, the difference between the permitted voltage limit and the corrected voltage at bus relating to the binding voltage constraint shows the error caused by the DSA method. In the studied test cases, the maximum error between the corrected voltage obtained by the LF study and the permitted voltage bound is found in cases A.3 and A.4 equal to 0.0015 pu. As it can be seen in figure 2-7, after the SSVCA action, the voltage at bus 30 (which created the binding voltage constraint) reaches 0.9715 pu instead of 0.97 pu. Considering the base voltage of 12.66 kV in the studied network, when converting into the real values, this error equals to 18.9 V, which is not considerable.

Furthermore, in the proposed formulation for inclusion of the branch ampacity limits, it is assumed that the reactive power changes of DGs will affect only the imaginary parts of the branch currents while the real parts of the branch currents remain constant. This is true when considering the branch current of a simple 2-bus system. However, in the larger-scale distribution systems, this assumption does not hold anymore. As a consequence, an error is found in the branch currents when using the proposed formulation. The simulation results confirm that as the system voltages are nearly close to 1 pu and the voltage angles are small, the error associated with the proposed formulation is within the reasonable values. In all studied test cases of this chapter, the error between the new branch current (obtained by the LF calculation considering DG reactive power changes) relating to the binding constraint and the predefined branch ampacity limit never exceeds 0.033 pu. Converting into the real values, this error equals to 1.5 A.

The SSVCA aims at returning all the violated voltages inside the permitted voltage range at once. As a consequence, the initial working point of system may be moved largely towards the new (corrected) point. Therefore, in the SSVCA, error due to using the simplified relations of voltages and currents with respect to reactive power changes of DGs is increased compared to that in the MSVCA. Consequently, it is seen that the SSVCA asks a bigger value of reactive power changes for solving the same problem in comparison with the MSVCA. For instance, considering the simulation results of cases A.1 and A.3 for multi-step and single-step formulations (given in tables 2-3 and 2-5), it is seen that for the same working point while the ampacity limits are neglected in both cases, the SSVCA demands a higher global reactive power changes. Similar results are found when considering results of cases A.2 and A.4 or B.1 and B.3.

Inside the MSVCA and SSVCA, the LF calculation is carried out on the basis of an iterative procedure. According to [63], convergence of the DLF approach on the studied 33-bus system is guaranteed when all line resistances are multiplied by the coefficients as big as 4.3. In general, when the input data of the DLF program are within the acceptable magnitudes, its convergence is guaranteed. Given that in this work, reactive power limitations of DGs are taken into account, the solution of the optimization problem will not demand unrealistic values of reactive power changes that can cause divergence of the DLF program. Consequently, convergence of the proposed VCAs is guaranteed when there are sufficient available reactive powers in DGs and enough free ampacities in the branches connected to DGs.

In the end, it should be stated that the proposed sensitivity-based voltage control approach has very short execution time. In all studied cases of this chapter, the calculation time of the SSVCA and MSVCA does not exceed 0.2 s using an ordinary desktop computer (processor core i5, CPU 3.1 GHz, RAM 8 GB). The notable speed of the proposed VCAs comes from the fact that the DLF method is developed for the distribution systems and it does not need the time-consuming procedure of the classical LF approaches. More importantly, thanks to information provided by the sensitivity analyses, the LF program is not embedded in the optimization problem of the VCAs and only effects of the control variables (i.e. reactive power changes of DGs) on node voltages and branch currents are employed in the optimization part. Therefore, number of the equality and inequality constraints as well as decision variables reduces noticeably compared to the ones in the VCA according to the OPF formulation. In the studied 33-bus test system, an OPF formulation consists of two non-linear equality constraints per each node associating with the balance of nodal active and reactive powers, beside one non-linear inequality constraint per each node relating to the voltage limit and one non-linear inequality constraint per each branch linking to the branch ampacity limit. In contrast, in the MSVCA, there is one voltage constraint regarding the worst voltage violation and 8 constraints for the branch limits in 4 considered zones which are all of the linear type. Similarly, in the SSVCA, there are 8 linear inequality constraints for the branch limits and $[L]$ or $[U]$ linear inequality constraints regarding the voltage violated buses in the voltage drop or rise state, where $[L]$ and $[U]$ denote the cardinality of sets L and U.

2.9. Conclusion

In this chapter, a novel VSA method has been proposed that defines the dependencies between the system voltages and nodal powers on the basis of the topology of the network. Moreover, a new formulation has been introduced to determine the maximum reactive power changes of the branches while maintaining the branch currents within their predefined limits. Then, a sensitivity-based voltage control approach has been developed to manage the voltage and current violations using the reactive power control of DGs. Simulation results reveal that the proposed VCAs are capable of keeping the system voltages and currents within their predefined limits. Moreover, fast execution speed of the sensitivity-based voltage control approach makes it suitable for the on-line management of the voltage and current in the MV distribution systems. Furthermore, simulation results confirm that the proposed sensitivity analysis formulations with a reasonable accuracy can estimate the node voltages and branch currents when reactive powers of DGs are modified by the VCA.

In addition, based on the simulation results, it is concluded that consideration of ampacity limits of the system branches can lead to an important increase of the total needed reactive powers of DGs. It happens when there is not enough free ampacity in the branches connected to DGs. In this case, it will not be possible to use the most efficient DGs with their maximum available reactive powers defined by their capability curves. Consequently, it is needed to use DGs with smaller effects on the violated voltages, which results in increasing total needed reactive power changes for the voltage regulation purpose.

In the next chapter, we go one step further and we consider that in addition to the reactive power control, active power curtailment of DGs can be employed in the VCAs. A 77-bus 11 kV radial distribution system with 8 feeders, which accommodates 22 DG units is used to test performance of the proposed SSVCA and MSVCA.

2.10. Chapter publication

This chapter has led to the following publications:

- B. Bakhshideh Zad, H. Hasanvand, J. Lobry and F. Vallée, "Optimal reactive power control of DGs for voltage regulation of MV distribution systems using sensitivity analysis method and PSO algorithm," *International Journal of Electric Power and Energy Systems*, vol. 68, pp. 52-60, 2015.

- B. Bakhshideh Zad, J. Lobry, F. Vallée and H. Hasanvand, "Optimal reactive power control of DGs for voltage regulation of MV distribution systems considering thermal limit of the system branches," *International Conference on Power System Technology (POWERCON)*, China, 2014.

Chapter 3: Optimal control of DG active and reactive powers for managing the voltage constraints

3.1. Abstract

The functionality of the SSVCA and MSVCA presented in chapter 2 is evolved here by adding the possibility of curtailing the active powers of DGs beside the reactive power control of DGs. Therefore, the proposed VCAs of this chapter can modify both active and reactive powers of DG units in order to bring back the violated voltages within the permitted voltage range while keeping the ampacity limits of the system branches. The voltage control problem is formulated as a linear optimization problem using the sensitivity analysis. The DSA method developed in chapter 2 is utilized to define the linearized relationships between the system voltages and nodal active and reactive powers. Also, ampacity limits of the branches are taken into account using the method introduced in chapter 2. The proposed VCA in the single-step or multi-step form distinguishes between the cheap and expensive control actions using the defined weighting coefficients in the objective function of the optimization problem. The numerical validation of the proposed VCAs is carried out on the 77-bus 11 kV radial distribution system that hosts 22 DG units. The effectiveness of the SSVCA and MSVCA in the voltage management of the aforementioned network is tested considering different values for the weighting coefficients of active and reactive powers.

3.2. Sensitivity-based voltage control approach managing DG active and reactive powers

The proposed voltage control approach of this chapter relies on the linear approximation of the relations between the system voltages and the control variables (namely active and reactive power changes of DGs) provided by the VSA. Therefore, similarly to the VCAs presented in the previous chapter, the LF-related constraints will not be considered in the optimization problem of the VCA given that the effects of control variables on node voltages are known through the DSA method. The MSVCA and SSVCA are adapted as follows in order to consider active power curtailment of DGs beside the reactive power control of DGs.

3.2.1. Multi-step voltage control algorithm

The MSVCA developed in this chapter has the same structure as the one presented in chapter 2 (section 2.5.1). The only difference is that the active power curtailment is also involved here in the voltage management procedure. As mentioned before, the MSVCA starts with running an initial LF calculation. If the voltage violations are found in the system, the main loop of the MSVCA starts with I=1. Then, the bus with the biggest voltage violation is selected. The voltage violation of that bus from the permitted voltage limit is calculated. It gives us the required value of voltage modification (ΔV_w^{req}) in order to return the voltage of the worst bus (bus w) inside the permitted voltage range. Voltage control problem of the MSVCA at I=1 is formulated as an optimization problem which aims at minimizing the total weighted changes of active and reactive powers of DGs subject to the voltage constraint of the bus with the biggest voltage violation as well as the branch ampacity limits and bounds on DG powers. The optimization problem of the MSVCA corresponding to the voltage rise state is given as follows.

$$\textbf{Minimize: } OF = \sum_{x=1}^{N_G} \left(C_Q \left| \Delta Q_{DGx}^{ind} - \Delta Q_{DGx}^{cap} \right| + C_P \Delta P_{DGx} \right) \tag{3-1}$$

$$\sum_{x=1}^{N_G} \left(\frac{\partial V_w}{\partial Q_{DGx}} (\Delta Q_{DGx}^{ind} - \Delta Q_{DGx}^{cap}) + \frac{\partial V_w}{\partial P_{DGx}} \Delta P_{DGx} \right) \le \Delta V_w^{req} \tag{3-2}$$

$$I_{brs} \le I_{brs}^{\max} \quad \forall s,\ s \in C \tag{3-3}$$

$$\Delta Q_{DGx}^{\min} \le \Delta Q_{DGx}^{ind} - \Delta Q_{DGx}^{cap} \le \Delta Q_{DGx}^{\max} \quad \forall x,\ x \in G \tag{3-4}$$

$$0 \le \Delta P_{DGx} \le \left| P_{DGx} \right| \ \forall x,\ x \in G \tag{3-5}$$

$$\Delta Q_{DGx}^{ind}, \Delta Q_{DGx}^{cap} \ge 0 \ \ \forall x,\ x \in G \tag{3-6}$$

where N_G is the total number of the DG units that contribute in the voltage control problem. P_{DGx} and ΔP_{DGx} give the injected active power and active power curtailment of the DG number x, respectively. Also, C_P and C_Q denote the weighting coefficients defined for active and reactive power changes of DGs. They are used to give a priority to the control action of DGs and can be associated with the operating costs of the DG active and reactive powers. The voltage sensitivity coefficients relevant to the bus with the biggest voltage violation (bus w) with respect to active and reactive power changes at the DG-connected buses are extracted from matrices **R** and **X** to construct the inequality constraint given in (3-2). It considers the fact that the DG power changes must return the voltage of the bus with the biggest violation into the permitted upper limit. The LHS of (3-2) is equal to the voltage variation at bus w due to DG power changes. In the voltage rise state, ΔV_w^{req} is negative ($\Delta V_w^{req} = 1.03 - V_w$), given that the voltage sensitivity coefficients derived from matrices **R** and **X** are also negative (see (2-18) and (2-19)), the reactive power changes towards the inductive direction and active power curtailment (restricted to non-negative range) can satisfy the voltage constraint. The inequality constraint (3-3) takes into consideration the ampacity limits of the branches. For the sake of simplicity, the ampacity limits are considered in some selected branches given by the set C. The inclusion of ampacity limits in the voltage control problem is discussed further in section 3.3.1. The bounds on available reactive powers of DGs defined by their capability curves are considered in the optimization problem as another inequality constraint. The available active power productions of DGs for the generation curtailment are taken into account by (3-5).

In the above optimization problem, voltage sensitivity coefficients are known parameters obtained from the DSA method. The required value of voltage change for solving the voltage violation at the bus w is also a defined parameter but ΔQ_{DGx}^{ind}, ΔQ_{DGx}^{cap} and ΔP_{DGx} ($x \in G$, $G = \{1, 2, 3, \ldots, N_G\}$) are decision variables that must be optimally selected. Once the optimization problem of I=1 is solved, needed changes of DG powers in order to solve the voltage violation at the bus with the biggest violation is defined. Then, a new LF calculation considering the new values of DG powers is run to determine the corrected voltages and to check whether any other voltage violation exists or not. If a new voltage violation is found, iteration number two starts. A new optimization problem must be formed at I=2 for the voltage violation at this new worst bus subject to updated constraints (3-3) to (3-5) representing the remained branch ampacities and available capacities of DG powers. After solving this optimization problem, at the end of the iteration number two, the LF calculation again determines the iterative procedure must go to the next iteration or it can stop. The MSVCA stops when there is no voltage violation in the system. The above procedure can be found in figure 2-3.

It should be noted that in presence of the buses with the voltage drop, ΔV_w^{req} is determined with respect to the lower permitted voltage limit (i.e. 0.97 pu). Also, as generation curtailment is only applicable for managing the voltage rise problem, ΔP_{DGx} must be removed from the above optimization problem. Consequently, in the voltage drop state, the optimization problem of the MSVCA is equal to the one presented in chapter 2 (given in (2-34) to (2-38)).

3.2.2. Single-step voltage control algorithm

The SSVCA of this chapter works on the basis of the same procedure as explained in chapter 2 (section 2.5.2) with only one difference that it is used here to return simultaneously all the violated voltages inside the permitted voltage range by managing active and reactive powers of DGs. It leads to an optimization problem, which aims at minimizing the total weighted changes of DG active and reactive powers subject to the voltage constraints relating to all violated voltages, as well as limits on DG powers and restrictions on branch ampacity limits. The SSVCA working procedure is described within the following steps.

- Step 1: Load system data, run the DLF program.
- Step 2: If there is any voltage violation, go to the next step, otherwise, stop.
- Step 3: Calculate the needed voltage modifications at the buses with voltage violations and select the relevant voltage sensitivity coefficients from matrices **R** and **X**.
- Step 4: Construct the optimization problem of the SSVCA subject to the voltage constraints, DG power limitations, and branch ampacity restrictions.
- Step 5: Solve the optimization problem, run a new LF calculation considering the new set-points of DGs obtained from step 4, determine the node voltages, plot the corrected voltages, and stop.

In the voltage rise state, the optimization problem of the SSVCA is written as follows.

$$\textbf{Minimize: } OF = \sum_{x=1}^{N_G} \left(C_Q \left| \Delta Q_{DGx}^{ind} - \Delta Q_{DGx}^{cap} \right| + C_P \Delta P_{DGx} \right) \tag{3-7}$$

$$\sum_{x=1}^{N_G} \left(\frac{\partial V_u}{\partial Q_{DGx}} (\Delta Q_{DGx}^{ind} - \Delta Q_{DGx}^{cap}) + \frac{\partial V_u}{\partial P_{DGx}} \Delta P_{DGx} \right) \leq \Delta V_u^{req} \quad \forall u,\ u \in U \tag{3-8}$$

$$I_{brs} \leq I_{brs}^{\max} \quad \forall s,\ s \in C \tag{3-9}$$

$$\Delta Q_{DGx}^{\min} \leq \Delta Q_{DGx}^{ind} - \Delta Q_{DGx}^{cap} \leq \Delta Q_{DGx}^{\max} \quad \forall x,\ x \in G \tag{3-10}$$

$$0 \leq \Delta P_{DGx} \leq \left| P_{DGx} \right| \quad \forall x,\ x \in G \tag{3-11}$$

$$\Delta Q_{DGx}^{ind}, \Delta Q_{DGx}^{cap} \geq 0 \quad \forall x,\ x \in G \tag{3-12}$$

As mentioned before, u is index for the buses with the voltage rise and set U includes all the buses with the voltage rise issue. Cardinality of set U gives the number of voltage constraints taken from (3-8).

The active power curtailment of DGs cannot be used in order to manage the voltage constraints in presence of the buses with the voltage drop issue. Consequently, ΔP_{DGx} must be removed from the above optimization problem. Therefore, in the voltage drop state, the optimization problem of the SSVCA is identical to the one presented in chapter 2 given in (2-42) to (2-46).

3.3. 77-bus test system

In order to test effectiveness of the proposed VCAs, a 77-bus, 11 kV radial distribution system shown in figure 3-1 is considered. It is the so-called ''HVUG'' test case of the United Kingdom Generic Distribution System (UKGDS). In this investigated network, bus number 1 is considered as the slack node while all other buses are of PQ (load) type. The substation transformer located between nodes 1 and 2 is modelled with a pure reactance equal to 12.5% pu in the transformer base power (80 MVA) [64]. The studied network feeds 75 loads, which have total active and reactive powers equal to 24.27 MW and 4.85 Mvar, respectively. The line and load data are presented in appendix 3 [65]. In the studied network, loads are considered with the constant power model and lines are modelled with the series impedances similar to the most of the practical cases in the distribution systems [17], [47], [62], [66] and [67]. The average R/X ratio of the system lines is equal to 1.743. The UKGDS also hosts 22 DG units, which are identical with the rated powers equal to 3.5 MW. The capability curves of DGs are obtained from the points given in table 2-1. The DG active power is modelled as a negative load. The base voltage and power are equal to 11 kV and 100 MVA, respectively. The permitted upper and lower voltage limits are respectively equal to 1.03 pu and 0.97 pu.

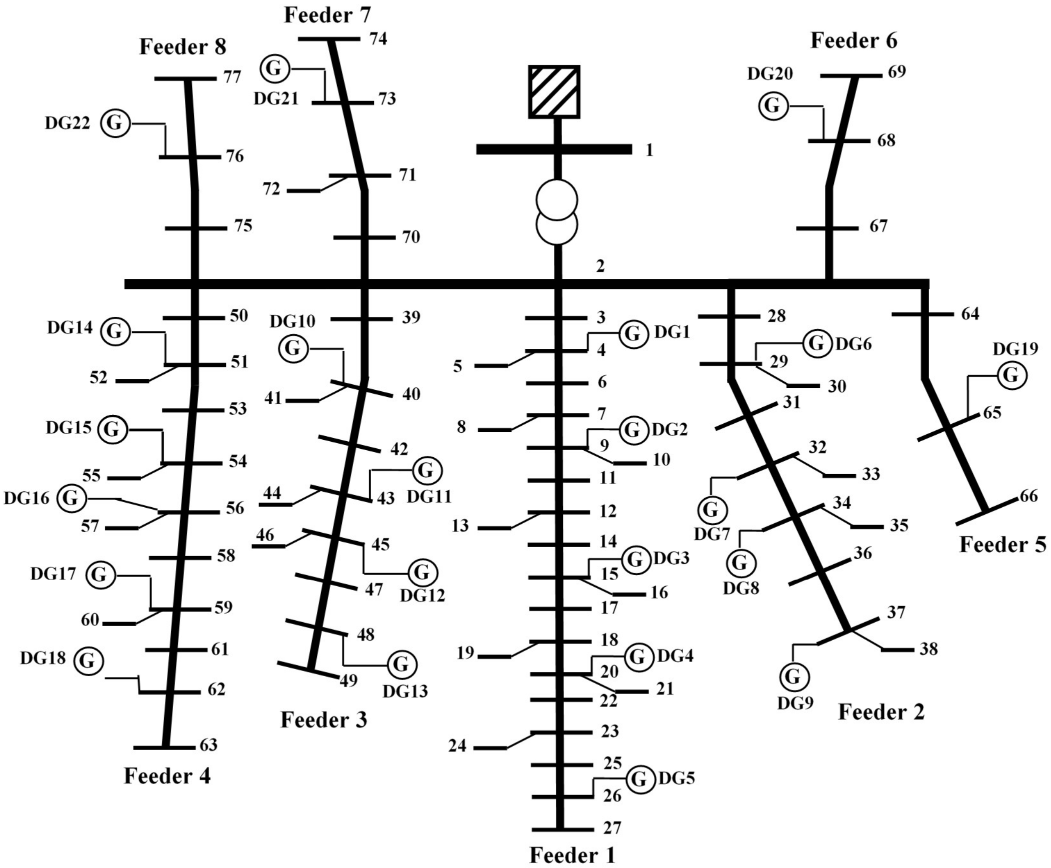

Figure 3-1: 77-bus radial distribution system (UKGDS)

3.3.1. On the consideration of ampacity limits of the branches in the studied test system

In this section, the methodology presented in the previous chapter regarding consideration of the branch ampacity limits in the VCAs is adapted for the studied test system of the current chapter. In the 77-bus UKGDS, the total powers of DGs are almost 3 times of the load powers. Therefore, it can be expected that the branch conductors have been sized according to the full-generation-and-min-load condition in order to be able to meet the maximum branch currents. In this work, it is supposed that the ampacity limits of the branches in the UKGDS are equal to the branch currents in the case that the load powers are zero and DG active powers are at 100% of their nominal values. Within such a network topology, it can be expected that the branch ampacity limits do not reach in the full-load-and-min-generation case.

In the previous chapter, we divided the 33-bus distribution system into 4 zones and we considered the currents in the beginning and ending branches of each zone. The former was responsible to keep the zonal branch currents within the predefined ampacity limit of the zone in the full-load-and-min-generation condition and the latter was considered to maintain the branch ampacity limit of that zone in the full-generation-and-min-load state. Given that in the 77-bus UKGDS, the full-load-and-min-generation condition does not cause the ampacity violation, there is no need to consider the first branch of each zone. As a result, it would be sufficient to take into account only the ampacity limit of the ending branch of each zone. In the

UKGDS, the branches that are located between two adjacent DGs are supposed to be in the same zone. This means that we need to consider the currents of branches which are directly connected to DGs in an upward direction (towards the slack bus). The choice is motivated by the fact that the branches connected to DGs in an upward direction (i.e. the ones located at the end of each zone) have the minimum free ampacities among the branches of their own zone. In addition to 22 branches accounted for 22 DG units, the current in the substation transformer is also taken into account in the optimization problem of the VCAs. Table 3-1 gives the list of the considered branches in the 77-bus UKGDS.

TABLE 3-1: CONSIDERED BRANCH LIMITS IN THE UKGDS

Branch	Between nodes	Feeder	Branch	Between nodes	Feeder
1	1-2	-	44	43-45	3
3	3-4	1	47	47-48	3
8	7-9	1	50	50-51	4
14	14-15	1	53	53-54	4
19	18-20	1	55	54-56	4
25	25-26	1	58	58-59	4
28	28-29	2	61	61-62	4
31	31-32	2	64	64-65	5
33	32-34	2	67	67-68	6
36	36-37	2	72	71-73	7
39	39-40	3	75	75-76	8
42	42-43	3			

In this chapter, active power curtailment of DGs is added to the VCAs. Given that curtailing active powers of DGs decreases the branch currents, it cannot cause current violations in the VCAs. Therefore, in the constraints relating to the branch currents in the VCAs, we consider only reactive power changes of DGs as a source that can increase the branch currents. The maximum reactive power changes of branches while keeping their ampacity limits are determined using the formulation presented in chapter 2 (equation (2-27)). The relations between DG reactive power changes and reactive power changes in the selected branches are obtained through the **DGIB** matrix.

$$[\mathbf{\Delta Q_{br}}] = [\mathbf{DGIB}][\mathbf{\Delta Q_{DG}}] \tag{3-13}$$

The **DGIB** matrix is constructed from the **BIBC** matrix in the DLF approach while the rows related to the selected branches and columns associated with the DG-connected buses are only kept, and all other rows and columns of the **BIBC** matrix are deleted. Therefore, the DGIB matrix has 23 rows and 22 columns. The following inequality constraint is introduced in the VCAs in order to maintain the currents of the selected branches within the predefined limits when reactive powers of DGs change for the voltage regulation purpose.

$$\Delta Q_{brs}^{\max 1} \leq \sum_{x=1}^{N_G} DGIB_{b,x}(\Delta Q_{DGx}^{ind} - \Delta Q_{DGx}^{cap}) \leq \Delta Q_{brs}^{\max 2} \quad \forall s, \mathrm{s} \in \mathrm{C} \tag{3-14}$$

where s is index for branches with the current limits ($s \in C$, set C can be found in table 3-1) and b is an index equal to order of element s in set C. For instance, for s=8 denoting the 8th branch, b is equal to 3, as 8 is the third element of set C. Considering (3-14), reactive powers of DGs are changed within the roots of (2-27) namely ΔQ_{brs}^{max1} and ΔQ_{brs}^{max2} in branch s. As a consequence, the current in the branch s is kept within its predefined ampacity limit. The above constraint is introduced in the MSVCA and SSVCA, in order to take the current limits of the selected branches into account when the reactive powers of DGs are changed.

3.4. Simulation results

The proposed MSVCA and SSVCA are coded in the MATLAB environment. The linear programming toolbox of MATLAB is used to solve the optimization problem of the VCAs. The numerical validation of the proposed VCAs is carried out on the presented 77-bus UKGDS. The VCAs manage the voltage violations of the considered working point of the UKGDS through optimal control of DG active ad reactive powers while keeping the branch currents within their limits.

According to the literature (e.g. [16], [17], [19]), for a voltage regulation end, reactive power changes of DGs are preferred rather than the curtailment of DG active powers given that the former is considered to be cheaper than the latter. Thus, the curtailment of DGs is penalized and the first priority is given to the reactive power control of DGs. When the available reactive powers of DGs are not enough or in the case that active power curtailment of DGs is more optimal, generation curtailment of DGs will be carried out in order to regulate the system voltages.

In this work, in order to validate the proposed VCAs for whole range of the DG actions, three different cases are considered as mentioned in table 3-2. In case A, the objective is to use only reactive power control capability of DGs, therefore, C_P (relating to active power changes of DGs) is penalized with a coefficient 100 times greater than C_Q (belonging to reactive power changes of DGs). Case B is an inverse situation of case A, thus, the VCAs employ the active power curtailment of DGs. Finally, in case C, the same weighing coefficients are defined for active and reactive power controls of DGs, consequently, according to the impacts of each control option (known from the DSA) on the violated voltages and considering free ampacities of the branches connected to DGs, the optimization procedure determines the contribution of DG active and reactive powers.

TABLE 3-2: WEIGHTING COEFFICIENTS OF DG POWER CHANGES IN THE STUDIED CASES

	C_Q	C_P
Case A	1	100
Case B	100	1
Case C	1	1

Performance of the MSVCA and SSVCA in each of the abovementioned studied cases is examined when solving the voltage control problem of an identical working point of the

UKGDS. It corresponds to the point that all the loads are at 10% of their nominal values while DGs produce active powers equal to 90% of their rated values (3.5×0.9=3.15 MW). The initial reactive powers of DGs are set to zero. In this situation, it is expected to deal with the voltage rise issue. It is worth noting that the working point regarding the full-load-and-min-generation state will not be studied here because the main objective of this chapter is to validate the new functionality of the VCAs, which is managing active and reactive powers of DGs. The full-load-and-min-generation working point creates voltage drop issue, which can be solved with capacitive reactive power changes of DGs, similarly to the simulated cases in chapter 2 (cases A.1 to A.4).

3.4.1. With multi-step voltage control algorithm

3.4.1.1. Case A

In the first studied case, the MSVCA is employed to manage the voltage violations of the considered working point using the reactive power control of DGs while maintaining ampacity limits of the branches. After running the initial LF calculation, the biggest voltage violation is found at bus 26 located in feeder 1. According to the information provided by the DSA, in a descending order, DG5 to DG1 are the most efficient DGs to be used in the voltage regulation of bus 26. Given that ampacity limits of the branches are taken into account, the MSVCA uses DG5 with its maximum contribution defined by the ampacity limit of the branch 25. In the first iteration, the branches 3, 8, 14, 19, 25 in feeder 1 are capable of transferring respectively up to 6.6077 Mvar, 5.1563 Mvar, 3.7273 Mvar, 2.4246 Mvar and 1.0965 Mvar inductive reactive power changes. Therefore, firstly, reactive power of DG5 is changed by 1.0965 Mvar according to the limit defined by the branch 25. Then, reactive power of DG4 is modified considering the restriction imposed by the branch 19. The initial free capability of branch 19 (=2.4246 Mvar) is now reduced due to reactive power changes of DG5. The branch 19 can pass up to 1.3281 (=2.4246-1.0965) Mvar reactive power changes of DG4. Similarly, contribution of DG3 is restricted by the ampacity limit of the branch 14. The remained available capability of branch 14 to transfer reactive power changes of DG3 is equal to 1.3028 (=3.7273 - ΔQ_{DG5} - ΔQ_{DG4}) Mvar. Finally, DG2 provides 1.4189 Mvar inductive reactive power changes to remove totally the voltage rise of bus 26. Table 3-3 gives the reactive power contributions of DGs in order to manage the voltage rise problem in the case A. Note that hereafter, only the DGs with the power changes are mentioned in the table and for the rest of DGs (which are not listed), power changes are equal to zero.

TABLE 3-3: SIMULATION RESULTS IN CASE A USING THE MSVCA

	I=1	I=2
ΔV_w^{req} (pu) w	-0.0298 26	-0.0134 62
ΔQ_{DGx} (Mvar) $x \in \{1, 2, 3, \ldots, 22\}$	DG2=1.4189 DG3=1.3028 DG4=1.3281 DG5=1.0965	DG17= 1.0612 DG18= 1.1067
OF Tot (Mvar)	7.3142	

In the optimization problem of the MSVCA in I=1, the constraints relating to branches 14, 19 and 25 are the binding ones. The difference between the corrected current values in these branches and their ampacity limits gives us the error arisen from the proposed formulation for considering the branch limits. This error for the branches 14, 19 and 25 equals respectively to 0.003 pu, 0.002 pu and 8.43×10^{-4} pu which are equal to 16.12 A, 10.51 A and 4.42 A when converting into the real values.

In the second iteration of the MSVCA, a similar procedure is followed to return the voltage rise at bus 62 (i.e. the one with the biggest violation) within the permitted voltage limit. DG18 which has the highest impact on the voltage at bus 62, is firstly used to this end. Given that branch 61 is able to pass a reactive power change from DG18 up to 1.1067 Mvar, and this would not be sufficient to remove voltage violation of bus 62, DG17 should be used as well. In I=2, the constraint relating to branch 61 is the binding one. The error between the ampacity limit of the latter and its corrected current is equal to 0.0012 pu or 6.4 A. Within two iterations of the MSVCA, all the system voltages are returned into the permitted voltage range, as a consequence, the iterative-procedure of the MSVCA stops at the end of I=2. Figure 3-2 shows the initial system voltages and the corrected ones obtained by the MSVCA.

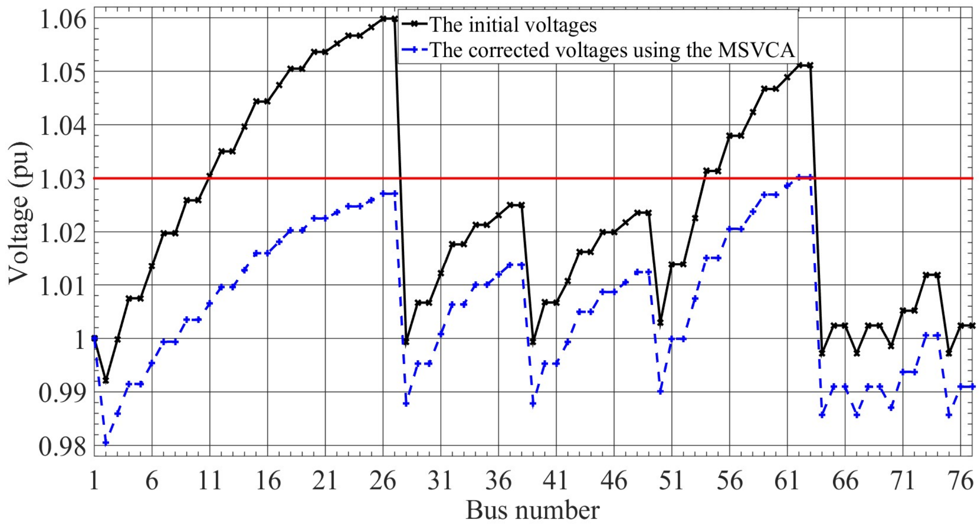

Figure 3-2: The initial voltages as well as the corrected ones obtained by the MSVCA in case A

As it can be seen in figure 3-2, all the system voltages are returned inside the permitted voltage range with a total objective function (*OF Tot*) equal to 7.3142 Mvar (given in table 3-3).

3.4.1.2. Case B

In case B, a big weighing coefficient is assigned to reactive power utilization of DGs (i.e. C_Q=100). The objective is to examine performance of the MSVCA when only active power control of DGs is employed. Given that the active power curtailment of DGs will reduce the branch currents, the ampacity limits do not restrict the optimization problem of the MSVCA and there will be no binding constraint relating to the branch limits in this case. Consequently, regardless of the branch limits, the MSVCA can employ the DGs which have the biggest impacts on the violated voltages. Table 3-4 presents the curtailed active powers of DGs at each iteration of the MSVCA and figure 3-3 shows the initial and corrected node voltages in case B.

TABLE 3-4: SIMULATION RESULTS IN CASE B USING THE MSVCA

	I=1	I=2	I=3	I=4	I=5
ΔV_w^{req} (pu) w	-0.0298 26	-0.0219 62	-0.0047 20	-0.0029 59	-6×10^{-4} 20
ΔP_{DGx} (MW) $x \in \{1, 2, 3, \ldots, 22\}$	DG4=0.3261 DG5=3.15	DG17=0.0816 DG18=3.15	DG4= 0.7167	DG17= 0.5526	DG4= 0.091
OF Tot (MW)	8.0686				

As it can be seen in table 3-4, the MSVCA needs 5 iterations in order to bring back the violated voltages within the permitted voltage range. In the first iteration, the biggest voltage rise is found at bus 26. Active power of DG5, which has the biggest impact on the voltage of node 26, is curtailed by 3.15 MW and reaches zero. DG4 is also involved in I=1 to remove the voltage rise of node 26. In I=2, voltage rise at bus 62 is the biggest one. In order to bring back the voltage rise of node 62, active power of DG18 is curtailed totally, as it is changed by 3.15 MW. In addition, DG17 is used to provide the rest of needed power curtailment. In the next iterations, DG18 and DG5 have no more active powers to be curtailed, thus, DG17 and DG4 are employed to remove the voltage rises of buses 59 and 20, respectively.

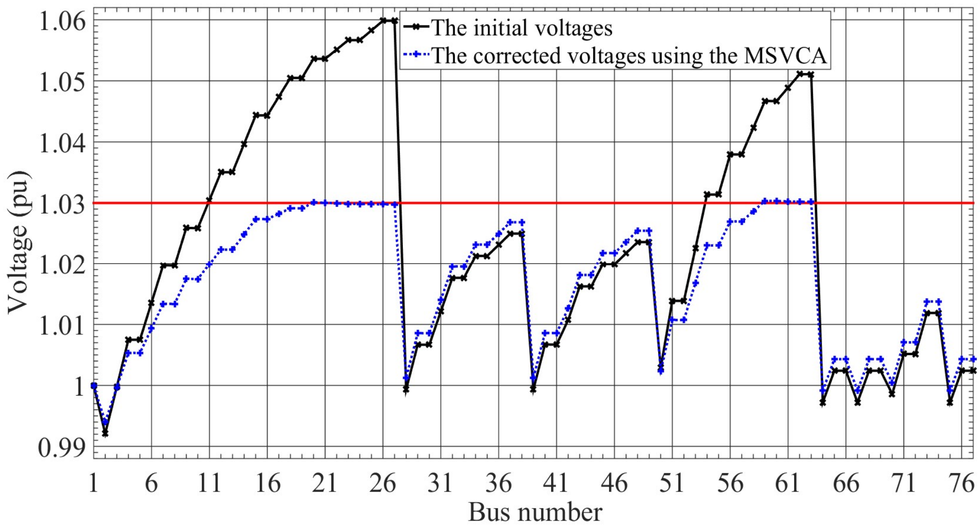

Figure 3-3: The initial voltages as well as the corrected ones obtained by the MSVCA in case B

Compared to the case A, in the current case, the MSVCA needs more iterations to manage the voltage violations. Given that the substation transformer has been modelled as a pure reactance (i.e. relatively big) located between the slack bus and every single node of the system, it has a direct influence on all the entries of the matrix **X**. As a consequence, when the DG reactive power varies in one feeder, it not only changes the voltages of that feeder, but it has also has a big impact on the voltages of other feeders. This is not the case when active power of DGs is changed because the matrix **R** is not affected by the transformer reactance. Referring to the simulation results in table 3-4, in the first iteration, active powers of DG4 and DG5 in feeder 1 are curtailed. These power variations (performed in feeder 1) do not have a considerable impact on the voltage at bus 62 (in feeder 4). It is seen in figure 3-3 that the initial voltage at bus 62 is 1.0511 pu, while in table 3-4 at iteration 2 (after active power changes in feeder 1), it increases to 1.0519 (=1.03+0.0219) pu. It means that the curtailed powers of DG4 and DG5 (i.e. equal to 0.326+3.15=3.47 MW) in feeder 1 have changed the voltage at bus 62 in feeder 4 by 0.0008 (=1.0519-1.0511) pu. In case A, however, the difference between the initial voltage at bus 62 and the corrected one after I=1 is equal to 0.0077 pu (=1.0511-1.0434 where 1.0434=1.03+0.0134, in table 3-3).

Considering figure 3-3, it is confirmed that the MSVCA removes all the initial voltage violations by employing active power curtailment of DGs such that the corrected voltages are placed within the permitted voltage range.

3.4.1.3. Case C

In the last case study on the MSVCA, the same weighting coefficients are considered for active and reactive power changes of DGs. Therefore, active or reactive power control of DGs can be employed in the MSVCA according to the impacts that they have on the violated voltages. Table 3-5 presents the iterative procedure of returning the system voltages into the permitted voltage range using the MSVCA. Also, figure 3-4 shows the initial and corrected node voltages in case C.

TABLE 3-5: SIMULATION RESULTS IN CASE C USING THE MSVCA

	I=1	I=2	I=3	I=4
ΔV_w^{req} (pu) w	-0.0298 26	-0.0215 62	-0.0050 20	-0.0029 59
ΔP_{DGx} (MW) $x \in \{1, 2, 3, \ldots, 22\}$	DG5=3.15	DG18=3.1476	DG4= 0.751	NA
ΔQ_{DGx} (Mvar) $x \in \{1, 2, 3, \ldots, 22\}$	DG5=0.26	NA	NA	DG17=0.5163
OF Tot	7.8249			

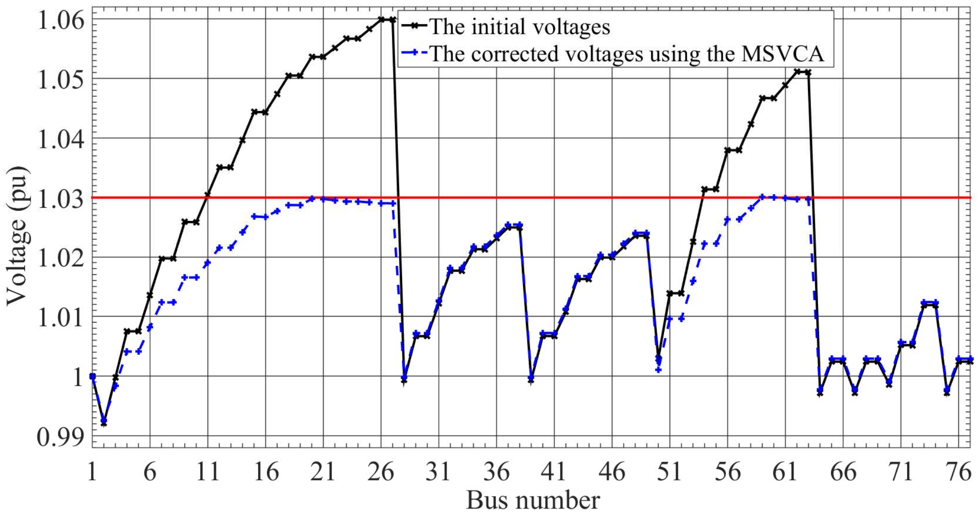

Figure 3-4: The initial voltages as well as the corrected ones obtained by the MSVCA in case C

In table 3-5 and hereafter, NA is used to indicate that a specific control action is not applied. It is known from the DSA that active power of DG5 has a bigger effect on the voltage at bus 26 compared to its reactive power, therefore, in I=1, the former is changed by 3.15 MW and the latter by 0.26 Mvar to remove the voltage violation at bus 26. In the second and third iterations, active powers of DG18 and DG4 are curtailed to manage the voltage violations of buses 62 and 20, respectively. Finally, in the last iteration, the reactive power change of DG17 solves the voltage rise of bus 59. It is worth noting that since the MSVCA has mostly used the active power curtailment of DGs, the branch currents do not reach their own ampacity limits and there is no binding constraint relating to the ampacity limits in any of 4 iterations of the MSVCA. Moreover, from figure 3-4, it can be noticed that the initial voltage violations are efficiently removed using the MSVCA and all the corrected voltages are within the permitted voltage range.

3.4.2. With single-step voltage control algorithm

In the second part of simulations, the SSVCA is used to manage the voltage violations of the considered working point of the UKGDS while keeping the ampacity limits of the branches. As discussed before, in the SSVCA, all the violated voltages are considered simultaneously, and the main aim is to return the violated voltages inside the permitted voltage range at once. Performance of the SSVCA is tested on three cases A, B and C introduced in table 3-2.

3.4.2.1. Case A

In the first case of study on the SSVCA, the reactive power control of DGs is used to solve the voltage control problem while the active power curtailment of DGs has been penalized with a big C_P. Table 3-6 presents the reactive power changes of DGs in order to manage the voltage rise problem of the considered working point. Figure 3-5 shows the system voltages along the feeders.

TABLE 3-6: SIMULATION RESULTS IN CASE A USING THE SSVCA

ΔQ_{DGx} (Mvar) $x \in \{1, 2, 3, \ldots, 22\}$	DG2=0.4097 DG3=1.3028 DG4=1.3281 DG5=1.0965 DG16=0.0385 DG17=1.2418 DG18=1.1523
OF (Mvar)	6.5697

In the considered working point, the biggest voltage rises happened in the end of feeders 1 and 4 as it can be seen in figure 3-5. The binding voltage constraints in the optimization problem of the SSVCA relate to the buses 26 and 62. In a descending order, DG5 to DG1 have the biggest impacts on the voltage at bus 26 and, DG18 to DG14 have the highest effects on the voltage of node 62. Therefore, within the above orders, DGs are used to remove the voltage violations of buses 26 and 62 considering the restrictions imposed by the ampacity limits of the branches in feeders 1 and 4. The branches 14, 19, and 25 in feeder 1 restrict the reactive power changes of

DG3, DG4, and DG5. Similarly, branches 58 and 61 in feeder 4 limit contributions of DG17 and DG18. The abovementioned branches are associated with the binding constraints of the SSVCA optimization problem. On the contrary, needed reactive power changes of DG2 and DG16 can transfer from the branches 8 and 55, respectively, without reaching their ampacity limits. The errors arisen from the proposed formulation (regarding the ampacity limits) in branches 14, 19 and 25 are almost identical to the ones mentioned in case A using the MSVCA as the reactive power changes of DG3, DG4 and DG5 are the same in these two cases and the corrected node voltages are nearly similar in both cases A using the MSVCA and SSVCA. The errors between the currents in branches 58 and 61 (which are also the binding constraints) and their own ampacity limits are equal to 0.0023 pu and 0.0011 pu (i.e. 12 A and 5.7 A in the real values), respectively.

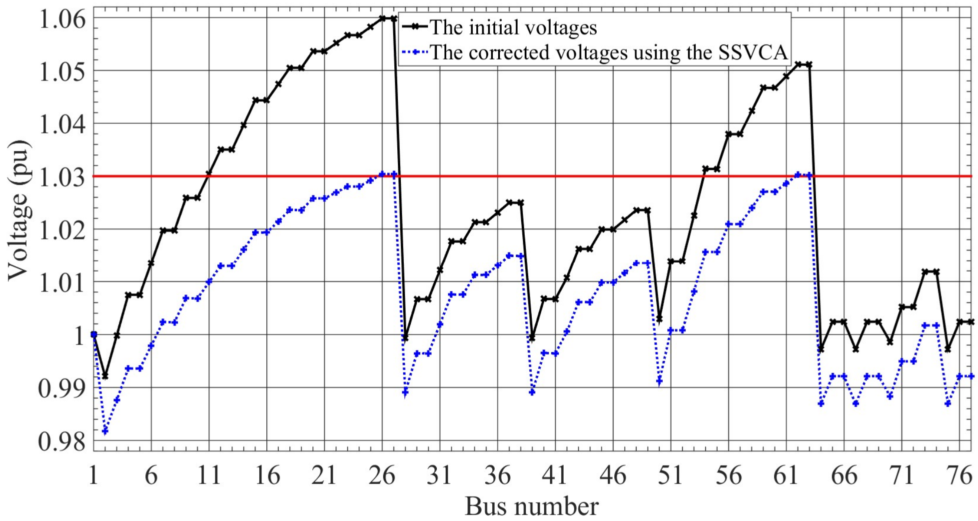

Figure 3-5: The initial voltages as well as the corrected ones obtained by the SSVCA in case A

Figure 3-5 confirms that the SSVCA employing reactive power control of DGs effectively removes the initial voltage violations of the studied working point such that the corrected voltages are placed within the permitted voltage range.

3.4.2.2. Case B

In this case, the SSVCA manages the voltage constraints of the considered working point through curtailment of DG active powers while the reactive power changes of DGs are penalized with a big weighing coefficient. Table 3-7 presents the curtailed active powers of DGs demanded by the SSVCA in order to remove the voltage violations. Also, figure 3-6 depicts the initial voltages as well as the ones obtained after the voltage regulation.

TABLE 3-7: SIMULATION RESULTS IN CASE B USING THE SSVCA

ΔP_{DGx} (MW) $x \in \{1, 2, 3, \ldots, 22\}$	DG4= 0.4973 DG5= 3.0833 DG17= 0.2307 DG18= 2.917
OF (MW)	6.7281

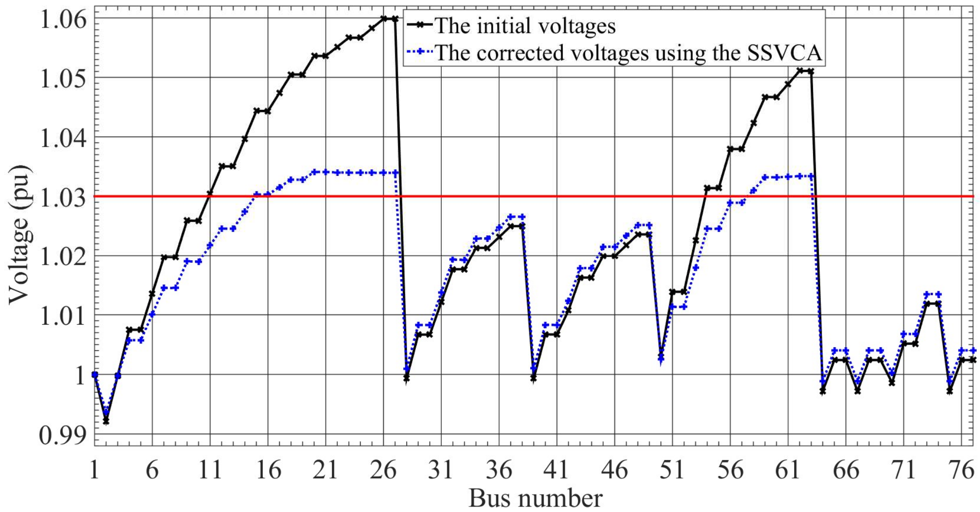

Figure 3-6: The initial voltages as well as the corrected ones obtained by the SSVCA in case B

As it can be noticed from figure 3-6, the initial voltage violations are not completely returned inside the permitted voltage range and some voltage rises are remained when the SSVCA action is completed. The voltage violations from the 1.03 pu voltage limit at the buses belonging to the binding constraints (i.e. buses 20 and 59) are equal to 0.0041 pu and 0.0033 pu. These errors are arisen from the DSA method, as the latter could not accurately linearize the relations between the violated voltages and DG active powers.

3.4.2.3. Case C

In the last case study of this chapter, active and reactive power changes of DGs are weighted equally. Therefore, the SSVCA employs the active or reactive power control of DGs that has the biggest impacts on the violated voltages while considering the ampacity limits of the branches. Table 3-8 gives the DG power changes in case C and figure 3-7 shows the initial voltages as well as the ones obtained after the SSVCA action.

TABLE 3-8: SIMULATION RESULTS IN CASE C USING THE SSVCA

ΔQ_{DGx} (Mvar) $x \in \{1, 2, 3, \ldots, 22\}$	DG4=0.233 DG5=1.0965 DG18=1.1523
ΔP_{DGx} (MW) $x \in \{1, 2, 3, \ldots, 22\}$	DG5=1.9924 DG18=1.6591
OF	6.1334

In case C, buses 20, 26 and 62 correspond to the binding voltage constraints. Reactive powers of DG5 and DG18 are changed according to the limits defined by the branches 25 and 61, respectively. In addition, reactive power of DG4 and active powers of DG5 and DG18 are modified in order to manage the voltage violations. However, as it can be seen in figure 3-7, after the voltage regulation by the SSVCA, the system voltages are not completely returned into the permitted voltage range and similar to the previous case, some voltage violations are remained. It is worth observing that in the current case, the remained voltage violations are smaller than the ones of case B since a smaller value of active power curtailment is applied here (due to the reactive power contribution of DGs). The mismatches between the corrected voltages obtained by the SSVCA at the buses 20, 26, and 62 (relating to the binding constraints) and the targeted 1.03 pu voltage limit are equal to 0.0027 pu, 0.0033 pu, and 0.0022 pu, respectively.

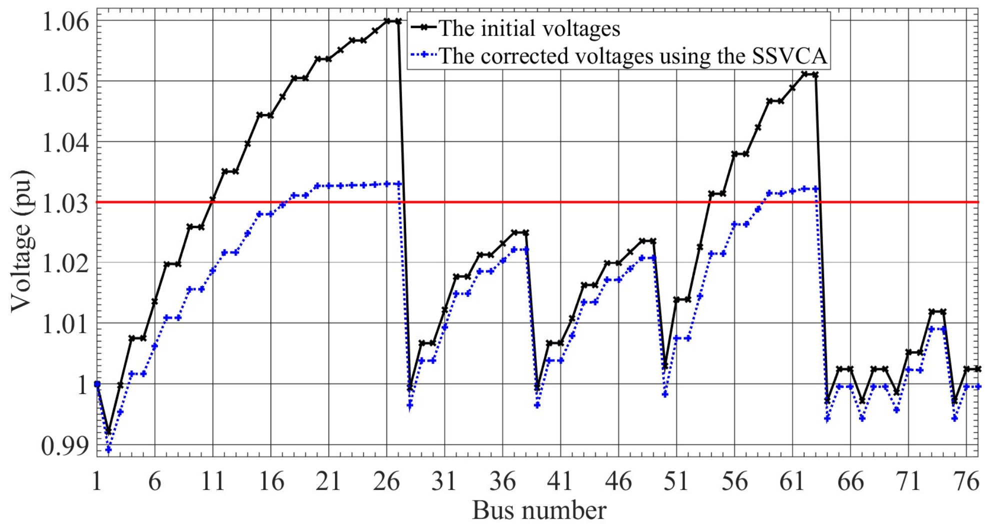

Figure 3-7: The initial voltages as well as the corrected ones obtained by the SSVCA in case C

3.5. Discussion on the results

On the basis of the simulation results, it is concluded that the MSVCA can effectively bring back the violated voltages within the permitted voltage range in the three studied cases. It is also found that the SSVCA employing the reactive power changes of DGs is capable of managing the voltage violations. However, when the SSVCA uses the generation curtailment of DGs in case B or C, some voltage violations are remained after the voltage regulation procedure. The voltage violations are arisen due to the error in the DSA method. The SSVCA works as an open-loop control system and it has no feedback on the corrected voltages. As a result, in case of error in the sensitivity analysis, it would not be possible anymore to return the system voltages within the permitted voltage limits.

In the simulated cases, it is seen that the error arisen from the proposed formulation regarding the branch limit inclusion increases when moving from end of the feeders towards the slack node. For instance, in case A using the MSVCA, the biggest error has been found in branch 14, while a smaller one is seen in branch 19, and branch 25 has the smallest error. This is explained by the fact that the error in branch 14 includes also errors linked to branches 19 and 25 since the power flows in these two branches pass through the branch 14. Given that bigger reactive power changes are needed for voltage regulation of the 77-bus UKGDS in this chapter, the errors arisen from the proposed formulation are increased compared to the ones found in chapter 2 (related to the 33-bus test system).

Moreover, based on the simulation results, it can be concluded that the substation transformer has very important impact on the performance of the VCAs. Given that the substation transformer is located in the starting point of the network in series with all the system branches, it has an effect on all entries of the matrix **X**. Consequently, it affects the contribution of DG reactive powers in the voltage regulation procedure. Furthermore, the transformer reactance is considerably bigger than the line reactances. Therefore, in figures 3-2 to 3-7, it is seen that there are always big voltage variations between nodes 1 and 2 which belong to the voltage drop on the transformer reactance.

Comparing the multi-step and single-step voltage control algorithms in case A (when only reactive power control of DGs is used), it is observed that the SSVCA solves the same voltage control problem with a smaller objective function (see tables 3-3 and 3-6). The studied UKGDS consists of 8 feeders. Due to presence of the transformer reactance, reactive power changes in one feeder have considerable impacts on the node voltages of other feeders. Therefore, the SSVCA which considers voltage violations of all feeders can manage the voltage control problem in a more optimal manner than the MSVCA which takes into consideration the worst voltage violation of the system in each iteration. The latter point can be further verified considering the voltage results of the abovementioned cases. As it can be seen, in figure 3-5 corresponding to the SSVCA results, the voltages in feeder 1 are closer to 1.03 pu than the ones in figure 3-2 (obtained from the MSVCA). This means that smaller reactive power changes are demanded by the SSVCA.

3.6. Conclusion

In this chapter, functionality of the VCAs presented in chapter 2 is evolved by adding the possibility of curtailing the active powers of DGs beside the reactive power control of DGs. The sensitivity-based VCAs adopting the open-loop and closed-loop forms are designed to manage DG active and reactive powers in order to maintain the node voltages and branch currents with their own permitted limits. Based on the simulation results, it can be concluded that using the MSVCA, even in presence of an inaccurate sensitivity data, the node voltages are returned inside the permitted voltage range thanks to its closed-loop framework. This is not the case in the SSVCA relying on an open-loop control system (e.g. cases B and C with the SSVCA). On the other hand, when the voltage violations are found in different feeders of the studied system, if an accurate sensitivity analysis is in our disposal, the SSVCA can solve the same voltage control problem in a more optimal way than the MSVCA given that the former has a global view of all the violated voltages.

Furthermore, it has been found that the substation transformer has very important impact on the performance of the VCAs. Considering the substation transformer, all entries of the voltage sensitivity matrix with respect to node reactive powers (i.e. matrix **X**) will be increased by a value equal to the reactance of transformer. The latter is considerably bigger than the line reactances. As a consequence, despite the high R/X ratio of the distribution system lines, the reactive power control of DGs becomes an efficient method for the voltage regulation of the distribution systems. For instance, in studied UKGDS having an average R/X of lines equal to 1.743, when comparing cases A and B using the MSVCA, it is seen that the same voltage control problem has been solved with smaller objective function when reactive power control of DGs is employed.

In the next chapter, it is attempted to cover the drawback of the DSA method in voltage estimation subject to active power variation. To this end, a new VSA method will be proposed that incorporates power losses in the system branches and their eventual impacts on the node voltages. A comprehensive analysis is carried out in order to test the effectiveness of the proposed VSA method in the voltage estimation subject to active and reactive power changes. Performance of the proposed method is evaluated in comparison with other VSA methods.

3.7. Chapter publication

This chapter has led to the following publication:

- B. Bakhshideh Zad, J. Lobry and F. Vallée, "A centralized approach for voltage control of MV distribution systems using DGs power control and a direct sensitivity analysis method," in *2016 IEEE International Energy Conference (ENERGYCON)*, Belgium, 2016.

Chapter 4: Introducing a new voltage sensitivity analysis method incorporating power losses

4.1. Abstract

In this chapter, a novel VSA method is developed which presents a complementary formulation of the DSA approach introduced in chapter 2. The proposed method named Improved Direct Sensitivity Analysis (IDSA) incorporates variations of power losses in the system branches due to the nodal power changes and their eventual impacts on the node voltages. Effectiveness of the IDSA in the voltage estimation is investigated and compared with the voltage results obtained by the DSA, JBSA, and Perturb-and-Observe Sensitivity Analysis (POSA) methods. To this end, firstly, the introduced VSA methods are tested when active or reactive power is changed at the selected nodes of the studied test system. Accuracy of voltage responses obtained by each of the considered VSA methods is evaluated with respect to the exact voltage value obtained from the LF study. Then, performance of the studied VSA methods is examined when they are separately embedded in the MSVCA and SSVCA. The main aim of this chapter is to demonstrate importance of incorporating the power losses in the VSA formulation by proposing the IDSA method and through comparative studies of the IDSA with the DSA, POSA and JBSA approaches, which are conducted on different working points of the studied test system.

4.2. Voltage variation in a simple 2-bus distribution system considering the branch power losses

Let consider the simple 2-bus distribution system shown in figure 4-1. When there is only power consumption at node 2, active and reactive powers that flow between nodes 1 and 2 (i.e. P_{br1} and Q_{br1}) are equal to the sum of load consumption (P_L+jQ_L) at bus 2 and the power losses associated with the line between nodes 1 and 2 (i.e. P_{Loss1}+jQ_{Loss1}).

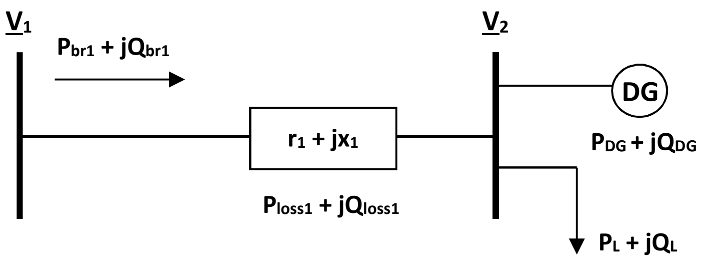

Figure 4-1: A simple 2-bus distribution system

As shown in section 1-3, voltage variation vector between nodes 1 and 2 is given by

$$\underline{\Delta V}_{12} = \frac{r_1 P_{br1} + x_1 Q_{br1}}{\underline{V}_1^*} + j\frac{x_1 P_{br1} - r_{12} Q_{br1}}{\underline{V}_1^*} \tag{4-1}$$

where r_1 and x_1 denote resistance and reactance of the line between nodes 1 and 2. In the distribution systems, as the voltage angles are small, the imaginary part of the voltage variation vector in (4-1) is negligible. Also, considering bus 1 as slack bus with the voltage magnitude equal to 1 pu and phase angle equal to zero, the above equation is simplified as

$$\Delta V_{12} = r_1 P_{br1} + x_1 Q_{br1} \tag{4-2}$$

Substituting for branch power flows from the load and DG powers at node 2 as well as the power losses of the branch, (4-2) is rewritten as

$$\Delta V_{12} = r_1 \left(P_L + P_{Loss1} + P_{DG} \right) + x_1 \left(Q_L + Q_{Loss1} + Q_{DG} \right) \tag{4-3}$$

In contrast with (1-5), it is seen that according to (4-3), the voltage variation at bus 2 not only is in function of DG active and reactive powers, load demand and the line impedance, but also it depends on the power losses associated with the line impedance. Therefore, in order to have a more accurate VSA, the line power losses should be incorporated in the formulation of the developed VSA method.

4.3. The improved direct voltage sensitivity analysis

As discussed in chapter 2, the DSA method defines the dependencies between the system voltages and the nodal powers directly on the basis of the topological structure of the network. This has an advantage in the sense that the voltage sensitivity coefficients are constant and independent of the network working point. On the other hand, the simple formulation of the DSA may lead to inaccurate voltage estimation as found in chapter 3 when modifying DG active powers. In this chapter, an attempt is made in order to cover this drawback of the DSA method by proposing a more accurate VSA approach.

It is known basically that by supposing the system loads and generations independent of the voltage, the power losses make the voltage-power relationships non-linear. Therefore, in order to have a more accurate VSA, the power losses should be taken into account, especially, in the case that the initial working point of the network is needed to be greatly moved. The IDSA presents a complementary formulation of the DSA method. Compared to the DSA and other existing approaches in the literature presented in section 2.3.1, the IDSA considers the variations in power losses of the system lines as a result of nodal power changes and their eventual impacts on the system voltages.

The IDSA method is developed based on the expression (4-3) that gives the voltage variation of the 2-bus system shown in figure 4-1 between node 1 (i.e. slack bus) and node 2. From (4-3), it can be observed that the active power that flows in the line is coupled with the resistance of the line and the reactive power that flows in the line is coupled with the reactance of the line. Supposing that node voltages are close to 1 pu and the imaginary parts of voltage variation vectors can be neglected, (4-3) can be applied recursively to all the adjacent nodes of the system. Let us refer again to the 5-bus radial system shown in figure 2-1. Voltage variations between bus 1 and other buses of the considered system are obtained as follows according to (4-3).

$$\begin{bmatrix} V_1 \\ V_1 \\ V_1 \\ V_1 \end{bmatrix} - \begin{bmatrix} V_2 \\ V_3 \\ V_4 \\ V_5 \end{bmatrix} = \begin{bmatrix} r_1 & 0 & 0 & 0 \\ r_1 & r_2 & 0 & 0 \\ r_1 & r_2 & r_3 & 0 \\ r_1 & r_2 & 0 & r_4 \end{bmatrix} \begin{bmatrix} P_{br1} \\ P_{br2} \\ P_{br3} \\ P_{br4} \end{bmatrix} + \begin{bmatrix} x_1 & 0 & 0 & 0 \\ x_1 & x_2 & 0 & 0 \\ x_1 & x_2 & x_3 & 0 \\ x_1 & x_2 & 0 & x_4 \end{bmatrix} \begin{bmatrix} Q_{br1} \\ Q_{br2} \\ Q_{br3} \\ Q_{br4} \end{bmatrix} \tag{4-4}$$

Given that sensitivity of system voltages with respect to nodal active and reactive powers is of interest, the branch power flows in (4-4) must be replaced by the nodal powers. In the DLF approach, relations between nodal powers and power losses in the branches with the power flows in the branches are given through the **BIBC** matrix as below.

$$\begin{aligned} \begin{bmatrix} P_{br1} \\ P_{br2} \\ P_{br3} \\ P_{br4} \end{bmatrix} &= [\mathbf{BIBC}] \begin{bmatrix} P_2 \\ P_3 \\ P_4 \\ P_5 \end{bmatrix} + [\mathbf{BIBC}] \begin{bmatrix} P_{loss1} \\ P_{loss2} \\ P_{loss3} \\ P_{loss4} \end{bmatrix} \\ &= [\mathbf{BIBC}] \begin{bmatrix} P_2 + P_{loss1} \\ P_3 + P_{loss2} \\ P_4 + P_{loss3} \\ P_5 + P_{loss4} \end{bmatrix} = \begin{bmatrix} 1 & 1 & 1 & 1 \\ 0 & 1 & 1 & 1 \\ 0 & 0 & 1 & 0 \\ 0 & 0 & 0 & 1 \end{bmatrix} \begin{bmatrix} P_2 + P_{loss1} \\ P_3 + P_{loss2} \\ P_4 + P_{loss3} \\ P_5 + P_{loss4} \end{bmatrix} \end{aligned} \tag{4-5}$$

where P_{loss1}, P_{loss2}, P_{loss3} and P_{loss4} stand for the active power losses in the branches 1, 2, 3 and 4, respectively. As it can be seen in the above equation, the **BIBC** matrix contains 1 or 0 elements to show whether the nodal powers and branch power losses are linked to the branch power flows, or not, respectively. Similarly to (4-5), relations between branch reactive power flows with nodal reactive powers and line reactive power losses are obtained through the **BIBC** matrix. Substituting for branch active power flows from (4-5) and doing the same for their reactive counterparts, (4-4) is rewritten as

$$\begin{aligned} \begin{bmatrix} V_1 \\ V_1 \\ V_1 \\ V_1 \end{bmatrix} - \begin{bmatrix} V_2 \\ V_3 \\ V_4 \\ V_5 \end{bmatrix} = &\begin{bmatrix} r_{12} & r_{12} & r_{12} & r_{12} \\ r_{12} & r_{12}+r_{23} & r_{12}+r_{23} & r_{12}+r_{23} \\ r_{12} & r_{12}+r_{23} & r_{12}+r_{23}+r_{34} & r_{12}+r_{23} \\ r_{12} & r_{12}+r_{23} & r_{12}+r_{23} & r_{12}+r_{23}+r_{35} \end{bmatrix} \begin{bmatrix} P_2 + P_{loss1} \\ P_3 + P_{loss2} \\ P_4 + P_{loss3} \\ P_5 + P_{loss4} \end{bmatrix} + \\ &\begin{bmatrix} x_{12} & x_{12} & x_{12} & x_{12} \\ x_{12} & x_{12}+x_{23} & x_{12}+x_{23} & x_{12}+x_{23} \\ x_{12} & x_{12}+x_{23} & x_{12}+x_{23}+x_{34} & x_{12}+x_{23} \\ x_{12} & x_{12}+x_{23} & x_{12}+x_{23} & x_{12}+x_{23}+x_{35} \end{bmatrix} \begin{bmatrix} Q_2 + Q_{loss1} \\ Q_3 + Q_{loss2} \\ Q_4 + Q_{loss3} \\ Q_5 + Q_{loss4} \end{bmatrix} \end{aligned} \tag{4-6}$$

In a matrix form, (4-6) can be written as

$$[\mathbf{V_1}]\text{-}[\mathbf{V_k}] = [\mathbf{R}][\mathbf{P}+\mathbf{P_{loss}}] + [\mathbf{X}][\mathbf{Q}+\mathbf{Q_{loss}}] \tag{4-7}$$

Considering bus 1 as slack bus, the sensitivity of voltage at bus k with respect to active or reactive power at bus n ($n \in NL$) is obtained by the following rules.

$$\frac{\partial\left(V_1-V_k\right)}{\partial P_n}=\frac{-\partial V_k}{\partial P_n}=R_{k-1,n-1}+\sum_{J=1}^{nbr}R_{k-1,J}\frac{\partial P_{lossJ}}{\partial P_n}+\sum_{J=1}^{nbr}X_{k-1,J}\frac{\partial Q_{lossJ}}{\partial P_n} \tag{4-8}$$

$$\frac{\partial\left(V_1-V_k\right)}{\partial Q_n}=\frac{-\partial V_k}{\partial Q_n}=X_{k-1,n-1}+\sum_{J=1}^{nbr}R_{k-1,J}\frac{\partial P_{lossJ}}{\partial Q_n}+\sum_{J=1}^{nbr}X_{k-1,J}\frac{\partial Q_{lossJ}}{\partial Q_n} \tag{4-9}$$

where J is index for the branch numbers ($J \in B, B = \{1, 2, 3, \ldots, nbr\}$) and nbr is total number of the system branches equal to cardinality of set B. In the IDSA method, in (4-8) and (4-9), the first term is a constant value that comes from the topology of the network (entry k-1,n-1 of the **R** or **X** matrix) similarly to the DSA method. On the contrary, the second and third terms representing the power loss variations in the system branches as a function of nodal power changes and their eventual impacts on the system voltages are in function of the network working point and they consequently change with it.

In [66], problem of the optimal placement and sizing of DG is addressed. An analytical method has been presented in order to obtain the sensitivity of total power losses with respect to the active power injection at a system bus. The partial derivatives of active and reactive power losses in the branch J with respect to active and reactive powers at node n needed in (4-8) and (4-9) are obtained according to [66] as follows.

Active and reactive power losses in the *Jth* branch of the system as a function of the real and imaginary parts of the nodal currents can be obtained using the **BIBC** matrix in the DLF method as below.

$$P_{lossJ}=r_J I_{brJ}{}^2=r_J\left[\left(\sum_{k=2}^{nbus}BIBC_{J,k-1}\,\mathrm{Re}(\underline{I}_k)\right)^2+\left(\sum_{k=2}^{nbus}BIBC_{J,k-1}\,\mathrm{Im}(\underline{I}_k)\right)^2\right] \tag{4-10}$$

$$Q_{lossJ}=x_J I_{brJ}{}^2=x_J\left[\left(\sum_{k=2}^{nbus}BIBC_{J,k-1}\,\mathrm{Re}(\underline{I}_k)\right)^2+\left(\sum_{k=2}^{nbus}BIBC_{J,k-1}\,\mathrm{Im}(\underline{I}_k)\right)^2\right] \tag{4-11}$$

where I_{brJ} is the absolute value of the *Jth* branch current. r_J and x_J are the resistance and reactance of the *Jth* branch, respectively. In above equations, the terms in the first and second parentheses give the real and imaginary parts of the current in the branch J, respectively, where $\mathrm{Re}(\underline{I}_k)$ and $\mathrm{Im}(\underline{I}_k)$ are the real and imaginary parts of the current in node k given by

$$\mathrm{Re}\left(\underline{I}_k\right)=\frac{P_k\cos\theta_{Vk}+Q_k\sin\theta_{Vk}}{V_k} \tag{4-12}$$

$$\mathrm{Im}(\underline{I}_k)=\frac{P_k\sin\theta_{Vk}-Q_k\cos\theta_{Vk}}{V_k} \tag{4-13}$$

where θ_{Vk}, P_k and Q_k are voltage angle, active and reactive powers at bus k, respectively. Substituting for real and imaginary parts of nodal currents from (4-12) and (4-13), sensitivity of active power loss in the branch *J* with respect to active or reactive power at node *n* is obtained from (4-10) as below.

$$\begin{aligned}\frac{\partial P_{lossJ}}{\partial P_n} &= 2r_J\left(\sum_{k=2}^{nbus} BIBC_{J,k-1}\,\mathrm{Re}(\underline{I}_k)\right)\times BIBC_{J,n-1}\frac{\cos\theta_{Vn}}{V_n}\\ &+2r_J\left(\sum_{k=2}^{nbus} BIBC_{J,k-1}\,\mathrm{Im}(\underline{I}_k)\right)\times BIBC_{J,n-1}\frac{\sin\theta_{Vn}}{V_n}\end{aligned} \tag{4-14}$$

$$\begin{aligned}\frac{\partial P_{lossJ}}{\partial Q_n} &= 2r_J\left(\sum_{k=2}^{nbus} BIBC_{J,k-1}\,\mathrm{Re}(\underline{I}_k)\right)\times BIBC_{J,n-1}\frac{\sin\theta_{Vn}}{V_n}\\ &-2r_J\left(\sum_{k=2}^{nbus} BIBC_{J,k-1}\,\mathrm{Im}(\underline{I}_k)\right)\times BIBC_{J,n-1}\frac{\cos\theta_{Vn}}{V_n}\end{aligned} \tag{4-15}$$

When the power at bus *n* passes through the branch *J*, the term $BIBC_{J,n-1}$ in the above equations is equal to 1, otherwise, it is zero. Consequently, if the power at node *n* does not pass through the branch *J*, sensitivity of power loss in branch *J* with respect to power at node *n* will be null. Similarly, derivatives of reactive power loss of branch *J* with respect to active and reactive powers of node *n* are obtained through (4-11) as

$$\begin{aligned}\frac{\partial Q_{lossJ}}{\partial P_n} &= 2x_J\left(\sum_{k=2}^{nbus} BIBC_{J,k-1}\,\mathrm{Re}(\underline{I}_k)\right)\times BIBC_{J,n-1}\frac{\cos\theta_{Vn}}{V_n}\\ &+2x_J\left(\sum_{k=2}^{nbus} BIBC_{J,k-1}\,\mathrm{Im}(\underline{I}_k)\right)\times BIBC_{J,n-1}\frac{\sin\theta_{Vn}}{V_n}\end{aligned} \tag{4-16}$$

$$\begin{aligned}\frac{\partial Q_{lossJ}}{\partial Q_n} &= 2x_J\left(\sum_{k=2}^{nbus} BIBC_{J,k-1}\,\mathrm{Re}(\underline{I}_k)\right)\times BIBC_{J,n-1}\frac{\sin\theta_{Vn}}{V_n}\\ &-2x_J\left(\sum_{k=2}^{nbus} BIBC_{J,k-1}\,\mathrm{Im}(\underline{I}_k)\right)\times BIBC_{J,n-1}\frac{\cos\theta_{Vn}}{V_n}\end{aligned} \tag{4-17}$$

Finally, using (4-14) to (4-17) and having the matrices **R** and **X**, we can obtain the voltage sensitivity coefficients of the IDSA method with respect to nodal active and reactive powers according to (4-8) and (4-9).

4.4. The studied voltage sensitivity analysis methods

In this chapter, the IDSA method is validated through the numerical simulations by changing active and reactive powers at the selected buses of the studied system. Moreover, performance of the IDSA is tested when it is embedded in the MSVCA and SSVCA. The IDSA results are compared with the responses obtained from the DSA, JBSA and POSA methods. The DSA, JBSA and POSA are briefly described in the following sections.

4.4.1. Direct sensitivity analysis

The DSA approach has been introduced in chapter 2. It is directly developed on the basis of the network topology, consequently, it remains independent of the network operating points. The DSA is a simplified version of the IDSA method neglecting the impacts of power losses in the system branches on the node voltages. Therefore, in the DSA method, the sensitivity coefficients are obtained from (2-18) and (2-19) which are equal to (4-8) and (4-9) relating to the IDSA method when disregarding their second and third terms.

4.4.2. Perturb-and-observe sensitivity analysis

Sensitivity of system voltages with respect to the nodal power changes can be obtained based on the perturb-and-observe concept. In this technique, two LF calculations are performed, once considering the initial network operating point and once more taking into account a small power variation at the perturbation point. The voltage variation at the observed point (ΔV_{obs}) due to the power change applied to the perturbation point (ΔP_{pert}) is calculated in order to derive the sensitivity of voltage at the observed node with respect to the power at the perturbation node using the following equation.

$$\frac{\partial V_{obs}}{\partial P_{pert}} = \frac{\Delta V_{obs}}{\Delta P_{pert}} \tag{4-18}$$

In case of applying reactive power change, ΔP_{pert} and P_{pert} in above equation are replaced by ΔQ_{pert} and Q_{pert}, respectively. In this chapter, the initial network operating point is perturbed by 1 kW (or 1 kvar) active (or reactive) power variation in order to calculate the voltage sensitivity coefficients. As it can be noticed, the drawback of this method is that the perturb-and-observe procedure should be repeated for each single node of the system.

4.4.3. Jacobian-based sensitivity analysis

Sensitivity of bus voltages with respect to nodal active and reactive powers is conventionally obtained from the inverse of the Jacobian matrix in the Newton-Raphson LF study. The Jacobian matrix is basically composed through expanding the equations of nodal active and reactive powers by the Taylor series while neglecting all the terms higher than the first order. The inverted Jacobian matrix gives us the linearized relationships between the small changes in nodal voltage angles and magnitudes with the small changes in the real and reactive powers as below.

$$\begin{bmatrix} \boldsymbol{\Delta\theta_V} \\ \mathbf{\Delta V} \end{bmatrix} = \mathbf{J}^{-1} \begin{bmatrix} \mathbf{\Delta P} \\ \mathbf{\Delta Q} \end{bmatrix} \tag{4-19}$$

where $\mathbf{J}^{-1}$ is the inverted Jacobian matrix. Also, $\boldsymbol{\Delta\theta}_V$, $\mathbf{\Delta V}$, $\mathbf{\Delta P}$ and $\mathbf{\Delta Q}$ denote vectors of small variations in voltage angles, voltage magnitudes, active and reactive powers at the PQ buses, respectively. Based on the Taylor series theorem, an analytical function can be represented as an infinite sum of terms that are calculated from the values of the function's derivatives at a single point. Therefore, the linearized relationships extracted from the Taylor series are valid for a single point. As a result, the voltage sensitivity analysis obtained from the Jacobian matrix is also valid for a single point and the sensitivity coefficients need to be updated for other network operating points.

In this work, the JBSA is obtained based on the generic formulation of the Jacobian matrix that can be found in [68] according to which, elements of the Jacobian matrix are partial derivatives of nodal active and reactive powers with respect to node voltage amplitudes and angles. Once the NRLF algorithm is converged, the lower half-part of the square matrix $\mathbf{J}^{-1}$ is used to derive the so-called Jacobian-based voltage sensitivity coefficients with respect to the nodal active and reactive powers.

4.5. Numerical validation of the introduced voltage sensitivity analysis methods through gradual variations of nodal powers

In this section, accuracy of the introduced VSA methods which are the DSA, IDSA, JBSA, and POSA in voltage estimation is examined. To this end, active or reactive power at a unique bus of the system is gradually changed while all other parameters are kept constant. For each point of power variation, voltage at bus k subject to power change at bus n is calculated using each of the studied VSA methods as follows.

$$V_k = V_k^{init} - \left|\frac{\partial V_k}{\partial P_n}\right| \Delta P_n \tag{4-20}$$

where V_k^{init} is the initial voltage value at bus k in the starting point of variation (with power change equal to zero). In case of reactive power changes, P_n and ΔP_n are replaced by Q_n and ΔQ_n in the above equation. In the starting point with power change at bus n equal to zero, the voltage sensitivity at bus k with respect to power at bus n $(\frac{\partial V_k}{\partial P_n})$ is calculated using each of the four abovementioned VSA methods. The voltage sensitivity coefficient corresponding to the starting point is kept constant and used to calculate the voltage at bus k when active or reactive power at bus n is changed. Moreover, LF calculation is carried out for each single point of power variations. Consequently, the latter gives the exact voltage values while using the voltage sensitivity coefficient according to (4-20) (or its reactive power counterpart), the estimated voltage values are obtained. The LF calculation is done using the DLF approach.

The numerical validation of the studied VSA methods is performed on the 77-bus UKGDS shown in figure 3-1. In the starting point of power variation, it is considered that all DGs produce active powers equal to 3.5 MW while their initial reactive powers are zero and the load powers are equal to 10% of their nominal values. The investigation is carried out on the active and reactive power changes (applied separately) at buses 26, 62 and 9. Buses 26 and 62 are selected as they are known to be influenced by the power losses given that they are located at the end of the feeders 1 and 4. Compared to buses 26 and 62, bus 9 is much less affected by the power losses as it is located closer to the slack bus. The simulation results regarding each of the studied buses are presented in the following sections.

4.5.1. On bus 26

The first analysis of this section is done on the active and reactive power changes of bus 26 which is located at the end of feeder 1. To this end, firstly, active power at bus 26 (where DG5 is located) is changed from 0 to 3500 kW by step changes of 1 kW. It corresponds to reducing the active power production of DG5 from its maximum value (3.5 MW) to zero. Figure 4-2 shows the voltage characteristics as a function of active power variations at bus 26 obtained by the studied VSA methods as well as the LF calculations.

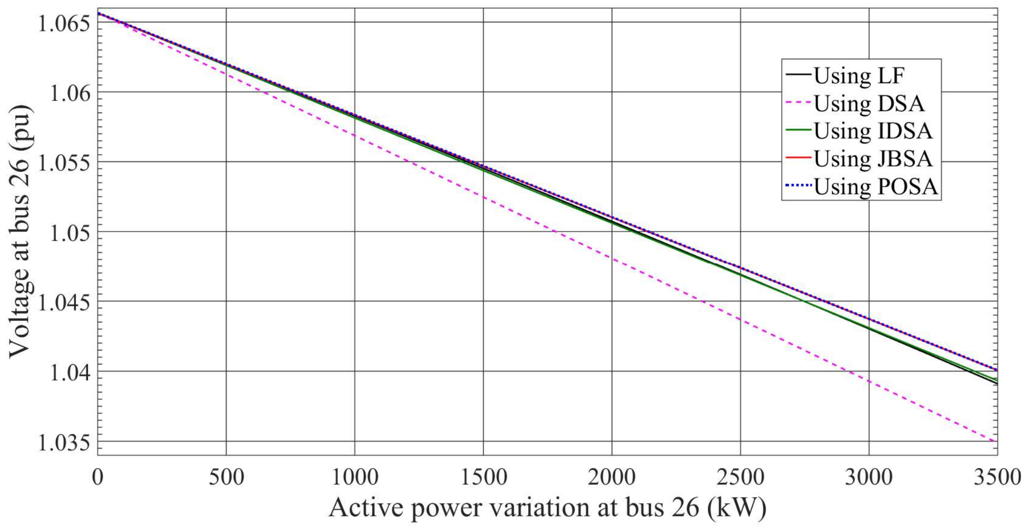

Figure 4-2: Voltage at bus 26 as a function of active power variations at bus 26

As it can be seen in figure 4-2, the DSA method produces high mismatches with regard to the exact value obtained from the LF study. Its error noticeably increases when the active power of bus 26 is largely moved from the starting point. Regarding the JBSA and POSA results, it is seen that they have both accurate voltage estimations at the beginning of power variations while for the active power variations greater than 2000 kW, errors appeared in their estimated voltages with respect to the reference values obtained from the LF. As mentioned before, the JBSA is valid for a single working point considering small changes of active and reactive powers. When the system working point is largely moved by the active or reactive power change, its accuracy is reduced. Similarly, the POSA derives the voltage sensitivity with respect to node power through extracting the slope of the voltage-power characteristic. Given that the latter is obtained by applying a step change equal to 1 kW (or 1 kvar), when the working point is largely moved, the accuracy of linearized relation based on the POSA method is reduced. From figure 4-2, it is noticed that the IDSA has led to the most accurate voltage estimations at bus 26 as the characteristic obtained according to the IDSA is the closest one to the LF-based characteristic.

In the second test, the reactive power at bus 26 is changed from 0 to 3500 kvar by step changes of 1 kvar. The same range of variation is applied to node active and reactive powers for ease of comparison of the voltage results. Given that the initial reactive power of DG5 is 0, the reactive power variations at bus 26 correspond to increasing the reactive power of DG5 towards the inductive direction. The voltage at bus 26 subject to reactive power variation applied at the same bus is calculated using the studied VSA methods and LF calculation similarly to the previous example. The voltage characteristics of bus 26 as a function of reactive power variations are depicted in figure 4-3.

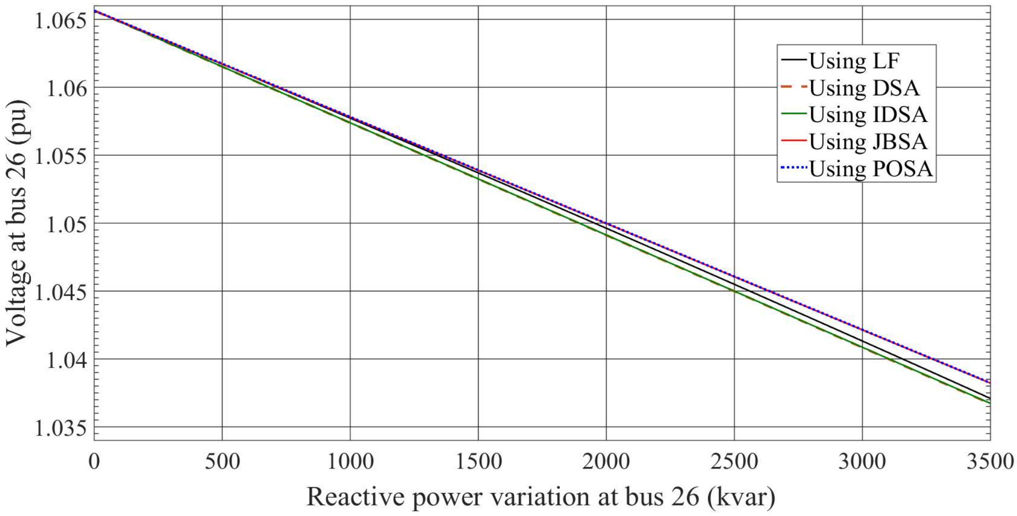

Figure 4-3: Voltage at bus 26 as a function of reactive power variations at bus 26

Taking the results depicted in figure 4-3 into consideration, it is seen that the DSA and IDSA methods have similar performances in response to reactive power changes. The voltage values obtained using these two methods are close to each other though the ones obtained by the IDSA are slightly closer to the points obtained by the LF. It can be concluded that for the studied network working point, the power loss variations (due to reactive power changes at bus 26) do not have a big impact on the voltage-reactive power relationships at bus 26 given that the performance of the IDSA is almost identical to the DSA one.

Moreover, from figure 4-3, it is observed that the JBSA and POSA work well for the reactive power changes smaller than 1500 kvar. Then, when reactive power increases more, the error in voltage estimation raises further such that at the ending point of variation (with reactive power changes equal to 3500 kvar), the mismatch between voltage obtained by the JBSA (or POSA) and LF clearly becomes bigger than the one obtained by the IDSA (or DSA) and LF.

Furthermore, taking figures 4-2 and 4-3 into account, it is noticed that the reactive power variation has slightly greater impact than active power change on the voltage of bus 26 given that the former finally reduces voltage to 1.0357 pu and the latter to 1.0359 pu according to the LF-based results.

4.5.2. On bus 62

The same investigation as performed on the bus 26 is repeated here on the active and reactive power variations at bus 62 (where DG18 is located) to examine the performance of the introduced VSA methods in the voltage estimation of a bus located in another feeder (i.e. feeder 4) of the UKGDS. Figures 4-4 and 4-5 present respectively the voltage at bus 62 subject to the active and reactive power changes (each one applied separately) at that bus.

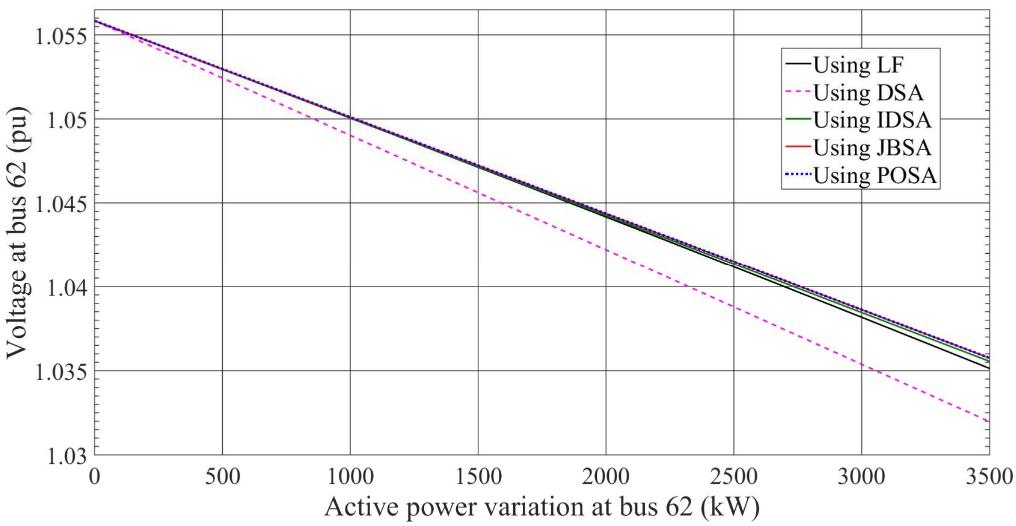

Figure 4-4: Voltage at bus 62 as a function of active power variation at bus 62

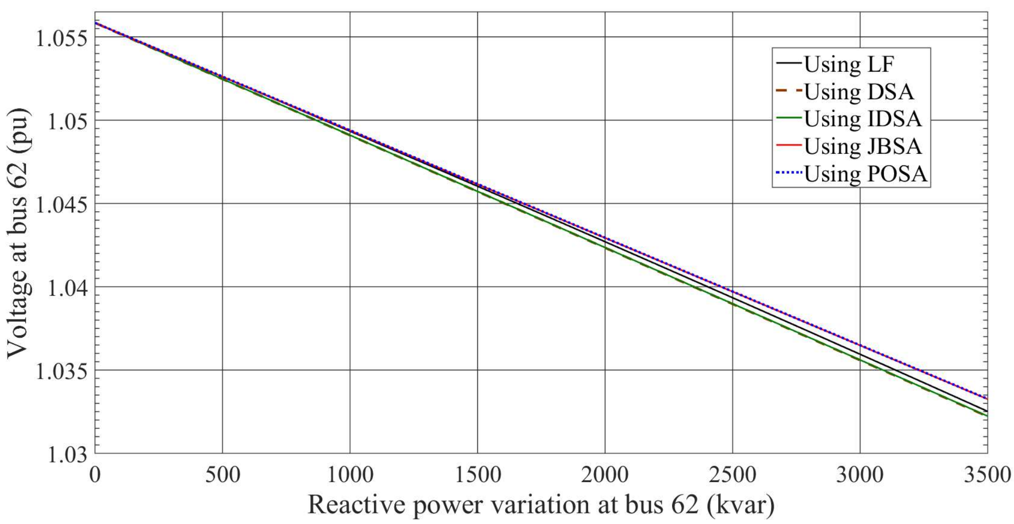

Figure 4-5: Voltage at bus 62 as a function of reactive power variation at bus 62

Considering the voltage characteristics shown in figure 4-4, the same conclusion as the one relating to study on bus 26 subject to active power variation can be made. The IDSA method has very good performance in case of active power changes while the DSA method shows big mismatches. In comparison with the the JBSA and POSA, the IDSA has led to slightly more accurate voltage estimations at the ending points of power variations as it can be seen in figure 4-4. Regarding reactive power changes, both IDSA and DSA methods show similar results (see figure 4-5). Also, small mismatches are found between voltages obtained by the JBSA (or POSA) and the LF-based ones when power variations are not relatively big. In the second half of power variation range, however, errors between the voltages obtained by the JBSA and POSA increase gradually with respect to the LF results.

4.5.3. On bus 9

Finally, the last analysis of this section is carried out on bus 9 (where DG2 is connected) in order to derive the voltage-active (or reactive) power characteristics of this node which is located closer to the slack bus and as a consequence, it is less affected by the power loss factor. In this regard, firstly, the active power at bus 9 is changed from 0 to 3500 kW. The voltage response at bus 9 as a function of the active power change at the same bus is depicted in figure 4-6.

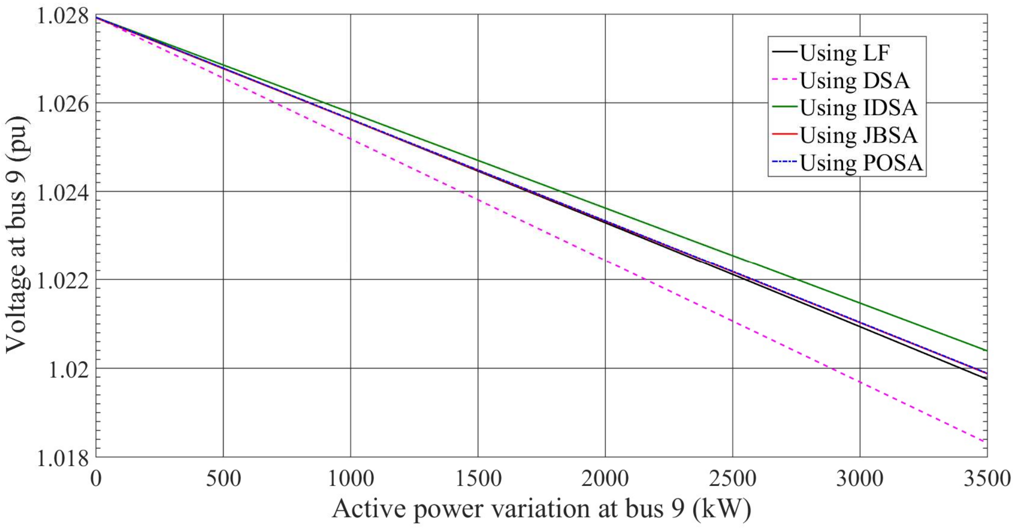

Figure 4-6: Voltage at bus 9 as a function of active power variation at bus 9

In figure 4-6, it is seen that unlike the two previous cases (on buses 26 and 62), for the analysis of bus 9, the JBSA and POSA methods have shown more accurate voltages compred to the ones obtained by the IDSA. Bus 9 is located close to the slack bus while bus 26 is placed at the end of feeder 1. The branch resistance between the transformer to bus 26 is almost 3.5 times bigger than the one from transformer to bus 9. Therefore, it can be expected that the voltage-power relationship at bus 9 is more linear than that of the bus 26 as the branch losses make this relationship non-linear. Consequently, it can be concluded that the JBSA or POSA can present more accurate voltage estimation at bus 9 compared to the case of bus 26. On the other hand, there is an approximation in formulation of the IDSA that neglects the imaginary part of the voltage variation vector since the voltage angles are expected to be small in the distribution systems. This assumption reduces the accuracy of the voltage estimation by the IDSA. Consequently, due to the introduced approximation of the IDSA and because of nearly linear nature of the voltage-power relationship at bus 9, the JBSA or POSA may show more accurate voltage estimation at this bus.

Figure 4-7 shows the voltage at bus 9 subject to the reactive power variations at the same bus. From this figure, it is noticed that all the VSA methods have led to almost accurate voltage estimations, while for reactive power changes greater than 3000 kvar, both DSA and IDSA methods show more accurate results than the JBSA and POSA ones. The IDSA results however are slightly closer to the LF-based values than the DSA ones.

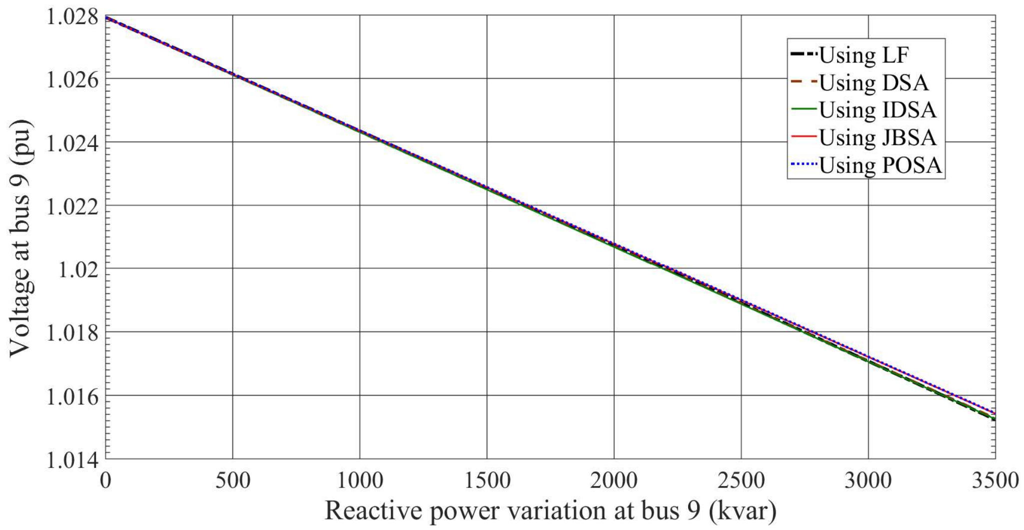

Figure 4-7: Voltage at bus 9 as a function of reactive power variation at bus 9

4.6. Numerical validation of the introduced voltage sensitivity analysis methods using the area between curves index

In this part, a new index is defined in order to evaluate and compare voltage responses obtained by the introduced VSA methods subject to the nodal active and reactive power changes. As it can be seen in figures 4-2 to 4-7, the characteristics of voltage-active (or reactive) power are sometimes very close to each other and it is not easy to distinguish them. In addition, we aim to validate the introduced VSA methods for some other working points of the system. This means that we need to deal with several figures, which cannot be easily interpreted. Consequently, a new index based on the concept of the Area Between Curves (ABC) is defined here. As known, the area between two curves shown in figure 4-8 with the given functions $y_1=f(x)$ and $y_2=g(x)$ between the points a and b is obtained by

$$ABC = \int_a^b f(x) - g(x)dx \tag{4-21}$$

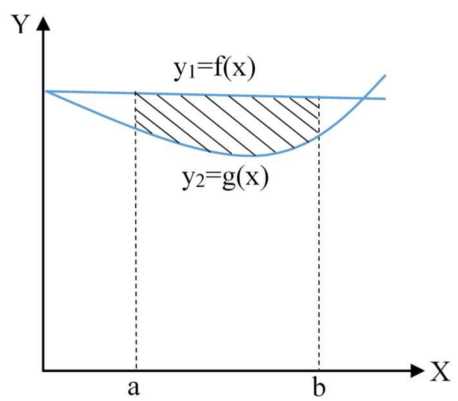

Figure 4-8: Area between the curves of y_1 and y_2

In our application, the error between the estimated voltages obtained according to the VSA and the exact voltages calculated by the LF study is of interest. In this regard, if one of the curves is considered to be obtained by the consecutive LF calculations and another one to be related to estimated points by the VSA, the area between two curves gives us an indicator of the overall accuracy of the VSA method between the studied points *a* and *b*. Thus, if the ABC of the LF and the VSA is small, it is concluded that the estimated voltages obtained by the VSA were close to the exact ones found from the LF study.

In order to implement this technique, the same procedure is followed as the previous section relating to gradual variations of nodal powers. Firstly, gradual changes of active or reactive power at one of the system nodes are applied. The voltage response subject to node power variations is calculated using the VSA method according to (4-20) or its reactive power counterpart. Also, for each point of the node power variations, LF is performed to calculate the exact voltage value. The voltage-active (or reactive) power characteristics obtained by the VSA and LF are now in our disposal. The mathematical function representing the characteristic related to the VSA is known, as it is a linear function with a constant slope equal to $\frac{\partial V_k}{\partial P_n}$ in (4-20). On the contrary, the mathematical function corresponding to the characteristic obtained by the consecutive LF calculations is unknown and its slope is not constant. Therefore, we cannot calculate the area between these two functions according to (4-21). The trapezoidal numerical integration method in MATLAB is utilized to obtain the area between two characteristics relating to LF and VSA results. The trapezoidal method determines the definite integral of *f(x)* over an interval by approximating the area under the curve of the function as trapezoids with more easily computable areas. Given that the gradual power changes are applied with the small steps of 1 kW (or 1 kvar), it is expected that the approximation in trapezoidal method will have negligible effect on the ABC result. Moreover, for all studied VSA methods, the above procedure is repeated separately, each time for the characteristic obtained by one of the studied VSA methods and the LF. Therefore, approximation of the trapezoidal method exists in all analyses of this section. It should be noted that if there are cross points between two characteristics (obtained by the LF and VSA), the total ABC is equal to the sum of the absolute values of the ABC in the subintervals during which one function is above another.

Four cases as presented in below are considered in order to evaluate performance of the studied VSA methods using the ABC factor. The investigation is done on the 77-bus UKGDS shown in figure 3-1. The gradual changes of active (or reactive) power are applied separately to the buses 9, 26 and 62 by step changes of 1 kW (or kvar). The voltage responses with respect to the power changes are calculated at the same bus where power changes are applied using the LF calculations as well as each of the introduced VSA methods.

4.6.1. Case 1

In the first case, it is assumed that DG active and reactive powers are equal to zero while the load powers are at 100% of their respective rated values. The reactive power variations from 0 to 3500 kvar towards the capacitive direction are applied at the selected buses. It simulates the case in which the capacitive reactive power compensation of DGs manages the existing voltage drop problem of the network. Table 4-1 presents the results of calculating the ABC obtained by each of the introduced VSA methods and the LF study at the selected buses.

TABLE 4-1: SIMULATION RESULTS IN CASE 1

	At bus 26	At bus 62	At bus 9
ABC of LF and DSA	1.7816	0.6541	0.7311
ABC of LF and IDSA	**1.0359**	**0.3298**	0.4105
ABC of LF and JBSA	1.7648	1.0635	0.2685
ABC of LF and POSA	1.7648	1.0638	**0.2684**

In table 4-1, it is clearly seen that at all selected buses, the IDSA method outperforms the DSA approach in terms of the accuracy of the performed voltage estimations. It is explained by the fact that the IDSA method presents a complementary formulation of the DSA by taking into account the power loss variation impacts on the node voltages. Similarly, for the study at buses 26 and 62, the IDSA leads to more accurate voltage results compared to the ones obtained by the JBSA and POSA. As known, by getting distance from the slack bus, the series impedance between the slack bus and each single point of the system is increased. Therefore, it can be expected that the voltage-power relationship at bus 26 (or 62) will be more influenced by the power losses than the one at bus 9. Due to the fact that the IDSA incorporates power loss variation impacts on node voltages, it shows a better performance for the study on buses 26 and 62 compared to the JBSA and POSA approaches. On the other hand, there is an approximation in formulation of the IDSA method, which neglects the imaginary part of the voltage variation vector. This approximation reduces the accuracy of the voltage estimation by the IDSA. Consequently, due to the introduced approximation of the IDSA, for the study on bus 9 where power loss impacts on the nodal voltages are not significant, the JBSA or POSA can show more accurate voltage results in comparison with the IDSA. In table 4-1, it is seen that the JBSA and POSA result in identical or very close ABC values.

4.6.2. Case 2

In the second studied case, DG active and reactive powers are equal to 0 and load powers are at 100% of their respective rated values similar to case 1. However, the active power (injection) is changed here from 0 to 3500 kW. It corresponds to the case of solving voltage drop problem by injecting the active power (for instance, from an energy storage device). Table 4-2 gives the ABC results corresponding to the investigation on the selected buses.

TABLE 4-2: SIMULATION RESULTS IN CASE 2

	At bus 26	At bus 62	At bus 9
ABC of LF and DSA	4.4956	1.9261	1.496
ABC of LF and IDSA	**0.7235**	**0.3717**	**0.1087**
ABC of LF and JBSA	1.9789	1.1189	0.241
ABC of LF and POSA	1.9662	1.1181	0.2407

In table 4-2, it is again seen that the IDSA clearly outperforms the DSA method at the selected buses of the studied network. Furthermore, the IDSA method shows more accurate voltage results in comparison with the JBSA and POSA ones too; even at the bus 9 that is known to be less affected by the power losses. From table 4-2, it can be also noticed that the JBSA and POSA have led to very close voltage results like the previous studied case.

4.6.3. Case 3

In case 3, DG active powers are considered to be at their maximum values and DG reactive powers are equal to 0.5 Mvar (inductive). The system loads are also at 10% of their respective rated values. The reactive power changes are done from 0 to 3500 kvar towards the inductive direction at the selected buses of the studied network. It corresponds to the case of solving voltage rise problem by absorbing the reactive power. Table 4-3 gives the ABC results corresponding to voltages obtained by the LF calculations and ones found through each of the VSA methods.

TABLE 4-3: SIMULATION RESULTS IN CASE 3

	At bus 26	At bus 62	At bus 9
ABC of LF and DSA	0.9750	0.802	0.8755
ABC of LF and IDSA	**0.4503**	**0.2904**	0.260
ABC of LF and JBSA	1.4726	0.9570	0.256
ABC of LF and POSA	1.4679	0.9544	**0.255**

In table 4-3, the IDSA method leads to more accurate voltage results compared to the DSA ones at the selected buses. In comparison with the JBSA and POSA, the IDSA shows superior results for the study as buses 26 and 62, and almost similar results at bus 9. The POSA performance remains in very close agreement with the JBSA one.

4.6.4. Case 4

The same working point as the one of the case 3 is considered here. However, in the current test case, the active power injection is changed from 3500 kW to 0 in order to simulate the situation in which the voltage rise problem is managed by the generation curtailment of DGs. Table 4-4 presents the same type of results for the study on case 4.

TABLE 4-4: SIMULATION RESULTS IN CASE 4

	At bus 26	At bus 62	At bus 9
ABC of LF and DSA	7.0716	5.2413	2.3752
ABC of LF and IDSA	**1.0843**	**1.334**	1.4159
ABC of LF and JBSA	1.1933	1.7668	0.1673
ABC of LF and POSA	1.1895	1.7645	**0.1667**

Regarding the results reported in table 4-4, it is seen that the IDSA clearly outperforms the DSA like all the previous cases. For the analyses of buses 26 and 62, the IDSA exhibits better performance compared to the JBSA and POSA ones too. Concerning the investigation on bus 9, however, the JBSA and POSA provide more accurate results compared to the IDSA one. Therefore, it can be noticed that the JBSA and POSA methods with an acceptable accuracy estimate the voltage-power relationships at the buses, which are close to the slack node. On the other hand, by getting distance from the slack bus, nodal voltage-power relationships will be more influenced by power loss variations (caused by the node power changes). As a consequence, the IDSA method can lead to more accurate voltage estimation for analysis of the buses which are relatively far from the slack node. The latter points can be verified considering the results reported in tables 4-1 to 4-4. It is worth noting that for a voltage regulation purpose, power variation at the buses, which are located far from the slack node (like buses 26 and 62) will be mostly demanded as the voltage violations usually occur at the end of the system feeders.

4.7. Comparative study of the introduced voltage sensitivity analysis methods embedded in the multi-step voltage control algorithm

In this section, the MSVCA presented in chapter 3 is used in order to evaluate performance of the studied VSA methods in a centralized closed-loop voltage control application. To this end, the studied VSA methods are embedded separately in the MSVCA. When the DSA, IDSA and POSA methods are tested, the DLF approach is used in the MSVCA. For the JBSA method, the NRLF method is employed. It should be noted that the voltage sensitivity coefficients obtained from the JBSA, POSA and IDSA methods are updated at the end of each iteration of the MSVCA (according to procedure shown in figure 2-3) by the new LF study while their counterparts in the DSA method are kept constant since they are independent of the network working point. The MSVCA including the studied VSA methods is coded in the MATLAB environment. It is applied to the 77-bus UKGDS shown in figure 3-1. Effectiveness of the studied VSA methods is examined in response to separate changes of DG active and reactive powers as well as the case that both active and reactive powers of DGs can be controlled by the MSVCA. In this regard, three cases with different values for weighting coefficients of DG active and reactive powers (i.e. C_P and C_Q) are taken into account as presented in table 4-5.

TABLE 4-5: WEIGHTING COEFFICIENTS OF DG POWER CHANGES IN THE STUDIED CASES

	C_Q	C_P
Case A	1	100
Case B	100	1
Case C	1	1

An identical initial working point is considered in the abovementioned cases. It is supposed that the system loads are at 10% of their respective nominal values, DG active powers are equal to 90% of their rated values (0.9×3.5=3.15 MW) while the initial reactive powers of DGs are set to zero. In this situation, it is expected to deal with the voltage rise problem at the DG-connected buses.

Performance of the four introduced VSA methods embedded in the MSVCA is evaluated and compared in terms of the errors associated with each method. In order to determine the accuracy of the VSA methods, two new parameters are defined by the following equations.

$$MM = 1.03 - V_w^{cor} \tag{4-22}$$

$$Err(\%) = \left| \frac{1.03 - V_w^{cor}}{\Delta V_w^{req}} \right| \times 100 \tag{4-23}$$

where V_w^{cor} is the corrected voltage of the bus with the biggest voltage violation (i.e. bus w). It is obtained by the LF calculation, which is done at the end of each iteration of the MSVCA (see figure 2-3). Given that voltage violation at bus w in each iteration of the MSVCA constructs the binding voltage constraint of the optimization problem, the mismatch between the targeted voltage point (i.e. the 1.03 pu voltage limit) and the corrected voltage at bus w gives us the error arisen from the VSA at each iteration of the MSVCA according to (4-22). Also, the relative error with regard to the required voltage modification (ΔV_w^{req}) at the bus with the biggest voltage violation at each iteration of the MSVCA is obtained using (4-23). These two parameters give us the error arisen from the VSA inside the MSVCA iterations. Therefore, there is no need to depict the node voltages obtained by the MSVCA.

It should be noted that the ampacity limits of the system branches are disregarded in the MSVCA given that we aim at evaluating accuracy of the introduced VSA methods. It is known that considering the ampacity limits, some errors are added to the voltage control problem due to simplification of the proposed formulation for considering the current limits. In this regard, the ampacity limits are neglected here to have the VSA as the only source of the error in the MSVCA.

4.7.1. Case A

In case A, the objective is to study performance of the presented VSA methods in response to only reactive power changes of DGs. To do so, active power curtailment of DGs is penalized with a big weighing coefficient which is 100 times bigger than C_Q as it can be seen in table 4-5. Table 4-6 presents the iterative procedure of returning all the violated voltages inside the permitted voltage range using the MSVCA employing DSA and IDSA methods. Table 4-7 gives the MSVCA results when using the JBSA and POSA approaches.

TABLE 4-6: SIMULATION RESULTS IN CASE A USING THE MSVCA INCORPORATING THE DSA AND IDSA METHODS

	DSA		IDSA	
	I=1	I=2	I=1	I=2
ΔV_w^{req} (pu) w	-0.0298 26	-0.0152 62	-0.0298 26	-0.0152 62
ΔQ_{DGx} (Mvar) x ∈ {1, 2, 3, …, 22}	DG4=1.6336 DG5=2.31	DG18=2.2491	DG4=1.6346 DG5=2.31	DG18= 2.2442
MM (pu)	-3.03×10^{-4}	-2.44×10^{-4}	-2.97×10^{-4}	-2.12×10^{-4}
Err (%)	1.019	1.6	0.998	1.4
OF Tot (Mvar)	6.1927		6.1888	
C_t (s)	0.19		0.5	

TABLE 4-7: SIMULATION RESULTS IN CASE A USING THE MSVCA INCORPORATING THE JBSA AND POSA METHODS

	JBSA		POSA	
	I=1	I=2	I=1	I=2
ΔV_w^{req} (pu) w	-0.0298 26	-0.0148 62	-0.0298 26	-0.0148 62
ΔQ_{DGx} (Mvar) x ∈ {1, 2, 3, …, 22}	DG4=1.8632 DG5=2.31	DG18=2.2736	DG4=1.8645 DG5=2.31	DG18=2.2736
MM (pu)	12.632×10^{-4}	3.2×10^{-4}	12.633×10^{-4}	3.19×10^{-4}
Err (%)	4.239	2.160	4.242	2.157
OF Tot (Mvar)	6.4468		6.4486	
C_t (s)	0.35		0.26	

As it can be seen in tables 4-6 and 4-7, in the first iteration (I=1), the biggest voltage rise is found at bus 26. Then, when the voltage rise at this bus is removed, in the second iteration, voltage at bus 62 has the biggest value of voltage violation. Using all four studied VSA methods, within 2 iterations of the MSVCA, the system voltages are returned to the permitted voltage range. Table 4-6 reveals that the DSA and IDSA methods have both very small errors and they exhibit better performances compared to the JBSA and POSA ones given in table 4-7. It is worth noting that the positive value of *MM* means that the estimated voltage using the VSA has passed the permitted upper limit and entered inside the permitted voltage range while its negative value corresponds to a voltage greater than 1.03 pu.

In I=1 and I=2, the IDSA has estimated the new voltage of bus *w* with the minimum errors while the maximum errors are found in the POSA and JBSA methods. Therefore, it can be concluded that the VSA with respect to reactive power changes in the IDSA (or DSA) method is more accurate than the JBSA and POSA ones for the studied network operating point. Consequently, in case A, the IDSA method solves the voltage control problem with the smallest value of reactive power changes (*OF Tot* = 6.1888 Mvar). It is also observed that the DSA embedded in the MSVCA has led to the shortest calculation time (C_t=0.19 s) given that the latter has a simple formulation.

4.7.2. Case B

In the second case, the MSVCA is used for testing accuracy of the studied VSA methods in response to active power curtailment of DGs. In this regard, C_P is set to 1 and C_Q (relating to DG reactive power variations) is assigned to 100. Table 4-8 shows the performance of the MSVCA employing the DSA method and table 4-9 gives the MSVCA results when incorporating IDSA, JBSA and POSA methods.

TABLE 4-8: SIMULATION RESULTS IN CASE B USING THE MSVCA INCORPORATING THE DSA METHOD

	DSA				
	I=1	I=2	I=3	I=4	I=5
ΔV_w^{req} (pu) w	-0.0298 26	-0.0219 62	-0.0047 20	-0.0029 59	-6×10^{-4} 20
ΔP_{DGx} (MW) x ∈ {1, 2, 3, …, 22}	DG4= 0.321 DG5=3.15	DG17= 0.0816 DG18=3.15	DG4=0.7167	DG17=0.5526	DG4=0.0916
MM (pu)	-0.0037	-0.0026	-4.92×10^{-4}	-3.2×10^{-4}	-0.6×10^{-4}
Err (%)	12.4275	12.032	10.4244	10.9274	9.775
OF Tot (MW)	8.0686				
C_t (s)	0.202				

TABLE 4-9: SIMULATION RESULTS IN CASE B USING THE MSVCA INCORPORATING THE IDSA, JBSA AND POSA METHODS

	IDSA		JBSA		POSA	
	I=1	I=2	I=1	I=2	I=1	I=2
ΔV_w^{req} (pu) w	-0.0298 26	-0.0221 62	-0.0298 26	-0.0221 62	-0.0298 26	-0.0221 62
ΔP_{DGx} (MW) x ∈ {1, 2, 3, …, 22}	DG4=1.0278 DG5=3.15	DG17=0.766 DG18=3.15	DG4=1.166 DG5=3.15	DG17=0.8284 DG18=3.15	DG4=1.1661 DG5=3.15	DG17=0.8285 DG18=3.15
MM (pu)	4.4×10^{-4}	4.56×10^{-4}	12.65×10^{-4}	7.27×10^{-4}	12.63×10^{-4}	7.26×10^{-4}
Err (%)	1.479	2.068	4.241	3.292	4.233	3.287
OF Tot (MW)	8.0938		8.2944		8.2946	
C_t (s)	0.5		0.385		0.25	

Based on the results of table 4-8, it can be concluded that the DSA method cannot estimate accurately the voltage response when active power of DGs is changed. The relative error in all iterations is high and reaches 12.42%. Regarding the results given in table 4-9, it is seen that the IDSA, JBSA and POSA methods show more accurate voltage estimations compared to those of the DSA. In the IDSA method, the maximum relative error is 2.068% while in the JBSA and POSA, it increases to 4.241% and 4.233% which confirms that the IDSA has led to the most accurate voltage estimations in case B.

Considering the total objective function of the MSVCA, the DSA method solves the voltage control problem with the smallest value since in each iteration, the voltage of the bus *w* (i.e. the one with the biggest violation) does not enter inside the permitted voltage range due to its inaccuracy (see *M.M* in table 4-8 which is always negative). Using the JBSA and POSA methods, the system voltages go more inside the permitted voltage range compared to the ones obtained by the IDSA, consequently, the JBSA and POSA solve the voltage control problem with bigger values of total objective function.

4.7.3. Case C

In case C, performance of the MSVCA employing each of the introduced VSA methods is examined when active and reactive power changes of DGs are weighted equally. Consequently, the voltage sensitivity coefficients define which control action should be taken. Table 4-10 presents the MSVCA results when the DSA method is used. Also, table 4-11 gives the results relating to the IDSA, JBSA, and POSA methods.

TABLE 4-10: SIMULATION RESULTS IN CASE C USING THE MSVCA INCORPORATING THE DSA METHOD

	DSA			
	I=1	I=2	I=3	I=4
ΔV_w^{req} (pu) At bus	-0.0298 26	-0.0215 62	-0.0050 20	-0.0029 59
ΔP_{DGx} (MW) $x \in \{1, 2, 3, \ldots, 22\}$	DG5=3.15	DG18=3.147	DG4=0.751	NA
ΔQ_{DGx} (Mvar) $x \in \{1, 2, 3, \ldots, 22\}$	DG5=0.26	NA	NA	DG4=0.1515 DG5=0.3648
MM (pu)	-0.0035	-0.0026	-5.34×10^{-4}	-0.63×10^{-5}
Err (%)	11.8062	12.0261	10.7817	2.185
OF Tot	7.8249			
C_t (s)	0.209			

TABLE 4-11: SIMULATION RESULTS IN CASE C USING THE MSVCA INCORPORATING THE IDSA, JBSA AND POSA METHODS

	IDSA		JBSA		POSA	
	I=1	I=2	I=1	I=2	I=1	I=2
ΔV_w^{req} (pu) w	-0.0298 26	-0.0180 62	-0.0298 26	-0.0181 62	-0.0298 26	-0.0181 62
ΔP_{DGx} (MW) $x \in \{1, 2, 3, \ldots, 22\}$	DG5= 1.406	DG18= 0.41	DG5= 1.57	DG18= 0.5228	DG5= 1.5706	DG18= 0.5236
ΔQ_{DGx} (Mvar) $x \in \{1, 2, 3, \ldots, 22\}$	DG5=2.31	DG18=2.31	DG5=2.31	DG18=2.31	DG5=2.31	DG18=2.31
MM (pu)	-4×10^{-4}	-2.6×10^{-4}	8.83×10^{-4}	3.81×10^{-4}	8.83×10^{-4}	3.8×10^{-4}
Err (%)	1.3449	1.4454	2.9645	2.1101	2.963	2.108
OF Tot	6.4355		6.7127		6.7143	
C_t (s)	0.5		0.37		0.26	

Considering the results of table 4-10, it is noticed that the DSA method shows high errors in I=1, I=2 and I=3 when mostly active powers of DGs are curtailed by the MSVCA. At I=4, as the reactive power changes are applied, the voltage estimation is more accurate. Moreover, from table 4-11, it is noticed that the IDSA, JBSA and POSA methods show better performances than the DSA one. It is also seen that the MSVCA employing the IDSA has resulted in the smallest errors. Consequently, the MSVCA with the IDSA solves the voltage control problem with the lowest control effort.

4.8. Comparative study of the introduced voltage sensitivity analysis methods embedded in the single-step voltage control algorithm

In the last part of this chapter, performance of the introduced VSA methods is tested when they are separately embedded in the SSVCA. Similar to the analysis carried out on the MSVCA, three cases having different weighting coefficients for active and reactive power changes of

DGs are considered here according to table 4-5. Also, an identical initial working point is taken into account in the three cases which is equal to the one presented in the study on the MSVCA (section 4.7). It should be noted that the branch ampacity limits are not taken into account in the SSVCA (similar to the previous section using the MSVCA) as the main aim is to investigate the accuracy of the introduced VSA methods. The simulation results relating to the three studied cases are presented in the following sections.

4.8.1. Case A

As discussed before, the SSVCA is designed to return simultaneously all the violated voltages within the permitted voltage range. In the case A, performance of the studied VSA methods in voltage regulation of the considered working point is tested when reactive power control of DGs is employed by the SSVCA. Table 4-12 presents the SSVCA results when each of the studied VSA methods is utilized. Figure 4-9 shows the initial and corrected voltages obtained by the SSVCA considering each of the studied VSA methods.

TABLE 4-12: SIMULATION RESULTS IN CASE A USING THE SSVCA

	DSA	IDSA	JBSA	POSA
ΔQ_{DGx} (Mvar) $x \in \{1, 2, 3, \ldots, 22\}$	DG4=1.0908 DG5=2.31 DG17=0.0705 DG18=2.31	DG4=1.0923 DG5=2.31 DG17=0.0749 DG18=2.31	DG4=1.291 DG5=2.31 DG17=0.1627 DG18=2.31	DG4=1.292 DG5=2.31 DG17=0.1636 DG18=2.31
OF (Mvar)	5.7812	5.7872	6.0738	6.0757
C_t (s)	0.155	0.355	0.36	0.35

From the results given in table 4-12, it is noticed that the DSA and IDSA methods show very close results when reactive power control of DGs is used, similarly to case A using the MSVCA. This point can be verified by the corrected voltages shown in figure 4-9. As it is seen in that figure, the system voltages obtained by these two methods are very close such that it is difficult to distinguish them. In the considered working point, the initial reactive powers of DGs are zero, which indicate that the reactive power variations do not have considerable effects on branch active and reactive power losses. According to (4-13), assuming that voltage angle at bus *k* is small, the imaginary part of current in node *k* is produced by the reactive power of that node. Therefore, when node reactive powers are zero, (4-15) and (4-17) representing sensitivity of active and reactive power losses with respect to reactive power change are small. As a result, the second and third terms in formulation of the IDSA with respect to reactive power (equation (4-9)) are small too that result in eventually having almost similar sensitivity coefficients from the DSA and IDSA methods.

Moreover, from table 4-12, it is observed that using the JBSA and POSA methods, the voltage control problem is solved with bigger objective functions compared to the DSA and IDSA ones. As a consequence, the system voltages obtained by the JBSA and POSA methods are entered into the permitted voltage range as it can be seen in figure 4-9. This indicates that an error is arisen in the voltage regulation procedure due to inaccuracy of the JBSA and POSA. The maximum errors arisen from the DSA, IDSA, POSA and JBSA methods respectively equal to 3.45×10^{-4} pu, 3.28×10^{-4} pu, 11.56×10^{-4} pu and 11.54×10^{-4} pu, which are the biggest mismatch between the corrected voltages relating to the binding constraints of the SSVCA optimization problem and the 1.03 pu voltage limit in each case.

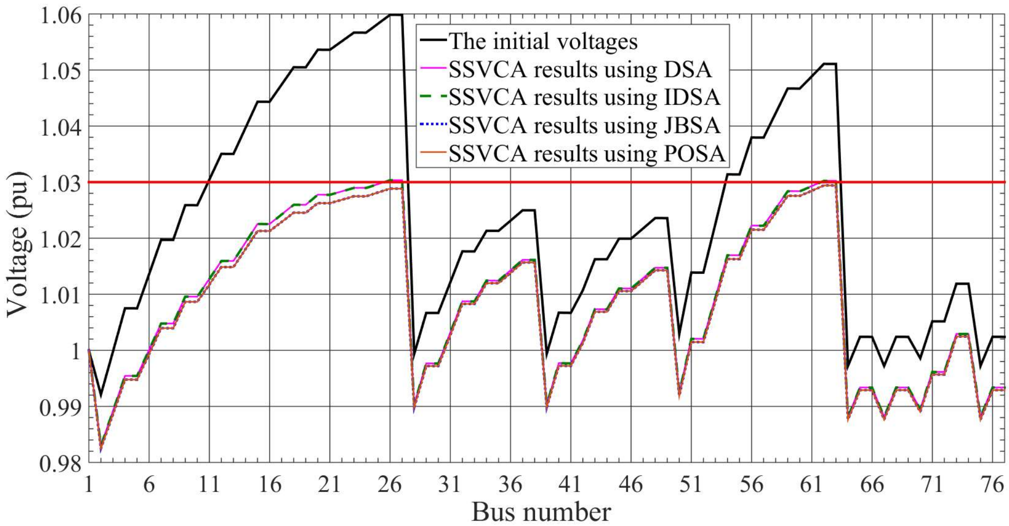

Figure 4-9: The initial and corrected voltages using the SSVCA in case A

4.8.2. Case B

In case B, effectiveness of the studied VSA methods in response to active power curtailment of DGs is tested by the SSVCA. Table 4-13 presents the needed active power curtailment of DGs defined by the SSVCA according to information provided by each of the VSA methods. The initial system voltages as well as the corrected ones obtained by the SSVCA using the studied VSA methods are depicted in figure 4-10.

TABLE 4-13: SIMULATION RESULTS IN CASE B USING THE SSVCA

	DSA	IDSA	JBSA	POSA
ΔP_{DGx} (MW) x ∈ {1, 2, 3, …, 22}	DG4=0.5674 DG5=3.0131 DG17=0.0793 DG18=3.0684	DG4=1.7165 DG5=2.8708 DG17=1.2926 DG18=2.9272	DG4=1.4116 DG5=3.102 DG17=0.9177 DG18=3.1145	DG4=1.4114 DG5=3.1018 DG17=0.9176 DG18=3.1144
OF (MW)	6.7281	8.8071	8.5458	8.5452
C_t (s)	0.155	0.38	0.365	0.34

Taking figure 4-10 into consideration, it is seen that using the DSA, the violated voltages are not completely returned into the permitted voltage range (similarly to the case B using the SSVCA in chapter 3). Therefore, the solution obtained by the SSVCA according to the DSA is not sufficient to remove all the voltage violations. On the contrary, using the IDSA, JBSA and POSA methods, the system voltages are returned into the permitted voltage range. However, as it can be seen in figure 4-10, the corrected voltages are taken back more than the needed values into the permitted voltage range which indicates that these obtained solutions do not correspond to the most optimal one and as a result, an unnecessary amount of active power has been curtailed due to inaccuracy of the IDSA, JBSA and POSA methods. The maximum errors arisen from the DSA, IDSA, POSA and JBSA are respectively equal to 0.0041 pu, 0.0017 pu, 0.0014 pu and 0.0015 pu.

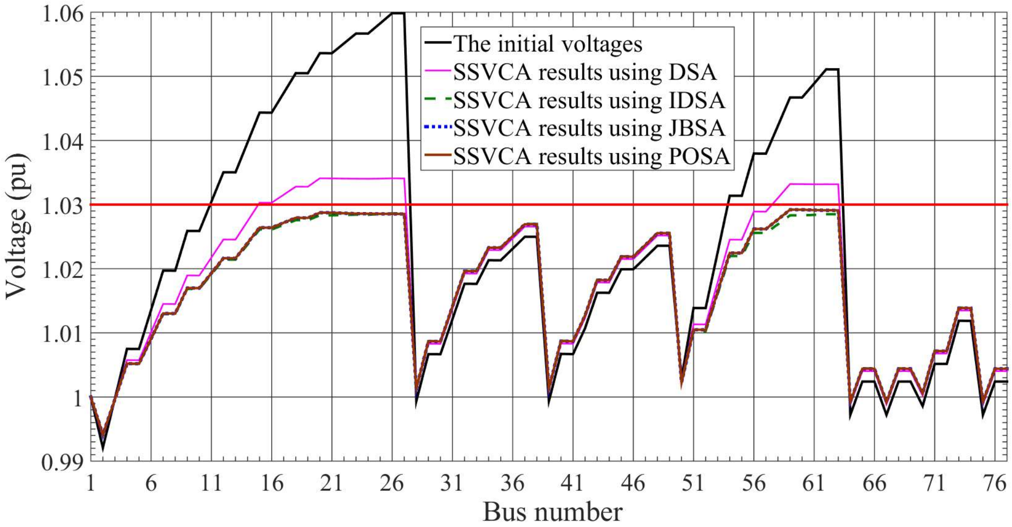

Figure 4-10: The initial and corrected voltages using the SSVCA in case B

4.8.3. Case C

In the last case, considering similar weighting coefficients for active and reactive power changes of DGs, performance of the VSA methods is tested by the SSVCA. The simulation results are reported in table 4-14 and node voltages are depicted in figure 4-11.

TABLE 4-14: SIMULATION RESULTS IN CASE C USING THE SSVCA

	DSA	IDSA	JBSA	POSA
ΔQ_{DGx} (MW) $x \in \{1, 2, 3, \ldots, 22\}$	DG5=2.31 DG18=2.31	DG4=1.0923 DG5=2.31 DG17=0.0749 DG18=2.31	DG4=1.291 DG5=2.31 DG17=0.1627 DG18=2.31	DG4=1.292 DG5=2.31 DG17=0.1636 DG18=2.31
ΔP_{DGx} (Mvar) $x \in \{1, 2, 3, \ldots, 22\}$	DG5=0.8279 DG18=0.2976	NA	NA	NA
OF	5.7455	5.7872	6.0738	6.0757
C_t (s)	0.15	0.35	0.36	0.35

Considering the voltages shown in figure 4-11, it is seen that after voltage regulation by the SSVCA using the DSA, there are small voltage violations remained at the buses located in the end of feeders 1 and 4. It occurs due to inaccuracy of the DSA method with respect to active power changes (relating to ΔP_{DG5} and ΔP_{DG18}). Taking into account the SSVCA results employing other VSA methods, it is found that the corrected voltages are within the permitted voltage range while with the POSA and JBSA, the corrected voltages entered into the permitted voltage range. It indicates that an error exists in the VSA that does not let the SSVCA to find the most optimal solution. The maximum errors arisen form the DSA, IDSA, JBSA and POSA are respectively equal to 0.0015 pu, 0.0003 pu, 0.0012 pu and 0.0012 pu. Given that a smaller error exists in the IDSA, the latter solves the voltage control problem with the lowest objective function (excluding the DSA results as the voltage violations are not completely removed in this case).

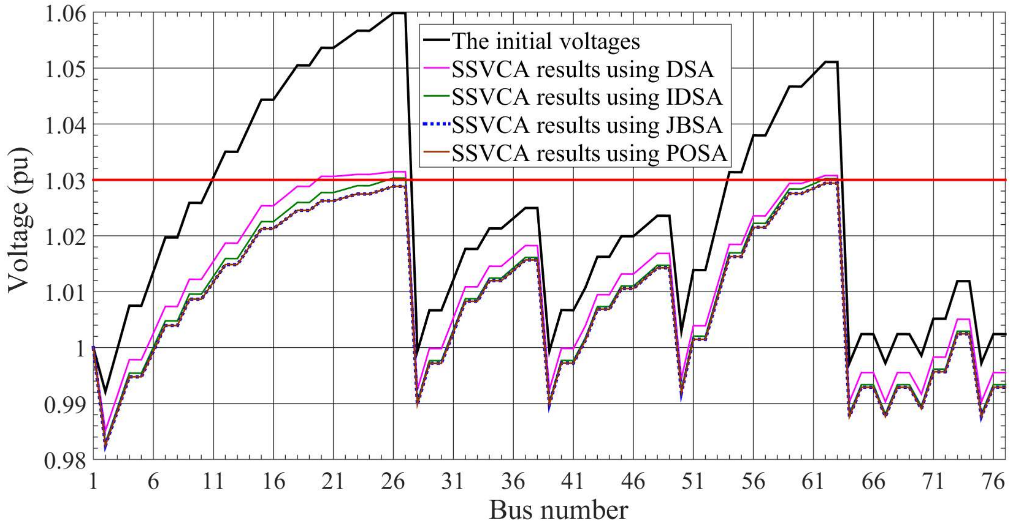

Figure 4-11: The initial and corrected voltages using the SSVCA in case C

4.9. Discussion on the results

4.9.1. Regarding the numerical validation of the voltage sensitivity analysis methods through gradual variations of node powers

The analyses of this section have been carried out on a working point corresponding to the full-generation-and-min-load state resulting in the voltage rise problem in the studied system. Given that the initial reactive powers of DGs are set to zero, node reactive power changes do not have considerable effects on branch active and reactive power losses. Consequently, it is seen that both DSA and IDSA methods exhibit similar performances in case of reactive power changes, although the results obtained by the IDSA are slightly more accurate than the DSA ones. On the contrary, in the considered working point, the initial DG active powers are maximal which means that active power changes have high impacts on the branch active and reactive power losses. Since power loss variations as a function of nodal power changes and their eventual impacts on node voltages are taken into account in the IDSA, it shows superior results to those of the DSA. The latter leads to big mismatches when active power changes are applied (see figures 4-2, 4-4 and 4-6). Therefore, it can be confirmed that the IDSA method is indeed an improved version of the DSA. For the same reason, at the buses which are far from the slack node (like bus 26 or 62) the IDSA shows more accurate voltage estimations compared to the JBSA and POSA ones too.

The JBSA derives analytically the nodal voltage-power relationships based on the Taylor series theorem. Generally, the JBSA has a high accuracy when power variations are small or in the case that the node voltage-power relationships are quite linear. The example for the former condition is when the JBSA is used in the NRLF study where the vectors of nodal power variations (known also as power residuals) are very small. The latter case is similar to the analyses performed at bus 9 of the UKGDS. Due to nearly linear voltage-power characteristic at bus 9 and because of the introduced approximation of the IDSA, the JBSA may show more accurate voltage estimation at this bus compared to the IDSA one (e.g. figure 4-6 corresponding to voltage response at bus 9 subject to active power variation). The last statement is also valid for the POSA method. The JBSA and POSA rely on the similar concept for extracting the voltage sensitivity coefficients; consequently, they lead to almost identical results.

4.9.2. Regarding the numerical validation of the voltage sensitivity analysis methods through the ABC index

On the basis of the investigation performed using the ABC index, it is verified once more that the power losses have direct impacts on the accuracy of the VSA. As it is shown in tables 4-1 to 4-4, the IDSA formulation incorporating power losses has led to considerably better performances compared to the DSA ones. Similarly, at the buses which are far from the slack bus (like buses 26 and 62), the IDSA can have more accurate voltage estimations than the JBSA and POSA ones too.

4.9.3. Regarding the multi-step voltage control algorithm

Performance of the studied VSA methods is tested using the MSVCA when only active or reactive power of DGs is used as well as in the case that both DG active and reactive powers are controlled for the voltage regulation end. In the three studied cases, the MSVCA incorporating the IDSA has led to the most accurate voltage estimations. It is due to the fact that the MSVCA has employed DGs located in the end of feeders for the voltage regulation purpose given that they have higher impacts on the violated voltages. As it has been shown before, the IDSA has a better performance compared to other studied VSA methods at the buses located in the end of feeders. In the IDSA formulation, sensitivity of power losses in all lines with respect to power changes at the DG-connected buses is needed. As a consequence, the calculation time of the MSVCA incorporating the IDSA is increased compared to case of using other studied VSA methods.

Furthermore, it is confirmed again that thanks to the closed-loop functioning mode of the MSVCA, it is capable of solving the voltage control problem even in presence of an inaccurate VSA data. For instance, in case B using the MSVCA, the DSA has led to wrong voltage estimations with the relative errors as big as 12.4%. The voltage violations however have been eventually removed using the DSA with some extra iterations compared to the MSVCA results using other VSA methods.

4.9.4. Regarding the single-step voltage control algorithm

In the SSVCA, when reactive power changes are applied (case A), using all introduced VSA methods, the system voltages are returned into the permitted voltage range while the IDSA leads to the most accurate voltage estimations. In case B when only active powers of DGs are curtailed, the SSVCA incorporating the DSA does not completely solve the voltage control problem and some voltage violations are remained after the voltage regulation. The inaccuracy of the DSA with respect to active power changes is covered in the IDSA. As it can be seen in figure 4-10, the corrected voltages obtained by the SSVCA employing IDSA are within the permitted voltage range. Similarly, using the POSA and JBSA, the voltage violations are removed in case B. However, the corrected voltages obtained according to the IDSA, POSA, and JBSA in case B are entered into the permitted voltage range as it can be seen in figure 4-10. This indicates that the solutions of the SSVCA obtained by these VSA methods do not belong to the most optimal one. From the figures 4-2, 4-4, and 4-6, it can be noticed that the IDSA, POSA and JBSA methods can estimate properly the node voltages subject to active power changes. However, those voltage-active power characteristics are obtained when active power varies only in a single bus of the system and all other parameters are assumed to remain unchanged. In the SSVCA, since the voltage violations at all buses should be removed simultaneously, this last assumption does not hold necessarily. For instance, regarding the considered working point, 27 buses of the UKGDS located in feeders 1 and 4 have different amounts of voltage violations. In order to manage this voltage control problem, contribution of more than one DG is needed. Consequently, because of the mutual impacts of the selected DGs on each other, the accuracy of the VSA is reduced such that the SSVCA cannot find the most optimal solution. It should be noted that the results of case B correspond to the studied working point where all DGs produce active powers equal to 90% of their rated values and load powers are at 10% of their respective nominal values. In the less extreme voltage violation situation, a smaller sum of the DG active power curtailment is needed for the voltage regulation, therefore, the mutual impacts of DG active powers are reduced.

4.9.5. Regarding the management cost of the system

In the proposed VCAs, the C_P and C_Q coefficients can be associated with the real operating costs of DG active and reactive powers. In this way, objective function of the VCA gives us the voltage management cost of the system. The costs of active power curtailment and reactive power control of DGs are equal to 100 €/MWh and 25 €/Mvarh, respectively, according to [19]. Supposing that the control command defined by the VCA will be kept constant for 60 minutes, the voltage management cost of the system can be calculated considering the sum of demanded power changes and its corresponding cost over a 60-minute horizon. For instance, regarding the results given in tables 4-6 and 4-7 (belonging to case A using the MSVCA), the voltage management costs related to the reactive power contribution of the selected DGs are 9289 €, 9283 €, 9670 € and 9673 € when the DSA, IDSA, JBSA and POSA methods have been used respectively. Therefore, it is noticed that having a more accurate VSA can lead to reduction of the system management costs.

4.10. Conclusion

In this chapter, the IDSA method is developed which presents a complementary formulation of the DSA by incorporating variations of power losses in the system branches arisen from the nodal power changes and their eventual impacts on the node voltages. Effectiveness of the IDSA in the voltage estimation is investigated and compared with the voltage results obtained by the DSA, JBSA, and POSA methods. On the basis of the simulation results, it is found basically that the power losses have direct impacts on the accuracy of the VSA methods. When the working point is slightly changed or the power variations are applied at the buses close to the slack node, the power loss impact is small, as a result, the VSA can estimate voltage-power relationship with little error. Conversely, when power at the buses located at the end of feeders is changed, the power loss impacts become considerable. Consequently, it is observed that the DSA, JBSA and POSA cannot accurately estimate the voltage response subject to power variation. In this case, the IDSA method shows a better performance in comparison with other studied VSA methods. In a centralized voltage control application, given that the voltage violations occur mostly at the end of the system feeders, the power changes at the buses located at the end of feeders are demanded. Consequently, it is seen that the VCA employing the IDSA has led to the most accurate voltage estimation.

In the next chapter, the MSVCA and SSVCA are equipped with a complementary functionality to control the voltage level at the secondary side of the substation transformer through the transformer OLTC. The proposed VCAs in the single-step and multi-step forms are utilized in order to manage the voltage control problem of the UKGDS through controlling the DG powers and OLTC set-point.

4.11. Chapter publication

This chapter has led to the following publication:

- B. Bakhshideh Zad, J. Lobry and F. Vallée, "A new voltage sensitivity analysis method incorporating power losses impact," *Electric Power Components and Systems (Under review: initial submission on August 2017, revised paper has been submitted on February 2018).*

Chapter 5: Optimal control of the transformer tap changer and DG powers for managing the voltage constraints

5.1. Abstract

Functionality of the proposed VCAs in the multi-step and single-step forms presented in chapter 3 is evolved here by adding the possibility of controlling the voltage level at the secondary side of the substation transformer through the OLTC. The proposed VCAs of this chapter will have the OLTC action, reactive power control of DGs and active power curtailment of DGs as available measures in order to manage the voltage constraints and will eventually use the most optimal combination of these control options to this end. A straightforward approach is proposed here in order to derive sensitivity of node voltages with respect to the OLTC action. Thanks to the use of the sensitivity data, the voltage control problem is formulated as a linear optimization problem like before. However, due to introduction of the transformer tap changer with a discrete model, the optimization problem is converted into the Mixed-Integer Linear Programing (MILP) having the DG active and reactive powers as the continuous variables and the OLTC set-point as the discrete one. The numerical validation of the proposed centralized sensitivity-based VCAs is carried out on the 77-bus UKGDS in the voltage rise and drop conditions as well as in the case that simultaneous voltage drop and rise violations occur in the system feeders. The accuracy of the voltage estimation obtained by the sensitivity analysis regarding the effect of the OLTC action on the node voltages is investigated.

5.2. On-load tap changer inclusion in the proposed sensitivity-based voltage control approach

On-load tap changer modifies the turn ratio of the transformer winding to provide the voltage regulation possibility at the secondary side of the transformer. The OLTC utilization for managing the voltage constraints has small effect on the branch currents since it directly controls the node voltages. Consequently, it will not cause congestion problem in the system branches and will not affect considerably the power losses. This is the important advantage of the OLTC utilization over the reactive power control of DGs.

Tap changing operation is done with a time delay due to the slow dynamics of the OLTC mechanism. Also, if more than one tap change is needed, each tap movement operation is performed with that specified delay. Dynamic behaviour of the OLTC will not be taken into consideration in this work and OLTC action is modelled by adjustment of the voltage set-point at the bus next to the slack bus (i.e. secondary side of the transformer substation).

The OLTC action is incorporated in the proposed voltage control approach through the sensitivity analysis. Supposing that sensitivity of nodal voltages with respect to transformer tap changes is available, the linearized optimization problems of the MSVCA and SSVCA (presented in chapter 3) will be extended here in order to include the OLTC action.

5.2.1. Sensitivity of node voltages with respect to transformer tap changes

Sensitivity of node voltages with respect to tap changes can be obtained based on the ''perturb-and-observe'' concept. Similarly to the POSA method giving the linearized relations between nodal voltages and powers (presented in section 4.4.2), in order to determine impacts of transformer tap changes on node voltages, two LF calculations are performed while the transformer tap is changed (perturbed) by one step. Then, the node voltages subject to this perturbation of the tap position are evaluated and effects of one step change of the transformer tap on the system voltages are extracted. In addition, an analytical method to derive voltage sensitivity coefficients with respect to the transformer tap position has been introduced in [31]. In this chapter, a straightforward approach is proposed to obtain the latter as follows.

Firstly, it is assumed that the load consumptions and DG powers are independent of the voltage so that the OLTC action will not change their actual values. Secondly, it is supposed that the OLTC will change the voltage of the secondary side of the transformer within the small range, which is defined based on the upper and lower permitted voltage limits of the system. When the transformer tap changes are limited to a small range and the node powers are constant, it can be expected that the tap changes will not affect considerably the node and branch currents. As a result, the voltage variations on the system branches arisen from the OLTC action can be neglected. Therefore, it can be expected that the voltage modification created by a small tap change will be reflected throughout the entire system nodes. In this chapter, impacts of the OLTC action on the system voltages are approximated by the idea that the same voltage change performed on the OLTC point is followed in all the system nodes. Accuracy of this approximation will be tested later through the numerical simulations.

According to [68], OLTC can provide voltage regulation possibility in the range of ±10% of the nominal voltage (i.e. 1 pu) within 40 steps. Therefore, each transformer tap change is equal to 0.005 pu voltage modification at bus 2 (secondary side of the substation transformer) of the studied network. However, the OLTC cannot use its whole range for the voltage regulation due to the limitation of changing the voltage at the tap changer node imposed by the permitted voltage limits. Considering the permitted voltage range which has a threshold of 0.06 pu (from the 0.97 pu lower voltage limit to the 1.03 pu upper voltage bound), it is concluded that in order to have the OLTC voltage within this range, the OLTC action should be limited to 12 steps (12×0.005=0.06 pu). Moreover, an extra limitation is defined for the OLTC action since it is known that there will be a big voltage variation on the impedance of the transformer. Consequently, the OLTC action is limited to 8 (±4) steps that correspond to a voltage regulation equal to ±0.02 pu around 1 pu at the secondary side of the substation transformer. Therefore, sensitivity of node voltages with respect to one step movement of the transformer tap position is equal to 0.005 (0.04/8) pu.

5.3. Sensitivity-based voltage control approach involving OLTC and DG powers

The proposed VCAs of this chapter rely on the linear approximation of the relations between system voltages and decision variables namely reactive power changes of DGs, active power curtailment of DGs and the OLTC set-point. While the first two control variables are continuous, the last one has a discrete or integer nature. In order to include the OLTC in the VCA formulation, it is possible to treat it as a continuous variable and then round the solution of the VCA to the nearest integer value similar to [17]. However, this approach will cause an error in the VCA since what has been demanded by the VCA and what is applied as the control decision is not the same. To avoid such an issue, the voltage control problem should be formulated as a MILP from.

5.3.1. Generic mixed-integer linear programming formulation

In the MILP formulation, the vector of decision variables **x** consists of the continuous and integer variables. The generic MILP formulation is written as

$$\textbf{Minimize: } \mathbf{C}^{T}\mathbf{x} \tag{5-1}$$

$$\mathbf{A}\mathbf{x} \le \mathbf{b} \tag{5-2}$$

$$\mathbf{A}_{eq}\mathbf{x} = \mathbf{b}_{eq} \tag{5-3}$$

$$\mathbf{l}_{b} \le \mathbf{x} \le \mathbf{u}_{b} \tag{5-4}$$

where $\mathbf{C}^{T}$ is the transpose vector of coefficients of linear objective function, **A** is the matrix of the linear inequality constraints and $\mathbf{A}_{eq}$ is the matrix of the linear equality constraints. The upper and lower bounds on the control variables are defined by $\mathbf{u}_{b}$ and $\mathbf{l}_{b}$, respectively. The linear equality and inequality constraints are limited to $\mathbf{b}_{eq}$ and **b**, respectively.

5.3.2. Multi-step voltage control algorithm

As mentioned before in chapters 2 and 3, in the MSVCA, the priority of the voltage regulation is given to the bus with the biggest voltage violation so that at each iteration of the MSVCA, the voltage at the bus with the biggest violation will be returned inside the permitted voltage limits. The MSVCA starts with running an initial LF calculation. If the voltage violations are found in the system, the main iterative-based procedure of the MSVCA starts with I=1. In the first iteration (I=1), the voltage at the bus with the biggest violation is selected and the value of voltage violation from the permitted voltage limit is determined at that bus. It gives us the required value of voltage change in order to return the voltage of that bus inside the permitted voltage range. The voltage regulation at I=1 is formulated as an optimization problem which aims at minimizing the total weighted changes of control variables subject to the voltage constraint relating to the worst voltage violation as well as the bounds on the control variables. The MILP optimization toolbox of MATLAB is used to solve the optimization problem of the MSVCA. Once the optimization problem is solved, the new set-points of DGs as well as the transformer tap position are defined in order to manage the biggest voltage violation in I=1. Then, a new LF calculation is done at the end of the iteration one (including the new set-points of control variables) in order to define whether the MSVCA must go to the next iteration or it can stop. If a new voltage violation is found, the iteration 2 starts, and a new optimization problem is composed to bring back the biggest voltage violation of the second iteration within the permitted voltage limits. By solving this new optimization problem, the control commands that return the biggest voltage violation of the second iteration within the permitted voltage range are defined. Again at the end of I=2, a new LF calculation is performed to decide if the next iteration of the MSVCA is needed or not. The iterative procedure of the MSVCA continues as long as a voltage violation exists.

In the voltage rise case, the required value of voltage change ($\Delta V_w^{req,ri}$) at the bus with the biggest voltage violation (i.e. bus w) is calculated with regard to the permitted upper voltage limit (i.e. the 1.03 pu limit) using the following equation.

$$\Delta V_w^{req,ri} = 1.03 - V_w^{ri} \tag{5-5}$$

where V_w^{ri} is the voltage value at the bus w which has the biggest voltage rise. In order to remove voltage violation of bus w relating to the first iteration of the MSVCA, the following optimization problem is formulated.

$$\textbf{Minimize: } OF = \sum_{x=1}^{N_G} \left(C_Q \Delta Q_{DGx} + C_P \Delta P_{DGx} \right) + C_{TR} \Delta Tap_{TR} \tag{5-6}$$

$$\sum_{x=1}^{N_G} \left(\frac{\partial V_w^{ri}}{\partial Q_{DGx}} \Delta Q_{DGx} + \frac{\partial V_w^{ri}}{\partial P_{DGx}} \Delta P_{DGx} \right) + \frac{\partial V_w^{ri}}{\partial V_{Tap}} \Delta Tap_{TR} \leq \Delta V_w^{req,ri} \tag{5-7}$$

$$0 \leq \Delta P_{DGx} \leq \left| P_{DGx} \right| \quad \forall x,\ x \in G \tag{5-8}$$

$$\Delta Q_{DGx}^{\min} \leq \Delta Q_{DGx} \leq \Delta Q_{DGx}^{\max} \quad \forall x,\ x \in G \tag{5-9}$$

$$\Delta Tap_{TR}^{\min} \leq \Delta Tap_{TR} \leq \Delta Tap_{TR}^{\max} \tag{5-10}$$

where N_G is the total number of DGs that contribute in the voltage control problem. ΔP_{DGx} and ΔQ_{DGx} are the active and reactive power changes of the DG number x. Also, C_P and C_Q are the weighting coefficients for the active and reactive power changes of DGs. ΔTap_{TR} and C_{TR} denote the transformer tap changes, and its corresponding weighting coefficient, respectively. The upper and lower bounds on the control variables are taken into account using (5-8) to (5-10).

In the presented optimization problem, the reactive power changes of DGs and the transformer tap position movements are restricted in the ranges from the negative to positive values while the active power curtailment of DGs is limited to the non-negative bound. In presence of control variables unrestricted in sign, when there is no constraint to limit them, the solution of the linear optimization problem would be the lower or upper bound of those control variables. This is not definitely a proper solution for the voltage control problem. Therefore, similarly to chapter 2, the control variables with the non-positive bounds should be modified such that the linear optimization problem only includes the control variables with the non-negative bounds. To this end, the reactive power changes of DGs will be presented with two auxiliary variables introduced in chapter 2 as

$$\Delta Q_{DGx} = \Delta Q_{DGx}^{ind} - \Delta Q_{DGx}^{cap} \quad (5\text{-}11)$$

where ΔQ_{DGx}^{ind} represents the reactive power changes of DGs towards the inductive direction and ΔQ_{DGx}^{cap} takes into account the capacitive reactive power changes of DGs. Both of these auxiliary variables are restricted in the non-negative ranges. Similarly, the OLTC operation is modelled by the use of two new auxiliary variables as below, which have also non-negative bounds.

$$\Delta Tap_{TR} = \Delta Tap_{TR}^{up} - \Delta Tap_{TR}^{down} \quad (5\text{-}12)$$

where ΔTap_{TR}^{up} and ΔTap_{TR}^{down} include respectively the upward and downward transformer tap position movements in the optimization problem. Substituting for auxiliary variables from (5-11) and (5-12), the above optimization problem is rewritten as follows including five sets of the control variables namely ΔQ_{DGx}^{ind}, ΔQ_{DGx}^{cap}, ΔTap_{TR}^{down}, ΔTap_{TR}^{up} and ΔP_{DGx} which are all restricted to non-negative bounds.

$$\textbf{Minimize: } OF = \sum_{x=1}^{N_G} \left(C_Q \left| \Delta Q_{DGx}^{ind} - \Delta Q_{DGx}^{cap} \right| + C_P \Delta P_{DGx} \right) + C_{TR} \left| \Delta Tap_{TR}^{up} - \Delta Tap_{TR}^{down} \right| \quad (5\text{-}13)$$

$$\sum_{x=1}^{N_G} \left(\frac{\partial V_w^{req,ri}}{\partial Q_{DGx}} (\Delta Q_{DGx}^{ind} - \Delta Q_{DGx}^{cap}) + \frac{\partial V_w^{req,ri}}{\partial P_{DGx}} \Delta P_{DGx} \right) + \frac{\partial V_w^{req,ri}}{\partial V_{Tap}} (\Delta Tap_{TR}^{up} - \Delta Tap_{TR}^{down}) \le \Delta V_w^{req,ri} \quad (5\text{-}14)$$

$$0 \le \Delta P_{DGx} \le \left| P_{DGx} \right| \ \forall x,\ x \in G \quad (5\text{-}15)$$

$$\Delta Q_{DGx}^{\min} \le \Delta Q_{DGx}^{ind} - \Delta Q_{DGx}^{cap} \le \Delta Q_{DGx}^{\max} \quad \forall x,\ x \in G \quad (5\text{-}16)$$

$$\Delta Tap_{TR}^{\min} \le \Delta Tap_{TR}^{up} - \Delta Tap_{TR}^{down} \le \Delta Tap_{TR}^{\max} \quad (5\text{-}17)$$

$$\Delta Q_{DGx}^{ind}, \Delta Q_{DGx}^{cap}, \Delta Tap_{TR}^{up}, \Delta Tap_{TR}^{down} \ge 0 \quad \forall x,\ x \in G \quad (5\text{-}18)$$

In order to have always a positive objective function, ΔQ_{DGx} and ΔTap_{TR} in (5-6) are replaced by the absolute values of their equivalences given in (5-11) and (5-12), respectively. The inequality constraint (5-14) represents the fact that the control variable changes must return the voltage of the bus with the biggest voltage rise inside the permitted voltage range. The voltage sensitivity coefficients in (5-14) are defined parameters. The required value of voltage change for solving the voltage violation at the bus *w* (having the biggest voltage rise) is also a defined parameter but the control variables are unknown that must be optimally selected.

Based on the formulation of the DSA method, it is known that the voltage sensitivity coefficients with respect to active and reactive power changes of DGs have negative values (see (2-18) and (2-19)). On the contrary, the sensitivity of node voltages with respect to the transformer tap movement is positive. Considering the fact that $\Delta V_w^{req,ri}$ is negative in the voltage rise state, in order to satisfy the constraint (5-14), based on the optimality of each of the control decisions, the MSVCA may demand DG reactive power changes towards the inductive direction, curtailment of the DG active powers and decrease of the tap position. It is worth mentioning that the capacitive reactive power changes of DGs and the upward transformer tap movement will not be used in the voltage rise case because they will worsen the voltage violation of the bus *w*.

In the voltage drop condition, given that the permitted lower voltage limit (=0.97 pu) is considered as the targeted point of the MSVCA, the required value of voltage change at the bus with the worst voltage drop is obtained according to

$$\Delta V_w^{req,dr} = 0.97 - V_w^{dr} \tag{5-19}$$

The inequality constraint that takes into account the needed value of voltage modification at the bus with the worst voltage drop violation (i.e. bus *w*) is given by

$$\sum_{x=1}^{N_G}\left(\frac{\partial V_w^{dr}}{\partial Q_{DGx}}(\Delta Q_{DGx}^{ind} - \Delta Q_{DGx}^{cap}) + \frac{\partial V_w^{dr}}{\partial P_{DGx}}\Delta P_{DGx}\right) + \frac{\partial V_w^{dr}}{\partial V_{Tap}}(\Delta Tap_{TR}^{up} - \Delta Tap_{TR}^{down}) \geq \Delta V_w^{req,dr} \tag{5-20}$$

In the voltage drop state, $\Delta V_w^{req,dr}$ is positive, $\frac{\partial V_w^{dr}}{\partial V_{Tap}}$ is also positive, but $\frac{\partial V_w^{dr}}{\partial Q_{DGx}}$ and $\frac{\partial V_w^{dr}}{\partial P_{DGx}}$ are negative, thus, in order to satisfy the abovementioned voltage constraint, reactive powers of DGs must change towards the capacitive direction and the tap position should move upward. It is worth noting that in the voltage drop state, active power curtailment of DGs will not be used since it will worsen the voltage violation issue. The optimization problem of the MSVCA mentioned in (5-13) to (5-18) is generally valid for the voltage regulation in the voltage drop state with one exception (difference) that the inequality constraint regarding the required value of voltage modification given in (5-14) must be replaced by the one in (5-20).

5.3.2.1. Multi-step voltage control algorithm adaptation to manage the simultaneous voltage rise and drop violations

So far, it has been supposed that there are homogeneous voltage violations in all the system feeders meaning that the voltage violations happen either from the permitted upper or lower voltage limit. However, it is possible to have voltage rise problem in one feeder and simultaneously voltage drop issue in another one. The MSVCA should be reformulated accordingly in order to be able to manage voltage violations of such a situation. First of all, when there are both voltage rise and drop issues, the MSVCA must be modified in order to consider simultaneously the biggest voltage violation from each of the upper and lower voltage limits. In this way, it is guaranteed that the corrective decision made for the voltage regulation at the bus with the biggest voltage rise will not exacerbate the voltage violation at the bus with the worst voltage drop issue and vice versa.

Moreover, in each iteration of the MSVCA, in addition to the constraints corresponding to the current biggest voltage violations from the upper and lower voltage limits, the ones related to the previous iterations should be taken into account in order to ensure that the voltage regulation in the current iteration will not create problem for the voltages that have been already corrected. The optimization problem of the MSVCA to manage the voltage constraints while having simultaneous voltage rise and drop issues is written as follows.

$$\textbf{Minimize: } OF=\sum_{x=1}^{N_G}\left(C_Q\left|\Delta Q_{DGx}^{ind}-\Delta Q_{DGx}^{cap}\right|+C_P\Delta P_{DGx}\right)+C_{TR}\left|\Delta Tap_{TR}^{up}-\Delta Tap_{TR}^{down}\right| \tag{5-21}$$

$$\sum_{x=1}^{N_G}\left(\frac{\partial V_w^{dr}}{\partial Q_{DGx}}(\Delta Q_{DGx}^{ind}-\Delta Q_{DGx}^{cap})+\frac{\partial V_w^{dr}}{\partial P_{DGx}}\Delta P_{DGx}\right)+\frac{\partial V_w^{dr}}{\partial V_{Tap}}(\Delta Tap_{TR}^{up}-\Delta Tap_{TR}^{down})\geq \Delta V_w^{req,dr} \tag{5-22}$$

$$\sum_{x=1}^{N_G}\left(\frac{\partial V_w^{ri}}{\partial Q_{DGx}}(\Delta Q_{DGx}^{ind}-\Delta Q_{DGx}^{cap})+\frac{\partial V_w^{ri}}{\partial P_{DGx}}\Delta P_{DGx}\right)+\frac{\partial V_w^{ri}}{\partial V_{Tap}}(\Delta Tap_{TR}^{up}-\Delta Tap_{TR}^{down})\leq \Delta V_w^{req,ri} \tag{5-23}$$

$$0\leq \Delta P_{DGx}\leq \left|P_{DGx}\right| \quad \forall x,\ x\in G \tag{5-24}$$

$$\Delta Q_{DGx}^{\min}\leq \Delta Q_{DGx}^{ind}-\Delta Q_{DGx}^{cap}\leq \Delta Q_{DGx}^{\max} \quad \forall x,\ x\in G \tag{5-25}$$

$$\Delta Tap_{TR}^{\min}\leq \Delta Tap_{TR}^{up}-\Delta Tap_{TR}^{down}\leq \Delta Tap_{TR}^{\max} \tag{5-26}$$

$$\Delta Q_{DGx}^{ind},\Delta Q_{DGx}^{cap},\Delta Tap_{TR}^{up},\Delta Tap_{TR}^{down}\geq 0 \quad \forall x,\ x\in G \tag{5-27}$$

The inequality constraint (5-22) represents the needed voltage modification at the bus with the worst voltage drop violation while constraint (5-23) gives the required value of voltage change to return the biggest voltage rise within the 1.03 pu voltage limit. Constraints (5-24) to (5-27) take into account the upper and lower bounds of the control variables.

5.3.3. Single-step voltage control algorithm

The SSVCA as introduced before in chapters 2 and 3 is designed to return simultaneously all the violated voltages inside the permitted voltage range. It is formulated as an optimization problem which aims at minimizing the total weighted changes of the control variables subject to the voltage constraints regarding all the violated voltages as well as the limits on the control variables. The MILP optimization toolbox of MATLAB is used to solve the optimization problem of the SSVCA. Once the optimization problem is solved, the needed contribution of each control variable to solve the voltage control problem is defined. Then, a new LF calculation is carried out including the new set-points of control variables. At this stage, the corrected system voltages obtained by the LF study are plotted and the SSVCA stops.

The SSVCA starts with running an initial LF calculation. If voltage violations are found in the system, all buses with the voltage violations are selected. Set U includes the buses with the voltage rise issue. For each bus with the voltage rise, the required value of voltage modification to remove the voltage violation is calculated with regard to the 1.03 pu voltage limit using the equation given in below.

$$\Delta V_u^{req}=1.03-V_u \quad \forall u,u\in U \tag{5-28}$$

where u is index for the buses with the voltage rise violation. Regarding the voltage drop state, at each bus with the voltage violation, the needed value of voltage modification is obtained with reference to the 0.97 pu voltage limit as

$$\Delta V_l^{req} = 0.97 - V_l \quad \forall l, l \in L \tag{5-29}$$

where l is index for the buses with the voltage drop and set L contains all buses with the voltage drop issue. The optimization problem of the SSVCA is given by

$$\textbf{Minimize: } OF = \sum_{x=1}^{N_G} \left(C_Q \left| \Delta Q_{DGx}^{ind} - \Delta Q_{DGx}^{cap} \right| + C_P \Delta P_{DGx} \right) + C_{TR} \left| \Delta Tap_{TR}^{up} - \Delta Tap_{TR}^{down} \right| \tag{5-30}$$

$$\sum_{x=1}^{N_G} \left(\frac{\partial V_l}{\partial Q_{DGx}} (\Delta Q_{DGx}^{ind} - \Delta Q_{DGx}^{cap}) + \frac{\partial V_l}{\partial P_{DGx}} \Delta P_{DGx} \right) + \frac{\partial V_l}{\partial V_{Tap}} (\Delta Tap_{TR}^{up} - \Delta Tap_{TR}^{down}) \geq \Delta V_l^{req} \quad \forall l, l \in L \tag{5-31}$$

$$\sum_{x=1}^{N_G} \left(\frac{\partial V_u}{\partial Q_{DGx}} (\Delta Q_{DGx}^{ind} - \Delta Q_{DGx}^{cap}) + \frac{\partial V_u}{\partial P_{DGx}} \Delta P_{DGx} \right) + \frac{\partial V_u}{\partial V_{Tap}} (\Delta Tap_{TR}^{up} - \Delta Tap_{TR}^{down}) \leq \Delta V_u^{req} \quad \forall u, u \in U \tag{5-32}$$

$$0 \leq \Delta P_{DGx} \leq \left| P_{DGx} \right| \ \forall x,\ x \in G \tag{5-33}$$

$$\Delta Q_{DGx}^{\min} \leq \Delta Q_{DGx}^{ind} - \Delta Q_{DGx}^{cap} \leq \Delta Q_{DGx}^{\max} \quad \forall x,\ x \in G \tag{5-34}$$

$$\Delta Tap_{TR}^{\min} \leq \Delta Tap_{TR}^{up} - \Delta Tap_{TR}^{down} \leq \Delta Tap_{TR}^{\max} \tag{5-35}$$

$$\Delta Q_{DGx}^{ind}, \Delta Q_{DGx}^{cap}, \Delta Tap_{TR}^{up}, \Delta Tap_{TR}^{down} \geq 0 \quad \forall x,\ x \in G \tag{5-36}$$

The aforementioned optimization problem presents the generic formulation of the SSVCA. In the case that there is only voltage drop or rise issue, the corresponding voltage constraint to that case which would be either (5-31) or (5-32), respectively, is considered in the optimization problem.

5.4. Simulation results

The numerical validation of the proposed VCAs in the multi-step and single-step forms will be carried out on the 77-bus UKGDS presented in figure 3-1. The VCAs will be used to manage the voltage control problem when there is only voltage rise or drop violation as well as in the case of having simultaneous voltage drop and rise issues in the system feeders.

In the studied cases, it is supposed that the OLTC action has the smallest weighing coefficient compared to other control variables in order to have a dominant involvement of the OLTC in the voltage control problem. In this regard, C_{TR} is set to 1 while the reactive power changes of DGs are weighted by the coefficient which is 50% bigger than the OLTC one (C_Q=1.5). Also, the active power curtailment of DGs is penalized by the coefficient which is 100% bigger than the OLTC one (C_P=2). It should be noted that since the main focus is to evaluate performance of the OLTC in the VCAs and the latter does not cause congestion problem while managing the voltage constraints, ampacity limits of branches are disregarded in the simulated cases of this chapter.

5.4.1. Using the multi-step voltage control algorithm

In the first part of the simulated cases, the MSVCA is utilized in order to manage the system voltages in three considered cases when dealing with only voltage rise and voltage drop issue as well as the case where both voltage drop and rise violations exist simultaneously.

5.4.1.1. In the voltage rise state

In order to create voltage rise state, a working point is considered in which the loads are at 10% of their respective nominal values and DG active powers are equal to 90% of the rated values while the initial reactive powers of DGs are set to zero. Table 5-1 gives the optimal contribution of the control variables demanded by the MSVCA in order to solve the voltage control problem. As it can be seen, within 2 iterations of the MSVCA, the voltage violations are returned into the permitted voltage range. The initial system voltages as well as the corrected ones obtained by the MSVCA are depicted in figure 5-1.

TABLE 5-1: MSVCA RESULTS IN THE VOLTAGE RISE CONDITION

	I=1	I=2
$\Delta V_w^{req,ri}$ (pu)	-0.0298	-0.008
w	26	62
ΔQ_{DGx} (Mvar)	DG5=2.31	DG18= 0.4396
ΔP_{DGx} (MW)	DG5=0.0848	NA
ΔTap_{TR}	-2	-1
OF Tot	7.293	

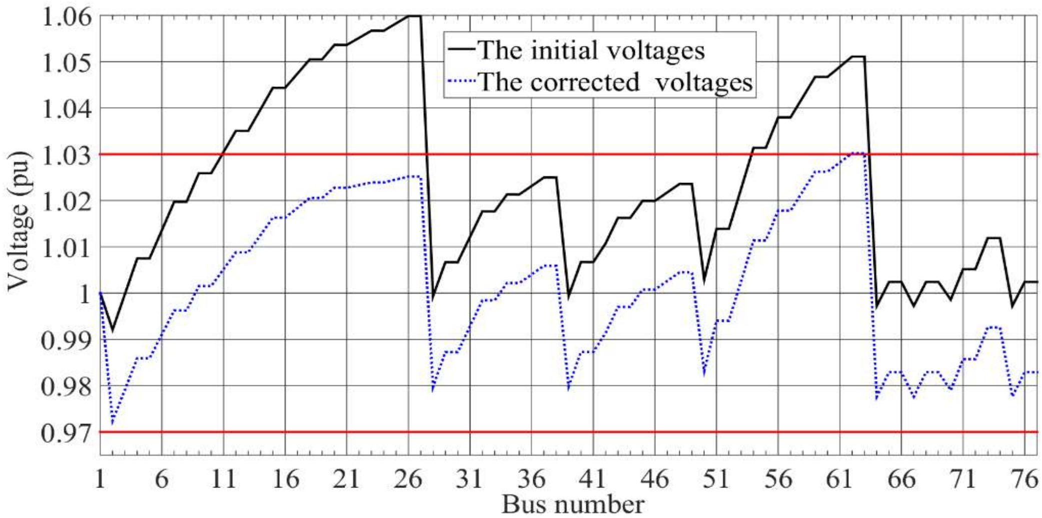

Figure 5-1: System voltages obtained by the MSVCA in the voltage rise condition

In the studied working point, the biggest initial voltage violation is found at bus 26. In the first iteration of the MSVCA, DG5 has been used with its maximum available reactive power (=2.31

Mvar) as it has the biggest influence on the voltage at bus 26. The rest of needed voltage correction is provided by decreasing the OLTC position to two lower steps and curtailing the active power of DG5 equal to 0.0848 MW. At I=2, the inductive reactive power changes of DG18 and one step decrease of the tap position manage the voltage violation at bus 62. In the end of I=2, the voltage at bus 62 reaches the 1.03 pu voltage limit and since there is no other voltage violation, the MSVCA stops at this point.

5.4.1.2. In the voltage drop state

In the working point regarding the voltage drop state, all loads are considered to be at their maximum values while DG active and reactive powers are equal to zero. It leads to voltage violations, which are found in the feeder 1 from buses 9 to 27 and in the end of feeder 4 at the buses 61, 62, and 63. Table 5-2 presents the MSVCA results to return theses violated voltages within the permitted voltage range. The initial system voltages and the ones obtained after the voltage regulation by the MSVCA are shown in figure 5-2.

TABLE 5-2: MSVCA RESULTS IN THE VOLTAGE DROP CONDITION

	I=1	I=2
$\Delta V_w^{req,dr}$ (pu) w	0.0217 27	0.008 21
ΔQ_{DGx} (Mvar)	DG5=-2.621	DG5=-0.113
ΔTap_{TR}	NA	NA
OF Tot	4.102	

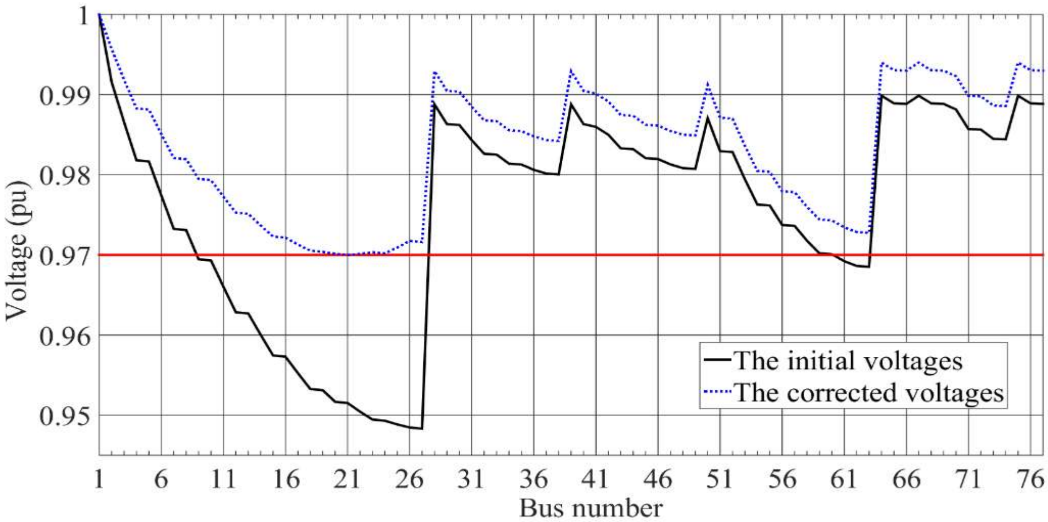

Figure 5-2: System voltages obtained by the MSVCA in the voltage drop condition

In the studied working point for the voltage drop condition, active power productions of all DGs are equal to zero, therefore, the available reactive power capacities of DGs are increased to 3.325 (=0.95×3.5) Mvar according to table 2-1 presenting the capability curve of DGs. Consequently, the MSVCA will only use reactive power changes of DG5 in the iterations one and two to solve the voltage drop of the buses 27 and 21 located in feeder 1. The initial voltage drop of the buses located at the end of the feeder 4 is managed while solving the voltage violations at the buses 27 and 21 in the feeder 1.

5.4.1.3. In the simultaneous voltage drop and rise problems

In order to create simultaneous voltage rise and drop violations, it is supposed that in the feeder 1, all the loads are at their maximal values and active power productions of DGs are equal to zero while in all other feeders, loads are equal to 10% of the nominal values and active powers of DGs are equal to 90% of their rated powers. The considered working point creates violations of lower permitted voltage limit in the feeder 1 while, in the feeder 4, voltage violations from the 1.03 pu limit are found at the buses 54 to 63. Table 5-3 summarizes the MSVCA performance for managing the voltage constraints. Also, figure 5-3 depicts the node voltages of the studied case.

TABLE 5-3: MSVCA RESULTS HAVING SIMULTANEOUS VOLTAGE RISE AND DROP VIOLATIONS

	I=1		I=2			
V_w (pu) w	0.9507 26	1.0523 62	0.9708 26	1.0315 62	1.032 59	0.9691 20
ΔQ_{DGx} (Mvar) $x \in \{1, 2, 3, \ldots, 22\}$	DG5= -2.8 DG18=2.31		DG4= -0.24 DG17= 0.425			
ΔP_{DGx} (MW) $x \in \{1, 2, 3, \ldots, 22\}$	DG18=1.591		NA			
ΔTap_{TR}	NA		NA			
OF Tot	11.844					

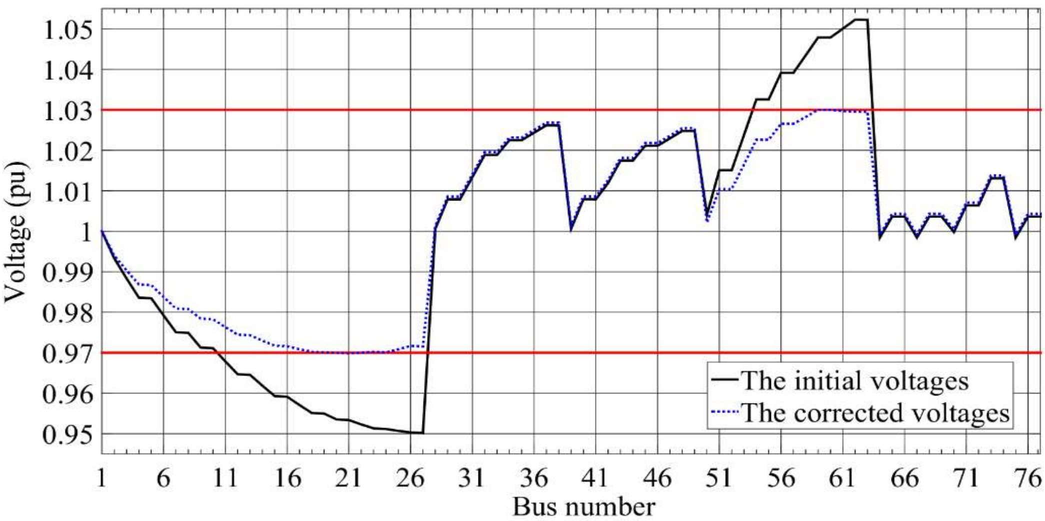

Figure 5-3: System voltages obtained by the MSVCA when having simultaneous voltage rise and drop violations

As it can be seen in table 5-3, in I=1, the biggest voltage rise and drop violations happen at buses 62 and 26, respectively. In order to manage the voltage violations at I=1, the active power production of DG18 located at bus 62 is curtailed by 1.591 MW and its reactive power is changed by 2.31 Mvar (inductive utilization). Also, DG5 located at bus 26 is asked to provide

2.8 Mvar capacitive reactive power (to increase the voltages of feeder 1). In I=2, the biggest voltage rise and drop violations occur at buses 59 and 20, respectively. In addition to the voltage constraints regarding buses 59 and 20, the previous corrected voltages at buses 26 and 62 should be also taken into account. In I=2, DG4 is used to increase the voltage values in the end of the feeder 1 by providing 0.24 Mvar capacitive reactive power and DG17 is asked to increase its reactive power to 0.425 Mvar to reduce the voltages in the feeder 4. Figure 5-3 confirms that the corrected voltages obtained at the end of I=2 have been effectively placed within the permitted voltage range.

It is worth mentioning that the OLTC has not been employed in the voltage regulation procedure because when both voltage rise and drop issues exist, the OLTC action solves the voltage violations of one direction but it simultaneously worsens the voltage violations of another direction.

5.4.2. Using the single-step voltage control algorithm

In the second part of the simulations, the SSVCA is used to manage the voltage violations of the same working points as mentioned in the previous section corresponding to the voltage rise case, voltage drop state, and simultaneous violations of the upper and lower voltage limits.

5.4.2.1. In the voltage rise state

As known, the SSVCA manages all the voltage violations at once. In the voltage rise state, there will be number of $[U]$ inequality constraints taken from (5-32) where $[U]$ is cardinality of set U that includes all buses with the voltage rise. Table 5-4 presents the SSVCA results in the voltage rise case. Given that the transformer tap changer has a high impact on all violated voltages and its impact is identical on all nodes, the tap changer position is decreased by 4 steps which is its maximum possible movement. The reactive power of DG5 is also changed by 1.191 Mvar (inductive) to provide the rest of the needed voltage change for satisfying the voltage constraints. The initial voltages and the ones obtained after the voltage regulation by the SSVCA are depicted in figure 5-4.

TABLE 5-4: SSVCA RESULTS IN THE VOLTAGE RISE CONDITION

ΔQ_{DGx} (Mvar) $x \in \{1, 2, 3, \ldots, 22\}$	DG5=1.191
ΔP_{DGx} (MW) $x \in \{1, 2, 3, \ldots, 22\}$	NA
ΔTap_{TR}	-4
OF	5.786

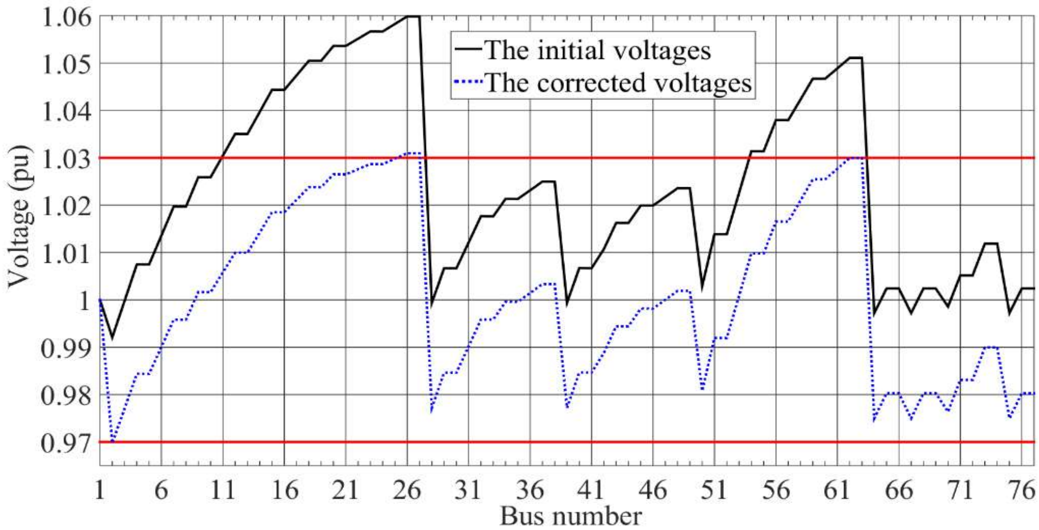

Figure 5-4: System voltages obtained by the SSVCA in the voltage rise condition

In figure 5-4, it is seen that after voltage regulation, the voltage at bus 2 (secondary side of the substation transformer) reaches 0.97 pu while the OLTC position has been decreased by 4 steps. It verifies the necessity of the extra limit that was defined for the OLTC action to restrict it within 8 steps (±4 step changes from 1 pu). As stated before, there is a big voltage variation on the transformer impedance that should be taken into account when defining the OLTC bounds.

Furthermore, when the voltage regulation using the SSVCA has been completed, it is observed from figure 5-4 that small voltage violations remain at the buses located in the end of feeder 1. This is due to the inaccuracy of the sensitivity data used inside the SSVCA to linearize impacts of the control variables on the node voltages.

5.4.2.2. In the voltage drop state

In the voltage drop case, the main voltage violations happen in feeder 1. Reactive power change of DG5 which has the biggest impact on the voltages at the end of the feeder 1 together with the transformer tap movement are employed by the SSVCA in order to remove the voltage violations. Table 5-5 presents the SSVCA results in the voltage drop case. The initial and corrected voltages are depicted in figure 5-5.

TABLE 5-5: SSVCA RESULTS IN THE VOLTAGE DROP CONDITION

ΔQ_{DGx} (Mvar) $x \in \{1, 2, 3, \ldots, 22\}$	DG5=-1.44
ΔTap_{TR}	2
OF	4.16

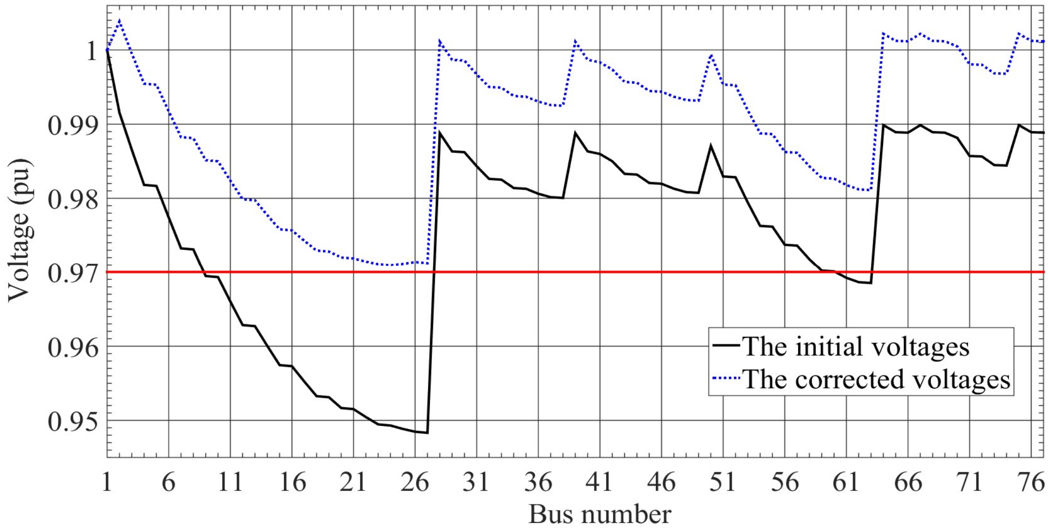

Figure 5-5: System voltages obtained by the SSVCA in the voltage drop condition

In the voltage drop case, the initial voltage violation at bus 24 constructs the only binding voltage constraint of the SSVCA. Therefore, the error arisen from the VSAs (relating to reactive power change of DG5 and OLTC action) can be found from the corrected voltage of bus 24 in figure 5-5. The latter is equal to 0.9709 pu which indicates that an error equal to 0.0009 pu is arisen in the SSVCA due to the VSA inaccuracies.

5.4.2.3. In the simultaneous voltage drop and rise problems

In the considered working point for simultaneous voltage rise and drop violations, the lower voltage limit violations are found in feeder 1 while the upper voltage limit violations happen in feeder 4. Table 5-6 presents the optimal values of the control variable changes to manage the voltage constraints and the corrected voltages are shown in figure 5-6.

TABLE 5-6: SSVCA RESULTS HAVING SIMULTANEOUS VOLTAGE RISE AND DROP VIOLATIONS

ΔQ_{DGx} (Mvar) x ∈ {1, 2, 3, …, 22}	DG5=-3.189 DG17=0.686 DG18=2.31
ΔP_{DGx} (MW) x ∈ {1, 2, 3, …, 22}	DG18=1.116
ΔTap_{TR}	NA
OF	11.509

As it can be seen in table 5-6, the transformer tap changer has not been employed by the SSVCA since using OLTC to solve the voltage rise problem in feeder 4 will worsen the voltage drop issue of the feeder 1 and vice versa. Moreover, reactive power changes of DGs in one feeder have impacts on voltages of other feeders due to presence of the transformer reactance which is like a common point among all feeders. Therefore, in presence of both voltage rise and drop problems, an efficient control option should have big impacts on the violated voltages of its own feeder while having less undesired effects on the voltages of the other feeders. Considering the impacts of the control variables on the violated voltages, the SSVCA asked capacitive reactive changes of DG5 in order to increase the voltages in feeder 1. It also employed active power curtailment of DG18 and inductive reactive power changes of DG17 and DG18 to decrease the voltages in feeder 4.

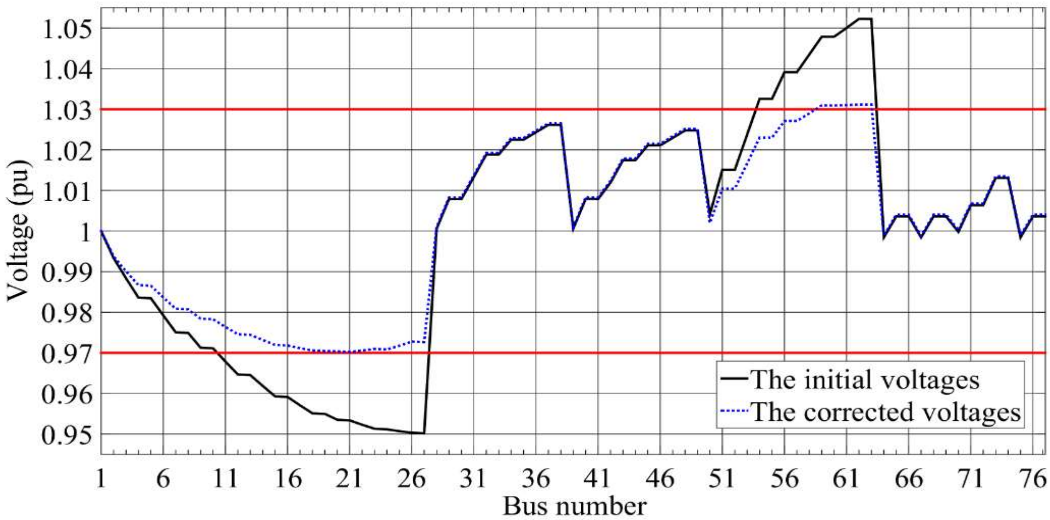

Figure 5-6: System voltages obtained by the SSVCA when having simultaneous voltage rise and drop violations

5.5. Evaluating accuracy of the sensitivity analysis regarding effects of OLTC action on node voltages

In the sensitivity analysis regarding effects of transformer tap changer on node voltages, it was supposed that for a small range of the transformer tap movement, the voltage modification created by the OLTC action will be reflected exactly throughout all the system nodes. This approximation can lead to errors in the voltage control procedure. Moreover, because of the transformer tap movement, the turn ratio of transformer varies. This has an effect on the internal impedance of the transformer. The tap changing transformer with the nominal turn ratio is modelled with a series impedance Z_T or its equivalent admittance Y_T (=1/Z_T). When the transformer turn ratio is off-nominal, the transformer impedance (or admittance) should be modified accordingly. References [68] and [69] have suggested a formulation for the exact modelling of the transformer impedance incorporating impact of the off-nominal turn ratio. According to [68] and [69], a transformer with a per-unit admittance Y_T in series with an ideal transformer representing the off-nominal turn ratio is considered as shown in figure 5-7.

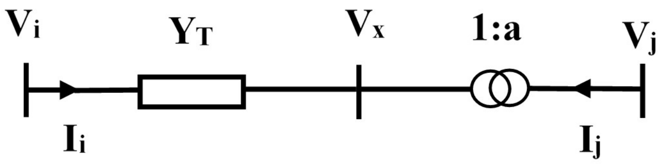

Figure 5-7: Equivalent model of the tap changing transformer

where a is per-unit off-nominal tap position varying in a small range. Bus x is fictitious one located between nodes i and j. Bus i is the non-tap side and bus j is the tap side one. Voltage at bus x is obtained by

$$V_x = \frac{1}{a} V_j \tag{5-37}$$

Given that the complex powers on both sides of the ideal transformer are equal, we have

$$I_j = -\frac{I_i}{a} \tag{5-38}$$

The current I_i is expressed by

$$I_i = Y_T (V_i - V_x) \tag{5-39}$$

Substituting for V_x from (5-37), (5-39) is rewritten as

$$I_i = Y_T V_i - \frac{Y_t}{a} V_j \tag{5-40}$$

Substituting for I_i from (5-40) gives the I_j according to (5-38) as

$$I_j = \frac{-Y_T}{a} V_i + \frac{Y_T}{a^2} V_j \tag{5-41}$$

In the admittance matrix form, the currents I_i and I_j given in (5-40) and (5-41) are written as

$$\begin{bmatrix} I_i \\ I_j \end{bmatrix} = \begin{bmatrix} Y_T & -\frac{Y_T}{a} \\ -\frac{Y_T}{a} & \frac{Y_T}{a^2} \end{bmatrix} \begin{bmatrix} V_i \\ V_j \end{bmatrix} \tag{5-42}$$

Consequently, in case of having an off-nominal turn ratio equal to a, the admittance matrix between nodes i and j should be modified according to (5-42). Figure 5-8 presents the equivalent π-model of the tap changing transformer located between nodes i and j.

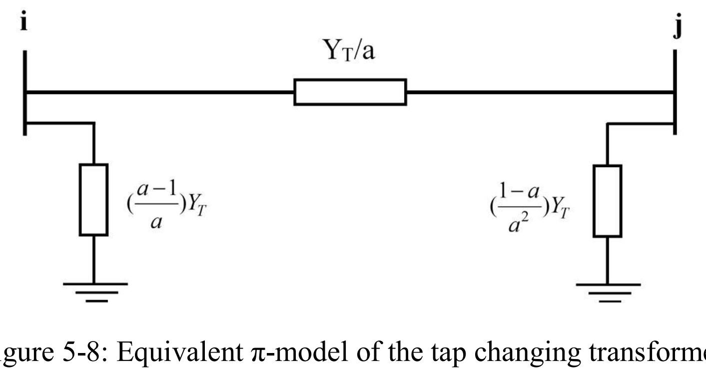

Figure 5-8: Equivalent π-model of the tap changing transformer

5.5.1. Numerical tests

The accuracy of the proposed sensitivity analysis approach regarding effects of transformer tap changes on node voltages is investigated here through the numerical simulations carried out on the introduced working point relating to the voltage rise case. To this end, the transformer tap is changed within the wide range of ± 20 steps around its initial point corresponding to the nominal transformer turn ratio. For each single movement of the tap position, the LF calculation including the exact formulation according to (5-42) is carried out in order to evaluate impacts of the tap changing operations on the node voltages. In the end, characteristics of node voltages in function of tap position changes are obtained which give us the exact relations between node voltages and transformer tap changes. In addition, node voltages subject to tap changes are obtained using the proposed sensitivity analysis method of this chapter (assuming that the nodal voltage modifications are the same as the voltage changes applied by the OLTC action). The obtained characteristics through the exact method (based on the consecutive LF calculations) as well as the approximated one (using the proposed sensitivity analysis method) are compared in figure 5-9. It is basically known that the relation between the transformer tap movement and the node voltage becomes more non-linear by getting distance from the slack node. Therefore, the voltage characteristic subject to the transformer tap changes at bus 26 located at the end of the feeder 1 has been chosen for the illustration in figure 5-9.

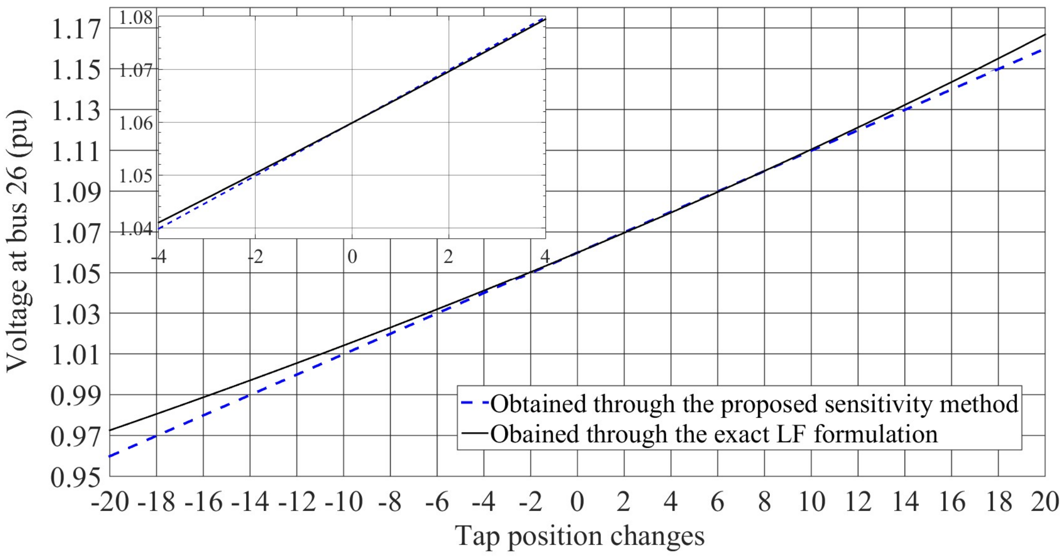

Figure 5-9: Voltage characteristics at bus 26 as function of the tap position movements obtained by the proposed sensitivity analysis method and the exact LF calculations

According to figure 5-9, when the transformer tap position is moved within the defined range of this chapter (i.e. ±4 steps around the nominal turn ratio), a close agreement is observed between the voltage values approximated by the proposed sensitivity analysis approach and the exact voltages obtained using the LF calculations.

Furthermore, the error arisen from the sensitivity analysis in the VCA is evaluated here by the numerical tests performed in the voltage rise and drop conditions. The SSVCA is used in this regard since in the MSVCA, the errors will be covered in the end of the voltage regulation procedure due to its closed-loop model. In the SSVCA, it is supposed that the weighing coefficients related to the active and reactive power changes of DGs are 100 times bigger than that of the transformer OLTC in order to have eventually maximum contribution of the OLTC in the voltage regulation. The obtained set-point from the SSVCA will be verified once with the simple LF calculation (neglecting impact of tap changes on transformer impedance) and once more using the so-called exact LF study that takes the off-nominal turn ratio into account according to (5-42). The voltage results obtained through these two LF study methods are analysed and discussed.

In the studied voltage rise condition as presented before, the SSVCA will ask to decrease the transformer tap position by 4 steps and to change the reactive power of DG5 equal to 1.191 Mvar (inductive). The system voltages obtained by the simple LF calculation as well as the exact approach are shown in figure 5-10. Also, the absolute value of errors between the voltages obtained by these two LF methods is presented in figure 5-10.

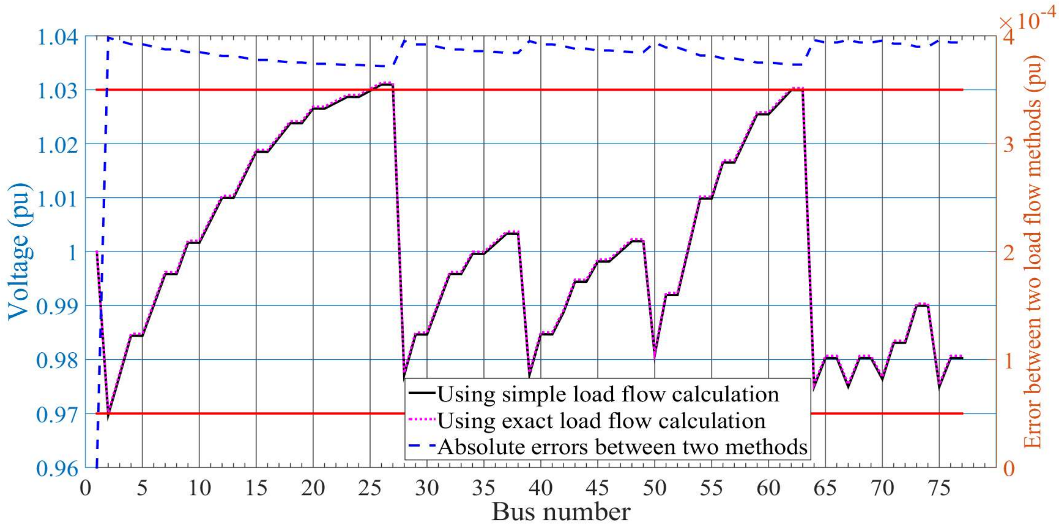

Figure 5-10: System voltages obtained by the simple and exact LF calculations in the voltage rise case

As it can be seen in figure 5-10, due to the error in the sensitivity analysis, small voltage violations are found after the voltage regulation at the buses located at the end of feeder 1. Bus 26 creates the binding constraint of the SSVCA optimization problem. The error between the corrected voltage of bus 26 and the targeted 1.03 pu voltage limit is equal to 0.0013 pu. Considering the initial voltage violation at bus 26 which was equal to 0.0298 pu, the relative error arisen from the sensitivity analysis will be equal to (0.0013/0.0298)×100=4.3%. Also, in figure 5-10, it is seen that the voltage values obtained by both of the LF methods are very close. The biggest error between the values obtained by the simple LF method and the exact one is equal to 3.98×10^{-4} at bus 2.

In the voltage drop state, in order to manage the voltage violations, the tap changer position is increased by 4 steps to its highest possible position and DG5 is asked to provide 0.185 Mvar capacitive reactive power. The system voltages obtained by the two methods of LF calculations are presented in figure 5-11.

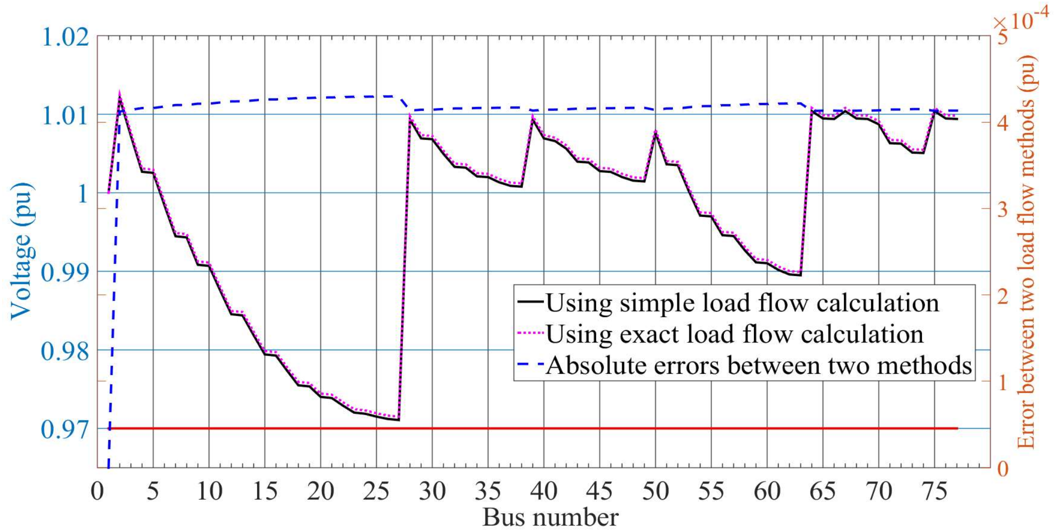

Figure 5-11: System voltages obtained by the simple and exact LF calculations in the voltage drop case

In the voltage drop condition, the initial voltage violation at bus 27 constructs the binding constraint of the SSVCA optimization problem. The mismatch between the corrected voltage of bus 27 (=0.9715 pu) and the 0.97 pu voltage limit gives us the error due to the sensitivity analysis. Considering the initial voltage drop at bus 27, which was equal to 0.0223 pu, the relative error arisen from the sensitivity analysis is equal to (0.0015/0.0223)×100=6.7%. Since a small amount of reactive power change is asked by the SSVCA, it can be stated that the mentioned error is mostly arisen from the voltage sensitivity analysis with respect to the OLTC action. Like the voltage rise case, in figure 5-11, it is seen that errors between two methods of LF are small with a maximum of 4.3×10^{-4} at bus 27.

It is worth mentioning that the case of having simultaneous voltage rise and drop violations has not been studied here because the OLTC action will not be used for the voltage regulation in such a situation.

5.6. Adaptation of the proposed sensitivity-based voltage control approach with the practical context of the MV distributions systems

The proposed sensitivity-based voltage control approach relies on the LF results to determine the network state. In order to perform the LF study, the branch parameters (i.e. resistance and reactance of the lines) and bus parameters (i.e. load and DG powers) are needed. In the practical MV distribution systems, the branch parameters coming from the network model are known but the node powers which are in function of the network working point are not fully available due to lack of the sufficient measurement. Consequently, we do not have access to all the needed parameters for carrying out the LF study. In order to adapt the proposed voltage control approach with the realistic cases, we can replace the LF program with some limited voltage measurements on the selected buses. As known, the objective of using the LF program is to find the voltage violations of the system and to validate the VCA results after applying the corrective actions. Thus, the limited measurements can provide us these data instead of doing the LF study.

In the studied UKGDS, it has been shown that the voltage violations happen in the end of the feeders 1 and 4. Therefore, we need to monitor the voltages at buses 20 and 26 in feeder 1 as well as buses 59 and 62 in feeder 4 where mostly voltage violations occur. The DG powers should be also provided by the measurement, as we need to know the available DG powers for the voltage regulation end. From the voltage and power measurements, we have finally the voltage violations as well as the bounds on the control variables; therefore, we can construct the optimization problem of the presented VCAs in the single-step and multi-step forms using the proposed voltage sensitivity analysis methods (which are independent of network working point). In this way, the proposed sensitivity-based voltage control approach is adapted with the realistic cases of the voltage management in the MV distribution systems. It should be noted that if the branch ampacity limits are needed to be taken into account in the voltage control procedure, the current phasors in the selected branches (as presented in section 3.3.1) must be provided by the measurement as well. Also, in the MSVCA, if the OLTC movement is required, the dynamic response (delay) of the OLTC is considered inside the MSVCA, and its next iteration starts when the corrective control actions regarding the previous iteration have been completed.

5.7. Conclusion

In this chapter, application of the transformer on-load tap changer in a centralized sensitivity-based voltage control scheme is investigated. The voltage control algorithms presented in the chapter 3 are adapted in order to include the OLTC action beside the control of DG active and reactive powers. The OLTC impacts on the node voltages are linearized through the sensitivity analysis. A straightforward technique is introduced to obtain the sensitivity of node voltages with respect to the OLTC action. It is supposed that, if the transformer tap changes are limited to a small range and the node powers are constant, the voltage modification at the OLTC node will be reflected to all nodes. Thanks to the use of the sensitivity analysis, the voltage control problem formulation remains linear as before. However, due to introduction of the OLTC action, it is formulated as a mixed-integer linear programming aiming at minimizing the total weighted changes of the control variables subject to the voltage constraints. The numerical simulations are carried out to validate the performance of the VCAs in the multi-step and single-step forms. Moreover, the numerical tests are performed to evaluate the accuracy of the proposed sensitivity analysis approach regarding effects of the transformer tap changes on the node voltages. The impacts of the off-nominal transformer turn ratio on the system voltages are also studied in this chapter.

Based on the simulation results, it is concluded that the proposed sensitivity-based VCAs can optimally manage the OLTC set-point and DG active and reactive powers in order to remove the voltage violations happened in the voltage rise, voltage drop, and simultaneous voltage drop and rise conditions. In all the studied cases, the corrective control decisions have been made within a very short time, which does not exceed 0.35 s. This confirms that the proposed sensitivity-based voltage control approach can comply with the framework of the on-line voltage constraints management. Moreover, the numerical simulations verify that the proposed approach to extract the node voltage sensitivity with respect to tap changes has an acceptable accuracy. In addition, it is found that impact of the off-nominal transformer turn ratio on the node voltages is negligible.

In the next chapter, we consider that the network model is not constant and deterministic anymore (as it was in chapters 2 to 5) and it changes within the predefined bounds due to uncertainties associated with the network components. The main idea is to analyse when we have a VCA solution determined on the basis of the deterministic simplified network model, how the model uncertainty can affect the corrected voltages obtained by the VCA. Our investigation focuses on the model uncertainty associated with the voltage dependency of loads, power factor of loads, thermal dependency of lines, shunt admittances of lines and internal resistance of substation transformer.

Chapter 6: Model uncertainty impacts on the voltage control algorithm results

6.1. Abstract

Given that the accurate and up-to-date models of the system components are not available, the calculations and analyses of the previous chapters have been performed by relying on their simplified models. This may lead to erroneous analyses and eventually wrong control decisions by the voltage control algorithm. In this chapter, a framework is proposed in order to evaluate impacts of the uncertain models of the system components on the voltage control problem of the MV distribution systems. The investigation focuses on the model uncertainties associated with the voltage dependency of loads, power factor of loads, thermal dependency of lines, shunt admittances of lines and internal resistance of substation transformer. To this end, firstly, the voltage constraints are managed using the SSVCA relying on the simplified deterministic models of the system components (as before). The system loads and lines as well as the substation transformer are then modelled with the uncertain variables, which are bounded in the predefined ranges. Monte Carlo (MC) simulations are used to create series of scenarios that cover the possible values that the parameters of the system components can take due to their uncertain nature. The model uncertainty impacts on the voltage control problem are finally evaluated by the LF calculations considering the scenarios created by the MC simulations and the set-point obtained by the SSVCA. The proposed framework of this chapter brings useful information regarding the possible deviations that the node voltages can have due to uncertain models of the studied components.

6.2. Introduction

Voltage control problem is known as one of the main challenges in the MV distribution systems integrating high level of DGs. Different voltage control schemes have been proposed in the literature in order to remove the voltage violations and to keep the system voltages within the predefined voltage limits. Despite the differences of the existing VCAs, they have been developed relying on the similar assumptions that the system loads are of the voltage-independent type (e.g.: [4], [13], [16], [19], [20], [29], [31], [46], [70], [71]), system lines are equivalent to the series impedances which have constant values over the time (e.g.: [4], [13], [16], [17], [19], [20], [29], [31], [46], [70], [71]) and the substation transformer is a pure reactance (e.g.: [4], [17], [72]) that can be even negligible (e.g.: [29], [31], [70]). In reality, however, these assumptions do not hold since the load powers are in function of the voltage, shunt admittances of the lines cannot be neglected, branch resistances vary with respect to the conductor temperatures, and internal resistance of the substation transformer is needed to be taken into account. Therefore, the models based on which the VCAs were developed in the abovementioned works and in the chapters 2 to 5 do not represent the real characteristics of the network. Consequently, corrective control decisions of these VCAs obtained by relying on the simplified network models may be insufficient to solve a specific voltage violation problem of the real case.

In this chapter, a framework is proposed in order to evaluate impacts of the uncertainties associated with the voltage dependency of loads, power factor of loads, thermal dependency of lines, shunt admittances of lines and internal resistance of substation transformer on the output results of the studied VCA. The voltage control problem is firstly solved by relying on the simplified models of the system components. Due to the fact that the exact and up-to-date models of the network components are not available, the studied components are considered with the uncertain variables which are bounded in the predefined ranges. The MC simulations are used to create series of scenarios that characterize the uncertain models of the studied components. The uncertainty impacts associated with models of the studied components on the voltage constraints of the VCA are evaluated by the LF calculations. The NRLF study is reformulated in this regard in order to incorporate the effect of the voltage dependency of loads. Evaluating the cumulative uncertainty effects of the studied components brings us useful information regarding the maximum deviations that the node voltages can have from the values obtained by the VCA. This can be utilized in order to reset the targeted bounds of the VCA such that it makes the VCA solutions robust against uncertainty of the system component models.

6.3. The proposed framework in order to evaluate impacts of the model uncertainty on the voltage constraints

The SSVCA presented in chapter 5 is used here to provide the basic set of the voltage results. Assuming that the errors arisen from the voltage sensitivity analyses are negligible, it can be expected that in the output point of the SSVCA, the voltage constraints are managed and the system voltages are returned into the permitted voltage range. However, in the studied VCA, loads are considered to be of the voltage-independent type, exact power factor of loads is supposed to be known, lines are modelled with the series impedances, which are supposed to remain unchanged with respect to the loading conditions, and the substation transformer is considered as a pure reactance. Therefore, the corrected voltages obtained by the SSVCA are subject to the variations due to utilization of these simplified models. The main objective of this chapter is to evaluate impacts of the uncertain models of the network components on the performance of the studied VCA. In this regard, a 3-stage method as shown in figure 6-1 is proposed. It consists of the SSVCA, MC simulations, and LF calculations.

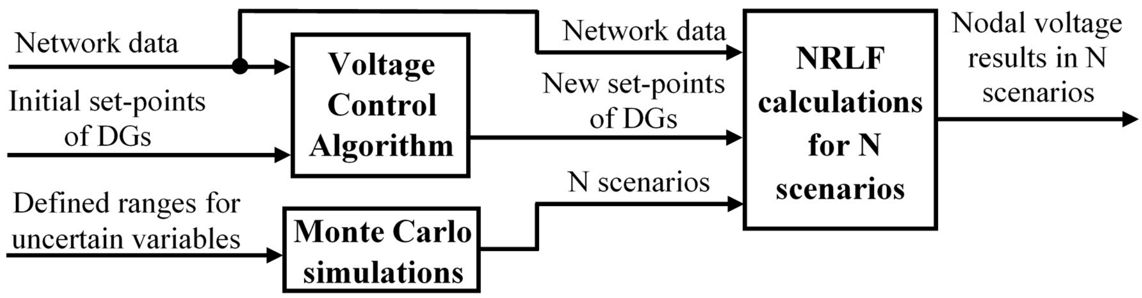

Figure 6-1: The proposed approach to evaluate the model uncertainty impact on the voltage control algorithm results

The first part of the proposed method is the SSVCA. It receives the network data (according to the simplified models of the system components) and initial values of DG powers. If the voltage violations are found in the system, it defines the new set-points of DGs as well as the tap changer position in order to remove those voltage violations. The SSVCA results are kept constant for the further analyses. The second part is the scenarios creation by the MC simulations. Given that the exact models of the studied components are not available, MC simulations are used to generate N scenarios within the predefined ranges for the parameters of the models under study in order to cover the possible values that those parameters can take in reality. The final stage is the LF calculations considering the set-points obtained by the SSVCA, N scenarios for the uncertain models of the network components and rest of the network data. The LF calculations are repeated for each of the N scenarios created by the MC technique. Therefore, finally, N sets of node voltages will be available that will be transformed into the Cumulative Distribution Function (CDF) form. The CDFs of nodal voltages give possible ranges of the voltage variations at the system buses in the generated scenarios. They show also the probability of having a specific voltage value within the obtained ranges. If the CDFs of the system voltages are found to be within the permitted voltage range, it can be concluded that the uncertain models of the studied components will not create voltage violation problem in the VCA. The three parts of the proposed method are described in the following sections.

6.3.1. Voltage control algorithm

The single-step voltage control algorithm is used here for the voltage regulation purpose. Being based on the open-loop control system, the corrective commands defined by the SSVCA can be analysed in order to evaluate impacts of the uncertainties associated with the network component models. It should be noted that when the MSVCA receives the updated state of the network (in each iteration) through the measurement channels, errors related to the simplified network component models will be eventually covered in the voltage control procedure due to its closed-loop functionality. Therefore, the MSVCA could not be used for the investigation of this chapter. The SSVCA as presented in chapter 5 manages the active and reactive powers of DGs as well as the transformer tap position in order to return simultaneously all the violated voltages inside the permitted voltage range. The branch ampacity limits are not considered in the SSVCA as the main objective is to evaluate impacts of the model uncertainty on the voltage constraints of the MV distribution systems. In the SSVCA, the DSA is used to determine the dependencies between nodal voltages and powers. Also, the proposed VSA method presented in chapter 5 is employed for taking into account tap position impacts on the node voltages. It should be noted that the error arisen in the VCA from inaccuracy of the VSA methods is out of scope of this chapter given that the latter has been studied in the previous chapters.

6.3.2. Monte Carlo simulations

In the literature, the MC technique has been utilized in order to analyse the uncertain and unobservable nature of the distribution systems. In [73] and [74] using MC simulations, uncertainty impacts associated with the nodal generations and consumptions have been investigated. Application of the sensitivity analysis in a probabilistic context based on the MC simulations for characterizing the LV distribution systems has been studied in [75] . Also, a state estimation technique has been developed in [76] where MC simulations are employed to validate it.

The MC technique in the proposed framework of this chapter adopts the procedure presented in [73], which is introduced as follows. Firstly, the possible variation range of the random (uncertain) variable is defined (for instance $\pm x$). Then, proper number of points is created between the lower and upper bounds of the defined range according to the desired accuracy. It is assumed that the probability of having a point within this range is normally distributed. Therefore, it can be assigned to a normal distribution function like [73] and [74]. Afterwards, the probability density function corresponding to those points is obtained by calculating their standard deviation and mean value. Also, by definition, a probability density function can be transformed into a CDF by

$$CDF(x) = P(X \leq x) \tag{6-1}$$

where X is the random variable associated with the uncertain parameter of the model under study and x is the upper bound on the variation range of the uncertain parameter. In order to create N scenarios for the parameter of the model under study, a sampling procedure is applied to the obtained CDF as follows [73]. A uniformly distributed random value between 0 and 1 is chosen. It is assigned to the CDF on the vertical axis and its corresponding value on the horizontal axis gives the variation that the uncertain parameter of the model under study can have in one scenario. The sampling procedure is repeated N times in order to create N scenarios. In the end, a vector with N elements is built that covers possible variations that the uncertain parameter of the model under study can have. Considering the created scenarios and the basic (simplified) model, the uncertain nature of the studied component is taken into account.

6.3.3. Newton-Raphson load flow study

The NRLF study is used in the proposed framework in order to evaluate the system voltages in the scenarios created by the MC simulations. In the NRLF, the non-linear algebraic equations of the nodal powers are linearized by expanding them through the Taylor series. It constitutes the so-called Jacobian matrix, which gives the linearized relationships between small changes in real and reactive powers with respect to small changes in nodal voltage angles and magnitudes as below.

$$\begin{bmatrix} \mathbf{\Delta P} \\ \mathbf{\Delta Q} \end{bmatrix} = \begin{bmatrix} \mathbf{J}_1 & \mathbf{J}_2 \\ \mathbf{J}_3 & \mathbf{J}_4 \end{bmatrix} \begin{bmatrix} \mathbf{\Delta \theta} \\ \mathbf{\Delta V} \end{bmatrix} \tag{6-2}$$

where $\mathbf{\Delta\theta}$ and $\mathbf{\Delta V}$ denote the vectors of small variations in the voltage angles and magnitudes at the PQ buses, respectively. Also, $\mathbf{\Delta P}$ and $\mathbf{\Delta Q}$ are the vectors of errors between the scheduled and calculated powers at the PQ buses. The mathematical relations to obtain the elements of the Jacobian matrix have been given in [68]. Once the Jacobian matrix is composed, using $\mathbf{\Delta P}$ and $\mathbf{\Delta Q}$ that are known parameters and inverted Jacobian matrix according to (6-2), system voltages are updated. Then, the new voltages are employed to update $\mathbf{\Delta P}$ and $\mathbf{\Delta Q}$ vectors as well. In the next iteration of the NRLF, the Jacobian matrix elements will be updated in order to obtain the new voltages and eventually new $\mathbf{\Delta P}$ and $\mathbf{\Delta Q}$. The NRLF in this iterative-based procedure tries to minimize the errors (i.e. $\mathbf{\Delta P}$ and $\mathbf{\Delta Q}$). The iterative procedure stops when a predefined error is met.

6.4. Studied sources of the model uncertainty

As stated before, the model based on which the proposed voltage control approach of the previous chapters has been developed does not represent the real characteristics of the studied network. There are different factors that have been neglected due to the uncertainty, unobservability and complexity of the network model. An accurate and up-to-date network model should incorporate factors such as the working point, loading condition, ambient temperature, voltage, frequency, ageing of the equipment etc. Given that it is not possible to take all these factors into account, in this chapter, the most dominant ones in the MV distribution systems are considered. The current investigation focuses on the impacts of the uncertainties associated with the voltage dependency of loads, power factor of loads, thermal dependency of lines, shunt admittances of lines and internal resistance of substation transformer. The above sources of the model uncertainty are described in the following sections. The numerical simulations will be carried out on the 77-bus UKGDS in order to determine effects of the studied uncertainties on the output results of the considered VCA (i.e. the SSVCA) in section 6.5.

6.4.1. Voltage dependency of loads

The load demand in an electric device is rated at the nominal voltage, but regarding the nature of the load, it can vary when the system voltage is not equal to the nominal value. In order to represent the dependency degree of the load to the voltage, polynomial and exponential models have been widely used in the literature [32], [77], [78], [79], [80]. In the polynomial (known also as ZIP) model, a typical load is considered to be a combination of the power constant, current constant and impedance constant loads. The power constant load type is supposed to be independent of the voltage, while the current constant model is a linear function of the voltage, and the impedance constant type is proportional to the square voltage. The polynomial load model is expressed by the following equations for active and reactive powers.

$$P_L^* = P_L\left[a_P V^2 + b_P V + c_P\right] \tag{6-3}$$

$$Q_L^* = Q_L\left[a_Q V^2 + b_Q V + c_Q\right] \tag{6-4}$$

where P_L and Q_L stand for the rated active and reactive powers of the load at the nominal voltage equal to 1 pu. Also, P_L^* and Q_L^* denote the actual consumed active and reactive power values of the load at the voltage equal to V. The coefficients a_P, b_P, c_P, a_Q, b_Q and c_Q of the polynomial model determine the voltage dependency characteristic of the load. In the exponential model, actual consumed active and reactive powers of load (P_L^* and Q_L^*) are obtained by

$$P_L^* = P_L V^{\alpha} \tag{6-5}$$

$$Q_L^* = Q_L V^{\beta} \tag{6-6}$$

In the exponential model, voltage dependency of the load for active and reactive powers is defined by the exponents α and β, respectively.

In this work, in order to study the uncertainty of the load-voltage dependency, the exponential load model is used because of the following reasons. Firstly, in the exponential model, the uncertain variables for active and reactive powers of load are exponents α and β while in the polynomial model, there will be three uncertain variables (i.e. a_P, b_P and c_P) for active power and three other variables (i.e. a_Q, b_Q and c_Q) for reactive power of load. Therefore, in the polynomial model, there will be three times more uncertain variables for each of the load buses compared to the case of the exponential model. Secondly, in the polynomial model, sum of the coefficients in (6-3) and (6-4) must be always equal to one ($a_P+b_P+c_P=a_Q+b_Q+c_Q=1$). It means that the scenarios for the polynomial coefficients of active and reactive powers cannot be created independently and one of these three coefficients in (6-3) and (6-4) must be always used to make the summation of each three coefficients equal to one. Consequently, it is concluded that the exponential model can be implemented in a more efficient and straightforward manner than the polynomial approach. It is worth noting that the polynomial and exponential models generally lead to quite similar results such that they can be used interchangeably for representing the voltage dependency of load in the MV and LV levels, according to [78] and [79], respectively.

Furthermore, possible values that the exponents α and β can take for different types of loads have been fully investigated in the literature. It is known that for instance, α and β related to industrial motors, fans, pumps as well as incandescent and compact fluorescent lamps are between 0 and 2 while the exponents can have relatively bigger values (up to 2.6 for α and 4 for β) in some other groups of loads such as conventional fluorescent lamps, room air conditioner, and battery charger [32], [80]. On the contrary, possible ranges of values for the polynomial coefficients in (6-3) and (6-4) are not clear. The polynomial coefficients of residential loads such as motors, incandescent and compact fluorescent lamps are found to be within a narrow range from negative to positive values (approximately from -1.5 to 2) [79]. However, wider bounds have been reported for the polynomial coefficients in [78] ranging from -19 to 11. In the end, it should be noted that the parameters of exponential load model give us a clearer idea regarding the level of the load-voltage dependency compared to the ones of the polynomial model.

Given that the exact dependency degree of load powers to the voltage is unknown, MC simulations are employed to create scenarios that can cover the uncertain nature of the loads in a probabilistic way. Two approaches as described in the following sections will be developed in order to take the voltage dependency of loads into consideration.

6.4.1.1. Approach based on the maximum values

In the first approach, the MC simulations are used to create the scenarios that cover the possible variations that the load powers can have due to the voltage dependency. According to (6-5) and

(6-6), the maximum variations of load powers with respect to the voltage are determined by having the maximum values of α and β as well as the maximum voltage magnitude. In the literature, it is found that based on the load nature, the voltage dependency exponents can be as big as 2.6 and 4 for α and β, respectively [32], [80]. Taking into account the worst case scenarios for the voltage rise and drop conditions, the biggest voltage variations in the studied UKGDS (presented in figure 3-1) would be approximately in the range of ±0.06 pu (around 1 pu). Considering the biggest possible α and β equal to 2.6 and 4, the maximum variations of load active and reactive powers with respect to the voltage in the voltage rise case are equal to +16% and +26% of their nominal values, respectively, according to (6-5) and (6-6). Similarly, in the voltage drop state, the variations of load active and reactive powers in function of voltage reach -15% and -22% of their nominal values, respectively, according to (6-5) and (6-6). In the voltage rise case, the lower bounds of load power variations are set to 0 to represent no load-voltage dependency while in the voltage drop case, the upper bounds of load power variations are equal to 0 that correspond to zero load-voltage dependency condition. The MC simulations will be used here to create scenarios within the predefined ranges for the load active and reactive power variations with respect to the voltage. It is expected that by having the rated load powers (P_L and Q_L) and their variations created by the MC, the uncertain nature of the load-voltage dependency can be properly taken into account.

6.4.1.2. Approach based on the adapted NRLF study

In the second approach for the investigation on the load-voltage uncertainty, the MC simulations are used to create scenarios for the levels of the voltage dependency of loads namely α and β. Therefore, based on the defined ranges for α and β, N scenarios are created for these coefficients. Then, the NRLF study is adapted in order to be able to recognize the load-voltage dependency such that the created α and β in each scenario are treated to determine the system state in that scenario. Similarly, by evaluating all scenarios, N sets of system voltages are obtained that will be transformed into the CDF form. The NRLF study is modified as follows in order to be capable of distinguishing the load-voltage dependency.

Assuming that the system loads are voltage dependent, the mathematical relations for calculating the elements of sub-Jacobian matrices (**J1**, **J2**, **J3** and **J4**) in (6-2) should be modified accordingly. The voltage dependency of loads affects all elements of the sub-Jacobian matrices. Considering (6-5) and (6-6), the diagonal elements of **J2** and **J4** will be obtained by

$$\frac{\partial P_k^*}{\partial V_k} = P_k \alpha_k V_k^{\alpha_k - 1} + \frac{\partial P_k}{\partial V_k} V_k^{\alpha_k} \tag{6-7}$$

$$\frac{\partial Q_k^*}{\partial V_k} = Q_k \beta_k V_k^{\beta_k - 1} + \frac{\partial Q_k}{\partial V_k} V_k^{\beta_k} \tag{6-8}$$

where k is index for the load buses ($k \in NL$). Also, the off-diagonal elements of **J2** and **J4** are given by

$$\frac{\partial P_k^*}{\partial V_n} = \frac{\partial P_k}{\partial V_n} V_k^{\alpha_k} \tag{6-9}$$

$$\frac{\partial Q_k^*}{\partial V_n} = \frac{\partial Q_k}{\partial V_n} V_k^{\beta_k} \tag{6-10}$$

Similarly, n is index for the load buses ($n \in NL$). The diagonal and off-diagonal elements of **J1** are written as

$$\frac{\partial P_k^*}{\partial \theta_k} = \frac{\partial P_k}{\partial \theta_k} V_k^{\alpha_k} \tag{6-11}$$

$$\frac{\partial P_k^*}{\partial \theta_n} = \frac{\partial P_k}{\partial \theta_n} V_k^{\alpha_k} \tag{6-12}$$

And, finally, the diagonal and off-diagonal elements of **J3** are obtained by

$$\frac{\partial Q_k^*}{\partial \theta_k} = \frac{\partial Q_k}{\partial \theta_k} V_k^{\beta_k} \tag{6-13}$$

$$\frac{\partial Q_k^*}{\partial \theta_n} = \frac{\partial Q_k}{\partial \theta_n} V_k^{\beta_k} \tag{6-14}$$

Apart from the modified formulations regarding the elements of the sub-Jacobian matrices, the NRLF principles as explained in section 6.3.3 remain unchanged for the LF study incorporating the load-voltage dependency. It should be noted that the entries of the Jacobian matrix relating to the DG-connected buses are obtained using the generic equations of the NRLF study (neglecting the voltage dependency). In other words, modified formulations of the NRLF according to (6-7) to (6-14) do not apply to the DG-connected buses and there is no voltage-power dependency at those nodes.

In the study based on the adapted NRLF approach, the MC simulations are used to create scenarios for α within the range of 0 to 2.6 and β in range of 0 to 4. Therefore, it is observed that the predefined bounds for α and β are identical to the ones selected in the approach based on the maximum values so that the obtained results of these two approaches can be equally compared later.

6.4.2. Power factor of loads

In the electric distribution systems, due to lack of the sufficient measurements, load power factors cannot be obtained accurately. As a result, an uncertainty is added to the load model regarding the power factor. Assuming that the active power of load is known, the power factor uncertainty affects the reactive power consumption of the load. In this work, in order to study impact of the uncertainty associated with the load power factor, it is supposed that the latter can vary within a specific range. Then, MC simulations are utilized to create N scenarios for the load power factor within that predefined range. The reactive power corresponding to the generated power factor in each scenario is calculated using (6-15). This procedure is followed for all the load buses independently. In the end, vectors of nodal reactive powers are built that can be used to evaluate impacts of load power factor uncertainties using the NRLF calculations.

$$Q_L = P_L \tan(\cos^{-1}(PF)) \tag{6-15}$$

where PF stands for the load power factor. It should be noted that for the analysis of this part, the voltage dependency of load is neglected and power constant load model is taken into consideration. The variation range of the load power factor is supposed to be from 0.9 (lagging) to 1. Within this range, considering the initial average power factors of loads in the UKGDS given in appendix 3 (= 0.98 lagging), the reactive powers of loads can increase by 138% of their respective initial values when PF is equal to 0.9 or decrease to 0 in the case of the unity power factor (PF=1).

6.4.3. Thermal dependency of the line resistances

The electrical resistance of the line increases with the conductor temperature rise. Therefore, the line resistance depends not only on the conductor size and type, but also on the temperature at which the line conductor is operating [81]. The temperature of the line conductor is in function of the current that passes through the line and the conductor ambient temperature. It means that, according to the actual level of the line loading and the conductor ambient temperature, the line electrical resistance should be recalculated. The overhead lines are more subject to the ambient temperature variations than the underground cable lines. In this work, the under study network (i.e. the 77-bus UKGDS) consists in underground cables. Thus, it is assumed that the cable loading has a dominant effect on the conductor temperature compared to the impact of the ambient temperature. Given that in the studied network, the actual (up-to-date) temperatures of the cable conductors are not available, we rely on the experimental results reported in [82] to obtain the possible variations that the cable conductor temperatures can have due to current intensity changes.

In [82], a test site has been constructed in order to measure the temperature changes of the underground MV power cable with constant and cyclic currents. The experiments have been done on a 15 kV underground cable, which has been placed in the duct bank with the soil temperature equal to 24°C. The maximum ampacity of the studied cable is 600 A. According to the introduced daily load cycle in that work, the cable current is changed from 8% to 83% of its nominal current. Within this range of current variation, the conductor temperature changes between 48 to 85°C. Also, in another test that was performed on the same cable in [82], it is reported that with a constant current equal to 50% of the cable rated ampacity, the conductor temperature reaches 62°C.

In the 77-bus UKGDS, total powers of DGs are almost 3 times bigger than sum of the load powers (see appendix 3). Therefore, the temperature variations of cable conductors as a function of the cable loadings in the voltage rise case are expected to be bigger than the ones of the voltage drop state. In the voltage rise case, the branch loadings are close to the maximal ampacities of the cables. As a result, the cable conductor temperatures can increase to 85°C based on [82]. Moreover, due to the ambient temperature in more severe conditions (greater than 24°C), the cable conductor temperatures can go up to 90°C which is usually considered as the maximum permitted temperature of the cable conductor insulation [83]. Assuming that the resistances of the lines have been initially adapted for 62°C (based on the temperature that corresponds to a 50% cable loading), maximal temperature variations of the cable conductors in the voltage rise case will be equal to 28°C (=90-62). It results in increasing the cable resistances up to 11% of their initial values (at 62°C) by the use of the equation (6-16) [84]. In addition, it is considered that in ambient temperatures below 24°C, the cable conductor temperatures can drop by 10°C which would decrease the line resistances to 4% of their initial values (at 62°C) according to (6-16).

$$R_{new} = R_0(1+\alpha_c \Delta T) \tag{6-16}$$

where R_0 is the initial cable resistance at 62°C (the temperature corresponding to a 50% cable loading) and R_{new} denotes the up-to-date cable resistance value by taking the conductor temperature variations (ΔT) around 62°C into account. In addition, α_c is the temperature coefficient of resistivity equal to 0.00393 for copper conductors.

In the voltage drop case, the cable loadings hardly exceed 50% of their rated ampacities. In this situation, it can be expected that the temperature variations of the cable conductors due to the loading condition and ambient temperature changes can fall in a range of ±15°C (around 62°C) that create resistance changes equal to ±5.8% of their initial values using (6-16).

By having the initial resistances of the lines (at 62°C) and their possible variations (ΔR) obtained by the MC simulations, the uncertainty in the line models due to the thermal dependency effect is taken into account. It is worth mentioning that in this study, the line inductance is considered constant as it depends mostly on the installation configuration of the cables.

6.4.4. Shunt admittances of the lines

Shunt admittances of the lines are usually neglected in the distribution systems while they can have important impacts on the system voltages in case of the long cable lines. According to [71], values of the charging capacitances of the lines are found to be in the range of 0.2 to 0.25 μF/km for the cables with sections varying from 95 to 245 mm^2. Considering the bigger value for the line capacity (0.25 μF/km) and having length of the lines in the studied network, the upper bounds of the predefined ranges for the admittances of all lines can be determined. Since in the UKGDS, shunt admittances of the lines have been totally neglected, the lower bounds of the admittance variations will be equal to 0. The MC simulations are employed here to create N scenarios according to the predefined bounds. It should be noted that in each scenario and for each line, the obtained admittance value is divided by two ($b/2$) to be assigned to each side of the corresponding line based on the π line model.

6.4.5. Internal resistance of the substation transformer

The power transformers are modelled with a series impedance while its resistive part is mostly considered negligible. Although internal resistance of the transformer is very small compared to its reactance, it can have considerable effects on the system voltages because of two main reasons. Firstly, in the distribution systems with the high ratio of resistance to reactance, the system voltages highly depend on the branch resistances. Secondly, the substation transformer is located in the starting point of the network in series with all other buses. Therefore, it has an impact on all nodal voltages. The typical reactance to resistance ratio of the normal power transformers is found to be in the range of 20 to 40 [85]. Furthermore, it is considered that the resistance of the transformer can vary based on its loading conditions. In this regard, an extension of ±10% with respect to the aforementioned range is adopted. Consequently, in this work, it is supposed that the resistance of the transformer (R_T) can take values from the range starting at 2.25% (1/40×0.9) and ending at 5.5% (1/20×1.1) of the transformer reactance. It should be noted that the reactance of the transformer is known and kept constant in all N scenarios.

6.4.6. Cumulative uncertainty effects of the load, line and transformer models

In the last part of this chapter, the cumulative uncertainty effects of the load, line and transformer models on the VCA performance are investigated. In section 6.4.2 studying the power factor uncertainty of the loads, the power constant load model has been taken into account. However, it is known that the power factor of the voltage dependent load is in function of α and β since by changing the voltage dependency exponents, the active and reactive powers of load, as well as the load power factor will be changed. This must be taken into consideration in (6-15) when creating vectors of nodal reactive powers. Considering the fact that the load is of the voltage dependent type, we have

$$\tan(\cos^{-1}(PF^*)) = \frac{Q_L^*}{P_L^*} = \frac{Q_L V^{\beta}}{P_L V^{\alpha}} = \frac{Q_L}{P_L} V^{\beta-\alpha}$$
$$= \tan(\cos^{-1}(PF)) V^{\beta-\alpha} \tag{6-17}$$

where PF^* and PF stand for the power factor in case of voltage dependent load and power constant load models, respectively. Equation (6-15) for the voltage dependent load is rewritten as follows.

$$Q_L^* = P_L^* \tan(\cos^{-1}(PF^*))$$
$$= P_L . \tan(\cos^{-1}(PF)) V^{\beta} \tag{6-18}$$

Therefore, in order to study the power factor uncertainty when load is of the voltage dependent type, vectors of nodal reactive powers should be built according to (6-18). It is worth noting that the active powers of loads will be obtained using (6-5) considering the generated scenarios for α. Apart from this modification, a similar procedure as developed before is followed here to evaluate the cumulative uncertainty associated with the load, line, and transformer models. To this end, the scenarios for the uncertain variables namely α, β, and PF for all loads, ΔR and $b/2$ for all lines and R_T for the substation transformer are generated independently using the MC simulations according to the defined ranges for each of the variables. The system voltages are then evaluated using the adapted NRLF study and the boxplots of obtained voltages will be illustrated eventually.

6.5. Simulation results

The proposed framework of this chapter including the SSVCA, MC tool, and NRLF program is implemented in the MATLAB environment. The simulations are carried out on the 77-bus UKGDS shown in figure 3-1 in the voltage drop and rise states. Two working points as follows are defined in order to create the voltage drop and rise conditions. In the first working point for the voltage drop case, all loads are considered to be at their maximum values while active powers of DGs are equal to zero. In the second working point corresponding to the voltage rise state, it is supposed that the load powers are at 10% of their respective nominal values and active powers of DGs are equal to 90% of their rated values. The initial reactive powers of DGs in both cases are set to zero. It should be noted that the working point relating to simultaneous voltage rise and drop violations is not considered here given that it leads to smaller voltage violations compared to the ones in the single voltage rise or drop case. Consequently, it can be expected that the model uncertainty effects in case of simultaneous voltage rise and drop violations are less than those of two considered working points.

In the proposed method for evaluating effects of the model uncertainty on the voltage constraints, in the first stage, the violated voltages will be removed using the VCA by relying on simplified models of the system components as shown in figure 6-1. Thus, the abovementioned working points are given separately to the VCA for the voltage regulation purpose. The initial system voltages as well as the corrected ones obtained by the VCA are depicted in figure 6-2. Table 6-1 presents the demanded power changes of DGs and necessary transformer tap movements in order to manage the voltage violations in both voltage rise and drop cases. In the VCA, it is supposed that the OLTC action has the smallest weighing coefficient compared to other control variables which is equal to 1 (C_{TR}=1) while the reactive power changes of DGs are weighted by a coefficient which is 50% bigger than the OLTC one (C_Q=1.5). Also, the active power curtailment of DGs is assigned to a coefficient which is 100% bigger than the OLTC one (C_P=2).

In the studied working point for simulating voltage rise case, voltage violations happen in the feeders 1 and 4 (at buses 11 to 27 and 54 to 63) as it can be seen in figure 6-2. In order to remove these voltage violations, tap changer position has decreased by 4 steps and DG5 which has a high impact on the voltages of feeder 1 has been used to provide 1.191 Mvar inductive reactive power. In the voltage drop case, the major voltage violations occur in the end of the feeder 1 at buses 9 to 27; thus, the VCA employs DG5 for a capacitive reactive power compensation equal to 1.44 Mvar at bus 26 beside two steps increase of the transformer tap position.

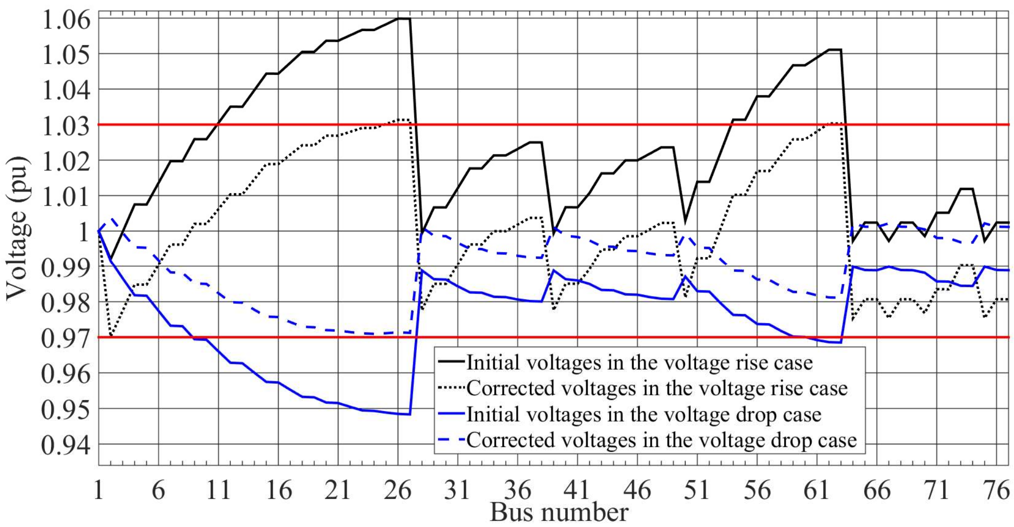

Figure 6-2: Initial system voltages as well as the corrected ones obtained by the VCA in the voltage drop and rise cases

TABLE 6-1: VCA RESULTS IN THE VOLTAGE RISE AND DROP CONDITIONS

	Voltage drop	Voltage rise
ΔQ_{DGx} (Mvar) $x \in \{1, 2, 3, \ldots, 22\}$	DG5= -1.44	DG5= 1.191
ΔP_{DGx} (MW) $x \in \{1, 2, 3, \ldots, 22\}$	NA	NA
ΔTap_{TR}	2	-4
OF	4.16	5.786

The second step of the proposed method is characterizing the uncertain model of the studied components. In order to take the model uncertainty into account, number of 1000 scenarios (N=1000) are generated by the MC simulations for the uncertain variables relating to each of the studied components according to the predefined ranges. The system voltages are finally evaluated by the NRLF calculations considering each of the generated scenarios as well as the initial network data and demanded changes of the control variables by the VCA (reported in table 6-1). The voltage results will be presented in the CDF form. In the voltage drop state, the CDF of the voltage at bus 24 is selected for the illustration because it corresponds to the binding constraint of the VCA. Consequently, its corrected voltage will be the closest one to the permitted lower limit (see figure 6-2). This indicates that the voltage at bus 24 is more likely to be fallen outside of the permitted voltage range in response to the model uncertainty compared to other buses. In the voltage rise case, the CDF of the voltage at bus 26 is plotted since the latter belongs to the binding constraint and after the voltage regulation, voltage at bus 26 is the closest one to the permitted upper voltage limit. The corrected voltage values obtained by the VCA are equal to 1.0313 pu for bus 26 in the voltage rise case, and 0.971 pu at bus 24 in the voltage drop case.

In what follows, firstly, model uncertainty effects related to each of the studied components are investigated individually. In the end, the cumulative uncertainty effects regarding all the studied factors will be evaluated and the box plots of the resultant node voltages will be presented.

6.5.1. On the impact of the voltage dependency of the loads

The uncertainty effects due to the voltage dependency of loads are investigated here by the approaches based on the maximum values and the adapted NRLF study. Figure 6-3 shows the CDFs of the voltages at the selected buses corresponding to the study on the voltage drop and rise cases.

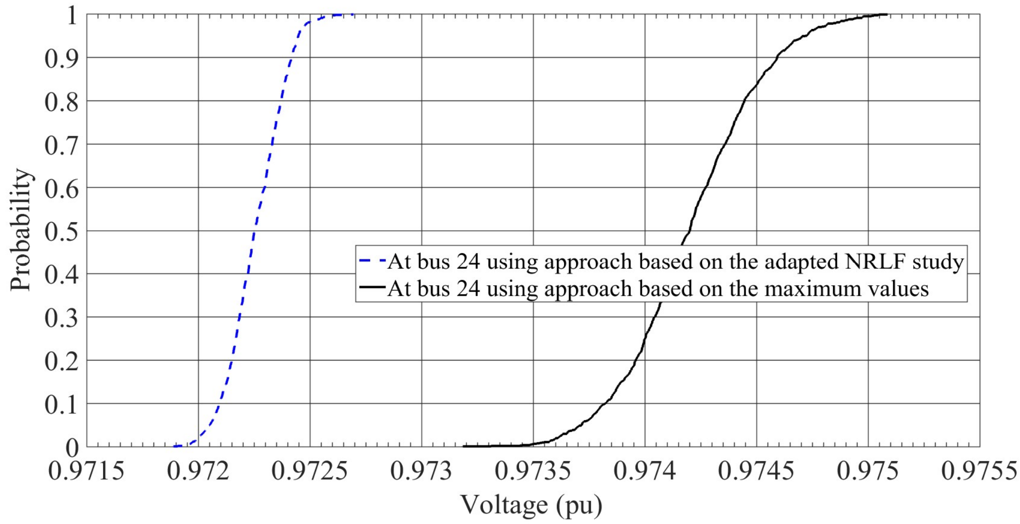

a

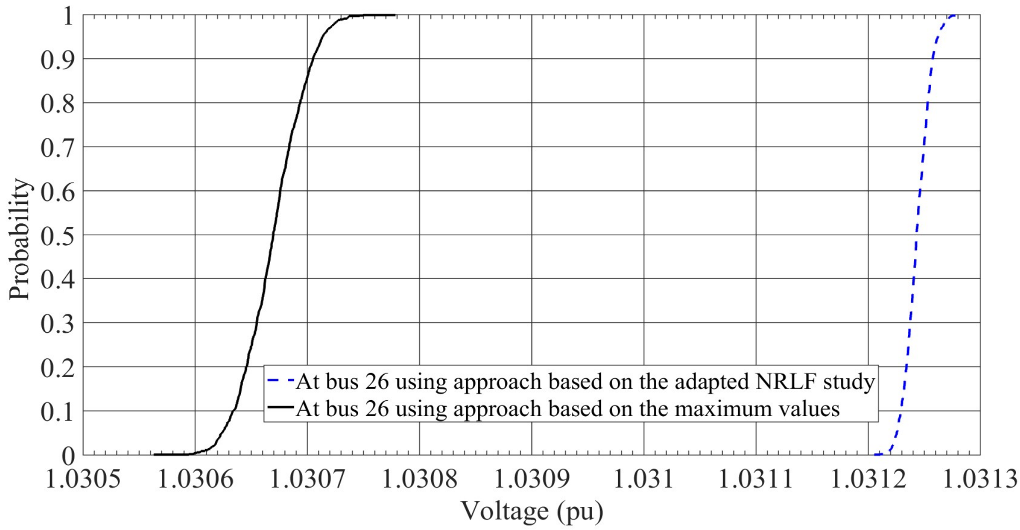

b

Figure 6-3: CDFs of the probability of voltages at the selected buses obtained by the NRLF study considering the model uncertainty due to the voltage dependency of loads (a) in the voltage drop case, (b) in the voltage rise case

Considering the results shown in figure 6-3, it is noticed that the uncertainty in the load model due to the voltage dependency effect does not create voltage violation problem in the VCA in both voltage drop and rise cases. It is explained by the fact that the load changes in function of voltage are on the proper direction of the voltage control purpose. According to (6-5) and (6-

6), in the voltage drop situation (V_k<1), the actual consumed loads are smaller than the rated ones; consequently, the system voltages increase compared to the ones obtained by the rated load values. In the voltage rise situation (V_k>1), the actual consumed loads are bigger than the rated ones so that the node voltages will reduce compared to the ones obtained by the rated load values. It is worth mentioning that the small voltage violation from the 1.03 pu voltage limit found in the voltage rise case at bus 26 (figure 6-3(b)) is not happened because of the voltage dependency of loads. As mentioned before, the corrected voltage obtained by the VCA is 1.0313 pu at bus 26. Therefore, in the voltage rise case, the voltage dependency of loads has decreased the voltage of bus 26 (see figure 6-3(b)).

Furthermore, by comparing figures 6-3(a) and 6-3(b), it is noticed that in the voltage drop situation, the load-voltage dependency creates a wider range of voltage variations compared to the one obtained in the voltage rise case. This is justified by the fact that in the voltage drop condition, load powers are maximal while in the voltage rise case, loads are at 10% of their nominal values. Consequently, in the former case, they can have bigger impacts on the system voltages.

Moreover, taking into account the voltage results obtained by the approach based on the maximum values and the ones based on the adapted NRLF study confirms that the latter leads to more moderate results. For instance, in figure 6-3(a), due to the voltage dependency of loads, using the approach based on the maximum values, the voltage at bus 24 is found to vary in a range between 0.9732 to 0.9751 pu while using the adapted NRLF approach, the voltage variation at that bus is limited to the range of 0.9719 to 0.9727 pu. A similar trend is found also in the voltage rise case in figure 6-3(b). It indicates that the approach based on the adapted NRLF study determines impacts of the voltage dependency of loads in a more realistic way than the method based on the maximum values. It is due to the fact that the approach based on the maximum values uses the worst voltage violations to define the ranges of load variations with respect to the voltage while in another approach, the adapted NRLF study takes into consideration the voltages which correspond to that specific studied working point.

6.5.2. On the impact of the power factor of loads

The impact analysis of the load power factor uncertainty is carried out in this section. Figure 6-4 presents CDFs of the voltage results at the selected buses when the power factor of loads varies within the predefined bounds.

Taking figure 6-4(a) corresponding to the voltage drop case into account, it is observed that big voltage violations occur from the 0.97 pu voltage limit. As the minimum effect of the load power factor uncertainty, the voltage at bus 24 decreases to 0.9671 pu that means the voltage violation from the permitted lower limit equals to 0.0029 pu. In the generated scenarios, with a probability of 90%, the voltage magnitude at bus 24 will be lower than 0.965 pu. The load power factor uncertainty can reduce the voltage at bus 24 to almost 0.96 pu that is nearly equal to 0.011 pu voltage drop with respect to the corrected voltage of bus 24 obtained by the VCA (=0.971 pu). On the contrary, in the voltage rise case, as it can be seen in figure 6-4(b), voltage variations due to the load power factor uncertainties have considerably smaller amplitudes. As the maximum impact of the load power factor uncertainty in the voltage rise state, voltage at bus 26 reduces to 1.0299 pu. With respect to the corrected voltage of bus 26 obtained by the VCA (=1.0313 pu), a voltage drop of 0.0014 pu is found at that bus. It is worth mentioning that the load power factor uncertainty has a great impact on the voltage drop situation since in that case, the load powers are maximal. On the other hand, in the voltage rise case, the load powers are equal to 10% of their nominal values; consequently, the eventual effects of the load power factor uncertainties are small.

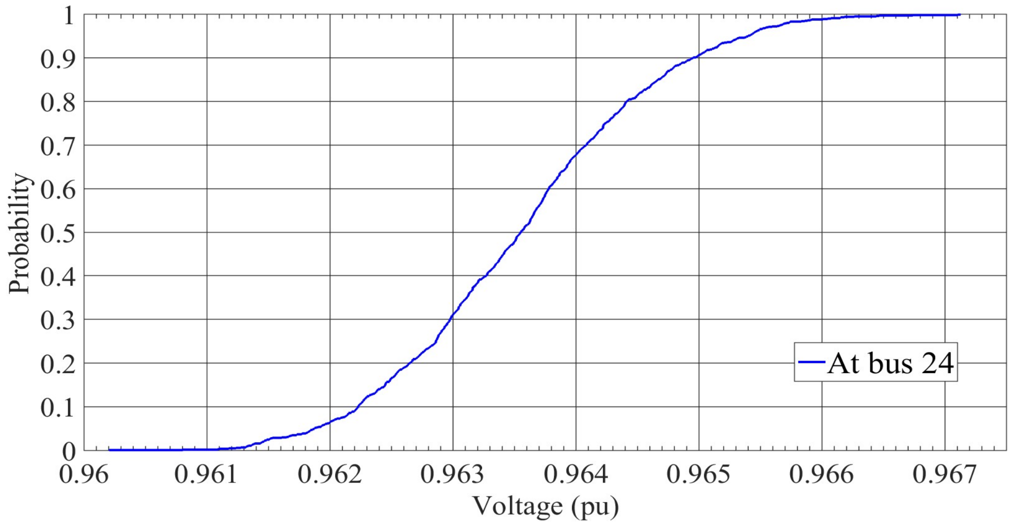

a

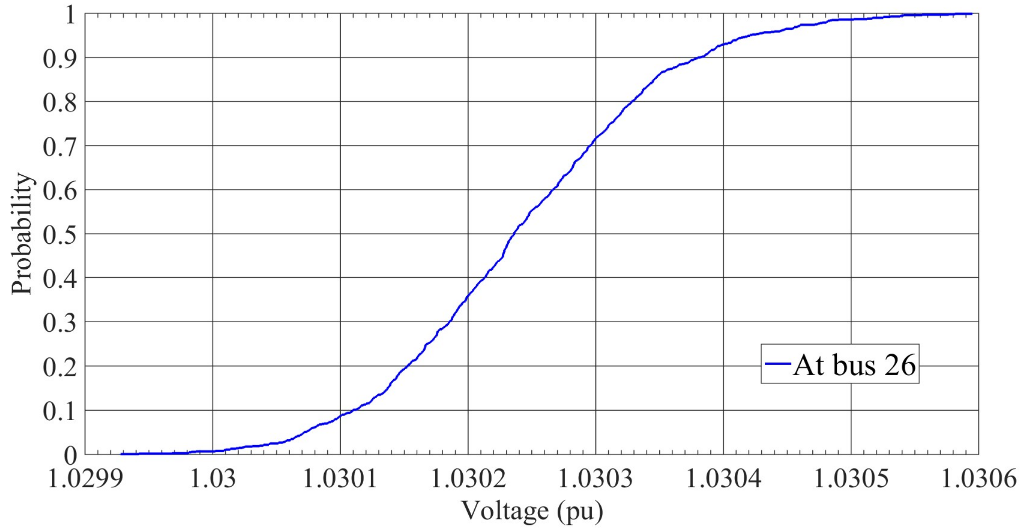

b

Figure 6-4: CDFs of the probability of voltages at the selected buses obtained by the NRLF study considering the model uncertainty due to the power factor of loads (a) in the voltage drop case, (b) in the voltage rise case

6.5.3. On the impact of the thermal dependency of the line resistances

The effect of the temperature dependency of the branch resistances is studied in this part. According to the defined ranges for resistance variations of the cables given in section 6-4-3, the MC simulations generate *N* scenarios and the LF calculations are performed in order to evaluate the nodal voltages. Figure 6-5 shows the obtained CDFs of the voltages at the selected buses in the voltage drop and rise conditions.

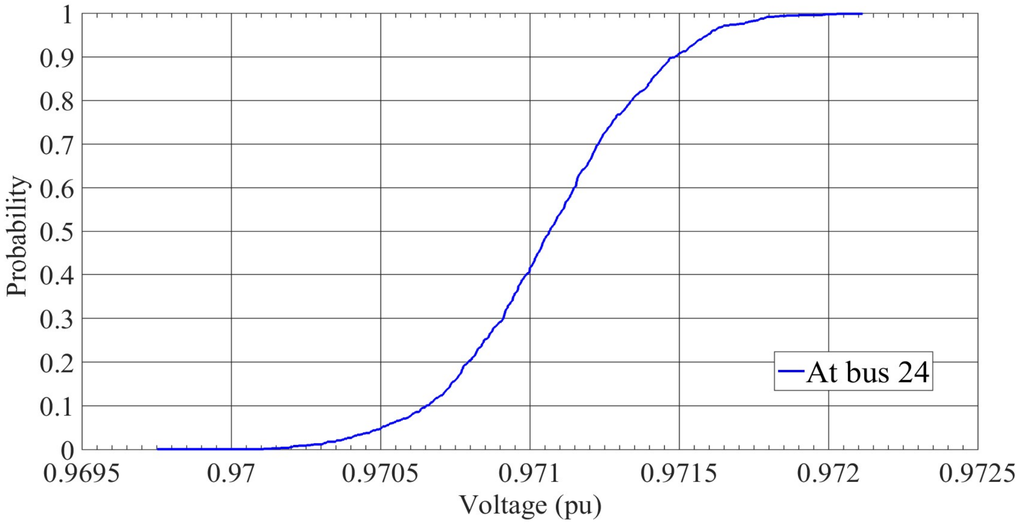

a

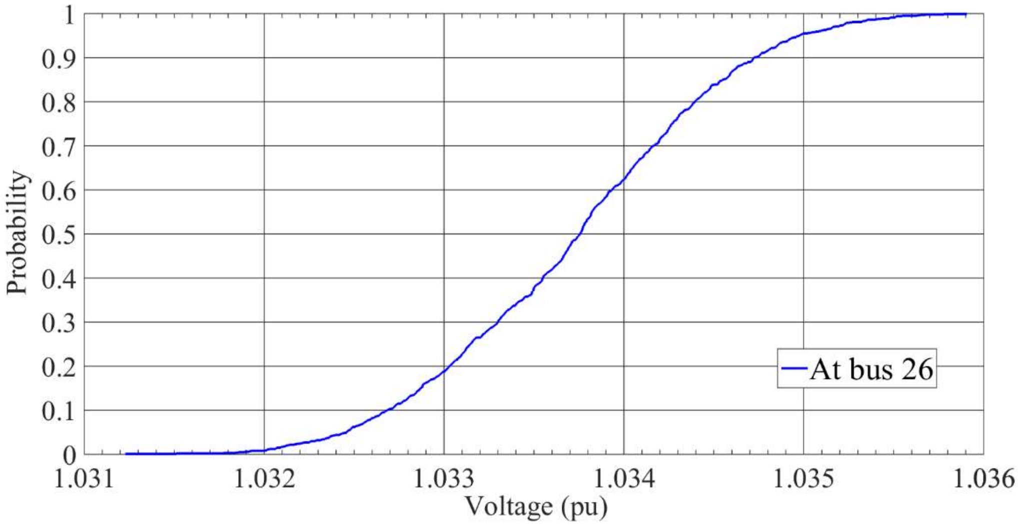

b

Figure 6-5: CDFs of the probability of voltages at the selected buses obtained by the NRLF study considering the model uncertainty due to the thermal dependency of the line resistances (a) in the voltage drop case, (b) in the voltage rise case

As it can be observed from figure 6-5(a), in the voltage drop case, the voltage variations at bus 24 due to the thermal dependency of the line resistances are limited to a range between 0.9697 to 0.9721 pu. Consequently, very small voltage violation from the permitted voltage range (its lower bound) is found in the voltage drop case. In addition, voltage variations are found to be around the corrected voltage of bus 24 obtained by the VCA (i.e. 0.971 pu). Unlike the voltage drop case, in the voltage rise state, big voltage violation from the permitted upper voltage limit occurs at bus 26. According to the figure 6-5(b), voltage at bus 26 can increase to 1.0359 pu due to impacts of the temperature dependency of the branch resistances. In figure 6-5, it is clearly seen that the voltage variations in the voltage rise case have a wider range than the one of the voltage drop state. It is due to the fact that the predefined ranges for the resistance variations of cables in the voltage rise state are bigger than the bounds of the resistance variations in the voltage drop case.

6.5.4. On the impact of the shunt admittances of the lines

In this section, impacts of incorporating shunt admittances of the lines on the system voltages are studied. It is expected that adding the shunt admittances of the lines will increase the system voltages and it can lead to the voltage rise issue. Figure 6-6 shows the CDF of the voltage at bus 26 obtained by the NRLF study in the voltage rise state considering the scenarios created by the MC simulations.

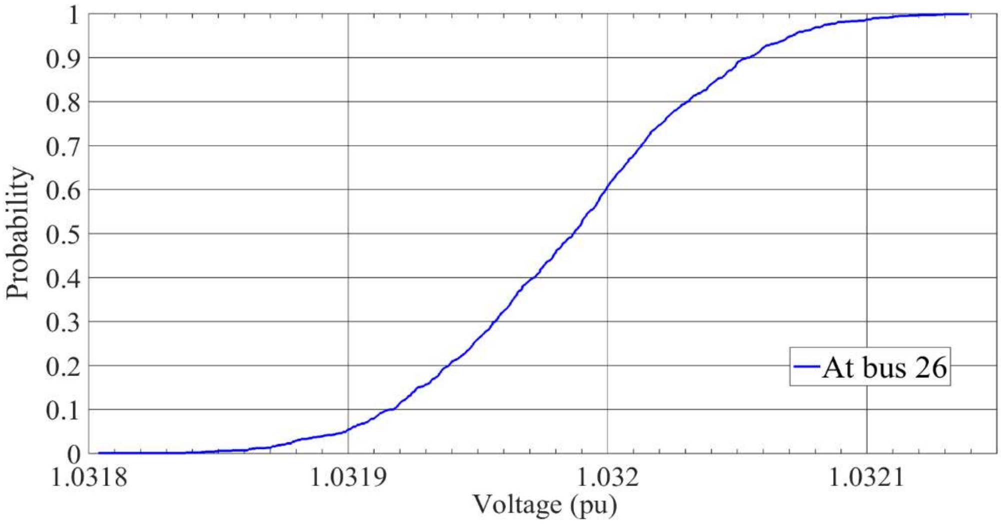

Figure 6-6: CDF of the probability of the voltage at bus 26 obtained by the NRLF study considering the model uncertainty due to the shunt admittances of the lines in the voltage rise case

Based on the figure 6-6, it is confirmed that adding shunt admittances of the lines creates small voltage increase with respect to the corrected voltage obtained by the VCA. In the simulated scenarios, as the minimum effect of the shunt admittances, the voltage at bus 26 is increased by 0.0005 (=1.0318-1.0313) pu. The voltage at that bus can reach 1.03214 pu. Concerning impacts of shunt admittances of the lines on the voltage drop case, it is observed that the system voltages increase similar to the voltage rise case but with slightly less extents. However, since the network is in the voltage drop state, it does not create voltage violation problem.

6.5.5. On the impact of the internal resistance of the substation transformer

Similar to the previous sections, the investigation on the transformer model is carried out on the voltage drop and rise states. Figure 6-7 depicts the CDFs of the voltages in the corresponding cases when the created scenarios are evaluated by the LF calculations. In figure 6-7, it is seen that the voltage violations occur from both upper and lower permitted voltage limits due to the uncertainty that exists in the transformer internal resistance value. In the voltage drop state, voltage at bus 24 decreases to nearly 0.969 pu and in the voltage rise case, voltage at bus 26 can reach 1.0366 pu. Therefore, it is concluded that the internal resistance of the substation transformer has an important influence on the system voltages, especially, in the voltage rise state. A wider range of voltage variation is observed in the voltage rise case since the transformer loading is heavier in this case compared to that of the voltage drop state. As mentioned before, in the studied UKGDS, the total powers of DGs are almost 3 times bigger than the total load consumptions.

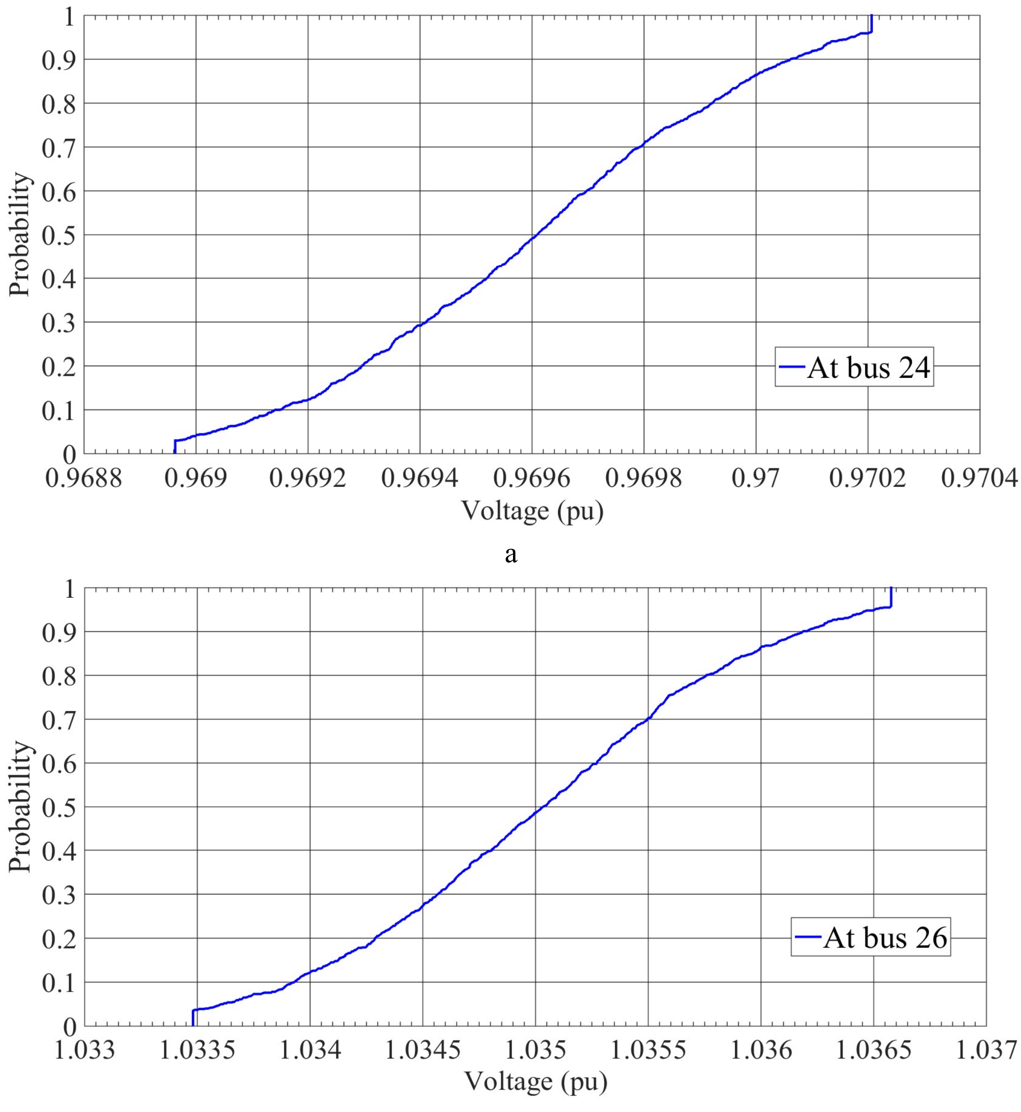

Figure 6-7: CDFs of the probability of voltage at the selected buses obtained by the NRLF study considering the model uncertainty due to the resistance of the substation transformer (a) in the voltage drop case, (b) in the voltage rise case

It is worth mentioning that in figure 6-7(a), the voltage value corresponding to the starting point of the plotted CDF relates to the scenarios in which the resistance of transformer has been equal to the upper bound of the considered range for R_T. Consequently, it leads to the point with the maximum voltage violation. Conversely, the voltage corresponding to the starting point of the plotted CDF in figure 6-7(b) belongs to the scenarios in which the resistance of transformer has been equal to the lower bound of the predefined range for R_T. Therefore, it gives the lower bound of the voltage violation.

6.5.6. On the cumulative uncertainty impacts associated with the models of loads, lines and substation transformer

In the last part of this chapter, the cumulative uncertainty effects of the load, line and transformer models on the system voltages are investigated. The MC simulations generate scenarios for the studied uncertain variables, which are α, β, and PF for the load buses, ΔR and $b/2$ for all lines and R_T for the substation transformer. Given that there are more uncertain variables in this case, the total number of scenarios is increased to 5000 in order to be able to capture all the possible realizations of the uncertain variables. The system voltages are obtained using the adapted NRLF study. Box plots of the node voltages are presented in figure 6-8. The corrected voltages obtained by the VCA (relying on the simplified deterministic models of the system components) are also plotted in the same figure in order to demonstrate clearly how the system voltages can vary as a result of the model uncertainty of the system components.

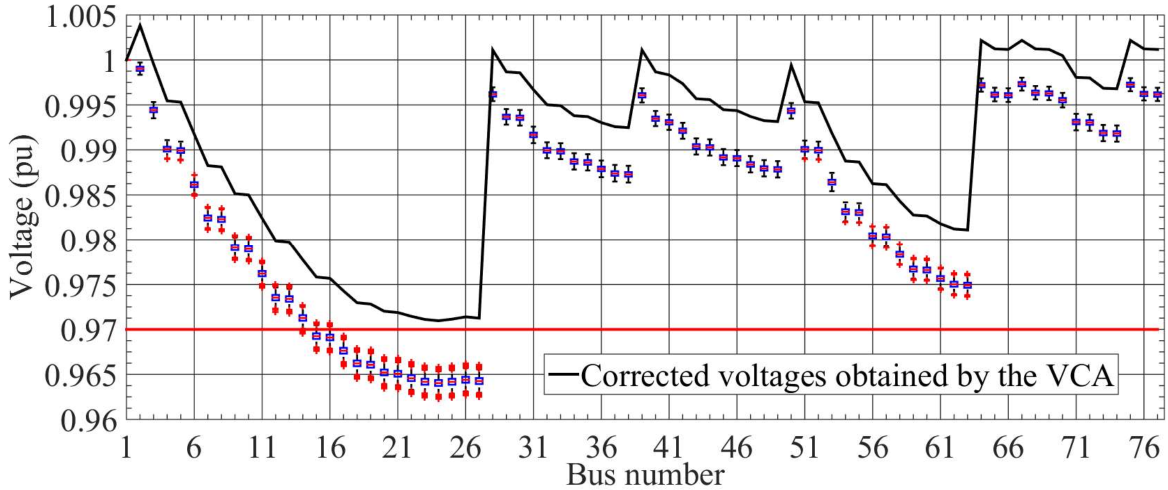

a

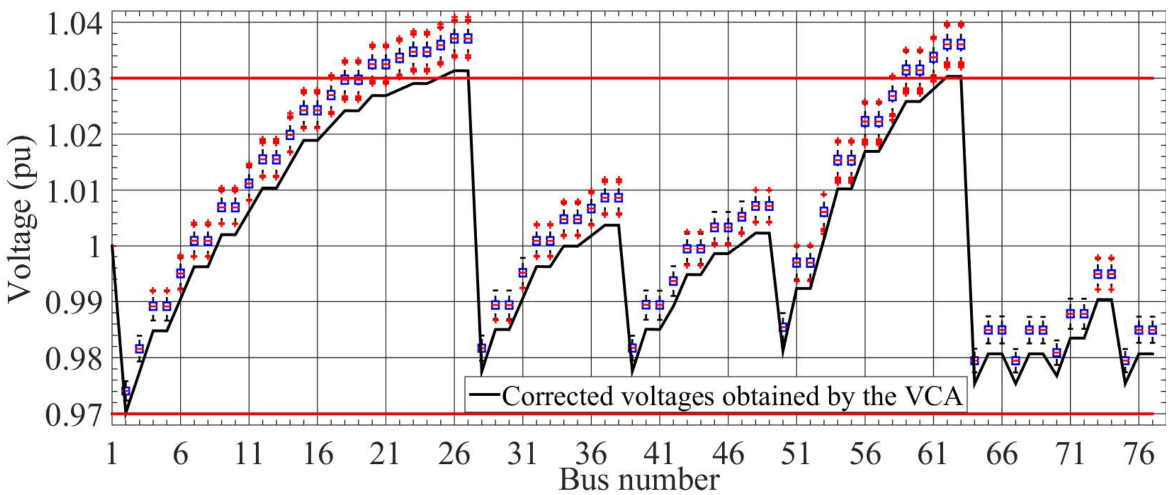

b

Figure 6-8: Box plots of the node voltages subject to the cumulative uncertainty effects of the studied components and the corrected voltages obtained by the VCA
(a) in the voltage drop case, (b) in the voltage rise case

In figure 6-8(a) corresponding to the investigation on the voltage drop case, it is seen that box plots of the node voltages exceed the permitted lower voltage limit. In the studies carried out on impact of each individual uncertain factor in the voltage drop situation, it was found that the voltage dependency of the loads and shunt admittances of the lines lead to a voltage increase while the internal resistance of the substation transformer and load power factor decrease the system voltages. Also, thermal dependency of the lines creates voltage variations around (in both directions) the corrected voltages. However, the uncertainty linked to the load power factors has the most dominant effect on the voltage results shown in figure 6-8(a) such that it can be stated that the voltage violations found in the voltage drop case mainly happen due to the power factor uncertainty of the loads. This point can be verified by taking into account the results shown in figure 6-4(a) according to which, voltage at bus 24 can decrease to nearly 0.96 pu due to the load power factor uncertainty. This big voltage drop has changed in figure 6-8(a) towards more moderate values due to compensating effects of $b/2$, α and β.

In the voltage rise case, cumulative uncertainty effects of the studied components create big voltage violations above the 1.03 pu voltage limit as it can be seen in figure 6-8(b). The maximum voltage violation occurs at bus 26 where the voltage amplitude can reach 1.041 pu. With regard to the voltages obtained by the VCA (relying on the simplified models), it is noticed that the node voltages can have violations up to nearly 0.01 (=1.041-1.0313) pu at bus 26 due to uncertain nature of the system component models. It is worth mentioning that in the voltage rise case, uncertainties related to the internal resistance of the substation transformer and thermal dependency of the branch resistances have the most dominant effects on the node voltages.

The obtained results in this section give us the maximum deviation that the node voltages can have due to cumulative uncertainty effects of the studied components. This can be utilized in order to reset the targeted voltage values of the VCA in such a way that it makes the VCA robust against possible deviations due to the inherent uncertainty related to the traditionally used (simplified) models of the network components. In this regard, in the studied VCA, in order to have the system voltages within the permitted 0.97 pu voltage limit, the targeted lower voltage value of the VCA should be changed to 0.9775 (=0.97+0.0075) pu, according to the maximum voltage deviation found in the voltage drop case at bus 24 which is equal to 0.0075 pu (see figure 6-8(a)). Similarly, the targeted upper voltage value of the VCA must be modified to 1.019 (=1.03-0.011) pu, based on the results shown in figure 6-8(b) regarding the maximum voltage deviation found at bus 26 (=0.011 pu). In this way, the VCA will be immunized against all possible realizations due to model uncertainty of the studied components. Figure 6-9 shows box plots of the system voltages as well as the corrected voltages obtained by the VCA when the targeted lower and upper voltage values of the VCA are modified to 0.9775 pu and 1.019 pu, respectively, in order to have system voltages within the permitted voltage range and consequently be robust against the intrinsic uncertainty in the models of the studied components. It should be noted that in adjusting the targeted bounds of the VCA, the errors arisen from the inaccuracy of the voltage sensitivity analyses have been considered as well.

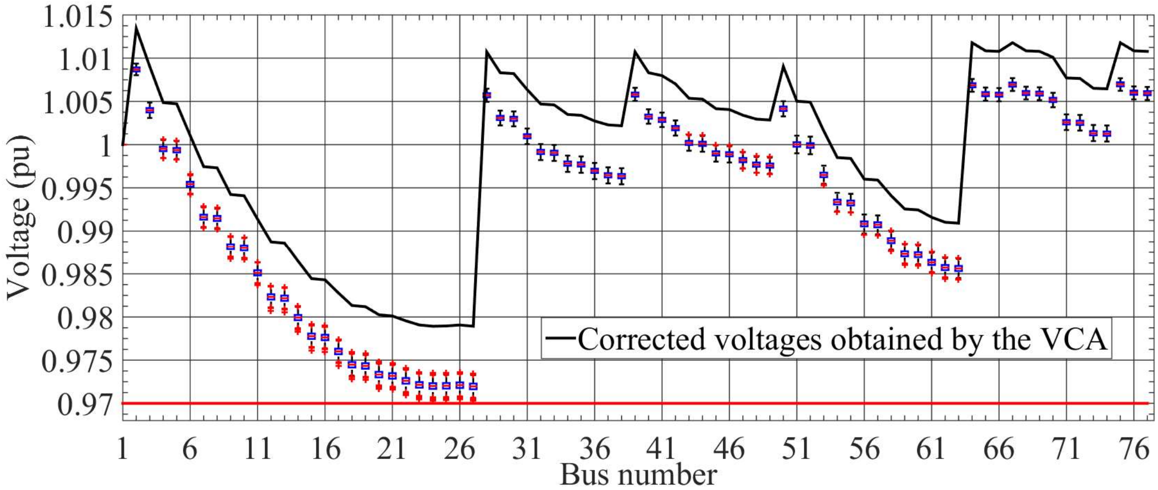

a

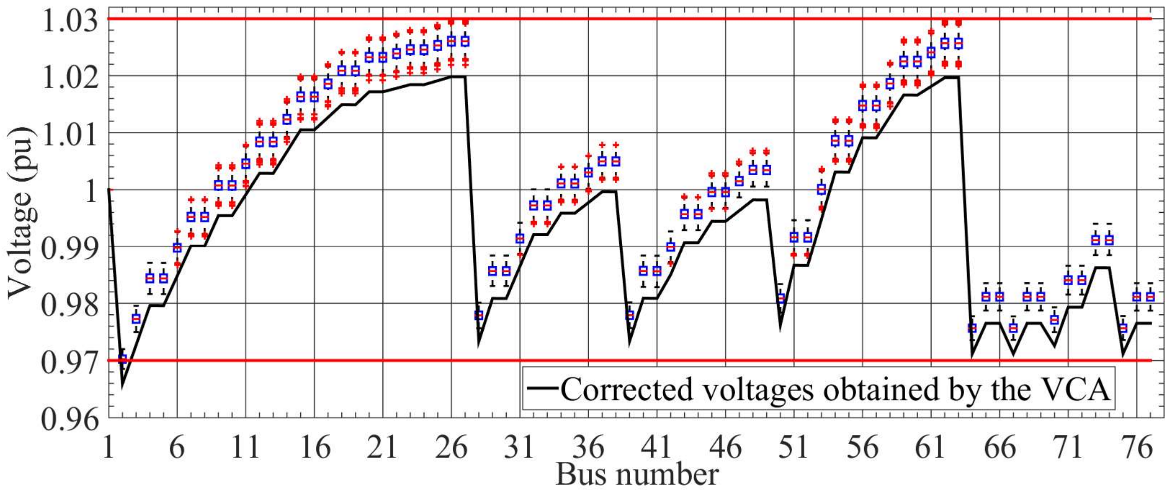

b

Figure 6-9: Box plots of the node voltages subject to the cumulative uncertainty effects of the studied components and the corrected voltages obtained by the VCA when the targeted voltage values of the VCA have been modified
(a) in the voltage drop case, (b) in the voltage rise case

As it can be seen in figure 6-9, in all created scenarios that take the model uncertainty effects into account, the system voltages do not violate the permitted voltage range in both voltage drop and rise conditions when applying the control actions undertaken by the VCA relying on the simplified models of the network components. On the other hand, as a consequence of modifying the targeted voltage bounds of the VCA, a conservative solution will be obtained by the VCA. To make it clearer, table 6-2 presents needed contributions of the control variables in order to solve the voltage control problem when the targeted voltage values of the VCA have been modified.

TABLE 6-2: VCA RESULTS IN THE VOLTAGE RISE AND DROP CONDITIONS WHEN THE TARGETED PERMITTED BOUNDS OF THE VCA HAVE BEEN MODIFIED

	Voltage drop	Voltage rise
ΔQ_{DGx} (Mvar) $x \in \{1, 2, 3, \ldots, 22\}$	DG5=-1.11	DG5= 2.288 DG18=1.282
ΔP_{DGx} (MW) $x \in \{1, 2, 3, \ldots, 22\}$	NA	NA
ΔTap_{TR}	4	-4
OF	5.665	9.35

As it can be seen in table 6-2, in the voltage rise state, when the targeted upper voltage value of the VCA is set to 1.019 pu, the VCA asks DG5 and DG18 to change their reactive powers by 2.288 Mvar and 1.282 Mvar, respectively. Also, the transformer tap changer is decreased by 4 steps. The objective function of the VCA in this case equals to 9.35 which is bigger than the one presented in table 6-1 (=5.786) when the targeted upper voltage point was 1.03 pu. The difference between the objective functions in these two cases indicates the control effort that should be added (or the price that we should pay) in order to make the VCA solutions fully robust against the effects of the model uncertainties. A similar trend can also be found considering the *OF* values corresponding to the voltage drop case in tables 6-1 and 6-2. In order to avoid such a conservative solution, a lower level of robustness can be eventually adopted that may result in some unwanted voltage violations.

6.6. Conclusion

In this chapter, impacts of the uncertainties associated with the models of the loads, lines, and substation transformer on the voltage constraints of the studied VCA are investigated. On the basis of the simulation results, it is concluded that the voltage dependency of loads does not cause voltage violation issue in the VCA. On the contrary, the load power factor uncertainty creates big voltage violations in the voltage drop case. Moreover, it is found that adding the shunt admittances of the lines results in increasing the system voltages and it can lead to voltage violation problem in the voltage rise state. Furthermore, it is shown that internal resistance of substation transformer and thermal dependency of branch resistances have considerable impacts on the system voltages in such a way that by taking them into account, voltage violations occur from both upper and lower voltage limits. Finally, through evaluating cumulative uncertainty effects of the studied components in the tested system, it has been demonstrated that the voltage violations from the permitted voltage range happen in both voltage drop and rise states. To avoid voltage violations due to the model uncertainty impacts, the targeted values of the VCA should be adjusted according to the results of the study on the cumulative uncertainty effects of the studied components.

The proposed framework of this chapter determines impacts of the model uncertainties on the node voltages on the basis of a posteriori analysis. **In the next chapter**, the studied uncertainties will be transferred inside the VCA. The robust optimization will be adopted to account for the model uncertainty. Solution of the robust optimization problem defines the control commands that remain immunized against all possible realizations of the uncertainties. Therefore, there will be no need to modify the targeted bounds of the VCA (as suggested in the current chapter) in order to maintain the system voltages within the permitted voltage limits given that the uncertainties will be included in the robust VCA formulation.

6.7. Chapter publication

This chapter has led to the following publications:

- B. Bakhshideh Zad, J. Lobry and F. Vallée, "Impacts of the model uncertainty on the voltage regulation problem of medium-voltage distribution systems," *IET Generation Transmission & Distribution*, vol. 12, no. 10, pp. 2359-2368, 2018.

- B. Bakhshideh Zad, J. Lobry, and F. Vallée, "Impacts of the load and line inaccurate models on the voltage control problem of the MV distribution systems," *52nd International Universities Power Engineering Conference (UPEC)*, Greece, 2017.

Chapter 7: A robust voltage control algorithm incorporating uncertainties related to the network component models

7.1. Abstract

In the last chapter of this thesis, uncertainties related to the network component models as presented in the previous chapter are considered in the VCA when taking corrective decisions of the control variables. The Robust Optimization (RO) is adopted to account for the uncertainties. The proposed VCA of this chapter determines a solution that remains robust against all possible realizations of uncertainties associated with the network component models. To this end, prior to formulating the voltage control problem, MC simulations are used to characterize uncertain models of the network components and LF calculations are carried out to evaluate their impacts. The RO under box uncertainty set is adopted to formulate the voltage control problem subject to the model uncertainty. The RO counterpart of the proposed VCA is derived based on the results obtained through the MC simulations and LF calculations. Once the RO problem is solved, in order to check robustness of the solution, system voltages are evaluated using the LF calculations considering the new set-points of control variables and uncertainties of the network component models.

7.2. Introduction

In many optimization applications, the problem data are assumed to be known with certainty. In practice, however, the realistic data are very often subject to uncertainty due to their random nature, measurement errors, or other reasons. Since the solution of the optimization problem exhibits high sensitivity to data perturbations, ignoring the data uncertainty could lead to solutions which are infeasible in practice [86]. Robust optimization presents methodology for dealing with the optimization problem subject to data uncertainty. Under this approach, we are willing to accept a suboptimal solution for the nominal values of data in order to ensure that this solution remains feasible when data change within the predefined ranges. In contrast to the stochastic optimization, RO formulates the uncertainty assuming that an uncertain value varies within a predefined interval rather than proposing a probability distribution function for it. Therefore, in the RO, uncertainty modelling is not stochastic, but rather determinate and set-based. Consequently, no assumption on the distribution of the uncertainty has to be made which is an attractive aspect of RO, especially, in the case of the lack of full information about the nature of the uncertainty [87].

In the electric power systems, data uncertainty can be arisen from the electricity price change, load or DG power variation, measurement noise, state estimation error, and the partial knowledge of the network model [88] and [89]. In the literature, RO techniques have been applied to problems such as volt-var control [90], voltage constraints management [46], optimal power flow [91], [92], economic dispatch [93], generation planning [94], [95], and microgrid planning [96].

7.3. Robust optimization problem

Consider the generic linear optimization problem presented in below.

$$\textbf{Maximize: } \mathbf{C}^{\mathrm{T}}\mathbf{x} \tag{7-1}$$

$$\mathbf{Ax} \le \mathbf{b} \tag{7-2}$$

$$\mathbf{l_b} \le \mathbf{x} \le \mathbf{u_b} \tag{7-3}$$

without loss of generality, it is assumed that data uncertainty only affects elements of matrix **A**. Consider a particular row i of the matrix **A** and let J_i be the set of column indices in row i that are subject to uncertainty. Each entry a_{ij} of matrix **A**, $j \in J_i$ is modelled as a symmetric and bounded random variable $\tilde{a}_{ij}$ that takes values from the range $[a_{ij} - \hat{a}_{ij}, a_{ij} + \hat{a}_{ij}]$ where a_{ij} is the nominal value of $\tilde{a}_{ij}$ and $\hat{a}_{ij}$ denotes its maximum positive perturbation. The uncertain data $\tilde{a}_{ij}$ is given by

$$\tilde{a}_{ij} = a_{ij} + \xi_{ij}\hat{a}_{ij} \tag{7-4}$$

where ξ_{ij} is a random variable which is subject to uncertainty and perturbs in the range [-1,1]. Under the uncertainty of matrix **A**, the robust optimization solution is the one that satisfies all constraints no matter what value the random variable ξ_{ij} takes within the range [-1,1]. In order to derive the robust counterpart of the presented generic linear optimization problem, the structural constraint (7-2) needs only to be modified as below given that the data uncertainty affects elements of matrix **A**.

$$\sum_{j \notin J_i} a_{ij}x_j + \sum_{j \in J_i} \tilde{a}_{ij}x_j \le b_i \quad \forall i \tag{7-5}$$

The above constraint can be reformulated further as

$$\sum_{j} a_{ij}x_j + \sum_{j \in J_i} \xi_{ij}\hat{a}_{ij}x_j \le b_i \quad \forall i \tag{7-6}$$

In the robust optimization with a predefined uncertainty set U, the robust solution is the one that remains feasible for any ξ in the given uncertainty set. The corresponding structural constraint of the RO problem under uncertainty set U is obtained by [86].

$$\sum_{j} a_{ij}x_j + \max_{\xi \in U} \sum_{j \in J_i} \xi_{ij}\hat{a}_{ij}x_j \le b_i \quad \forall i \tag{7-7}$$

The term $\max_{\xi \in U} \sum_{j \in J_i} \xi_{ij}\hat{a}_{ij}x_j$ provides the necessary protection of the *ith* constraint by maintaining a gap between $\sum_j a_{ij}x_j$ and b_i. In the following sections, the most prominent uncertainty sets are introduced and their corresponding RO problems are presented.

7.3.1. Robust optimization under box uncertainty set

In the box uncertainty set, it is assumed that ξ_{ij} is the random variable linked with each uncertain entry $\tilde{a}_{ij}$ in row i of matrix **A** which can vary independently between 0 and Ψ_i. The interaction of perturbations creates a box-shaped space, which represents the box uncertainty set described as follows.

$$U_b = \left\{ \tilde{a}_{ij} = a_{ij} + \xi_{ij}\hat{a}_{ij} \,\middle\|\, \xi_{ij} \right| \leq \Psi_i, \forall i \Big\} \tag{7-8}$$

where Ψ_i represents perturbation bounds for all uncertain coefficients of matrix A in row i. Figure 7-1 depicts the box uncertainty set for entry $\tilde{a}_j$ of matrix **A** where two elements of its *ith* row are subject to uncertainty (i.e., j=1,2).

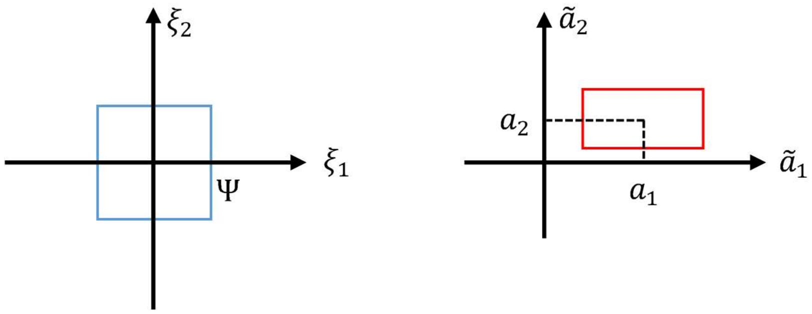

Figure 7-1: Illustration of the box uncertainty set

For the bounded uncertainty $\xi_j \in [-1,1]$, when Ψ is set to 1, the entire uncertain space $\tilde{a}_j$ is covered by the box uncertainty. This is a special case of the box uncertainty set which is known as interval uncertainty set. The robust counterpart optimization under box uncertainty is formulated as follows [86], [97], [98].

$$\textbf{Maximize: } \mathbf{c}^{\mathrm{T}}\mathbf{x} \tag{7-9}$$

$$\sum_j a_{ij}x_j + \left[\Psi_i \sum_{j \in J_i} \hat{a}_{ij} \left| x_j \right| \right] \leq b_i \quad \forall i \tag{7-10}$$

$$\mathbf{l_b} \leq \mathbf{x} \leq \mathbf{u_b} \tag{7-11}$$

Under the box uncertainty set, the solution of the optimization problem is robust for all perturbations smaller than Ψ_i. If Ψ_i is set to 1 (i.e. the interval uncertainty set), the above optimization problem results in the most conservative solution.

7.3.2. Robust optimization under ellipsoidal uncertainty set

As stated in the previous section, the interval uncertainty set leads to the most conservative solution, which has an advantage in the sense that it provides the highest protection against the uncertainties. On the other hand, conservatism of the interval uncertainty formulation can noticeably change the objective function value in comparison with its nominal one. In order to address this issue, the ellipsoidal uncertainty set has been proposed in [99] according to which, the uncertainty space is reduced through deleting a subset of uncertainty using the following set.

$$U_e = \left\{ \tilde{a}_{ij} = a_{ij} + \xi_{ij}\hat{a}_{ij} \,\middle|\, \sum_j \xi_{ij}^2 \le \Omega_i^2, \forall i \right\} \tag{7-12}$$

where Ω_i is an adjustable parameter associated with the *ith* row of matrix **A**, thanks to which, we can control the size (border) of the uncertainty set. Figure 7-2 illustrates the ellipsoidal uncertainty set where two uncertain coefficients (i.e., j=1,2) exist in the *ith* row of **A**.

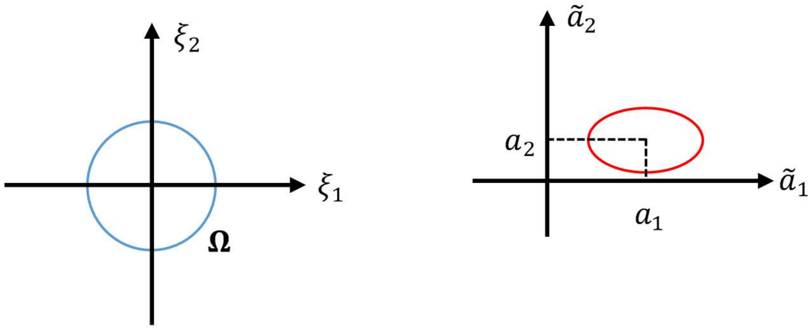

Figure 7-2: Illustration of the ellipsoidal uncertainty set

For the bounded uncertainty $\xi_j \in [-1,1]$, when $\Omega_i \ge \sqrt{|J_i|}$, $|J_i|$ is cardinality of the set J_i, the entire uncertain space $\tilde{a}_j$ is covered by the ellipsoidal uncertainty. Figure 7-3 shows the ellipsoidal uncertainty set for different values of Ω_i with respect to the interval uncertainty set (having $\Psi_i = 1$).

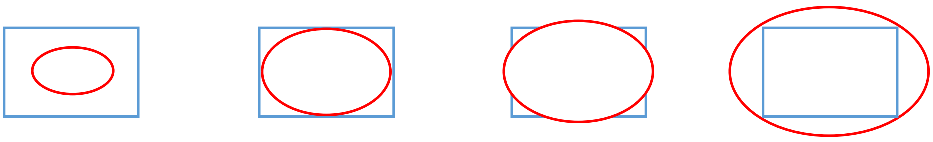

Figure 7-3: The ellipsoidal uncertainty set for different values of Ω

From figure 7-3, it is seen that when Ω_i=1, the ellipsoid is inscribed by the box and the whole uncertainty set is not covered in the ellipsoid. Consequently, the level of conservatism of the solution is reduced with respect to that of the interval set. The resulting RO problem under ellipsoidal uncertainty set is formulated as [86], [98].

$$\textbf{Maximize: } \mathbf{c}^{\mathrm{T}}\mathbf{x} \tag{7-13}$$

$$\sum_j a_{ij}x_j + \left[\Omega_i \sqrt{\sum_{j\in J_i} \hat{a}_{ij}^2 x_j^2}\right] \le b_i \quad \forall i \tag{7-14}$$

$$\mathbf{l_b} \le \mathbf{x} \le \mathbf{u_b} \tag{7-15}$$

In the bounded uncertainty $\xi_{ij} \in [-1,1]$, for any $\Omega_i < \left(\sqrt{|J_i|}\right)$, the ellipsoidal robust formulation leads to solution which is less conservative than the one obtained by the interval uncertainty set since every feasible solution of the former is a feasible solution to the latter. On the other hand, the robust model of the interval uncertainty set is a linear optimization problem while the ellipsoidal uncertainty set leads to a non-linear second-order cone optimization problem which demands more computational burden to solve and it will not be particularly attractive for the robust discrete optimization models [86], [98].

7.3.3. Robust optimization under polyhedral uncertainty set

In practice, it is needed to make a compromise between the optimization performance and the conservatism of the RO solution. In this regard, the robust formulation under polyhedral uncertainty set is developed in [98]. The polyhedral uncertainty set is defined as follows.

$$U_p = \left\{ \tilde{a}_{ij} = a_{ij} + \xi_{ij}\hat{a}_{ij} \middle| \sum_j |\xi_{ij}| \le \lfloor \Gamma_i \rfloor, \forall i \right\} \tag{7-16}$$

As defined before, consider J_i to be set of the column indices of the *ith* row that are subject to uncertainty. For every row i, a parameter Γ_i is introduced, not necessarily integer, that takes value in the range $[0, |J_i|]$. The role of parameter Γ_i is to adjust the robustness level of the solution. This choice is motivated by the fact that it is unlikely that all of the entries $a_{ij}, j \in J_i$ will change due to uncertainty. Figure 7-4 shows the uncertainty space under polyhedral set when two entries of the *ith* row of matrix **A** are subject to uncertainty.

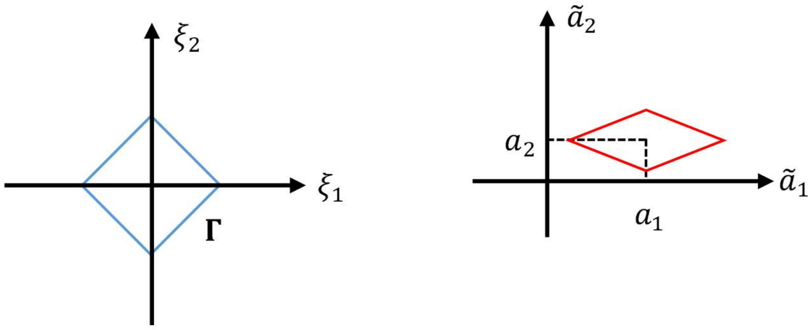

Figure 7-4: Illustration of the polyhedral uncertainty set

For the bounded uncertainty $\xi_j \in [-1,1]$, when $\Gamma_i \ge |J_i|$, the entire uncertain space $\tilde{a}_j$ is covered by the polyhedral uncertainty. Figure 7-5 shows the polyhedral uncertainty set for different values of Γ_i with respect to the interval uncertainty set (having $\Psi_i = 1$).

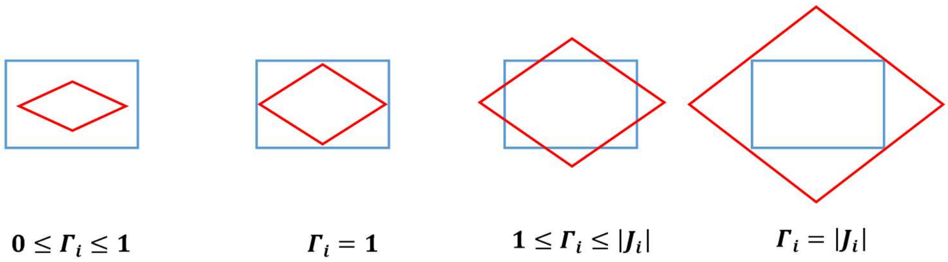

Figure 7-5: The polyhedral uncertainty set for different values of Γ

In figure 7-5, it is seen that when $\Gamma_i = 1$, the polyhedron is inscribed by the box of interval uncertainty set and the intersection between the polyhedron and the box is the polyhedron. Also, when $\Gamma_i = |J_i|$, the intersection between the polyhedron and the box is the box. The RO formulation under polyhedral uncertainty set is given by [86], [98], [100]:

$$\textbf{Maximize: } \mathbf{c}^{\mathrm{T}}\mathbf{x} \tag{7-17}$$

$$\sum_j a_{ij} x_j + \max_{\{S_i \cup \{t_i\} | S_i \subseteq J_i, |S_i| = \lfloor \Gamma_i \rfloor, t_i \in J_i \setminus S_i\}} \left[\sum_{j \in S_i} \hat{a}_{ij} y_j + (\Gamma_i - \lfloor \Gamma_i \rfloor) \hat{a}_{it} y_t \right] \le b_i \quad \forall i \tag{7-18}$$

$$-y_j \le x_j \le y_j \tag{7-19}$$

$$\mathbf{l_b} \le \mathbf{x} \le \mathbf{u_b} \tag{7-20}$$

$$\mathbf{y} \ge 0 \tag{7-21}$$

The solution of the above optimization problem is protected against all cases in which up to $\lfloor \Gamma_i \rfloor$ of coefficients are allowed to change and one coefficient a_{it}, changes by $(\Gamma_i - \lfloor \Gamma_i \rfloor \hat{a}_{it})$. If Γ_i is chosen to be an integer, the *ith* constraint is protected by $\max_{\{S_i | S_i \subseteq J_i, |S_i| = \Gamma_i\}} \{\sum_{j \in S_i} \hat{a}_{ij} |x_j|\}$. Moreover, when $\Gamma_i = 0$, the *ith* constraint is equal to that of the nominal problem and $\Gamma_i = |J_i|$ leads to the roust formulation under the interval uncertainty set. Therefore, by varying $\Gamma_i \in [0, |J_i|]$, it is possible to adjust the robustness of the polyhedral model against the level of the conservatism of solutions.

7.4. On the choice of the uncertainty set for the robust voltage control algorithm

The Robust VCA (RVCA) of this chapter adopts the model under box uncertainty set. This choice is motivated by the fact that the ellipsoidal robust formulation converts the initial linear optimization problem into a non-linear second-order one and results in increasing complexity and calculation burden of the RVCA. In addition, the polyhedral uncertainty set leads to a bi-level nested optimization problem. Although the latter has a linear dual model, due to introduction of dual variables, the size of the robust counterpart of the VCA increases in the polyhedral model. Consequently, given that under the box uncertainty, the RVCA has the same number of variables and constraints as the initial VCA and the RVCA formulation remains linear similarly to the initial VCA, the RO under the box uncertainty set is adopted in this chapter. In order to provide the highest protection against the worst uncertainty case, Ψ_i is set to 1 that eventually belongs to the interval uncertainty set.

7.5. The robust voltage control algorithm

As stated before, the RVCA aims at finding corrective control actions of the decision variables such that the obtained solution remains immunized against the uncertainties associated with the network component models. Figure 7-6 presents the proposed methodology of this chapter to this end, which consists of the pre-processing stage, RO formulation and post-processing stage.

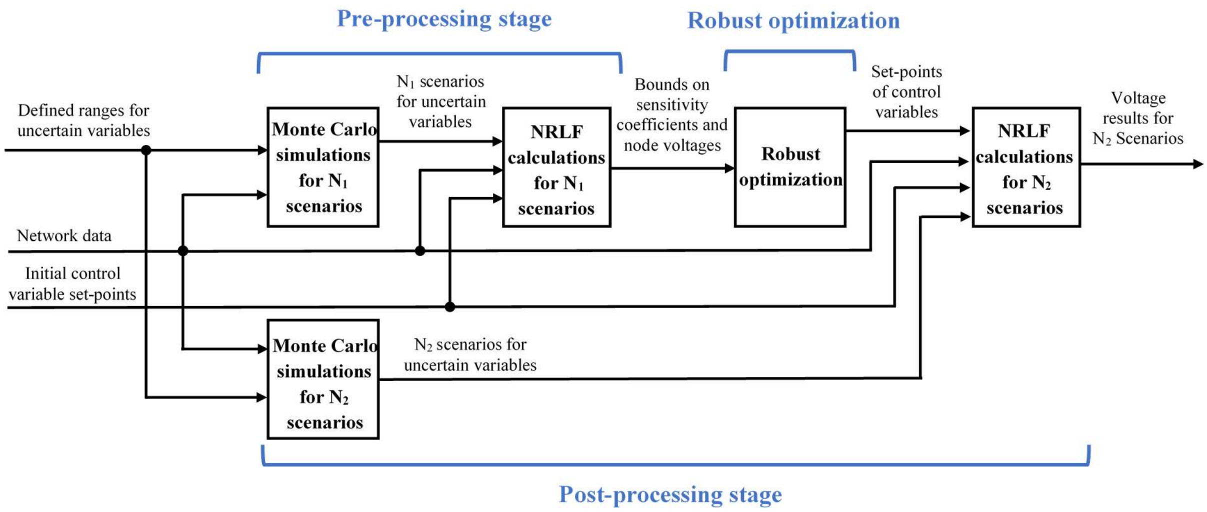

Figure 7-6: The proposed approach to develop a robust voltage control algorithm

As it can be seen in figure 7-6, the pre-processing stage determines impacts of the model uncertainties on the voltage control problem using MC simulations and LF calculations. The RO formulation is derived then on the basis of information provided by the pre-processing stage. The solution of the RO defines needed changes of control variables in order to solve the voltage control problem subject to model uncertainty. The obtained solution of the RO is finally validated in the post-processing stage and the robustness of the solution is evaluated. The three parts of the proposed approach are discussed further in the following sections.

7.5.1. The pre-processing stage

Similarly to chapter 6, the network components are considered here with uncertain variables which are bounded within the predefined ranges. The first step of the proposed method shown in figure 7-6 is to characterize the model uncertainties. To this end, MC simulations are utilized to create N_1 scenarios for the uncertain variables of the network component models. As a result of the model uncertainty, in each scenario, the elements of matrix **A** (i.e. the voltage sensitivity matrix) will be perturbed with respect to their initial values. Given that perturbation bounds of elements of matrix **A** are not known, in the second step, LF calculations are performed for each of N_1 scenarios created by the MC simulations. Beside the perturbations on elements of matrix **A** which correspond to the LHSs of the structural constraints of the generic RO problem, the model uncertainty will change the RHSs of those constraints. In a voltage control context, the RHS uncertainties of structural constraints can represent the errors associated with the state estimation interface or noise of the voltage measurement devices. When the RHS of the *ith* structural constraint is subject to uncertainty, we have

$$\tilde{b}_i = b_i + \xi_{i0}\hat{b}_i \tag{7-22}$$

where $\tilde{b}_i$ and $\hat{b}_i$ are the uncertain RHS of the *ith* structural constraint and its perturbation value, respectively. Also, ξ_{i0} is the random variable associated with uncertainty of RHS of the *ith* structural constraint. The structural constraint (7-7) of the generic RO problem is needed to be rewritten when uncertainties are in both of the RHS and LHS, as follows.

$$\sum_j a_{ij}x_j + \max_{\xi\in U}\left\{-\xi_{i0}\hat{b}_i + \sum_{j\in J_i}\xi_{ij}\hat{a}_{ij}x_j\right\} \le b_i \quad \forall i \tag{7-23}$$

Considering the box uncertainty set, the above constraint is equal to [86]

$$\sum_j a_{ij}x_j + \Psi_i\left[\sum_{j\in J_i}\hat{a}_{ij}\left|x_j\right| + \hat{b}_i\right] \le b_i \quad \forall i \tag{7-24}$$

When LF calculations for N_l scenarios are carried out, perturbations of voltage sensitivity coefficients (i.e. entries of **A**) as well as variations of node voltages (which define the uncertainties related to the RHSs of the structural constraints) are known. Therefore, the RO counterpart of the VCA under the interval uncertainty set subject to uncertainties in RHS and LHS of the structural constraints can be derived.

7.5.2. The robust optimization formulation

The RO counterpart of the sensitivity-based VCA optimization problem presented in chapter 5 ((5-30) to (5-36)) in the voltage rise case is given as follows when uncertainties are in RHS and LHS of the structural constraints.

$$\textbf{Minimize: } OF = \sum_{x=1}^{N_G}\left(C_Q\left|\Delta Q_{DGx}^{ind} - \Delta Q_{DGx}^{cap}\right| + C_P\Delta P_{DGx}\right) + C_{TR}\left|\Delta Tap_{TR}^{up} - \Delta Tap_{TR}^{down}\right| \tag{7-25}$$

$$\sum_{x=1}^{N_G}\left(\frac{\widetilde{\partial V_u}}{\partial Q_{DGx}}(\Delta Q_{DGx}^{ind} - \Delta Q_{DGx}^{cap}) + \frac{\widetilde{\partial V_u}}{\partial P_{DGx}}\Delta P_{DGx}\right) + \frac{\widetilde{\partial V_u}}{\partial V_{Tap}}(\Delta Tap_{TR}^{up} - \Delta Tap_{TR}^{down}) \le \widetilde{\Delta V}_u^{req} \quad \forall u, u\in U \tag{7-26}$$

$$0 \le \Delta P_{DGx} \le \left|P_{DGx}\right| \quad \forall x,\ x\in G \tag{7-27}$$

$$\Delta Q_{DGx}^{\min} \le \Delta Q_{DGx}^{ind} - \Delta Q_{DGx}^{cap} \le \Delta Q_{DGx}^{\max} \quad \forall x,\ x\in G \tag{7-28}$$

$$\Delta Tap_{TR}^{\min} \le \Delta Tap_{TR}^{up} - \Delta Tap_{TR}^{down} \le \Delta Tap_{TR}^{\max} \tag{7-29}$$

$$\Delta Q_{DGx}^{ind}, \Delta Q_{DGx}^{cap}, \Delta Tap_{TR}^{up}, \Delta Tap_{TR}^{down} \ge 0 \quad \forall x,\ x\in G \tag{7-30}$$

As before, u is index for the buses with the voltage rise and set U includes all the buses with the voltage rise violations. $\frac{\partial\widetilde{V}_u}{\partial Q_{DGx}}$, $\frac{\partial\widetilde{V}_u}{\partial P_{DGx}}$ and $\frac{\partial\widetilde{V}_u}{\partial V_{Tap}}$ stand for uncertain sensitivity coefficients of voltage at bus u with respect to reactive power of DGx, active power of DGx, and transformer tap, respectively. The RHS of the structural constraint (7-26) denoted by $\widetilde{\Delta V}_u^{req}$ gives the uncertain needed voltage modification at bus u in order to return its voltage within the permitted voltage range. Assuming that the model uncertainty will affect all elements of the *uth* row of the voltage sensitivity matrix, the structural constraint of the above RVCA optimization problem can be rewritten according to (7-24) as follows.

$$\begin{aligned}&\sum_{x=1}^{N_G}\left[\left[\left(\frac{\partial V_u}{\partial Q_{DGx}}+\frac{\widehat{\partial V_u}}{\partial Q_{DGx}}\right)(\Delta Q_{DGx}^{ind}-\Delta Q_{DGx}^{cap})\right]+\left[\left(\frac{\partial V_u}{\partial P_{DGx}}+\frac{\widehat{\partial V_u}}{\partial P_{DGx}}\right)\Delta P_{DGx}\right]\right]\\&+\left[\left(\frac{\partial V_u}{\partial V_{Tap}}+\frac{\widehat{\partial V_u}}{\partial V_{Tap}}\right)(\Delta Tap_{TR}^{up}-\Delta Tap_{TR}^{down})\right]+\widehat{\Delta V_u}^{req}\leq\Delta V_u^{req}\qquad\forall u,u\in U\end{aligned}\tag{7-31}$$

where $\frac{\widehat{\partial V_u}}{\partial Q_{DGx}}$, $\frac{\widehat{\partial V_u}}{\partial P_{DGx}}$ and $\frac{\widehat{\partial V_u}}{\partial V_{Tap}}$ are perturbations of voltage sensitivity coefficients of bus u with respect to the control variables. Also, $\widehat{\Delta V}_u^{req}$ is the perturbation of needed voltage modification at bus u due to model uncertainty imapct. Note that the perturbations of node voltages and voltage sensitivity coefficients are obtained by performing LF calculations in N_l scenarios of the pre-processing stage. In the voltage drop case, the corresponding structural constraint of the RO problem is given as below where index u is replaced by l referring to buses with voltage drop violations found in set L.

$$\begin{aligned}&\sum_{x=1}^{N_G}\left[\left[\left(\frac{\partial V_l}{\partial Q_{DGx}}+\frac{\widehat{\partial V_l}}{\partial Q_{DGx}}\right)(\Delta Q_{DGx}^{ind}-\Delta Q_{DGx}^{cap})\right]+\left[\left(\frac{\partial V_l}{\partial P_{DGx}}+\frac{\widehat{\partial V_l}}{\partial P_{DGx}}\right)\Delta P_{DGx}\right]\right]\\&+\left[\left(\frac{\partial V_l}{\partial V_{Tap}}+\frac{\widehat{\partial V_l}}{\partial V_{Tap}}\right)(\Delta Tap_{TR}^{up}-\Delta Tap_{TR}^{down})\right]+\widehat{\Delta V_l}^{req}\geq\Delta V_l^{req}\qquad\forall l,l\in L\end{aligned}\tag{7-32}$$

As before, the 0.97 pu voltage limit is selected as the targeted point for the buses with the voltage drop violations. Given that the model uncertainty does not necessarily create symmetrical variation around nominal value of each entry of the sensitivity matrix, perturbations of sensitivity coefficients in (7-31) or (7-32) must be selected such that the maximum protection against the worst uncertainty scenario is guaranteed. In this regard, the perturbation that reduces the absolute value of each entry of the sensitivity matrix at most is selected because in this way, the biggest value of control variable changes will be demanded. Consequently, the highest protection against the model uncertainty is provided. In addition, the perturbation that creates the biggest voltage violation at the *lth* or *uth* bus of the system (among N_l scenarios) will be chosen since it gives the worst voltage violation scenario at bus l or u.

The voltage sensitivity coefficients with respect to nodal active and reactive powers in each of N_l created scenarios are obtained based on the JBSA method as the Jacobian matrix is in our disposition in the NRLF study. The nodal voltage sensitivities with respect to transformer tap are calculated using the perturb-and-observe technique. To this end, the voltage variation in the observed point is calculated using the NRLF when the transformer tap position (i.e. the perturbation point) is moved by one step.

7.5.3. The post-processing stage

Once the abovementioned linear RO problem is solved, new set-points of control variables (i.e. active and reactive power changes of DGs as well as the transformer tap movement) are available. As stated before, the obtained solution of the RVCA must remain immunized against all possible realizations of uncertainties associated with the network component models. In order to verify the latter, further analyses are carried out on the new set-points of control variables. In this regard, MC simulations are used to create N_2 scenarios for uncertain parameters of the network component models. Then, LF calculations are done on each of the N_2 scenarios considering the set-points of control variables obtained by the RO and the rest of the network data. Finally, node voltages in N_2 scenarios will be in our disposition, which will present the robustness of the RVCA solution in N_2 realizations of uncertainties associated with the network component models.

In the proposed approach shown in figure 7-6, in the pre-processing stage (prior to composing the RO problem), when choosing needed number of scenarios (i.e. N_1) for characterizing uncertainties and defining their impacts, the requirement regarding the execution time of the RVCA must be taken into account. Such a limit does not exist when N_2 scenarios are created to validate the RVCA results since the corrective decisions have been already made. Consequently, N_2 can be much bigger than N_1. In this way, the RVCA results will be tested for extra scenarios that are not necessarily included among N_1 generated scenarios in the first stage of the MC simulations. It is worth noting that the defined variation ranges for uncertain variables of network component models are identical when creating scenarios in the pre-processing and post-processing stages.

7.6. Studied sources of the model uncertainty

Like the previous chapter, uncertainties associated with the voltage dependency of loads, power factor of loads, thermal dependency of lines, shunt admittances of lines and internal resistance of substation transformer are taken into consideration here. The proposed RVCA firstly manages the voltage constraints under uncertainty arisen from each of the abovementioned sources (individually). Then, all studied sources of uncertainties are considered to be present simultaneously and the RVCA solves the voltage control problem under uncertainties of load, line and transformer models. The investigations of this chapter are done on the voltage rise and drop conditions corresponding to the same working points as presented in the previous chapter. It should be noted that the defined ranges for the uncertain variables of the network component models are also identical with the ones given in chapter 6. In addition, MC creates scenarios on the basis of the procedure described in section 6.3.2.

7.7. Simulation results

The proposed RVCA including the MC simulation, NRLF calculation, and the presented RO formulation is implemented in the MATLAB environment. Performance of the RVCA is tested on the UKGDS shown in figure 3-1 in the voltage drop and rise states. Two working points as follows are defined in order to create the voltage drop and rise conditions. In the first working point for the voltage drop case, all loads are considered to be at their maximum values (=100%) while active powers of DGs are equal to zero. In the second working point corresponding to the voltage rise state, it is supposed that the load powers are at 10% of their respective nominal values and active powers of DGs are equal to 90% of their rated values. The initial reactive powers of DGs in both cases are set to zero.

In order to consider the constraint regarding the calculation time of the RVCA, in the pre-processing stage (prior to forming the RO problem), 500 scenarios (N_1=500) are created by the MC simulations. However, to validate the RO results, number of scenarios is increased to 2000 (N_2=2000). In the voltage control procedure, it is supposed that the OLTC action has the smallest weighting coefficient compared to other control variables which is equal to 1 (C_{TR}=1) while the reactive power changes of DGs are weighted by a coefficient which is 50% bigger than the OLTC one (C_Q=1.5). Also, active power curtailment of DGs is assigned to a coefficient which is 100% bigger than the OLTC one (C_P=2). The upper and lower permitted nodal voltage limits are equal to 1.03 pu and 0.97 pu, respectively.

Table 7-1 presents the demanded contributions of DGs and necessary transformer tap movements in order to manage voltage violations in the voltage rise and drop cases when the model uncertainty is neglected. The initial system voltages (with voltage violations) as well as the ones obtained after the voltage regulation using the simple VCA corresponding to the nominal network model are depicted in figure 7-7.

TABLE 7-1: VCA RESULTS IN THE VOLTAGE RISE AND DROP CONDITIONS CONSIDERING SIMPLE MODELS OF NETWORK COMPONENTS

	Voltage drop	Voltage rise
ΔQ_{DGx} (Mvar) $x \in \{1, 2, 3, \ldots, 22\}$	DG5=-1.266	DG5=1.363
ΔP_{DGx} (MW) $x \in \{1, 2, 3, \ldots, 22\}$	NA	NA
ΔTap_{TR}	2	-4
OF	3.897	6.044

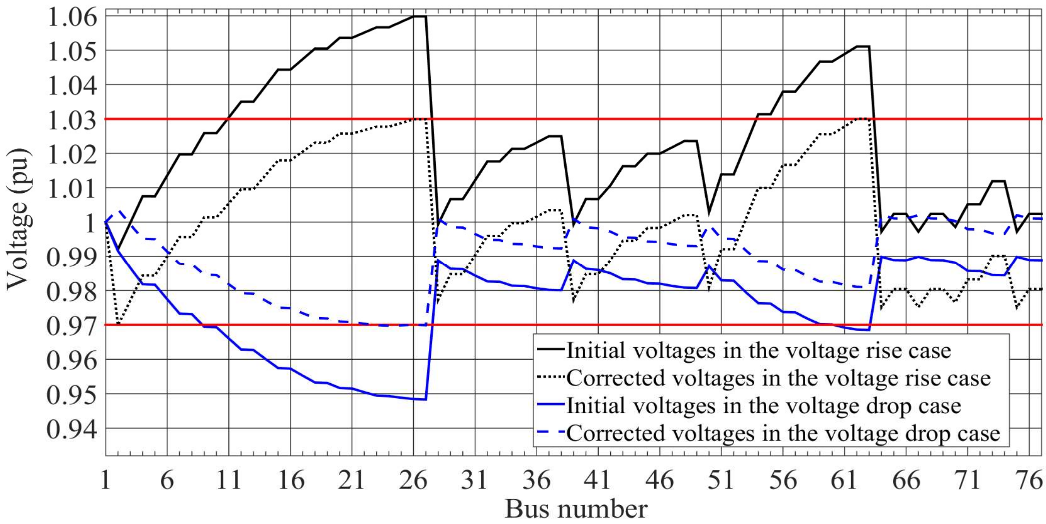

Figure 7-7: Initial nodal voltages as well as the corrected ones obtained by the simple VCA relying on simplified models of network components in the voltage drop and rise

In what follows, the RVCA is utilized to manage the voltage constraints in the voltage rise and drop conditions under uncertainty of the network component models. The RVCA results are compared with the ones obtained through the simple VCA (which does not consider the model uncertainty and relies on the simplified deterministic network model).

7.7.1. On the uncertainty linked with the voltage dependency of the loads

In the first studied case, the uncertainty due to the voltage dependency of loads is taken into consideration. The RVCA manages the node voltages in the voltage drop and rise conditions under uncertainty of the load-voltage dependency. Due to the fact that in the voltage rise condition, load powers are equal to 10% of their nominal values, it can be expected that the load-voltage dependency will not have important impact on this case. Conversely, in the voltage drop condition, load powers are maximal; therefore, study on the RVCA performance considering the load-voltage dependency in the voltage drop case will be of interest.

Table 7-2 presents the control variable changes demanded by the RVCA to manage the voltage violations in both voltage rise and drop conditions. For ease of comparison, the results obtained using the simple VCA are also given hereafter in the same table. Moreover, figure 7-8 shows the boxplots of initial and corrected voltages subject to the studied uncertainty of this section as well as the initial and corrected voltages obtained by relying on the simplified deterministic component model. The boxplots of initial voltages show the possible perturbations of node voltages due to the model uncertainty, which correspond to the uncertainty in RHSs of the structural constraints. The boxplots of corrected voltages give the voltage results obtained in N_2 scenarios considering the solution of the RO problem. Hereafter, boxplots of the initial voltages are shown in blue while ones related to the corrected voltages are illustrated in black.

TABLE 7-2: ROBUST VCA RESULTS CONSIDERING THE UNCERTAINTY ASSOCIATED WITH VOLTAGE DEPENDENCY OF LOADS IN COMPARISON WITH THE SIMPLE VCA RESULTS; IN THE VOLTAGE RISE AND DROP CONDITIONS

	Voltage drop		Voltage rise	
	RVCA	Simple VCA	RVCA	Simple VCA
ΔQ_{DGx} (Mvar) $x \in \{1, 2, 3, \ldots, 22\}$	DG5=-2.577	DG5=-1.266	DG5=1.364	DG5=1.363
ΔP_{DGx} (MW) $x \in \{1, 2, 3, \ldots, 22\}$	NA	NA	NA	NA
ΔTap_{TR}	NA	2	-4	-4
OF	3.845	3.897	6.046	6.044

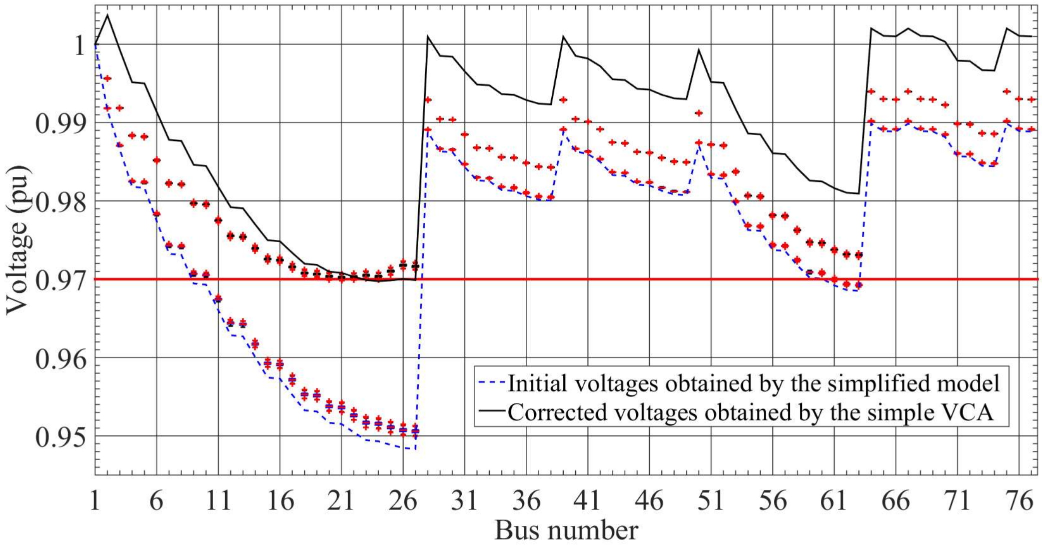

a

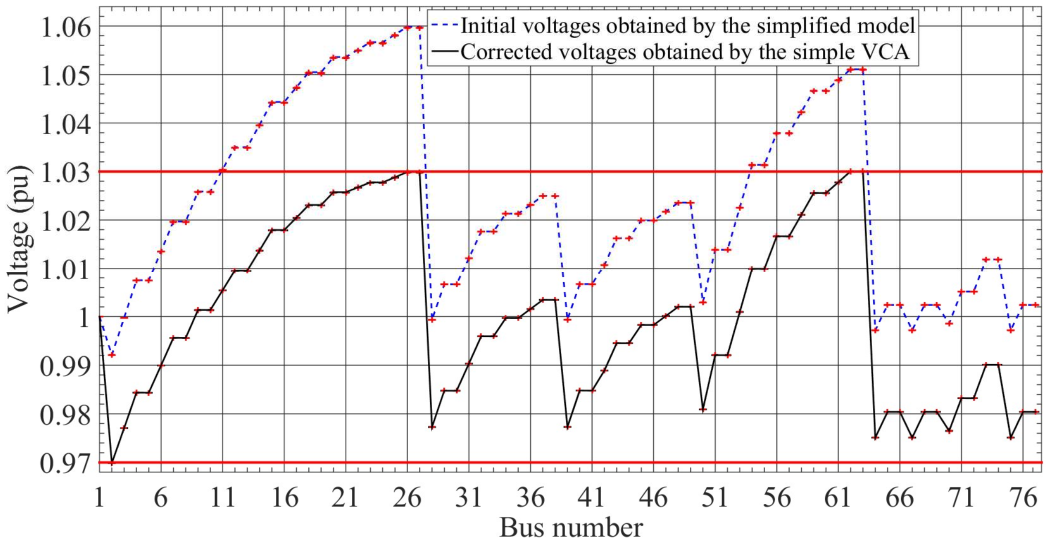

b

Figure 7-8: The voltages obtained using simplified network component models as well as boxplots of initial and corrected voltages considering the uncertainty associated with the voltage dependency of load
(a) in the voltage drop case, (b) in the voltage rise case

In the voltage drop condition, the voltage control problem considering the uncertainty has been solved with a smaller value of objective function compared to the one obtained by the simple VCA using the simplified (power constant) load model as it can be seen in table 7-2. This is due to the fact that in the voltage drop condition, node voltages are smaller than 1 pu; therefore, the load-voltage dependency reduces the load powers. Consequently, the load-voltage uncertainty decreases the severity of the voltage control problem. In other words, perturbations caused by the studied uncertainty release (smooth) the structural constraints of the RO problem such that less control effort is needed to solve the voltage control problem in the voltage drop condition. Similar interpretation can be also done on the basis of the voltage results shown in figure 7-8(a) where it is seen that boxplots of initial voltages are placed above the voltages obtained by the simplified load model.

Furthermore, from table 7-2, it can be concluded that the uncertainty impact due to the load-voltage dependency in the voltage rise condition is negligible since the RVCA and simple VCA have led to almost similar results in this case. The latter point can be verified further considering the figure 7-8(b) where it is seen that boxplots of initial and corrected voltages have very narrow bounds.

7.7.2. On the uncertainty linked with the power factor of the loads

Performance of the RVCA under uncertainty of load power factors is investigated here on the studied voltage rise and drop conditions. Similar to the previous case, it can be expected that the power factor uncertainty impact appears mostly on the voltage drop condition since the load powers are maximal in this case. Table 7-3 and figure 7-9 present the RVCA results under uncertainty of the load power factors.

TABLE 7-3: ROBUST VCA RESULTS CONSIDERING THE UNCERTAINTY ASSOCIATED WITH POWER FACTOR OF LOADS IN COMPARISON WITH THE SIMPLE VCA RESULTS; IN THE VOLTAGE RISE AND DROP CONDITIONS

	Voltage drop		Voltage rise	
	RVCA	Simple VCA	RVCA	Simple VCA
ΔQ_{DGx} (Mvar) $x \in \{1, 2, 3, \ldots, 22\}$	DG5=-1.327	DG5=-1.266	DG5=1.317	DG5=1.363
ΔP_{DGx} (MW) $x \in \{1, 2, 3, \ldots, 22\}$	NA	NA	NA	NA
ΔTap_{TR}	4	2	-4	-4
OF	5.991	3.897	5.976	6.044

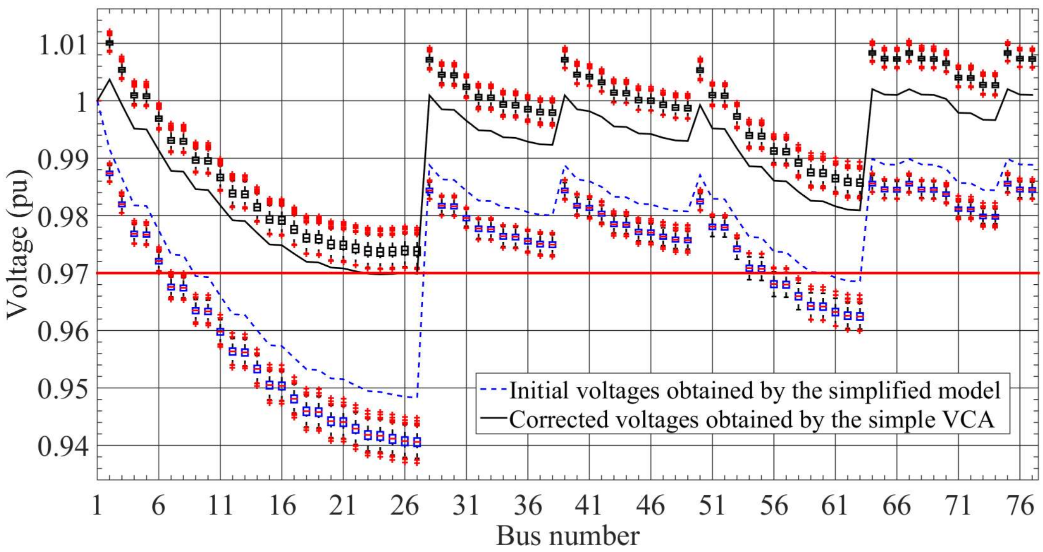

a

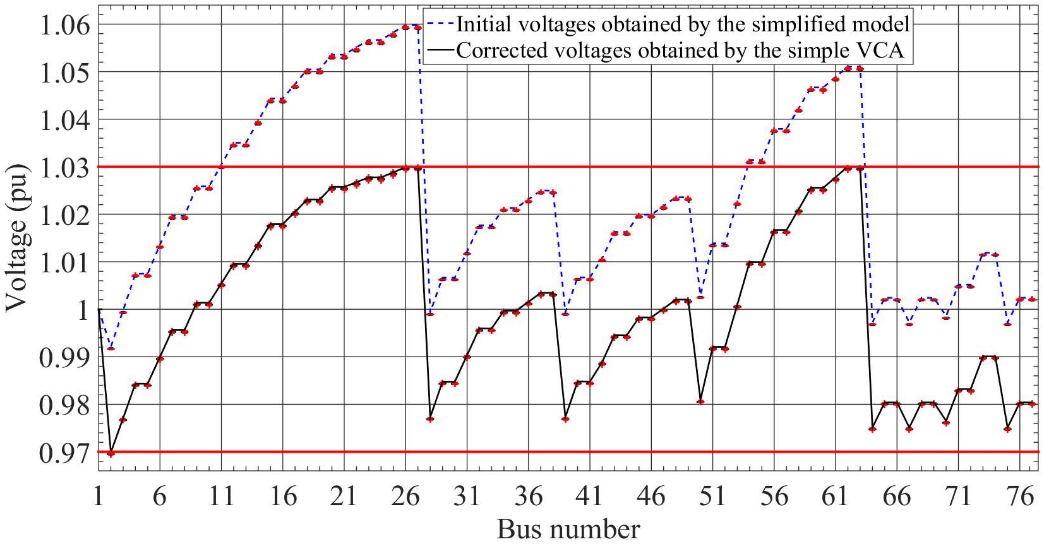

b

Figure 7-9: The voltages obtained using simplified network component models as well as boxplots of initial and corrected voltages considering the uncertainty associated with the power factor of load
(a) in the voltage drop case, (b) in the voltage rise case

As stated before (in section 6.5.2), the average power factor of loads in the studied UKGDS is equal to 0.98. Considering the defined range for the power factor variation from 0.9 to 1, the load reactive powers will increase because of the power factor uncertainties. Consequently, in figure 7-9(a), it is observed that boxplots of the initial node voltages are noticeably lower than the initial voltages obtained by neglecting load power factor uncertainties. The difference between the former and latter can reach almost 0.01 pu. Therefore, a bigger value of control variable changes is needed to manage the voltage control problem under uncertainty of load power factors in the voltage drop case as it can be seen in table 7-3.

In figure 7-9(b) regarding the voltage rise condition, it is seen that as a result of the load power factor uncertainty, boxplots of the initial voltages are placed under the voltages obtained by the simplified load model. It is due to the fact that power factor uncertainties have increased the load reactive powers with respect to their initial values. Consequently, in the voltage rise condition, the voltage control problem under load power factor uncertainties has been solved with a smaller value of objective function in comparison with the one of the simple VCA (see table 7-3). From figures 7-9(a) and 7-9(b), it is noticed that the boxplots of the corrected voltages in the voltage drop and rise conditions do not violate the permitted voltage range in all N_2 created scenarios. Therefore, it is verified that the RVCA solution remains immunized against all realizations of the studied uncertainty. It is worth observing that the solution of the simple VCA is optimal and feasible for the nominal value of the uncertain variable. If the latter takes any other value than its nominal one, the solution of the simple VCA would be either infeasible or non-optimal. In the current studied case, the solution of the simple VCA is infeasible in the voltage drop case and non-optimal in the voltage rise case (for any value of the uncertain variable other than the nominal one). In contrast, the solution of the RVCA remains feasible for all realizations of uncertainty (within the predefined range) and is optimal with respect to the worst uncertainty scenario.

7.7.3. On the uncertainty linked with the thermal dependency of lines

In this section, thermal dependency of lines is taken into consideration as the source of the uncertainty. The RVCA is utilized to manage the voltage control problem of the studied working points under uncertainty of the line resistances due to the thermal dependency effect. Table 7-4 and figure 7-10 present the RVCA results corresponding to the voltage rise and drop conditions.

TABLE 7-4: ROBUST VCA RESULTS CONSIDERING THE UNCERTAINTY ASSOCIATED WITH THERMAL DEPENDENCY OF LINES IN COMPARISON WITH THE SIMPLE VCA RESULTS; IN THE VOLTAGE RISE AND DROP CONDITIONS

	Voltage drop		Voltage rise	
	RVCA	Simple VCA	RVCA	Simple VCA
ΔQ_{DGx} (Mvar) $x \in \{1, 2, 3, \ldots, 22\}$	DG5=-1.403	DG5=-1.266	DG5=1.876 DG18=0.544	DG5=1.363
ΔP_{DGx} (MW) $x \in \{1, 2, 3, \ldots, 22\}$	NA	NA	NA	NA
ΔTap_{TR}	2	2	-4	-4
OF	4.103	3.897	7.631	6.044

In the voltage drop case, as stated in section 6.4.3, it is considered that the line resistances can vary within the range of ±5.8% of their nominal values due to the thermal dependency effect. This creates voltage variations around the initial voltages (obtained by neglecting thermal dependency of branch resistances) as it can be seen in figure 7-10(a). The RVCA solution must remain immunized against the worst possible realization of the uncertainty. Therefore, the perturbations that create the worst uncertainty scenarios are selected to compose the structural constraints of the RO problem. The worst uncertainty scenario in the voltage drop condition corresponds to the case in which the initial voltages are equal to their minimum in boxplots shown in figure 7-10(a) and the absolute values of voltage sensitivity indexes are reduced at most by the thermal dependency impact. Figure 7-10(a) confirms that when the RVCA solution is applied to N_2 simulated scenarios (that take the model uncertainty impact into account), the box plots of the corrected voltages do not violate the permitted voltage range. In order to be protected against the uncertainty associated with the thermal dependency of line resistances, the reactive power changes of DG5 has changed from -1.266 Mvar (i.e. the simple VCA results) to -1.403 Mvar as it can be seen in table 7-4.

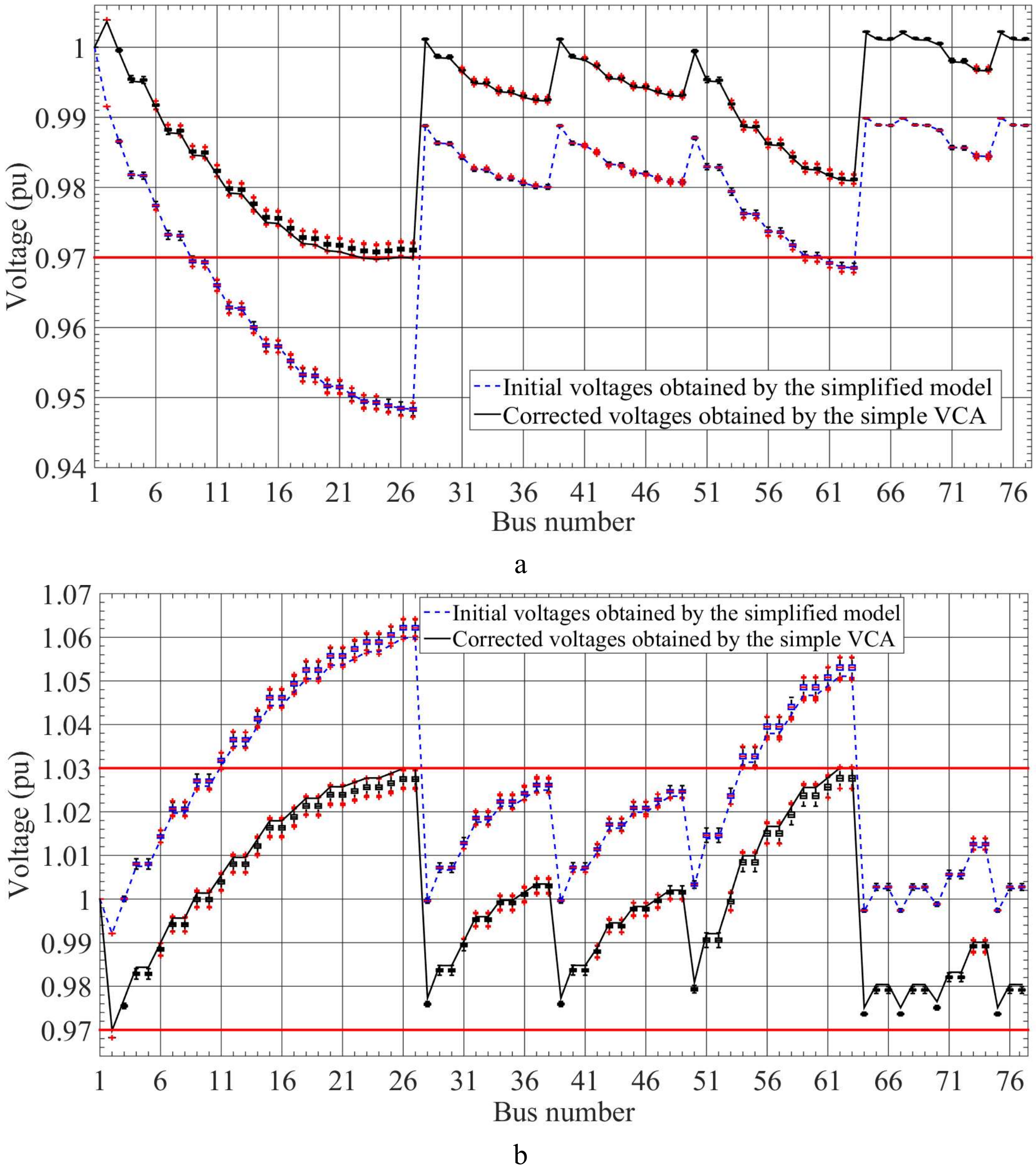

Figure 7-10: The voltages obtained using simplified network component models as well as boxplots of initial and corrected voltages considering the uncertainty associated with thermal dependency of lines
(a) in the voltage drop case, (b) in the voltage rise case

In the voltage rise condition, thermal dependency effect creates bigger voltage variations compared to the ones in the voltage drop situation as it can be noticed from boxplots of initial voltages shown in figures 7-10(a) and 7-10(b). It is explained by the fact that the defined range for the resistance variation (due to the thermal dependency effect) is wider in the voltage rise condition. In order to have a protected solution against the uncertainty effect in the voltage rise condition, the reactive powers of DG18 and DG5 are increased by 0.544 and 0.513 Mvar, respectively, with respect to the results of the simple VCA (see table 7-4). Figure 7-10(b) verifies that the solution of the RVCA is immunized against realization of N_2 scenarios in the voltage rise condition.

7.7.4. On the uncertainty linked with the shunt admittances of the lines

The RVCA performance is tested here when shunt admittances of the lines are considered as source of the uncertainty. Given that in the simplified line model, the shunt admittances have been totally neglected, it is expected that the consideration of shunt admittances will increase the node voltages in both voltage rise and drop conditions. Table 7-5 and figure 7-11 present the RVCA results under uncertainty of shunt admittances of the lines.

TABLE 7-5: ROBUST VCA RESULTS CONSIDERING THE UNCERTAINTY ASSOCIATED WITH SHUNT ADMITTANCES OF LINES IN COMPARISON WITH THE SIMPLE VCA RESULTS; IN THE VOLTAGE RISE AND DROP CONDITIONS

	Voltage drop		Voltage rise	
	RVCA	Simple VCA	RVCA	Simple VCA
ΔQ_{DGx} (Mvar) x=1, 2, …, N_G	DG5=-1.207	DG5=-1.266	DG5=1.485 DG18=0.062	DG5=1.363
ΔP_{DGx} (MW) x=1, 2, …, N_G	NA	NA	NA	NA
ΔTap_{TR}	2	2	-4	-4
OF	3.81	3.897	6.281	6.044

In table 7-5 regarding the RVCA results in the voltage drop condition, it is seen that as a result of incorporation of shunt admittances, objective function of the RVCA is reduced with respect to the one of the simple VCA from 3.897 to 3.81. It is due to the fact that shunt admittances of lines increase the initial node voltages with respect to the ones obtained by the simple line model as it can be seen in figure 7-11(a). Therefore, the severity of the voltage control problem is decreased when shunt admittances are taken into account. Consequently, a smaller value of control variable changes is needed for managing the voltage violations in the voltage drop condition in presence of uncertainties due to shunt admittances of lines.

Unlike the voltage drop condition, in the voltage rise situation, in order to have a protected solution against the uncertainty of shunt admittances, the objective function of the RVCA increases with respect to that of the simple VCA as it can be seen in table 7-5. From figure 7-11(b), it is noticed that boxplots of initial voltages in N_1 scenarios are found to be in above of the initial voltages obtained by the simple line model meaning that the studied uncertainty has raised the nodal voltages. As a consequence, the robust solution must have a bigger value to provide the needed protection against the worst uncertainty case. Figure 7-11(b) confirms that the solution of the RVCA remains protected under N_2 realizations of shunt admittance values.

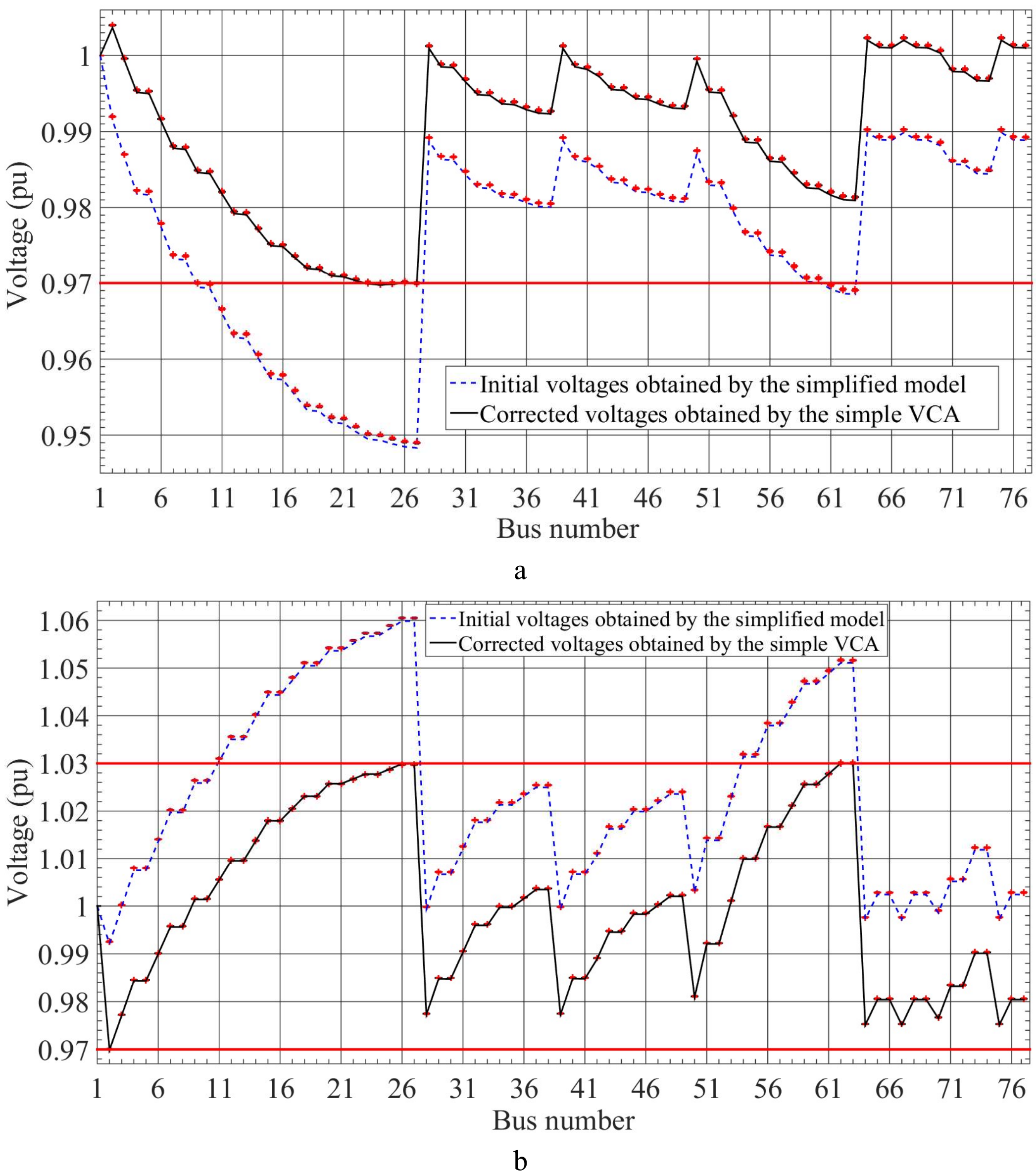

Figure 7-11: The voltages obtained using simplified network component models as well as boxplots of initial and corrected voltages considering the uncertainty associated with shunt admittances of the lines
(a) in the voltage drop case, (b) in the voltage rise case

7.7.5. On the uncertainty linked with the internal resistance of substation transformer

The internal resistance of the substation transformer is considered to be an uncertain variable in this section. The RVCA is employed to manage the voltage constraints in the voltage rise and drop conditions when the internal resistance of the transformer has a random but bounded value given in section 6.5.5. Table 7-6 and figure 7-12 present the RVCA results in the studied cases under uncertainty of the transformer resistance.

TABLE 7-6: ROBUST VCA RESULTS CONSIDERING THE UNCERTAINTY ASSOCIATED WITH INTERNAL RESISTANCE OF TRANSFORMER IN COMPARISON WITH THE SIMPLE VCA RESULTS; IN THE VOLTAGE RISE AND DROP CONDITIONS

	Voltage drop		Voltage rise	
	RVCA	Simple VCA	RVCA	Simple VCA
ΔQ_{DGx} (Mvar) x=1, 2, …, N_G	DG5=-1.534	DG5=-1.266	DG5=1.911 DG18=0.644	DG5=1.363
ΔP_{DGx} (MW) x=1, 2, …, N_G	NA	NA	NA	NA
ΔTap_{TR}	2	2	-4	-4
OF	4.298	3.897	7.864	6.044

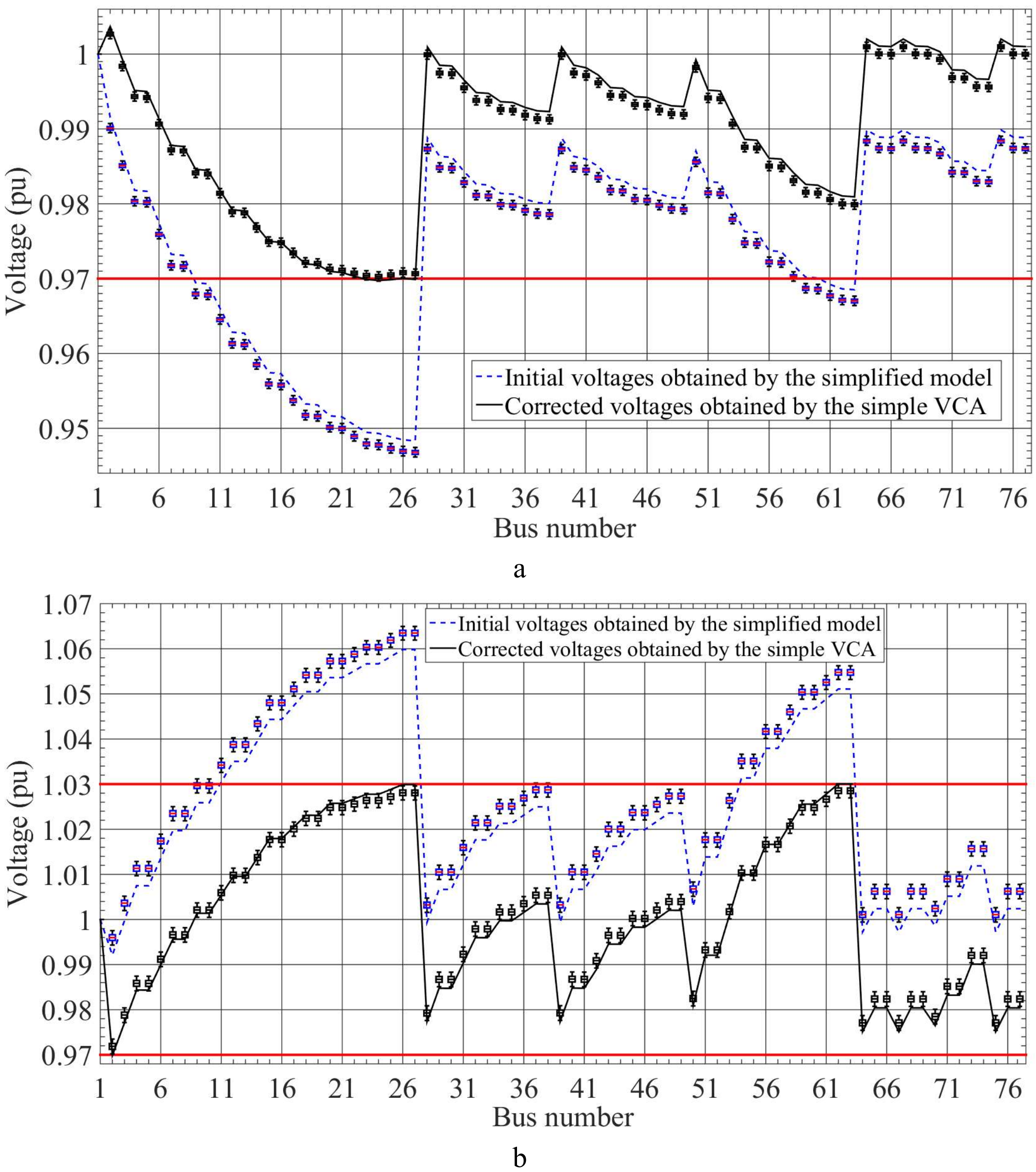

Figure 7-12: The voltages obtained using simplified network component models as well as boxplots of initial and corrected voltages considering the uncertainty associated with the internal resistance of transformer
(a) in the voltage drop case, (b) in the voltage rise case

From table 7-6, it can be noticed that in both voltage drop and rise cases, the RVCA solution has a bigger objective function value compared to its counterpart obtained by the simple VCA. This means that in practice, the solution obtained by the simple VCA will not be sufficient to solve the voltage control problem of the considered points due to the uncertainty that exists in the value of the transformer internal resistance. Figure 7-12 demonstrates that the solution of the RVCA remains immunized against N_2 realizations of the transformer resistance uncertainty in both voltage rise and drop conditions since boxplots of corrected voltages do not exceed the permitted voltage range.

In order to be protected against the uncertainty of the transformer resistance, the objective function of the RVCA has increased by 0.401 in the voltage drop and 1.824 in the voltage rise conditions (with respect to the objective function of the simple VCA). Therefore, it can be concluded that the studied uncertainty has a more important effect on the voltage rise case though the defined range for variation of the transformer resistance is identical in both voltage rise and drop cases. It is explained by the fact that in the studied UKGDS, total powers of DGs are almost three times bigger than sum of the load powers. Therefore, in the voltage rise case where DG powers are maximal, internal resistance of transformer can create bigger impact on the node voltages compared to the voltage drop case where the load powers are at their maximum values.

7.7.6. On the cumulative uncertainties linked with the load, line and transformer models

In the last case study, the uncertainties are considered to be arisen from the load, line, and transformer models. The RVCA performance under uncertainties of the network component models is evaluated on the same working points as before corresponding to the voltage rise and drop conditions. Prior to forming the RO formulation, in order to characterize the uncertainties and to evaluate their impacts, it is needed to create scenarios for the considered uncertain variables, which are α, β and PF for all loads, ΔR and $b/2$ for all lines and R_T for the substation transformer. Given that there are more uncertain variables in the current case, number of 500 scenarios (N_1=500) that is used in the previous cases would not be sufficient to capture all the important possible realizations of the mentioned uncertainties. On the other hand, due to the constraint regarding the execution time of the RVCA, it is not possible to increase N_1. In order to deal with this issue, in the pre-processing stage of the RVCA, the uncertain variables that have bigger impacts on the voltage control problem are only taken into consideration. In the voltage rise condition, it was shown that the transformer resistance and thermal dependency of line resistances have led to the biggest changes of the RVCA objective function (with respect to the one of the simple VCA). In the voltage drop condition, the uncertainties associated with the load models and transformer resistance have resulted in the biggest variations of the RVCA objective function. Therefore, the RO is constructed considering the selected sources of the uncertainty as mentioned in above in each of the voltage rise or drop case. Once the RO problem of the RVCA is solved, then, in order to validate the results, the nodal voltages are evaluated considering the solution of the RO when all uncertain variables of the network component models are taken into account simultaneously. In the post-processing stage, we increase the total number of scenarios to 5000 (N_2=5000) since the RVCA decision is already made. It should be noted that the total number of scenarios created in the pre-processing stage remains unchanged equal to 500. Table 7-7 shows the RVCA results for managing the voltage constraints under uncertainties of network component models, and figure 7-13 presents the corresponding boxplots of node voltages in the voltage rise and drop conditions.

TABLE 7-7: ROBUST VCA RESULTS CONSIDERING THE UNCERTAINTIES ASSOCIATED WITH MODELS OF LOAD, LINE AND TRANSFORMER IN COMPARISON WITH THE SIMPLE VCA RESULTS; IN THE VOLTAGE RISE AND DROP CONDITIONS

	Voltage drop		Voltage rise	
	RVCA	Simple VCA	RVCA	Simple VCA
ΔQ_{DGx} (Mvar) x=1, 2, …, N_G	DG5=-2.666	DG5=-1.266	DG4=0.0702 DG5=2.31 DG18=1.194	DG5=1.363
ΔP_{DGx} (MW) x=1, 2, …, N_G	NA	NA	NA	NA
ΔTap_{TR}	2	2	-4	-4
OF	5.993	3.897	9.361	6.044

As it can be noticed from table 7-7, the objective function of the RVCA has raised in both voltage rise and drop conditions (compared to that of the simple VCA) due to presence of the model uncertainty. This means that the solution of the simple VCA can be insufficient to solve the voltage control problem of the real case. Taking the voltage results shown in figure 7-13 into account reveals that the considered simplification of the uncertainty sources in the pre-processing stage of the RVCA does not create voltage violation when all uncertainties are included in the result validation (post-processing) stage since the boxplots of the corrected voltages are within the permitted voltage limits. Therefore, it can be concluded that within the considered variation range of the uncertain variables in this work, uncertainties linked with the thermal dependency of lines and internal resistance of transformer have the most important effects on the voltage control problem of the studied system in the voltage rise condition. For the voltage management in the voltage drop case, load and transformer models are recognized as the most important sources of the model uncertainty.

7.8. Conclusion

In the proposed voltage control algorithm of this chapter, the uncertainties associated with the network model are considered when taking the corrective decision of the control variables. The voltage control problem under uncertainty of the network model is formulated as a RO problem. Prior to forming the RO counterpart of the voltage control algorithm, MC simulation and LF calculation are employed to characterize and evaluate the impact of the model uncertainty. The needed time for the pre-processing stage of the RVCA is about 50 s which includes creation of N_I (=500) scenarios for the uncertain variables of the network component models and evaluation of their impacts by running LF calculations. Due to the fact that sensitivity of transformer tap changes to node voltages are obtained by the POSA method, for each scenario, two LF calculations must be done before and after the tap movement. Therefore, number of 1000 LF calculations is performed in the pre-processing stage.

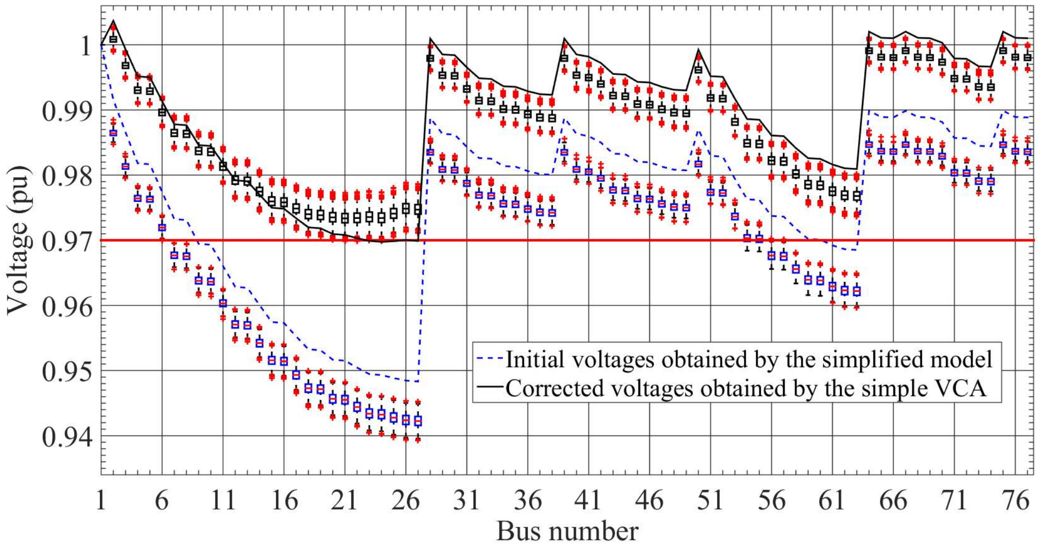

a

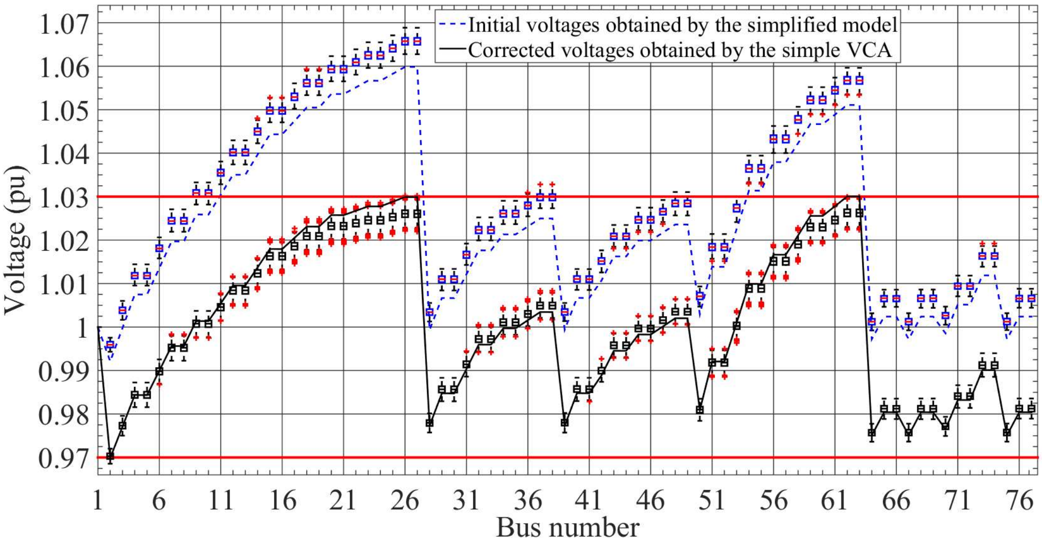

b

Figure 7-13: The voltages obtained using simplified network component models as well as boxplots of initial and corrected voltages considering the uncertainties associated with the load, line, and transformer models
(a) in the voltage drop case, (b) in the voltage rise case

On the basis of the simulation results, it is found that although the model uncertainty in most of the studied cases has led to an increase of the objective function of the RVCA with respect to that of the simple VCA, in special cases, the severity of the voltage control problem is reduced when considering the model uncertainty. For instance, the uncertainty linked with the voltage dependency of loads smooths the structural constraints of the RVCA such that the voltage control problem considering that source of uncertainty is solved with a smaller value of objective function compared to the case of neglecting the load-voltage uncertainty in the simple VCA. However, it is observed that when cumulative effects of the studied uncertainties are taken into account, in both voltage rise and drop conditions, the objective function of the RVCA is raised with respect to the simple VCA one. This indicates that the solution of the simple VCA can be insufficient to solve the voltage control problem of the real cases.

7.9. Chapter publication

This chapter has led to the following working paper to be submitted for publication:

- B. Bakhshideh Zad, J. Lobry and F. Vallée, "A robust voltage control algorithm incorporating the model uncertainty impacts," *Working paper*.

Chapter 8: General conclusion

8.1. Contributions

In this thesis, voltage control problem of the MV distribution systems under deterministic to uncertain model has been addressed. In the first part of the thesis, considering the simplified deterministic network model, a centralized sensitivity-based voltage control approach has been developed which manages the transformer tap position and DG powers in order to maintain the node voltages and branch currents within their permitted limits. The main contributions of the first part of the thesis which includes chapters 2 to 5 are as follows.

- A novel voltage sensitivity analysis method has been developed that determines impacts of the nodal active and reactive powers on the system voltages directly from the topology of the network.
- A new formulation has been suggested in order to consider the branch ampacity limits as a function of DG powers.
- Two voltage control algorithms relying on the open-loop and closed-loop functioning modes have been designed to manage the operational limits of the system. Thanks to the information provided by the proposed sensitivity analysis methods, the voltage control problem has been simplified to a linear optimization formulation aiming at minimizing the control variable changes while maintaining the node voltage constraints and branch ampacity limits.
- The performance of the proposed VCAs has been tested in chapters 2 and 3 in terms of the accuracy of the results and the execution time of the VCAs.
- The importance of incorporating the power losses in the VSA formulation has been demonstrated in chapter 4 by proposing the improved direct sensitivity analysis method and through comparative studies of the IDSA with the DSA, POSA and JBSA approaches.
- A straightforward approach has been suggested to derive impacts of the transformer tap changes on the node voltages.
- The performance of the sensitivity-based VCAs employing DG active and reactive powers as well as the transformer tap changer has been evaluated in chapter 5. Finally, in the end of this chapter, it has been explained that how the proposed sensitivity-based VCAs should be modified in order to comply with the practical limitations of the realistic MV distributions systems and to be used for the voltage constraints management of the real cases.

In the second part of the thesis, it has been considered that the network model is not anymore deterministic but it is rather uncertain varying within the predefined bounds. The voltage control problem under uncertainty of the network model has been studied in chapters 6 and 7. The contributions of this part are given in below.

- The uncertainties associated with the voltage dependency of loads, power factor of loads, thermal dependency of lines, shunt admittances of lines and internal resistance of substation transformer have been investigated using the Monte Carlo simulation technique.
- A probabilistic framework has been developed in chapter 6 in order to determine the upper and lower bounds of the voltage variations in the VCA due to uncertainty of the network model.
- The voltage control problem under uncertainty of the network model has been formulated as a robust optimization. The proposed robust VCA of the last chapter determines a solution that remains immunized against all possible realizations of uncertainties associated with the network component models.

The relevant publications of the current thesis are listed in appendix 4.

8.2. Conclusions

To get an overall conclusion regarding the first part of the thesis, we refer to section 1.7 introducing the motivation for carrying out the current research where it has been stated that:

''if the accuracy of the results obtained by the sensitivity-based voltage control approach is confirmed, then, it can be concluded that the proposed method is more suitable than the VCA based on the conventional OPF formulation particularly for the threefold reasons. Firstly, the sensitivity-based voltage control approach has a much simpler formulation compared to the OPF-based one and can give us a better understanding about the voltage control procedure. Secondly, due to its simplified formulation, the solution of the optimization problem of the sensitivity-based voltage control approach can be obtained in a faster way, which makes it more suitable for the on-line management of the operational limits. Finally, the sensitivity-based voltage control approach does not require the state estimation interface and with limited number of voltage and power measurements, it can manage the operational limits of the system''.

In the first part of the thesis, it is found that performance of the sensitivity-based voltage control approach depends on the accuracy of the sensitivity data. If the relations between the voltage constraints and decision variables can be linearized accurately, the sensitivity-based voltage control approach can manage the operational limits of the system in an efficient and optimal manner. In chapter 2, it has been shown that the DSA method and the proposed formulation for considering the branch ampacity limits can estimate the corrected node voltages and branch currents with little errors when reactive powers of DGs are changed for the voltage regulation end. In chapter 4, accuracy of the voltage results obtained by the IDSA has been verified when DG active and reactive powers are controlled. In addition, in chapter 5, it has been demonstrated that the suggested approach to derive the sensitivity of node voltages with respect to transformer tap changes with a negligible error can estimate the node voltages.

The sensitivity data however can be erroneous because of the non-linearity of the equations. In such a case, the multi-step VCA is preferred over the single-step VCA. The MSVCA functioning in a closed-loop mode has the advantage that can direct the system towards the targeted (safe) working point even in presence of the inaccurate sensitivity data. In addition, in the multi-step VCA, the priority of the voltage regulation is given to the bus with the biggest voltage violation such that in each step (or iteration), the biggest voltage violation of the system is removed. Thanks to this iterative procedure, the system working point moves gradually towards the safe point and the mutual impacts of the control variables are limited to the ones located in the feeder with the biggest voltage violation.

In all the simulated cases of chapters 2 to 5, the corrective control decisions of the SSVCA and MSVCA have been made within a very short time, which does not exceed 0.5 s. This confirms that the proposed sensitivity-based voltage control approach can comply with the framework of the on-line voltage constraints management.

Considering the results of chapters 6 and 7, it is concluded that the model uncertainty can have considerable impacts on the voltage constraints. In order to have a robust solution against the uncertainty effects, we can keep the VCA simple (relying on the simplified deterministic network model) and modify its targeted bounds based on the maximum deviations that the node voltages can have due to the model uncertainty. An alternative approach is to transfer the uncertainties inside the VCA and construct a robust optimization formulation. The latter method appears to be more optimal and less conservative since its solution is immunized against the considered working point while in the former approach, we modify the targeted bounds of the VCA based on the maximum deviations of the node voltages. On the other hand, the former method can be better scaled with the framework of the on-line voltage constraints management.

8.3. Applications

The sensitivity-based voltage control approach developed in the first part of the thesis can be used as the centralized decision-making tool of the DSOs to manage the voltage constraints of the MV distribution systems while keeping the ampacity limits of the branches. As discussed in the end of chapter 5, the sensitivity-based VCA by having the network data and relying on limited measurements can manage the operational limits of the system. The main advantage of the proposed approach over the classical centralized VCA methods is that it does not require the state estimation interface and its computation time is very fast that makes it suitable for the on-line management of the operational limits.

In addition, the proposed framework in chapter 6 can bring useful information to DSOs regarding the impacts of the model inaccuracy on their performed calculations and analyses. It determines the upper and lower bounds of voltage variations due to uncertainty of the network model. Finally, given that the voltage deviations arisen from the imperfect deterministic network model are inevitable, the DSOs can utilize the robust VCA developed in chapter 7. The corrective solution of the robust VCA remains immunized (at an extra cost) against any realization of the uncertainty within the predefined bounds.

8.4. Perspectives and future works

The VCAs developed in the first part of the thesis can be completed further by taking advantage of the other voltage control methods such as energy storage, load management, and power electronics-based devices. In addition, complementary constraints can be added to the VCAs regarding the impacts of the undertaken control decisions on the operational limits of the transmission system that is in the above of the MV system. For instance, to limit the power factor at the substation transformer of the MV distribution system to a predefined range.

The second part of the thesis could be improved further considering other sources of uncertainty. For instance, the line length can be different from that of the nominal model due to twist and turn of the cable in the duct along the feeder. This will affect both line resistance and reactance. In addition, the transformer reactance may have been changed with respect to its nominal value due to the aging or other reasons. More importantly, due to lack of the sufficient measurements in the MV distribution systems, load active powers are not known with certainty. Therefore, beside the considered uncertainty linked to the load reactive power (through the load power factor), load active power can be also an uncertain parameter. Similarly, in the case that the values of DG active and reactive powers are not available, assumptions on DG powers should be adopted as well. Consequently, in practice, the uncertainties are not only linked to the network model, but also they are arisen from the network working point. Developing a robust VCA that can take into account uncertainties associated with the network model as well as the network working point will be of a great interest as the future work of the current thesis. Moreover, reducing the needed number of scenarios using the improved Monte Carlo techniques can make the robust VCA compatible with the context of the real-time voltage management.

Acronyms

ABC	Area Between Curves
ANM	Active Network Management
APFC	Automatic Power Factor Control
AVC	Automatic Voltage Control
AVR	Automatic Voltage Regulation
BCBV	Branch Current to Bus Voltage
BIBC	Bus Injection to Branch Current
CDF	Cumulative Distribution Function
DFIG	Doubly-Fed Induction Generator
DG	Distributed Generation
DLF	Direct Load Flow
DSA	Direct Sensitivity Analysis
DSO	Distribution System Operator
FACTS	Flexible AC Transmission Systems
IDSA	Improved Direct Sensitivity Analysis
JBSA	Jacobian-Based Sensitivity Analysis
LF	Load Flow
LHS	Left-Hand Side
LV	Low Voltage
MC	Monte Carlo
NRLF	Newton-Raphson Load Flow
MILP	Mixed-Integer Linear Programming
MSVCA	Multi-Step Voltage Control Algorithm
MV	Medium-Voltage
OLTC	On-load Tap Changer
OPF	Optimal Power Flow
POSA	Perturb-and-Observe Sensitivity Analysis
RHS	Right-Hand Side
RO	Robust Optimization
RTU	Remote Terminal Unit

RVCA	Robust Voltage Control Algorithm
R/X	Resistance to Reactance
SCADA	Supervisory Control And Data Acquisition
SSVCA	Single-Step Voltage Control Algorithm
UKGDS	United Kingdom Generic Distribution System
VCA	Voltage Control Algorithm
VSA	Voltage Sensitivity Analysis

Nomenclature

Sets:

NL	Set of load buses
G	Set of DG units
U	Set of nodes with voltage rise issue
L	Set of nodes with voltage drop issue
C	Set of branches with the ampacity limits
B	Set of all branches
J	Set of column indices of matrix **A** which are subject to uncertainty

Indices:

k and n	Index for load buses
l	Index for buses with voltage drop issue
u	Index for buses with voltage rise issue
x	Index for DG unit number
J	Index for branch number
s	Index for branches with the ampacity limits
i	Index for entries of matrix **A** which are subject to uncertainty

Parameters:

I_{br}	Branch current
I	Node current
I_{br}^{init}	Initial current of branch
$I_{br}^{\max}$	Maximum current of branch
I^{it}	Node current at iteration number *it*
V	Node voltage
$\Delta Q_{br}^{\max}$	Maximum reactive power variation of branch while keeping the ampacity limit
P_{br}, Q_{br}	Branch active and reactive power flows, respectively

P_L , Q_L	Load active and reactive powers, respectively
r , x	Branch resistance and reactance, respectively
P_{DG}	Active power production of DG
$\Delta Q_{DG}^{\max}$, $\Delta Q_{DG}^{\min}$	Maximum and minimum possible variations of DG reactive power, respectively
$\Delta Tap_{TR}^{\max}$, $\Delta Tap_{TR}^{\min}$	Maximum and minimum possible movements of transformer tap changer, respectively
$\frac{\partial V}{\partial P}$	Sensitivity of voltage with respect to active power
$\frac{\partial V}{\partial Q}$	Sensitivity of voltage with respect to reactive power
$\frac{\partial V}{\partial V_{Tap}}$	Sensitivity of voltage with respect to transformer tap changes
θ_V , θ_I	Voltage and current phase angles, respectively
ΔV_w^{req}	Required voltage modification to remove the biggest voltage violation found at bus *w*
V_w	Voltage value at the bus with the biggest voltage violation, i.e., bus *w*
$\Delta V_w^{req,ri}$	Required voltage modification to solve voltage rise violation at bus *w*
$\Delta V_w^{req,dr}$	Required voltage modification to solve voltage drop violation at bus *w*
V_w^{ri} , V_w^{dr}	Voltage values at the bus with the biggest voltage violation in the voltage rise and drop states, respectively
$\frac{\partial V_{obs}}{\partial P_{pert}}$	Sensitivity of voltage at the observed point with respect to power variation at the perturbation point
ΔV_{obs}	Voltage variation at the observed point
ΔP_{pert}	Power variation at the perturbation point
$\mathrm{Re}(\underline{I})$, $\mathrm{Im}(\underline{I})$	Real and imaginary parts of the node current, respectively
P_{loss} , Q_{loss}	Branch active and reactive power losses, respectively
MM, $Err(\%)$	Mismatch and relative error of the voltage estimation, respectively
V_w^{cor}	Corrected voltage at bus *w*

Y_T	Transformer admittance
a	Transformer turn ratio
a_P , b_P , c_P	The coefficients of voltage dependency related to load active power
a_Q , b_Q , c_Q	The coefficients of voltage dependency related to load reactive power
α , β	Voltage dependency exponents related to load active and reactive powers, respectively
P_L^* , Q_L^*	Actual load active and reactive power consumptions, respectively
PF	Power factor of load
R_0 , R_{new}	The initial and modified branch resistances, respectively
ΔT	Temperature variation of the cable conductor
α_c	Temperature coefficient of resistivity
N	Number of scenarios created by the MC simulations in the probabilistic framework of chapter 6
N_1, N_2	Number of scenarios created by the MC simulations in the pre-processing and post-processing stages of the robust VCA, respectively
$nbus$, nbr	Total number of the system buses and branches, respectively
ξ	Random variable subject to uncertainty
Ω , Γ , Ψ	Parameters defining the borders of the uncertainty sets
$\frac{\widehat{\partial V}}{\partial P_{DG}}$, $\frac{\widehat{\partial V}}{\partial Q_{DG}}$, $\frac{\widehat{\partial V}}{\partial V_{Tap}}$	Perturbations of the voltage sensitivity coefficients related to DG active power, DG reactive power, and transformer tap changes, respectively
$\frac{\widetilde{\partial V}}{\partial P_{DG}}$, $\frac{\widetilde{\partial V}}{\partial Q_{DG}}$, $\frac{\widetilde{\partial V}}{\partial V_{Tap}}$	Uncertain voltage sensitivity coefficients related to DG active power, DG reactive power, and transformer tap changes, respectively

Variables:

ΔQ_{DG}	Reactive power change of DG
ΔQ_{DG}^{ind}	Reactive power change of DG towards inductive direction

ΔQ_{DG}^{cap}	Reactive power change of DG towards capacitive direction
ΔP_{DG}	Active power change of DG
ΔTap_{TR}	Transformer tap movement
ΔTap_{TR}^{down}	Downward transformer tap movement
ΔTap_{TR}^{up}	Upward transformer tap movement

Matrices:

BIBC	Bus injection to branch current matrix
BCBV	Branch current to bus voltage matrix
DLF	Direct load flow matrix
DGIB	DG injections to branch parameters matrix
$\mathbf{R}$, $\mathbf{X}$	Matrices including the line resistances and reactances, respectively
$\mathbf{V_k}$	Vector of nodal voltages at the load buses
$\mathbf{V_1}$	Vector of reference voltages equal to 1 pu
$\mathbf{I}$, $\mathbf{I_{br}}$	Vectors of nodal and branch currents, respectively
$\mathbf{P}$, $\mathbf{Q}$	Vectors of nodal active and reactive powers, respectively
$\mathbf{J}^{-1}$	Inverted Jacobian matrix
$\mathbf{J_1}$, $\mathbf{J_2}$, $\mathbf{J_3}$, $\mathbf{J_4}$	Sub-Jacobian matrices
$\mathbf{\Delta P}$, $\mathbf{\Delta Q}$	Vectors of nodal active and reactive powers, respectively
$\mathbf{\Delta V}$, $\mathbf{\Delta \theta}$	Vectors of nodal voltages magnitudes and phase angles, respectively
$\mathbf{l_b}$, $\mathbf{u_b}$	Lower and upper bounds of the control variables
$\mathbf{C}^{T}$	Transpose vector of coefficients of linear objective function
$\mathbf{A}$, $\mathbf{A_{eq}}$	Matrices of linear inequality and equality constraints, respectively
$\mathbf{b}$, $\mathbf{b_{eq}}$	LHSs of the inequality and equality structural constraints, respectively
$\mathbf{x}$	Vector of decision variables

Appendix 1: Direction of active and reactive powers

Let consider the circuit enclosed in the box shown in figure A-1 with entering current I and voltage V [69].

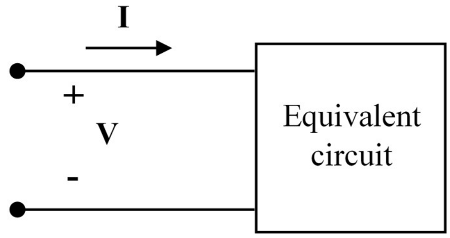

Figure A-1: Circuit enclosed in the box

We can determine active and reactive powers supplied or absorbed by the circuit according to the relation $S = VI^*$, where S is the apparent power and I^* is the conjugate current. When current I lags the voltage by an angle between 0 and 90°, we find that active and reactive powers (P and Q) are both positive, indicating that watts and vars are being absorbed by the inductive circuit or element inside the box. Conversely, when I leads voltage by an angle between 0 and 90°, active power is still positive but reactive power is negative meaning that negative vars are being absorbed or positive vars are being supplied by the capacitive circuit inside the box. Finally, when active power P is negative, circuit inside the box is supplying active power. Therefore, circuit inside the box

- absorbs real power if $P > 0$
- supplies real power if $P < 0$
- absorbs reactive power if $Q > 0$
- supplies reactive power if $Q < 0$

It should be noted that the box shown in figure A-1 could include a (portion of) network or an element such as DG or load.

Appendix 2: Parameters of the 33-bus system

Base power =1 MVA
Base voltage =12.66 kV
Total active power of loads: 3.72 MW
Total reactive power of loads: 2.3 Mvar
Average resistance of the lines: 0.6731 ohm
Average reactance of the lines: 0.5870 ohm

Branch data

Branch number	Sending node	Ending node	Resistance (ohm)	Reactance (ohm)
1	1	2	0.0922	0.0477
2	2	3	0.4930	0.2511
3	3	4	0.3660	0.1864
4	4	5	0.3811	0.1941
5	5	6	0.8190	0.7070
6	6	7	0.1872	0.6188
7	7	8	1.7114	1.2351
8	8	9	1.0300	0.7400
9	9	10	1.0040	0.7400
10	10	11	0.1966	0.0650
11	11	12	0.3744	0.1238
12	12	13	1.4680	1.1550
13	13	14	0.5416	0.7129
14	14	15	0.5910	0.5260
15	15	16	0.7463	0.5450
16	16	17	1.2890	1.7210
17	17	18	0.7320	0.5740
18	2	19	0.1640	0.1565
19	19	20	1.5042	1.3554
20	20	21	0.4095	0.4784
21	21	22	0.7089	0.9373
22	3	23	0.4512	0.3083
23	23	24	0.8980	0.7091
24	24	25	0.8960	0.7011
25	6	26	0.2030	0.1034
26	26	27	0.2842	0.1447
27	27	28	1.0590	0.9337
28	28	29	0.8042	0.7006
29	29	30	0.5075	0.2585
30	30	31	0.9744	0.9630

31	31	32	0.3105	0.3619
32	32	33	0.3410	0.5302

Load data

Bus number	Active power (kW)	Reactive power (kvar)
2	100	60
3	90	40
4	120	80
5	60	30
6	60	20
7	200	100
8	200	100
9	60	20.0
10	60	20
11	45	30
12	60	35
13	60	35
14	120	80
15	60	10
16	60	20
17	60	20
18	90	40
19	90	40
20	90	40
21	90	40
22	90	40
23	90	50
24	420	200
25	420	200
26	60	25
27	60	25
28	60	20
29	120	70
30	200	600
31	150	70
32	210	100
33	60	40

Appendix 3: Parameters of the 77-bus system

Base power =100 MVA
Base voltage =11 kV
Number of loads: 75
Total active power of loads: 24.274 MW
Total reactive power of loads: 4.854 Mvar
Total length of the system lines: 56.82 km
Longest feeder of the system: feeder 1, 11.15 km
Average resistance of the lines: 0.0898 ohm
Average reactance of the lines: 0.0515 ohm
Transformer reactance (X_T): 12.5% pu in the transformer base power (80 MVA)

Branch data

Branch number	Sending node	Ending node	Resistance (ohm)	Reactance (ohm)
1	1	2	0	X_T
2	2	3	0.0665	0.0512
3	3	4	0.0665	0.0512
4	4	5	0.0729	0.0198
5	4	6	0.0665	0.0512
6	6	7	0.0665	0.0512
7	7	8	0.0729	0.0198
8	7	9	0.0665	0.0512
9	9	10	0.0729	0.0198
10	9	11	0.0665	0.0512
11	11	12	0.0665	0.0512
12	12	13	0.0729	0.0198
13	12	14	0.0665	0.0512
14	14	15	0.0665	0.0512
15	15	16	0.0729	0.0198
16	15	17	0.0665	0.0512
17	17	18	0.0665	0.0512
18	18	19	0.0729	0.0198
19	18	20	0.0665	0.0512
20	20	21	0.0729	0.0198
21	20	22	0.0665	0.0512
22	22	23	0.0665	0.0512
23	23	24	0.0729	0.0198
24	23	25	0.0665	0.0512
25	25	26	0.0665	0.0512
26	26	27	0.0729	0.0198
27	2	28	0.0745	0.0574
28	28	29	0.0745	0.0574
29	29	30	0.0542	0.0147
30	29	31	0.0745	0.0574
31	31	32	0.0745	0.0574
32	32	33	0.0542	0.0147
33	32	34	0.0745	0.0574
34	34	35	0.0542	0.0147
35	34	36	0.0745	0.0574

36	36	37	0.0745	0.0574
37	37	38	0.0542	0.0147
38	2	39	0.0745	0.0574
39	39	40	0.0745	0.0574
40	40	41	0.164	0.1565
41	40	42	0.0542	0.0147
42	42	43	0.0745	0.0574
43	43	44	0.0542	0.0147
44	43	45	0.0745	0.0574
45	45	46	0.0542	0.0147
46	45	47	0.0745	0.0574
47	47	48	0.0745	0.0574
48	48	49	0.0542	0.0147
49	2	50	0.0917	0.0706
50	50	51	0.0917	0.0706
51	51	52	0.0571	0.0155
52	51	53	0.0917	0.0706
53	53	54	0.0917	0.0706
54	54	55	0.0571	0.0155
55	54	56	0.0917	0.0706
56	56	57	0.0571	0.0155
57	56	58	0.0917	0.0706
58	58	59	0.0917	0.0706
59	59	60	0.0571	0.0155
60	59	61	0.0917	0.0706
61	61	62	0.0917	0.0706
62	62	63	0.0571	0.0155
63	2	64	0.2038	0.1056
64	64	65	0.2038	0.1056
65	65	66	0.0624	0.017
66	2	67	0.2038	0.1056
67	67	68	0.2038	0.1056
68	68	69	0.0624	0.017
69	2	70	0.266	0.1378
70	70	71	0.266	0.1378
71	71	72	0.0663	0.018
72	71	73	0.266	0.1378
73	73	74	0.0663	0.018
74	2	75	0.2038	0.1056
75	75	76	0.2038	0.1056
76	76	77	0.0624	0.017

Load data

Bus number	Active power (MW)	Reactive power (Mvar)
1	0	0
2	0	0
3	0.342	0.0684
4	0.342	0.0684
5	0.222	0.0444
6	0.344	0.0688
7	0.344	0.0688
8	0.222	0.0444
9	0.344	0.0688
10	0.224	0.0448
11	0.344	0.0688
12	0.344	0.0688
13	0.224	0.0448
14	0.344	0.0688
15	0.344	0.0688
16	0.224	0.0448
17	0.344	0.0688
18	0.344	0.0688
19	0.224	0.0448
20	0.344	0.0688
21	0.224	0.0448
22	0.344	0.0688
23	0.344	0.0688
24	0.224	0.0448
25	0.344	0.0688
26	0.344	0.0688
27	0.224	0.0448
28	0.426	0.0852
29	0.426	0.0852
30	0.212	0.0424
31	0.426	0.0852
32	0.426	0.0852
33	0.212	0.0424
34	0.426	0.0852
35	0.212	0.0428
36	0.426	0.0852
37	0.426	0.0852
38	0.212	0.0428
39	0.426	0.0852
40	0.426	0.0852
41	0.212	0.0424
42	0.426	0.0852
43	0.426	0.0852
44	0.212	0.0424
45	0.426	0.0852
46	0.212	0.0428
47	0.426	0.0852
48	0.426	0.0852
49	0.212	0.0428
50	0.434	0.0868
51	0.434	0.0868
52	0.216	0.0432
53	0.436	0.0872
54	0.436	0.0872

55	0.216	0.0432
56	0.436	0.0872
57	0.216	0.0432
58	0.436	0.0872
59	0.436	0.0872
60	0.216	0.0432
61	0.436	0.0872
62	0.436	0.0872
63	0.216	0.0432
64	0.392	0.0784
65	0.392	0.0784
66	0.116	0.0232
67	0.392	0.0784
68	0.392	0.0784
69	0.116	0.0232
70	0.394	0.0788
71	0.394	0.0788
72	0.102	0.0204
73	0.396	0.0792
74	0.1	0.02
75	0.392	0.0784
76	0.392	0.0784
77	0.116	0.0232

Appendix 4: The relevant publications

1. B. Bakhshideh Zad, J. Lobry and F. Vallée, "Impacts of the model uncertainty on the voltage regulation problem of medium-voltage distribution systems," *IET Generation Transmission & Distribution*, vol. 12, no. 10, pp. 2359-2368, 2018.
2. B. Bakhshideh Zad, H. Hasanvand, J. Lobry and F. Vallée, "Optimal reactive power control of DGs for voltage regulation of MV distribution systems using sensitivity analysis method and PSO algorithm," *International Journal of Electric Power and Energy Systems*, vol. 68, pp. 52-60, 2015.
3. B. Bakhshideh Zad, J. Lobry and F. Vallée, "A new voltage sensitivity analysis method incorporating power losses impact," *Electric Power Components and Systems (<u>Under review</u>: initial submission on August 2017, revised paper has been submitted on February 2018)*.
4. B. Bakhshideh Zad, J. Lobry and F. Vallée, "A robust voltage control algorithm incorporating the model uncertainty impacts," *<u>Working paper</u>*.
5. B. Bakhshideh Zad, J. Lobry, and F. Vallée, "Impacts of the load and line inaccurate models on the voltage control problem of the MV distribution systems," *52nd International Universities Power Engineering Conference (UPEC)*, Greece, 2017.
6. B. Bakhshideh Zad, J. Lobry and F. Vallée, "A centralized approach for voltage control of MV distribution systems using DGs power control and a direct sensitivity analysis method," in *IEEE International Energy Conference (ENERGYCON)*, Belgium, 2016.
7. B. Bakhshideh Zad, J. Lobry, F. Vallée and H. Hasanvand, "Optimal reactive power control of DGs for voltage regulation of MV distribution systems considering thermal limit of the system branches," *International Conference on Power System Technology (POWERCON)*, China, 2014.
8. B. Bakhshideh zad, J. Lobry, F. Vallée and O. Durieux, "Improvement of on-load tap changer performance in voltage regulation of MV distribution systems with DG units using D-STATCOM," *in 22nd International Conference on Electricity Distribution (CIRED)*, Sweden, 2013.
9. B. Bakhshideh Zad, J. Lobry and F. Vallée, "Coordinated control of on-load tap changer and D-STATCOM for voltage regulation of radial distribution systems with DG units," in *Electric Power and Energy Conversion Systems Conference*, Turkey, 2013.
10. H. Hasanvand, B. Bakhshideh Zad, A. Parastar, J. Lobry, and, F. Vallée, "Voltage support and damping of low frequency oscillations in a large scale power system using STATCOM," in *IEEE International Energy Conference (ENERGYCON)*, Belgium, 2016.
11. V. Klonari, B. Bakhshideh Zad, J. Lobry, and F. Vallée, "Application of voltage sensitivity analysis in a probabilistic context for characterizing low voltage network

operation," in *2016 International Conference on Probabilistic Methods Applied to Power Systems (PMAPS)*, China, 2016.

Bibliography

[1] J. A. Pecas and N. Hatziagyriou, “Integrating distributed generation into electric power systems: a review of drivers, challenges and opportunities,” *Journal of Electric Power Systems Research,* vol. 77, pp. 1189-1203, 2007.

[2] J. Mutale, “Benefits of active management of distribution networks with distributed generation,” in *IEEE PES Power Systems Conference and Exposition*, USA, 2006.

[3] N. C. Scott, D. J. Atkinson and J. E. Morrell, “Use of load control to regulate voltage on distribution networks with embedded generation,” *IEEE Transactions on Power Systems,* vol. 17, no. 2, pp. 510-515, 2002.

[4] P. N. Vovos, A. E. Kiprakis, A. R. Wallace and G. P. Harrison, “Centralized and distributed voltage control impact on distributed generation penetration,” *IEEE Transactions on Power Systems,* vol. 22, no. 1, pp. 476-483, 2007.

[5] E. Chabod, L. Karsenti, J. Witkowski and G. Malarange, “Local voltage regulation influence on DG and distribution network,” in *international conference on electricity distribution (CIRED)*, 2012.

[6] A. E. Kiprakis and A. R. Wallace, “Hybrid control of distributed generators connected to weak rural networks to mitigate voltage variations,” in *international conference and exhibition on electricity distribution (CIRED)*, 2003.

[7] S. Engelhardt, I. Erlich and C. Feltes, “Reactive power capability of wind turbines based on doubly-fed induction generators,” *IEEE Transaction on Energy Conversion,* vol. 26, no. 11, pp. 364-372, 2011.

[8] k. Turitsyn, P. Sulc, S. Backhaus and M. Chertkov, “Options for Control of Reactive Power by Distributed Photovoltaic Generators,” *Proceedings of the IEEE,* vol. 99, no. 6, pp. 1063 - 1073, 2011.

[9] G. Won Kim and K. Y. Lee, “Coordination control of ULTC transformer and STATCOM based on an artificial neural network,” *IEEE Transactions on Power Systems,* vol. 20, no. 2, pp. 580-586, 2005.

[10] M. S. El Moursi, B. Bak-Jensen and M. H. and Abdel-Rahman, “Coordinated voltage control scheme for SEIG-based wind park utilizing substation STATCOM and ULTC transformer,” *IEEE Transactions on Sustainable Energy,* vol. 2, no. 3, pp. 246-255, 2011.

[11] B. Bakhshideh zad, J. Lobry, F. Vallée and O. Durieux, “Improvement of on-load tap changer performance in voltage regulation of MV distribution systems with DG units using D-STATCOM,” in *22nd International Conference on Electricity*, Sweden, 2013.

[12] B. Bakhshideh Zad, J. Lobry and F. Vallée, "Coordinated control of on-load tap changer and D-STATCOM for voltage regulation of radial distribution systems with DG units," in *Electric Power and Energy Conversion Systems*, Turkey, October 2013.

[13] M. Bahramipanah, R. Cherkaoui and M. Paolone, "Decentralized voltage control of clustered active distribution network by means of energy storage systems," *Electric Power Systems Research,* vol. 136, pp. 370-382, 2016.

[14] M. Nayeripoura, H. W. E. Fallahzadeh-Abarghouei and S. Hasanvand, "Coordinated online voltage management of distributed generation using network partitioning," *Electric Power Systems Research,* vol. 141, pp. 202-209, 2016.

[15] M. E Elkhatib, R. El-Shatshat and M. A. Salama, "Novel coordinated voltage control for smart distribution networks with DG," *IEEE Transactions on Smart Grid,* vol. 2, no. 4, pp. 598-605, 2011.

[16] F. Capitanescu, I. Bilibin and E. Romero Ramos, "A comprehensive centralized approach for voltage constraints management in active distribution grid," *IEEE Transaction on Power Systems,* vol. 29, no. 2, pp. 933-942, 2013.

[17] G. Valverde and T. Van Cutsem, "Model predictive control of voltages in active distribution networks," *IEEE Trans. on Smart Grid,* vol. 4, no. 4, pp. 2152-2161, 2013.

[18] H. Soleimani Bidgoli, M. Glavic and T. Van Cutsem, "Receding-horizon control of distributed Generation to correct voltage or thermal violations and track desired schedules," in *Power Systems Computation Conference (PSCC)*, 2016.

[19] F. Pilo, G. Pisano and G. G. Soma, "Optimal coordination of energy resources with a two-stage online active management, IEEE Transactions on Industrial Electronics," *IEEE Transactions on Industrial Electronics,* vol. 58, no. 10, pp. 4526-4537, 2011.

[20] A. Borghetti, M. Bosetti, S. Grillo, S. Massucco, C. Alberto Nucci, M. Paolone and F. Silvestro, "Short-term scheduling and control of active distribution systems with high penetration of renewable resources," *IEEE Systems Journal,* vol. 4, no. 3, pp. 313-322, 2010.

[21] J. G. Robertson, G. P. Harrison and A. Robin Wallace, " OPF Techniques for Real-Time Active Management of Distribution Networks," *IEEE Transactions on Power Systems,* vol. 32, no. 5, pp. 3529-3537, 2017.

[22] M. Brenna, E. De Beradinis, F. Foiadelli, G. Sapienza and D. Zaninelli, "Voltage control in smart grid an approach based on sensitivity analysis," *Journal of Electromagnetic and Applications,* vol. 2, no. 8, pp. 467-474, 2010.

[23] A. Borghetti, "Using mixed integer programming for the volt/var optimization in distribution feeders," *Electric Power Systems Research,* vol. 98, pp. 39-50, 2013.

[24] A. Borghetti, F. Napolitano and C. Alberto Nucci, “Volt/Var Optimization of Unbalanced Distribution Feeders via Mixed Integer Linear Programming,” in *Power Systems Computation Conference*, August 2014.

[25] L. Peng, J. Haoran, W. Chengshan and e. al., “ Coordinated Control Method of Voltage and Reactive Power for Active Distribution Networks Based on Soft Open Point,” *IEEE Transactions on Sustainable Energy ,* vol. 8, no. 4, pp. 1430-1442, 2017.

[26] H. Soleymani Bidgoli and T. Van Cutsem, “Combined Local and Centralized Voltage Control in Active Distribution Networks,” *IEEE Transactions on Power Systems,* vol. 33, no. 2, pp. 1374-1384, 2018.

[27] N. Efkarpidis, T. De Rybel and J. Driesen, “Technical assessment of centralized and localized voltage control strategies in low voltage networks,” *Sustainable Energy, Grids and Networks,* vol. 8, pp. 85-97, 2016.

[28] F. A. Viawana, A. Sanninob and J. Daaldera, “Voltage control with on-load tap changers in medium voltage feeders in presence of distributed generation,” *Electric Power Systems Research,* vol. 77, no. 10, pp. 1314-1322, 2007.

[29] Q. Zhou and J. W. Bialek, “Generation curtailment to manage voltage constraints in distribution networks,” *IET Generation Transmission Distribution,* vol. 1, no. 3, pp. 492-498, 2007.

[30] A. Abur, “A modified linear programming method for distribution system reconfiguration,” *International Journal of Electrical Power & Energy Systems ,* vol. 18, no. 7, pp. 469-474, 1996.

[31] K. Christakou, J. Y. LeBoudec, M. Paolone and D. C. Tomozei, “Efficient computation of sensitivity coefficients of node voltages and line currents in unbalanced radial electrical distribution networks,” *IEEE Transactions on Smart Grid,* vol. 4, no. 2, p. 741–750, 2013.

[32] N. Mithulananthan, M. M. A. Salama, C. A. Cañizares and J. Reeve, “Distribution system voltage regulation and Var compensation for different static load models,” *International Journal of Electrical Engineering Education,* vol. 37, no. 4, pp. 384-395 , 2000.

[33] C. M. Hird, H. Leite, N. Jenkins and H. Li, “Network voltage controller for distributed generation,” *IEE Proceedings - Generation, Transmission and Distribution,* vol. 151, no. 2, pp. 150 - 156, 2004.

[34] S. Frank, I. Steponavice and S. Rebennack, “Optimal power flow: a bibliographic survey I Formulations and deterministic methods,” *Energy Systems,* vol. 3, no. 3, p. 221–258, 2012.

[35] S. Frank, I. Steponavice and S. Rebennack, “Optimal power flow a bibliographic survey II, Non-Deterministic and Hybrid Methods,” *Energy Systems,* vol. 3, no. 2, p. 259–289, 2012.

[36] S. K. chang, “Optimal real-time voltage control’’, IEEE Transactions on Power Systems,” *IEEE Transactions on Power Systems,* vol. 5, no. 3, pp. 750-758, 1990.

[37] G. P. Harrison and A. R. Wallace, “Optimal power flow evaluation network capacity for the connection of distributed generation,” *IEE Proceedings - Generation, Transmission and Distribution ,* vol. 152, no. 1, pp. 115 - 122, 2005.

[38] D. Pudjianto, D. M. Cao, S. Grenard and G. Strbac, “Method for monetarisation of cost and and Benefits of DG Options,” Research project supported by the european commission, 2006.

[39] K. Almeida and F. D. Galiana, “Critical cases in the optimal power flow,” *IEEE Transactions on Power Systems ,* vol. 11, no. 3, pp. 1509-1518, 1996.

[40] R. Madani, S. Sojoudi and J. Lavaei, “Convex Relaxation for Optimal Power Flow Problem: Mesh Network,” *IEEE Transactions on Power Systems,* vol. 30, no. 1, pp. 199-211, 2015.

[41] M. Nick, R. Cherkaoui, J.-Y. Le Boudec and M. Paolone, “ An Exact Convex Formulation of the Optimal Power Flow in Radial Distribution Networks Including Transverse Components,” *IEEE Transactions on Automatic Control ,* vol. 63, no. 3, pp. 682-697, 2018.

[42] X. W. H. Bai, K. Fujisawa and Y. Wang, “Semidefinite programming for optimal power flow problems,” *International Journal of Electrical Power & Energy Systems,* vol. 30, no. 6-7, pp. 383-392, 2008.

[43] R. A. Jabr, “Radial distribution load flow using conic programming,” *IEEE Transactions on Power Systems,* vol. 21, no. 3, pp. 1458-1459, 2006.

[44] S. H. Low, “Convex Relaxation of Optimal Power Flow—Part I: Formulations and Equivalence,” *IEEE Transactions on Control of Network Systems,* vol. 1, no. 1, pp. 15-27, 2014.

[45] H. Lefebvre, D. Fragnier, J. Boussion, P. Mallet and M. Bulot, “Secondary coordinated voltage control system: feedback of EDF,” in *Power Engineering Society Summer Meeting* , USA, 2000.

[46] K. Christakou, M. Paolone and A. Abur, “Voltage Control in Active Distribution Networks Under Uncertainty in the System Model: A Robust Optimization Approach,” *IEEE Transactions on Smart Grid,* vol. DOI 10.1109/TSG.2017.2693212, 2017.

[47] J. Teng, “A direct approach for distribution system load flow solutions, IEEE Trans. on Power Delivery,” *IEEE Transaction on Power Delivery,* vol. 18, no. 3, pp. 882-887, 2003.

[48] D. Shirmohammadi, H. W. Hong, A. Semlyen and G. X. Luo, “A compensation-based power flow method for weakly meshed distribution and transmission networks,” *IEEE Transactions on Power Systems,* vol. 3, no. 2, pp. 753-762, 1988.

[49] M. H. Haque, “Efficient load flow method for distribution systems with radial or mesh configuration,” *IEE Proceedings- Generation, Transmission and Distribution,* vol. 143, no. 1, pp. 33-38, 1966.

[50] Q. Zhou and J. W. Bialek, "Simplified calculation of voltage and loss sensitivity factors in distribution networks," in *The16th Power Systems Computation Conference (PSCC)*, Scotland, 2008.

[51] D. Khatod, V. Pant and J. Sharma, "A novel approach for sensitivity calculations in the radial distribution system," *IEEE Transactions on Power Delivery,* vol. 21, no. 4, p. 2048–2057, 2006.

[52] S. Conti, S. Raiti and G. Vagliasindi, "Voltage sensitivity analysis in radial MV distribution networks using constant current models," in *2010 IEEE International Symposium on Industrial Electronics (ISIE)*, 2010.

[53] J. Teng, "Modelling distributed generations in three-phase distribution load flow," *IET Generation, Transmission and Distribution,* vol. 2, no. 3, pp. 330-340, 2008.

[54] F. Tamp and P. Ciufo, "A sensitivity analysis toolkit for the simplification of MV distribution network voltage management," *IEEE Transactions on Smart Grid,* vol. 5, no. 2, pp. 559-568, 2015.

[55] R. Gurram and B. Subramanyam, "Sensitivity analysis of radial distribution network-adjoint network method," *International Journal of Electric Power and Energy Systems,* vol. 11, pp. 323-326, 1999.

[56] J. W. Bandler and M. A. El-Kady, "A unified approach to power system sensitivity analysis and planning, Part I: Family of adjoint systems," *in Proc. IEEE Int. Symp. Circuits Syst.,* pp. 681-687, 1980.

[57] J. W. Bandler and M. A. El-Kady, "A unified approach to power system sensitivity analysis and planning, Part II: Special class of adjoint systems," *in Proc. IEEE Int. Symp. Circuits Syst.,* pp. 688-692, 1980.

[58] B. Bakhshideh Zad, J. Lobry, F. Vallée and H. Hasanvand, "Optimal reactive power control of DGs for voltage regulation of MV distribution systems considering thermal limit of the system branches," in *Int. conf. on power system technology (POWERCON)*, China, 2014.

[59] C. L. Masters, " Voltage rise: the big issue when connecting embedded generation to long 11 kV overhead lines," *Power Engineering Journal,* vol. 16, no. 1, pp. 5-12, 2002.

[60] M. Adibi and D. Milanicz, "Reactive capability limitation of synchronous machines," *IEEE Transactions on Power Systems,* vol. 9, no. 1, pp. 29-40, 1994.

[61] R. Sioshansi and A. J. Conejo, Optimization in Engineering; Models and Algorithms, Springer, 2017.

[62] F. F. W. Baran M E, "Network reconfiguration in distribution systems for loss reduction and load balancing," vol. 4, no. 2, pp. 1401-1407, 1989.

[63] M. R. Shakarami, H. Beiranvand, B. Beiranvand and E. Sharifipour, “A recursive power flow method for radial distribution networks:Analysis, solvability and convergence,” *Electrical Power and Energy Systems,* vol. 86, pp. 71-80, 2017.

[64] IEC60076-5, “Power transformers: Ability to withstand short circuit,” 2000.

[65] United Kingdom Generic Distribution Network (UKGDS), http://www.sedg.ac.uk/.

[66] T. Gozel and H. Hoacaoglu, “An analytical method for sizing and siting of distributed generators in radial distribution systems,” *Electric Power Systems Research,* vol. 79, pp. 912-918, 2008.

[67] D. Das, D. P. Kothari and A. Kalam, “Simple and efficient method for load flow solution of radial distribution networks,” *International Journal of Electrical Power & Energy Systems,* vol. 17, no. 5, pp. 335-346, 1995.

[68] H. Saadat, Power system analysis, mcgraw hill, 1999.

[69] J. J. Grainger and J. Stevenson, Power system analysis, Mcgraw Hill, 1994.

[70] B. Bakhshideh Zad, H. Hasanvand, J. Lobry and F. Vallée, “Optimal reactive power control of DGs for voltage regulation of MV distribution systems using sensitivity analysis method and PSO algorithm,” *International Journal of Electric Power and Energy Systems,* vol. 68, pp. 52-60, 2015.

[71] M. Brenna, E. D. Berardinis, L. D. Carpini and F. Foiadelli, “Automatic Distributed Voltage Control Algorithm in Smart Grids Applications,” *IEEE Transactions on Smart Grid,* vol. 4, no. 2, pp. 877-885, 2013.

[72] B. Bakhshideh Zad, J. Lobry and F. Vallée, "A centralized approach for voltage control of MV distribution systems using DGs power control and a direct sensitivity analysis method," in *IEEE international energy conference (ENERGYCON)*, Belgium, 2016.

[73] F. Vallée, V. Klonari, T. Lisiecki, O. Durieux and J. Lobry, “Development of a probabilistic tool using Monte Carlo simulation and smart meters measurements for the long term analysis of low voltage distribution grids with photovoltaic generation,” *International Journal of Electrical Power & Energy Systems,* vol. 53, pp. 468-477, 2.13.

[74] S. Conti and S. Raiti, “Probabilistic load flow using Monte Carlo techniques for distribution networks with photovoltaic generators,” *Solar Energy,* vol. 81, no. 12, pp. 1473-1481, 2007.

[75] V. Klonari, B. Bakhshideh Zad, J. Lobry and F. Vallée, “Application of Voltage Sensitivity Analysis in a Probabilistic Context for Characterizing Low Voltage Network Operation,” in *International Conference on Probabilistic Methods Applied to Power Systems (PMAPS)*, China, 2017.

[76] R. Singh, B. C. Pal and R. A. Jabr, “Distribution system state estimation through Gaussian mixture model of the load as pseudo-measurement,” *IET Generation, Transmission & Distribution,* vol. 4, no. 1, pp. 50-59, 2009.

[77] M. H. Haque, “Load flow solution of distribution systems with voltage dependent load models,” *Electric Power Systems Research ,* vol. 36, no. 3, pp. 151-156, 1996.

[78] L. M. Korunovic, D. P. Stojanovic and J. V. Milanovic, “Identification of static load characteristics based on measurements in medium voltage distribution network,” *IET Generation, Transmission & Distribution,* vol. 2, no. 2, pp. 227-234, 2008.

[79] A. J. Collin, G. Tsagarakis, A. E. Kiprakis and e. al, “'Development of Low-voltage Load Models for the Residential Load Sector,” *IEEE Transactions Power Systems,* vol. 29, no. 5, pp. 2180-2188, 2014.

[80] T. Van Cutsem and C. Vournas, Voltage Stability of Electric Power System, Springer, 2008.

[81] A. B. William, “A guide to installation of medium voltage cable,” *IEEE Transactions on Industry Applications,* Vols. IA-13, no. 6, pp. 527-529, 1977.

[82] A. Bernath, D. B. Olfe and B. W. Ferguson, “Heat transfer measurements on unequally loaded underground power cables with constant and cyclic currents,” *IEEE Power Trans. Power Appar. Syst.,* Vols. PAS-103, no. 10, pp. 2799-2806, 1984.

[83] Nexans, “6-36 kV medium voltage underground power cables,” 2010.

[84] U. A. Bakshi and M. V. Bakshi, Power System-I, India: Technical Publications, 2009.

[85] C37.010-1979, “IEEE application guide for AC high-voltage circuit breakers rated on a symmetrical current basis,” 1989.

[86] L. Zukui, D. Ran and A. F. Christodoulos, “A Comparative Theoretical and Computational Study on Robust Counterpart Optimization: I. Robust Linear Optimization and Robust Mixed Integer Linear Optimization,” *Industrial & Engineering Chemistry Research,* vol. 50, no. 18, pp. 10567-10603, 2011.

[87] M. Aien, A. Hajebrahimi and M. Fotuhi-Firuzabad, “A comprehensive review on uncertainty modeling techniques in power system studies,” *Renewable and Sustainable Energy Reviews,* vol. 57, pp. 1077-1089, 2016.

[88] B. Bakhshideh Zad, J. Lobry and F. Vallée, “Impacts of the model uncertainty on the voltage regulation problem of Medium Voltage distribution systems,” *IET Generation Transmission & Distribution,* vol. 12, no. 10, pp. 2359-2368, 2018.

[89] B. Bakhshideh Zad, J. Lobry and F. Vallée, “Impacts of the load and line inaccurate models on the voltage control problem of the MV distribution systems,” in *52nd International Universities Power Engineering Conference (UPEC)*, Heraklion, Greece, 2017.

[90] Z. Weiye, W. Wenchuan, Z. Boming and W. Yongjie, "Robust Reactive Power Optimization and Voltage Control Method for Active Distribution Networks via Dual Time-scale Coordination," *IET Generation, Transmission & Distribution,* vol. 11, no. 6, pp. 1461-1471, 2017.

[91] A. Ahmad, A. Nima and J. C. Antonio, "Adaptive robust AC optimal power flow considering load and wind power uncertainties," *International Journal of Electrical Power & Energy Systems,* vol. 196, pp. 132-142, 2018.

[92] J. Chengquan and W. Peng, "Optimal power flow with worst-case scenarios considering uncertainties of loads and renewables," in *International Conference on Probabilistic Methods Applied to Power Systems (PMAPS)*, China, 2016.

[93] L. Álvaro and A. S. Xu, "Adaptive Robust Optimization with Dynamic Uncertainty Sets for Multi-Period Economic Dispatch Under Significant Wind," *IEEE Transactions on Power Systems,* vol. 30, no. 4, pp. 1702-1713, 2015.

[94] A. Soroudi, "Robust optimization based self scheduling of hydro-thermal Genco in smart grids," *Energy,* vol. 61, pp. 262-271, 2013.

[95] A. Parisio, C. Del Vecchio and A. Vaccaro, "A robust optimization approach to energy hub management," *International Journal of Electrical Power & Energy Systems,* vol. 42, no. 1, pp. 98-104, 2012.

[96] B. Martin, E. De Jaeger and F. Glineur, "A robust convex optimization framework for autonomous network planning under load uncertainty," in *2017 IEEE Manchester PowerTech*, UK.

[97] A. L. Soyster, "Convex Programming with Set-Inclusive Constraints and Applications to Inexact Linear Programming," *Operations Research,* vol. 21, no. 5, pp. 1154-1157, 1973.

[98] D. Bertsimas and M. Sim, "The Price of Robustness," *Operations Research,* vol. 52, no. 1, pp. 35-53, 2004.

[99] A. Ben-Tal and A. Nemirovski, "Robust convex optimization," *Mathematics of Operations Research,* vol. 23, no. 4, pp. 769-805, 1998.

[100] A. Jalilvand-Nejad, R. Shafaei and H. Shahriari, "Robust optimization under correlated polyhedral uncertainty set," *Computers & Industrial Engineering,* vol. 90, pp. 82-94, 2016.